Development of Hydrogel-Based Strategies for Tissue Vascularisation

by

Pau Atienza Roca

A thesis submitted for the Degree of Doctor in Philosophy

Department of Orthopaedics and Musculoskeletal Medicine

University of Otago, Christchurch

October 2020

Abstract

The tissue engineering field and regenerative medicine has emerged as a promising strategy to overcome the lack of availability of organs and tissue grafts for transplantation. One of the main challenges in the field is to generate tissue analogues of relevant size with adequate nutrient and oxygen supply that promote graft integration and long-term functionality. The main strategies to promote tissue vascularisation are to either deliver bioactive cues such as growth factors (GFs), which attract the host vessels towards the area of interest, or to directly generate tissue analogues including a vessel network that can anastomose with the host blood vessels after implantation.

This thesis aims to develop novel platforms to improve tissue vascularisation by delivering GFs and generating *in vitro* vascularised tissues. Firstly, a literature review summarises the main strategies to deliver GFs and to generate *in vitro* vascularised tissues, together with their present limitations for clinical translation. Next, a GF delivery system based on tyraminated poly(vinyl alcohol) (PVA-Tyr) is developed, which has the ability to covalently incorporate a range of native GFs and then release them in a controlled profile and during a tailorable time frame. The flexibility of this GF delivery system allowed its adaptation to the revascularisation of the femoral head in an *in vivo* model of avascular necrosis, which was done by adjusting the incorporated GF, the GF release time, the cell-material interactions of the system and its delivery method. This research is followed by the development of a gelatin-norbornene (Gel-NOR) platform that allows biofabrication of large vascularised tissues. The fabricated tissues combined a controllable pore structure, which mimicked larger vessels in native tissues, with encapsulated endothelial cells that were able to assemble into micro-capillary structures, mimicking the capillary beds in native tissues. These fabricated tissues were used as a model to study how design parameters can affect the behaviour of endothelial cells, demonstrating that pore diameter and fibre diameter could have an impact on the ability of endothelial cells to form micro-capillaries. Finally, the developed platforms were combined using bioassembly, which allowed understanding how different cell arrangements can affect endothelial cell behaviour within fabricated scaffolds and to develop tissue analogues that combine GF delivery with pre-vascularisation techniques. Overall, this thesis combines materials chemistry and design with advanced fabrication techniques to develop new strategies that address current limitations in the field of tissue vascularisation.

Acknowledgements

I would like to thank my supervisors for their continuous guidance and advice during these years. Thanks to Khoon and Tim for giving me the opportunity to work at the CReaTE group and for all the growth opportunities provided.

Thanks to Khoon for all the time and effort spent to help me and my research become better. Thanks for your friendship and personal support during my first months here, they certainly made the changes easier to handle. I admire your intelligence, your hard work and your ability to see the big picture, and I'm hoping to take some of these qualities along on my next journey.

Thanks to Tim for your advice and your constant effort to look at the challenges from all possible points of view.

Thanks to Yogi and Lyn for welcoming me and dedicating your time and effort to my research. You helped me improve and taught me different ways to evaluate the constant challenges.

Thanks to the rest of the CReaTE members for the help provided during these years and for all the good times.

Thanks to all my friends that are or have been in this little island, especially Cesar, Michelle, Bram, Alice, Mitch, Gabby, Matt, Alasdair, Naveen and Jonas, for all the good moments that we have spent together.

Gràcies a la meva família per la paciència i el suport. Sé que la meva absència es nota, però aviat estaré de tornada.

Thanks to Lujay for the support, the patience, the company and the love. You have sacrificed part of your happiness to be here and the efforts are now coming to fruition. I'm impatient to see what awaits in the future.

Table of Contents

List of Figures

List of Tables

Chapter 1. Introduction

1.1. Tissue Engineering and the Challenge of Vascularisation

Since tissue and organ transplantation became a widespread medical procedure, there has been a tremendous disparity between the need and the availability of organs and tissue grafts. The inherent limitations associated with organ transplantation include immune rejection, risk of disease transmission and donor-site morbidity (1–3). The tissue engineering and regenerative medicine (TERM) field, which aims to regenerate or repair tissues or organs, has emerged as an attractive strategy to overcome these issues.

In order to successfully engineer tissues in the laboratory, it is vital to firstly understand the physiological processes of tissue development and regeneration. The main components in the developmental and regenerative microenvironments are cells, extracellular matrix (ECM) and soluble signalling molecules (4). Cells are the central unit of the tissue as they proliferate, migrate and differentiate in response to certain environmental inputs. The ECM acts as a physical support to these cells, while also providing the necessary biophysical and biochemical cues for tissue homeostasis. Finally, soluble signalling molecules circulate through the bloodstream and/or diffuse through interstitial fluid to modulate cellular behaviour. Tissue engineering focuses on controlling these three aspects within the regenerative microenvironment in order to trigger or enhance tissue regenerative/healing processes. This can be achieved by either delivering materials, cells and/or soluble signals directly into the injury site or by using these three components to generate tissue analogues that are maturated *in vitro* and implanted into the injury site.

Early stages of tissue regeneration usually involve the generation of a local vessel network that transports oxygen, cells and soluble signals to the injury site, initiating and promoting the wound-healing response (5). A good example of this process is bone fracture healing, where early vascularisation is essential. Reduced or inadequate blood flow during fracture healing has been associated to impaired regeneration, and reduced blood flow outside of the context of regeneration has been linked to disorders such as osteoporosis (6). Furthermore, enhancing the vascularisation process has consistently resulted in improved bone regeneration (7). Vascularisation is equally important in other tissues, and therefore promoting this process has been a major focus in TERM. However, generating a vascular network in tissue engineered

constructs remains one of the major challenges of the field (8,9). Vascular insufficiency is common in thick tissue engineered grafts, leading to poor cell survival and eventual failure of the graft (10).

This thesis focuses on promoting tissue vascularisation using two main strategies: delivering growth factors to the injury site and generating *in vitro* pre-vascularised tissue constructs. In this chapter, a brief introduction to vascularisation in the human body and the general strategies to promote it is provided, together with the main challenges in the strategies studied in this thesis.

1.2. Vascularisation in the Human Body

To develop strategies that promote vascularisation, it is necessary to understand the physiology of the vascularisation process. Blood vessels in the human body are formed by two distinct processes named vasculogenesis and angiogenesis (Figure 1.1) (11).

Vasculogenesis refers to the formation of a primitive capillary network from endothelial precursor cells (called angioblasts) that happens during embryonic development (Figure 1.1) (12). This capillary network is formed by the fusion of aggregates of stem cells called blood islands, which emerge from the mesoderm, in a complex process that involves interactions between stem cells, growth factors such as VEGFs (13,14), ECM molecules such as fibronectin and laminin (15) and cell adhesion molecules such as vascular endothelial cadherin (VE-cadherin), platelet-endothelial cell adhesion 1 (PECAM-1 or CD31) and CD34 (12). Notably, some studies have provided evidence of postnatal vasculogenesis initiated by endothelial progenitor cells (EPCs) present in human peripheral blood during wound healing and tumour development (16–18).

Angiogenesis refers to the formation of new capillaries from pre-existing vessels and is the predominant mechanism of blood vessel formation in later stages of embryonic development and in the adult body (11). The first instances of angiogenesis happen after the formation of a primitive capillary network through vasculogenesis. In this stage, new capillaries are formed by either sprouting of the endothelial cells (sprouting angiogenesis) or splitting of the capillaries (intussusceptive or non-sprouting angiogenesis) (Figure 1.1).

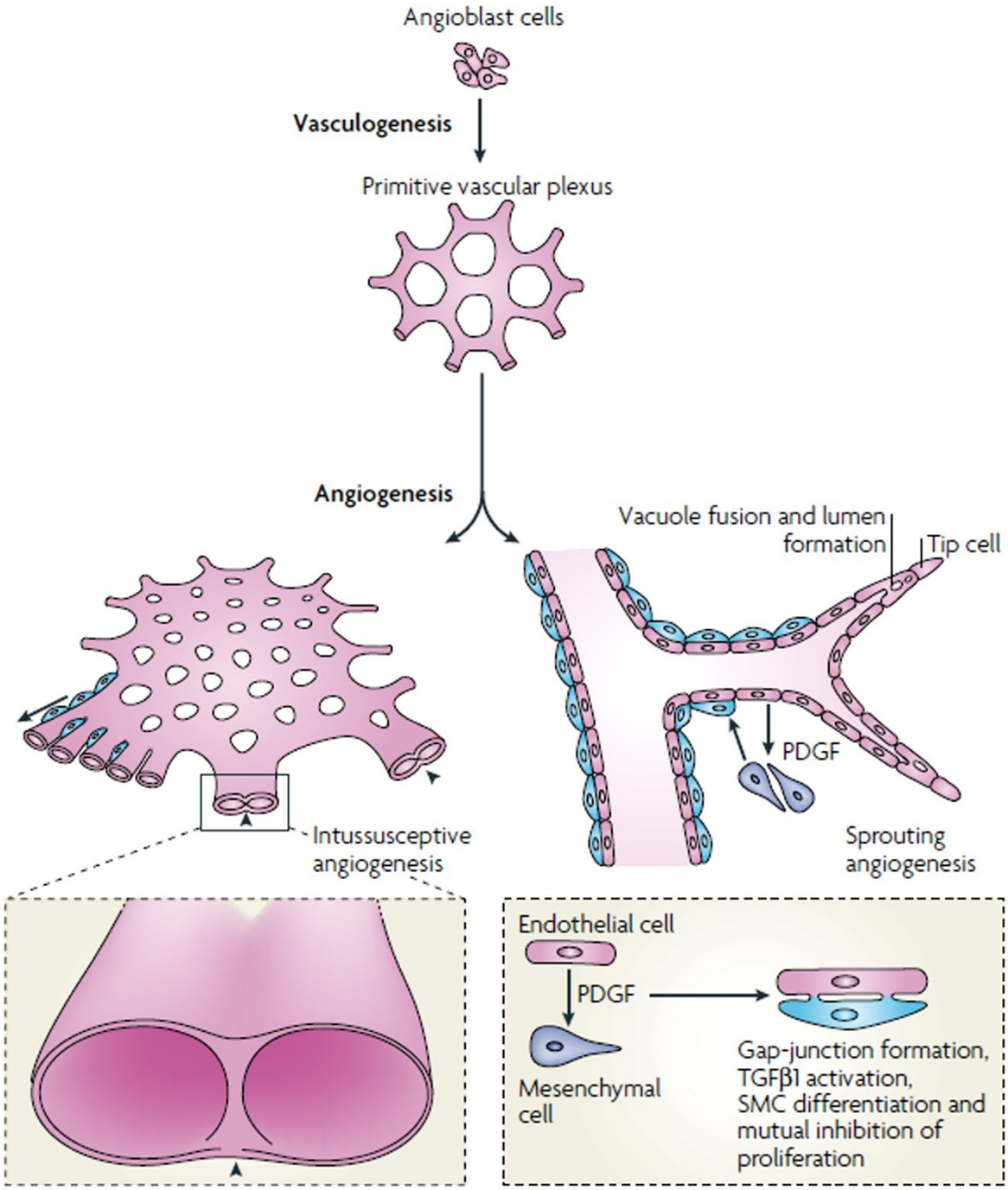

Figure 1.1. Vasculogenesis and Angiogenesis. *The differentiation of angioblasts, or endothelial precursor cells, from mesoderm and the formation of primitive vascular plexus from angioblasts are the two distinct steps during the onset of vascularization that together constitute vasculogenesis. Angiogenesis refers to the growth of new capillaries from pre-existing blood vessels either via sprouting or intussusception. Reproduced from (11).*

During sprouting angiogenesis, endothelial cells form sprouts with tip cells at their ending (polarized migratory endothelial cells that follow angiogenic stimuli, guiding vessel growth) followed by stalk cells (proliferative endothelial cells that form tubes and branches). This step is followed by pruning of unnecessary capillaries (19), recruitment of perivascular cells such as pericytes and smooth muscle cells and deposition of a basement membrane, resulting in a

more stable and mature vasculature (20,21). Angiogenesis in the adult body starts in fully developed blood vessels, therefore requiring an initial degradation of the basement membrane and detachment of mural cells before the sprouting of endothelial cells.

Non-sprouting angiogenesis starts with the protrusion of the vessel walls into the lumen, forming a contact between endothelial cells. This step is followed by the extension of cells from the interstitial tissue into this contact, the migration of pericytes and the growth of interstitial tissue, forming a transluminal pillar. This process has also been observed during tumour angiogenesis and in adult tissues such as kidney, bone, retina, heart and central nervous system (22).

1.3. Main Tissue Engineering Strategies to Promote Vascularisation

Tissue engineering has applied these biology concepts when designing strategies to promote vascularisation. There is a wide range of possibilities to do so, which are classified here in relation to the vascularisation process that they are trying to promote: angiogenesis or vasculogenesis.

In order to **promote angiogenesis**, the most extended strategy is to deliver bioactive clues that trigger angiogenic sprouting and attract tip cells towards the injury site (23,24). **Growth factors** that would naturally participate in the process of angiogenesis such as bFGF, VEGF, Angiopoietin-2 or PDGF have been one of the main focus of study (25). The delivery of **cells** is another strategy that is widely extended: mesenchymal stem cells (MSCs) and endothelial cells have been shown to promote angiogenesis by secreting signalling molecules into the environment (26). The use of **biomaterials** as vehicles to deliver these clues is one of the main pillars of tissue engineering (27). Biomaterials can be used to modulate the way in which delivered bioactive clues are presented, such as the release profile of growth factors, and they can also constitute angiogenic triggers by themselves. By using **ECM molecules** that participate in the vascularisation process such as fibrin or laminin as part of the delivery vehicle, it is possible to promote the penetration of angiogenic sprouts into the injury site (27). On the other hand, the **physico-mechanical properties and the degradation rate of the material** are huge determinants of the resulting regenerative process. A material that is too stiff will not allow the penetration of angiogenic sprouts into the area, and the degradation rate should match the matrix remodelling of cells that participate in tissue regeneration (28). Finally, the **3D architecture** of the scaffold is also an important. The generation of empty channels within the delivery vehicle through fabrication techniques has been demonstrated to

promote angiogenesis by facilitating the penetration of angiogenic sprouts from the body into the injury site (29).

The **stimulation of vasculogenesis** *in vitro* has been another major focus in tissue engineering during the last decade (9). It has been demonstrated that the co-encapsulation of endothelial cells or stem cells in ECM-derived hydrogels can promote their self-organisation into mature vessel networks including lumen, a tunica media and a basement membrane (30,31). This process happens after *in vitro* culture in media including vascularisation-promoting growth factors such as VEGF and bFGF (31,32). Furthermore, these pre-vascularised constructs are capable of forming anastomosis with the host vessel network after implantation, resulting in levels of tissue vascularisation that are significantly higher than after delivery of these cells and materials without the *in vitro* maturation step (33).

1.4. Challenges in Growth Factor Delivery

Growth factors (GFs) have been a main focus in tissue engineering due to the critical roles that they play during tissue development and regeneration. GFs are highly bioactive molecules, but they have a very short half-life in the physiological environment (34). Using biomaterial vehicles to deliver these GFs helps to mitigate the problem by protecting them from the physiological environment and providing a longer term release into the injury site as compared to direct injection. One of the main challenges in this field is to provide controlled release that fits the time frames of the targeted regenerative process. Adapting the GF release profiles of these delivery vehicles usually requires complex methodologies that may affect GF bioactivity or require the combination of multiple materials. Additionally, these methods can be very specific to a small range of GFs, limiting their application.

1.5. Challenges in the Generation of In Vitro Vascularised Tissue Analogues

The development of highly vascularised tissues has followed two main directions during recent years: top-down and bottom-up strategies (9).

Top-down strategies aim to use 3D fabrication techniques to generate a pre-designed channel network that is then seeded with endothelial cells, mimicking native vessels (35–37). While these techniques offer a lot of flexibility in the design of the channel network, they are limited in the minimum diameter of the channel (50 μm) due to the resolution of the fabrication techniques and the need of perfusing cells that can clog small channels (9,38). Another limitation of these techniques is in the high stiffness that is needed for long term

shape fidelity of the constructs, which is often in direct conflict with the material properties required for optimal cell spreading and differentiation.

Bottom-up approaches rely on the self-organisation of encapsulated cells to form a microvessel network by reproducing the natural processes of angiogenesis and vasculogenesis (32,39). The main limitation of bottom-up approaches to reproduce the native vessel network of tissues and organs is that the vessels formed are only in the size range of capillaries, which fails to reproduce the whole architecture of vessel networks. The need to use naturally-derived materials with very low stiffness limits their application to 3D fabrication techniques that would enable generating vessels of larger diameter (100 μm or larger). Furthermore, the scalability of these techniques also needs to be further studied for clinical translation, as research up to date only focuses on the generation of small tissue analogues.

1.6. General Aims of the Thesis

The present work aims to develop and study new tools to promote tissue vascularisation by promoting angiogenesis and vasculogenesis.

I. **Developing a growth factor delivery system to promote vascularisation.**
   Aim: To develop a growth factor delivery system that can incorporate a range of different growth factors and release them in a controlled manner and adapt it to promote vascularisation in a specific clinical context.

II. **Combining top-down and bottom-up approaches for the generation of large vascularised tissue analogues.**
   Aim: To develop and apply a material platform that can promote *in vitro* vasculogenesis and be biofabricated with controllable endothelialised porous networks to generate large vascularised tissue analogues that recapitulate different architectural resolutions of native vasculature.

III. **Combining approaches for tissue vascularisation through bioassembly.**
   Aim: To use bioassembly techniques for the biofabrication of large vascularised tissues that combine the developed growth factor delivery and pre-vascularisation platforms.

The theoretical and experimental research to achieve these goals has been organised in the following chapters:

Chapter 2. Literature review: Strategies to Promote Tissue Vascularisation in Tissue Engineering and Regenerative Medicine.

This chapter provides a thorough review of the present strategies and challenges in GF delivery and in the generation of *in vitro* vascularised tissue analogues.

Chapter 3. Visible Light Mediated PVA-Tyramine Hydrogels for Covalent Incorporation and Controlled Release of Functional Growth Factors.

This chapter describes the study of tyraminated poly-vinyl-alcohol (PVA-Tyr) hydrogels as a growth factor delivery vehicle. It focuses on demonstrating that the system can covalently incorporate tyrosine-containing growth factors without prior chemical modification, and release them in a controlled manner without altering their bioactivity. The research in this chapter is part of Aim I.

Chapter 4. Adaptation of the PVA-Tyr Growth Factor Delivery System for the Treatment of Perthes Disease.

This chapter describes the adaptation of PVA-Tyr hydrogels to promote angiogenesis in cases of avascular necrosis by releasing VEGF. The functionality of the system is improved by covalently incorporating gelatin, which allows the attachment of endothelial cells to the material. It is also confirmed that the addition of gelatin does not alter the degradation properties or release profile of GFs from PVA-Tyr hydrogels. A method for the injection of the delivery system is developed and the system is tested in an *in vivo* model of avascular necrosis. The research in this chapter is part of Aim I.

Chapter 5. Fabrication of multi-scale vascularised tissues with controllable 3D architecture using Gel-NOR.

In this chapter, the combination of a top-down and a bottom-up approach for the biofabrication of vascularised constructs with different levels of vascularisation is reported. To do that, Gelatin is functionalised with norbornene groups to finely control its mechanical properties using photo-crosslinking. Hydrogels with low stiffness that promote the assembly of endothelial cells and support cells into interconnected micro-capillary networks are fabricated. This formulation is then used to 3D fabricate large constructs with a controlled channel network, which allows studying the effects of fabrication parameters on endothelialisation of the channels and endothelial cell network formation. The research in this chapter is part of Aim II.

Chapter 6. Bioassembly of Gel-NOR and PVA-Tyr for Combinatory Approaches in Tissue Vascularisation.

In this chapter, both PVA-Tyr and Gel-NOR microspheres are fabricated to enable their bioassembly into larger scaffolds. The effects of the fabrication method on the ability of Gel-NOR encapsulated endothelial cells to form interconnected networks is evaluated. The growth factor release profile and degradation time of PVA-Tyr microspheres is also studied. Pilot experiments are executed to demonstrate the capabilities of bioassembly to generate *in vitro* models and to combine strategies for tissue vascularisation. The research in this chapter is part of Aim III.

Finally, the conclusions and suggestions for future directions are developed in **Chapter 7**.

1.7. Publications Arising from this Thesis

1. **Atienza-Roca P.**, Cui X., Hooper G.J., Woodfield T.B.F., Lim K.S. (2018) Growth Factor Delivery Systems for Tissue Engineering and Regenerative Medicine. In: Chun H., Park C., Kwon I., Khang G. (eds) Cutting-Edge Enabling Technologies for Regenerative Medicine. Advances in Experimental Medicine and Biology, vol 1078. Springer, Singapore

   Contribution: Pau Atienza wrote the manuscript. Co-authors assisted with literature search and editing for the final draft.
2. **Atienza-Roca P.**, Kieser D., Cui X., Ramaswamy Y., Hooper G., Clarkson A., Martens P., Wise L., Woodfield T. B. F., Lim K. S. Visible Light Mediated PVA-Tyramine Hydrogels for Covalent Incorporation and Controlled Release of Functional Growth Factors (2020). ***Biomater. Sci.***, 2020,8, 5005-5019. This article was selected for the HOT articles section of Biomaterials Science in August 2020.

   Contribution: Pau Atienza performed all the experimental work and wrote the manuscript. Co-authors assisted with experimental planning, scientific discussion and editing for final draft.
3. **Atienza-Roca P.**, Soliman B. G., Woodfield T. B. F., Lim K. S. Biofabrication of Multi-Scale Vascularised Tissues with Controllable 3D Architecture (2020) (In preparation).

Contribution: Pau Atienza performed most of the experimental work and wrote the manuscript. Co-authors assisted with experimental planning, execution of some of the experiments, scientific discussion and editing for final draft.

1.8. Publications Generated during the Candidature but not Part of the Thesis

1. Lim K. S., Abinzano F., Nuñez Bernal P., Albillos-Sanchez A., **Atienza-Roca P.**, Otto I., Woodfield T. B. F., Malda J., Levato R. One-step crosslinking of a dual-functionalized bioink as cell carrier and cartilage-binding glue for chondral regeneration (2020) (Submitted to Advanced Healthcare Materials).
   Contribution: Pau Atienza assisted with execution of some of the experiments and editing for final draft.

2. Alcala-Orozco C., Mutreja I., **Atienza-Roca P.**, Cui X., Hooper G., Lim K. S. Woodfield T. B. F. Hybrid biofabrication of bone regenerative constructs comprising nanocomposite support scaffolds and multi-functional bioinks with enhanced osteogenic tissue formation and growth factor localisation" (2020). (In preparation)
   Contribution: Pau Atienza assisted with the execution of some of the experiments.

1.9. Conference Presentations During the Candidature

1. **Atienza Roca, P.**, Soliman, B., Anten, J., Brown, G., Woodfield, T., & Lim, K. (2017, September). Photo-click gelatin-norbonene hydrogels for biofabrication of vascularized tissue. Verbal presentation at the Future Investigators of Regenerative Medicine (FIRM) Symposium, Girona, Spain.
2. **Atienza Roca, P.**, Anten, J., Brown, G., Woodfield, T., & Lim, K. (2017, April). Photo-click gelatin-norbornene hydrogels for tissue vascularisation. Verbal presentation at the Australasian Society for Biomaterials and Tissue Engineering (ASBTE) 25th Annual Conference and the 7th Indo-Australian Conference on Biomaterials, Implants, Tissue Engineering and Regenerative Medicine (BiTERM), Canberra, Australia.
3. **Atienza Roca, P.**, Soliman B. G., Anten, J., Brown, G., Woodfield, T., & Lim, K. (2018, April). *Development of a Visible Light Photo-Click Hydrogel System for Biofabrication of Vascularised Tissue*. Poster presentation at the Centre for Bioengineering and Nanomedicine 2018 Showcase, Dunedin, New Zealand. **Awarded the best poster presentation prize.**
4. **Atienza Roca, P.**, Soliman B. G., Anten, J., Brown, G., Woodfield, T., & Lim, K. (2018, April). *Development of a Visible Light Photo-Click Hydrogel System for Biofabrication of Vascularised Tissue*. Poster presentation at the MedTech in Christchurch 2018, Christchurch, New Zealand.
5. **Atienza-Roca P.**, Kieser D., Cui X., Ramaswamy Y., Hooper G., Clarkson A., Martens P., Wise L., Woodfield T. B. F., Lim K. S. (2019, October) Visible Light Mediated PVA-Tyramine Hydrogels for Covalent Incorporation and Controlled Release of Functional Growth Factors. Poster presentation at the Centre for Bioengineering and Nanomedicine 2019 Showcase, Dunedin, New Zealand.

1.10. References

1. Hulet C, Sonnery-Cottet B, Stevenson C, Samuelsson K, Laver L, Zdanowicz U, et al. The use of allograft tendons in primary ACL reconstruction. Knee Surgery, Sport Traumatol Arthrosc [Internet]. 2019;27(6):1754–70. Available from: https://doi.org/10.1007/s00167-019-05440-3

2. Cozzi E, Colpo A, De Silvestro G. The mechanisms of rejection in solid organ transplantation. Transfus Apher Sci [Internet]. 2017;56(4):498–505. Available from: http://www.sciencedirect.com/science/article/pii/S1473050217301337

3. Irwin L, Kotton CN, Elias N, Palafox J, Basler D, Shao SH, et al. Utilization of increased risk for transmission of infectious disease donor organs in solid organ transplantation: Retrospective analysis of disease transmission and safety. Transpl Infect Dis [Internet]. 2017 Dec 1;19(6):e12791. Available from: https://doi.org/10.1111/tid.12791

4. Lanza Langer, R. S., Vacanti, J. RP. Principles of Tissue Engineering. Amsterdam, The Netherlands: Elsevier Academic Press; 2007.

5. Barrientos S, Stojadinovic O, Golinko MS, Brem H, Tomic-Canic M. PERSPECTIVE ARTICLE: Growth factors and cytokines in wound healing. Wound Repair Regen [Internet]. 2008 Sep 1;16(5):585–601. Available from: https://doi.org/10.1111/j.1524-475X.2008.00410.x

6. Saran U, Gemini Piperni S, Chatterjee S. Role of angiogenesis in bone repair. Arch Biochem Biophys [Internet]. 2014;561:109–17. Available from: http://www.sciencedirect.com/science/article/pii/S0003986114002495

7. Hankenson KD, Dishowitz M, Gray C, Schenker M. Angiogenesis in Bone Regeneration. Injury [Internet]. 2011;42(6):556–61. Available from: http://www.ncbi.nlm.nih.gov/pmc/articles/PMC3105195/

8. Kant RJ, Coulombe KLK. Integrated approaches to spatiotemporally directing angiogenesis in host and engineered tissues. Acta Biomater [Internet]. 2018;69:42–62. Available from: https://doi.org/10.1016/j.actbio.2018.01.017

9. Song H-HG, Rumma RT, Ozaki CK, Edelman ER, Chen CS. Vascular Tissue Engineering: Progress, Challenges, and Clinical Promise. Cell Stem Cell [Internet].

2018 Mar 1;22(3):340–54. Available from: https://www.ncbi.nlm.nih.gov/pubmed/29499152

10. Yuchun L, Y CJK, Swee-Hin T. Review of vascularised bone tissue-engineering strategies with a focus on co-culture systems. J Tissue Eng Regen Med [Internet]. 2015;9(2):85–105. Available from: https://onlinelibrary.wiley.com/doi/abs/10.1002/term.1617

11. Kolte D, McClung JA, Aronow WS. Vasculogenesis and Angiogenesis [Internet]. Translational Research in Coronary Artery Disease: Pathophysiology to Treatment. Elsevier Inc.; 2016. 49–65 p. Available from: http://dx.doi.org/10.1016/B978-0-12-802385-3.00006-1

12. Risau W, Flamme I. Vasculogenesis. Annu Rev Cell Dev Biol. 1995;11:73–91.

13. Matsumoto K, Ema M. Roles of VEGF-A signalling in development, regeneration, and tumours. J Biochem [Internet]. 2014 May 16;156(1):1–10. Available from: https://doi.org/10.1093/jb/mvu031

14. Poole TJ, Finkelstein EB, Cox CM. The role of FGF and VEGF in angioblast induction and migration during vascular development. Dev Dyn [Internet]. 2001 Jan 1;220(1):1–17. Available from: https://doi.org/10.1002/1097-0177(2000)9999:9999%3C::AID-DVDY1087%3E3.0.CO

15. van Obberghen-Schilling E, Tucker RP, Saupe F, Gasser I, Cseh B, Orend G. Fibronectin and tenascin-C: Accomplices in vascular morphogenesis during development and tumor growth. Int J Dev Biol. 2011;55(4–5):511–25.

16. Asahara T, Murohara T, Sullivan A, Silver M, Zee R, Li T, et al. Asahara T, Murohara T, Sullivan A, Silver M, van der Zee R, Li T, Witzenbichler B, Schatteman G, Isner JMIsolation of putative progenitor endothelial cells for angiogenesis. Science 275:964-967. Science. 1997 Mar 1;275:964–7.

17. Asahara T, Masuda H, Takahashi T, Kalka C, Pastore C, Silver M, et al. Bone marrow origin of endothelial progenitor cells responsible for postnatal vasculogenesis in physiological and pathological neovascularization. Circ Res. 1999;85(3):221–8.

18. Shi Q, Rafii S, Wu MH, Wijelath ES, Yu C, Ishida A. Evidence for circulating bone marrow-derived endothelial cells. Blood. 1998;92:362–7.

19. Korn C, Augustin HG. Mechanisms of Vessel Pruning and Regression. Dev Cell [Internet]. 2015;34(1):5–17. Available from: http://www.sciencedirect.com/science/article/pii/S1534580715003937

20. Breier G. Angiogenesis in Embryonic Development—A Review. Placenta [Internet]. 2000;21:S11–5. Available from: http://www.sciencedirect.com/science/article/pii/S0143400499905258

21. Carmeliet P. Angiogenesis in life, disease and medicine. Nature [Internet]. 2005;438(7070):932–6. Available from: https://doi.org/10.1038/nature04478

22. Burri PH, Hlushchuk R, Djonov V. Intussusceptive angiogenesis: Its emergence, its characteristics, and its significance. Dev Dyn [Internet]. 2004 Nov 1;231(3):474–88. Available from: https://doi.org/10.1002/dvdy.20184

23. Almubarak S, Nethercott H, Freeberg M, Beaudon C, Jha A, Jackson W, et al. Tissue engineering strategies for promoting vascularized bone regeneration. Bone [Internet]. 2016;83:197–209. Available from: http://www.sciencedirect.com/science/article/pii/S8756328215004123

24. Shi Y, SHI HUI, NOMI A, Lei-lei Z, ZHANG BIN, QIAN HUI. Mesenchymal stem cell–derived extracellular vesicles: a new impetus of promoting angiogenesis in tissue regeneration. Cytotherapy [Internet]. 2019;21(5):497–508. Available from: http://www.sciencedirect.com/science/article/pii/S1465324918307047

25. Xu H-L, Yu W-Z, Lu C-T, Li X-K, Zhao Y-Z. Delivery of growth factor-based therapeutics in vascular diseases: Challenges and strategies. Biotechnol J [Internet]. 2017 May 1;12(5):1600243. Available from: https://doi.org/10.1002/biot.201600243

26. Yu H, Lu K, Zhu J, Wang J. Stem cell therapy for ischemic heart diseases. Br Med Bull [Internet]. 2017 Feb 6;121(1):135–54. Available from: https://doi.org/10.1093/bmb/ldw059

27. Saberianpour S, Heidarzadeh M, Geranmayeh MH, Hosseinkhani H, Rahbarghazi R, Nouri M. Tissue engineering strategies for the induction of angiogenesis using biomaterials. J Biol Eng. 2018;12(1):36.

28. Blatchley MR, Gerecht S. Acellular implantable and injectable hydrogels for vascular regeneration. Biomed Mater. 2015;10(3):34001.

29. Barabaschi GDG, Manoharan V, Li Q, Bertassoni LE. Engineering Pre-vascularized Scaffolds for Bone Regeneration BT - Engineering Mineralized and Load Bearing Tissues. In: Bertassoni LE, Coelho PG, editors. Cham: Springer International Publishing; 2015. p. 79–94.

30. Davis GE, Speichinger KR, Norden PR, Kim DJ, Bowers SLK. Endothelial Cell Polarization During Lumen Formation, Tubulogenesis, and Vessel Maturation in 3D Extracellular Matrices BT - Cell Polarity 1: Biological Role and Basic Mechanisms. In: Ebnet K, editor. Cham: Springer International Publishing; 2015. p. 205–20. Available from: https://doi.org/10.1007/978-3-319-14463-4_9

31. Wimmer RA, Leopoldi A, Aichinger M, Wick N, Hantusch B, Novatchkova M, et al. Human blood vessel organoids as a model of diabetic vasculopathy. Nature [Internet]. 2019;565(7740):505–10. Available from: http://dx.doi.org/10.1038/s41586-018-0858-8

32. Lesman A, Koffler J, Atlas R, Blinder YJ, Kam Z, Levenberg S. Engineering vessel-like networks within multicellular fibrin-based constructs. Biomaterials [Internet]. 2011;32(31):7856–69. Available from: http://www.sciencedirect.com/science/article/pii/S0142961211007745

33. Ben-Shaul S, Landau S, Merdler U, Levenberg S. Mature vessel networks in engineered tissue promote graft–host anastomosis and prevent graft thrombosis. Proc Natl Acad Sci [Internet]. 2019 Feb 19;116(8):2955 LP – 2960. Available from: http://www.pnas.org/content/116/8/2955.abstract

34. Hai-yang Z, Jiang W, Jing-jing Z, Ze-cong X, Chao-chao H, Hong-xue S, et al. Research Advances in Tissue Engineering Materials for Sustained Release of Growth Factors. Biomed Res Int. 2015;2015(Article ID 808202):1–7.

35. Miller JS, Stevens KR, Yang MT, Baker BM, Nguyen D-HT, Cohen DM, et al. Rapid casting of patterned vascular networks for perfusable engineered three-dimensional tissues. Nat Mater [Internet]. 2012;11(9):768–74. Available from: https://doi.org/10.1038/nmat3357

36. Bertassoni LE, Cecconi M, Manoharan V, Nikkhah M, Hjortnaes J, Cristino AL, et al. Hydrogel bioprinted microchannel networks for vascularization of tissue engineering constructs. Lab Chip [Internet]. 2014;14(13):2202–11. Available from:

http://dx.doi.org/10.1039/C4LC00030G

37. Abaci HE, Guo Z, Coffman A, Gillette B, Lee W, Sia SK, et al. Human Skin Constructs with Spatially Controlled Vasculature Using Primary and iPSC-Derived Endothelial Cells. Adv Healthc Mater [Internet]. 2016 Jul 1;5(14):1800–7. Available from: https://doi.org/10.1002/adhm.201500936

38. Heintz KA, Bregenzer ME, Mantle JL, Lee KH, West JL, Slater JH. Fabrication of 3D Biomimetic Microfluidic Networks in Hydrogels. Adv Healthc Mater [Internet]. 2016 Sep 1;5(17):2153–60. Available from: https://doi.org/10.1002/adhm.201600351

39. Kim S, Lee H, Chung M, Jeon NL. Engineering of functional, perfusable 3D microvascular networks on a chip. Lab Chip [Internet]. 2013;13(8):1489–500. Available from: http://dx.doi.org/10.1039/C3LC41320A

Chapter 2. Strategies to Promote Tissue Vascularisation in Tissue Engineering and Regenerative Medicine

2.1. Growth Factor Delivery

2.1.1. Introduction to Growth Factor Delivery

Growth factors (GFs) are defined as secreted, biologically active molecules that can affect the growth and differentiation of cells. They play critical roles in developmental and regenerative processes, and therefore have been a main focus in tissue engineering and regenerative medicine (TERM) strategies. Levi-Montalcini and Cohen firstly discovered GFs by studying the effect of sarcomas on axonal growth from chicken embryos (1). They identified the signalling molecule that triggered the growth of neuronal networks and termed it nerve growth factor (NGF) (2). Since then, several GFs that modulate many physiological processes have been discovered and applied to regenerative medicine (3). Some examples include bone morphogenetic proteins (BMP-2 and BMP-7) for bone regeneration (4) and vascular endothelial growth factor (VEGF) (5) or platelet-derived growth factor (PDGF) (6) for diabetic foot ulcers.

GFs act on cells by binding transmembrane receptors in a highly specific manner, which triggers a transduction cascade that generally starts with phosphorylation of the cytosolic domain of the receptor. Each GF is unique with specific roles in cellular behaviour (Table 2.1). For example, BMP-2 is essential for the maintenance of bone density (7). It has been reported that adult mice lacking BMP-2 showed spontaneous fractures and impaired bone repair (8). Due to these characteristics, BMP-2 has been used in clinical settings for spinal fusion procedures and for non-union fractures (9). A list of these GFs with their respective unique characteristics can be found in Table 2.1.

Table 2.1. Usage of growth factors in TERM applications.

Growth Factor	Main Receptors	Signal Transduction Pathways	Role in Adult Tissues	Application in Regenerative Medicine
BDNF (14–16)	TrkB LNGFR	Ras-MAPK PI3K PLC-γ1	Sensory Neuron Function Cortical Circuitry Function Synaptic Strength and Plasticity	Spinal Cord Injury Stroke
BMP2 and BMP7 (7,9)	BMPR-1A BMPR-1B BMP2-R ActR-1A ActR-2A/ 2B	Smad1/5/8 Ras-MAPK PI3K	Bone homeostasis and function. BMP-2: Indispensable for bone fracture healing, chondrocyte proliferation and maturation. BMP7: Kidney function	Spinal fusion Non-union fractures
EGF (16–18)	EGF-R	Ras-MAPK PI3K	Injury response, homeostasis and growth in mammary gland, GI tract, nervous system. Inhibits osteogenic and chondrogenic maturation.	Diabetic foot ulcers Stroke
FGF1 (12,19–22)	FGFR1-4	Ras-MAPK PI3K, STAT, PLC-γ	Maintenance of vascular tone, Adipogenesis.	Peripheral ischaemia Peripheral nerve lesions
FGF2 (bFGF) (16,19,20,22–27)	FGFR1-4	Ras-MAPK PI3K STAT PLC-γ	Heart homeostasis and repair, Vascular tone, Angiogenesis, Cartilage homeostasis	Skin wounds Bone lesions Myocardial infarction Stroke Ligament regeneration Tracheal defect repair
FGF7 (KGF) (19,20,22)	FGFR1-4	MAPK, PI3K, STAT, PLC-γ	Skin repair	Oral mucosa regeneration Skin wounds

Table 2.1. Usage of growth factors in TERM applications (Continued).

Growth Factor	Main Receptors	Signal Transduction Pathways	Role in Adult Tissues	Application in Regenerative Medicine
HGF (28–31)	c-Met	Gab-1 PLC-γ Ras-MAPK PI3K	Homeostasis and regeneration of Liver, Lung, Stomach, Pancreas, Heart, Brain and Kidney	Cirrhosis Liver regeneration Critical limb ischemia Chronic vocal cord lesions
NGF (14,32)	TrkA LNGFR	Ras-MAPK, PI3K, PLC-γ1	Sensory Neuron Function Cortical Circuitry Function	Peripheral nerve lesions
PDGF (33–37)	PDGFRα PDGFFRβ	PI3K, PLC-γ, Ras-MAPK	Postnatal angiogenesis and vascularization. Smooth muscle cell and fibroblast homeostasis.	Periodontal defects Skin wounds Bone regeneration Tissue vascularisation
SDF1-α (38–41)	CXCR4 CXCR7	Ras-MAPK, PI3K, JAK-STAT	Angiogenesis, Mesenchymal stem cell homing during tissue repair, Heart Homeostasis	Revascularisation Wound healing Tendon regeneration Muscle fibrosis
TGF-β(1-3) (42–45)	TβR-II TβR-I	Smad 2/3	Wound healing and skin homeostasis, Bone healing, Heart regeneration.	Bone regeneration Cartilage regeneration Periodontal tissue regeneration
VEGF-A (5,16,46–50)	VEGFR(1-2) Nrp (1-2)	PI3K PLC-γ MAPK	Angiogenesis. Brain, Liver, Bone and Lung homeostasis and regeneration,	Diabetic foot ulcers Bone regeneration Brain and myocardial ischemia

In the native microenvironment, GF concentrations are usually in the nanomolar to picomolar range, where their presence is continuous and can last up to several weeks or months (10). Initial clinical trials, which involved injection (11) or spraying (12) of GFs directly onto the wound site, showed limited therapeutic effects, mainly due to the short presence of the applied GFs at the wound area. To better mimic the natural spatio-temporal concentrations of GFs, continuous doses of the GF were administered, causing systemic overexposure that can result in undesirable increase risk of cancer and ectopic tissue formation (13).

These results led to the realisation of the need for a suitable GF delivery system, which has been the focus of many research groups in the past decades. This chapter will cover a list of criteria that should be followed when designing a GF delivery vehicle for a specific application, together with the different GF delivery approaches reported in the literature that aim to mimic key aspects of the regenerative microenvironment by controlling the spatio-temporal presence of GFs.

2.1.2. Design Criteria for Growth Factor Delivery Systems

When designing of a novel TERM therapy, the first aspect to consider is what GF to deliver. The selection of an adequate GF will not only depend on the type of organ or tissue that we are trying to regenerate, but also on the desired cell function. Some GFs trigger proliferation and differentiation of cells that are already present at the injury site. In other cases where the cells required for healing or regeneration are absent, chemotactic GFs are able to trigger migration of cells to the wound site (51,52). The ECM is another key factor that needs to be considered while designing any GF delivery system, since it can modulate the effects of GFs through different mechanisms. For example, heparan sulphate (53), decorin (54), betaglycan (55), versican (56), fibronectin (57), collagen (58), vitronectin (59), SPARC (60) and tenascin D (61) are ECM components that can bind GFs and modulate their diffusion and localization, further influencing their availability at the cell surface and their receptor-binding kinetics. Due to the dynamic remodelling of the ECM during regenerative processes (62,63), it is important to understand the interaction between GFs and the ECM for the design of an optimized delivery strategy. The interactions between cell receptor, ECM and GFs are represented in Figure 2.1.

In order to modulate these complex interactions, different parameters such as the localization of the GF, the concentrations released and the release pattern have been identified as relevant design criteria to be met when designing a delivery system. These aspects are further discussed in the sections below.

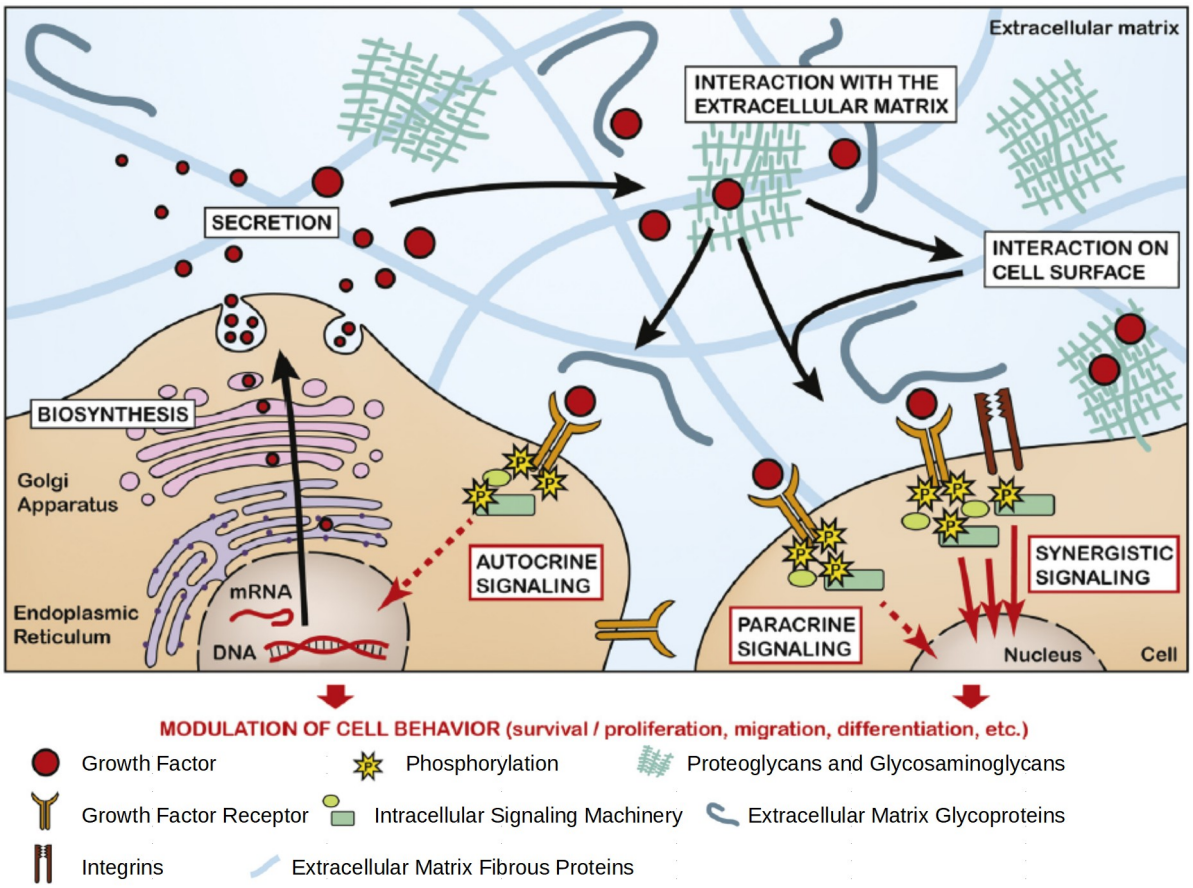

Figure 2.1. From biosynthesis to cell receptor signalling, a growth factor's journey within the physiological ECM. *After their biosynthesis, growth factors are secreted into the ECM, where they interact with ECM components before binding and activating their cognate receptors. Growth factors mainly signal to cell in autocrine and paracrine fashion, to instruct their behaviour during morphogenetic processes. Complexes formed between growth factors, ECM components, and cell surface receptors may lead to additive or synergistic cell signalling events. Reproduced from (64).*

2.1.2.1. Localization of the Delivery

GFs can have different effects in different tissues and cell types. For example, EGF promotes homeostasis in the GI tract (65) and mammary gland (66) but inhibits tissue maturation in the cartilage (67). In order to achieve only the desired therapeutic outcome, the GF has to be delivered and contained spatially at the targeted tissue. Moreover, unnecessary presence of GFs in non-targeted tissues might also trigger cancer development and progression due to excessive cell proliferation (13,68,69). In order to avoid these effects, different delivery systems that enable spatial containment of delivered GFs such as nanoparticles or scaffolds have been studied, which are further discussed in following sections.

2.1.2.2. Delivered Concentration

A major challenge in designing GF delivery approaches is optimising the concentration required for the desired therapeutic effect. A recent meta-analysis on the use of FGF-2 and PDGF-BB for periodontal defects reported thresholds of GF concentration below which the treatment failed to promote bone regeneration (70). These thresholds changed depending on the type of defect that was treated. The same study showed that excessive concentrations of FGF-2 resulted in insignificant promotion of bone growth. Furthermore, excessive concentrations of BMP-2 have been reported to promote apoptosis in osteoblasts, mesenchymal stem cells (MSCs) (71) and periosteal cells (72). Similarly, excessive VEGF concentrations promote the formation of aberrant and hyper-permeable blood vessels (73). Therefore, the optimal concentration of GFs to be delivered onsite has to be evaluated each TERM application.

The culmination of spatio-temporal control over GFs is the formation of concentration gradients that mimic regenerative and developmental processes. GFs are generally secreted from a focal spot, which can be a cluster of cells with a specific phenotype or the defined space of a regenerative process. Cells at different distances from the spot are exposed to different concentrations of the secreted GF, and specific concentration thresholds strictly define spatial differentiation patterns in many stages of embryonic development (74,75). Individual cells are able to detect spatial differences in the concentration of specific molecules, which makes gradients of chemotactic GFs a directional signal for cells to migrate to the wound site (76,77) and for vascularization and innervation of tissues (14,78). The specific characteristics of these gradients are crucial for organized tissue formation. Thus, their adequate mimicry would be one of the pinnacles of controlled GF delivery.

2.1.2.3. Release Patterns

The time period during which the GF is present on site is an essential parameter to achieve optimal therapeutic effects. The ordered presence and absence of specific factors corresponds to different stages of regeneration in natural processes (79,80). During bone regeneration, GFs that promote recruitment of MSCs and vascularization, such as stromal derived factor 1 (SDF-1) and VEGF are firstly expressed. This stage is followed by the generation of a cartilaginous callus in which other GFs such as TGF-β3 are highly expressed, and the process ends after a prolonged mineralisation and resorption phase in which expressions of TNF-α, IL-1 and BMP-2 are elevated (80,81). In an attempt to match these GF expression patterns,

delaying the administration of rhBMP-2-loaded calcium phosphate matrices for one week instead of 3 hours post-surgery resulted in accelerated healing in a primate fibular osteotomy model (82). It has also been reported that delaying the administration of an adenoviral BMP-2 vector by 5 to 10 days after surgery increases bone mineralisation in a rat critical-size defect model (83). It is also to be noted that the therapeutic effect of GFs is time-dependant. A 4 weeks sustained delivery of BMP-2 improves ectopic bone formation in comparison to just 5 days delivery (84), which agrees with the fact that the BMP-2 plays a major role in the long-term remodelling phase of bone regeneration (81). These results indicate that matching specific GF expression patterns can result in improved tissue regeneration and should be taken into account in designing GF delivery systems.

2.1.3. Use of Biomaterials for Growth Factor Delivery

The main limitations of delivered GFs are their low biochemical stability, short circulating half-life and rapid rate of cellular internalization. Combining GFs with a biomaterial is an effective approach to overcome these drawbacks. However, no single material or strategy has yet allowed the required spatio-temporal control over the delivered GFs for optimal therapeutic effect. In recent years, the convergence of different materials, chemistries and fabrication techniques has brought the field one step closer to its goal by enabling more complex release patterns, including coordinated release of different GFs. This section will provide an overview of all these strategies, focusing on the advanced materials and procedures that enable control over the outlined design criteria.

2.1.3.1. Incorporation Methods

GFs can be incorporated into biomaterials through different strategies. The simplest procedure involves directly submerging a material in a GF solution to facilitate the adsorption of the GF to the material (85). For example, GFs have been adsorbed on FDA approved polymers such as poly(lactic-co-glycolic) acid (PLGA) microspheres (86) and poly(caprolactone) (PCL) scaffolds (87). Changes in material surface roughness (88) or the addition of nanostructured features (89) can increase the overall surface area, resulting in increased GF adsorption. Another prominent strategy that involves mixing the material with the GF in a liquid phase prior to scaffold fabrication allows the fabrication of scaffolds entrapped with GFs. Common scaffold fabrication techniques include freeze drying, phase separation, molding or *in situ* polymerization (90). An important limitation of these strategies

is the requirement to protect the GFs from harsh conditions during scaffold fabrication in order to maintain their bioactivity. For example, melt molding can expose GFs to high temperatures, whereas radical based polymerization systems can facilitate GF oxidation/denaturation (91).

2.1.3.2. Interaction between Growth Factor and Biomaterial

The interaction between GF and biomaterial plays a key role in all incorporation methods, affecting not only the release profile (85,92), but also the biological effects of the GF (92). The different types of material-GF interaction are summarized in Figure 2.2.

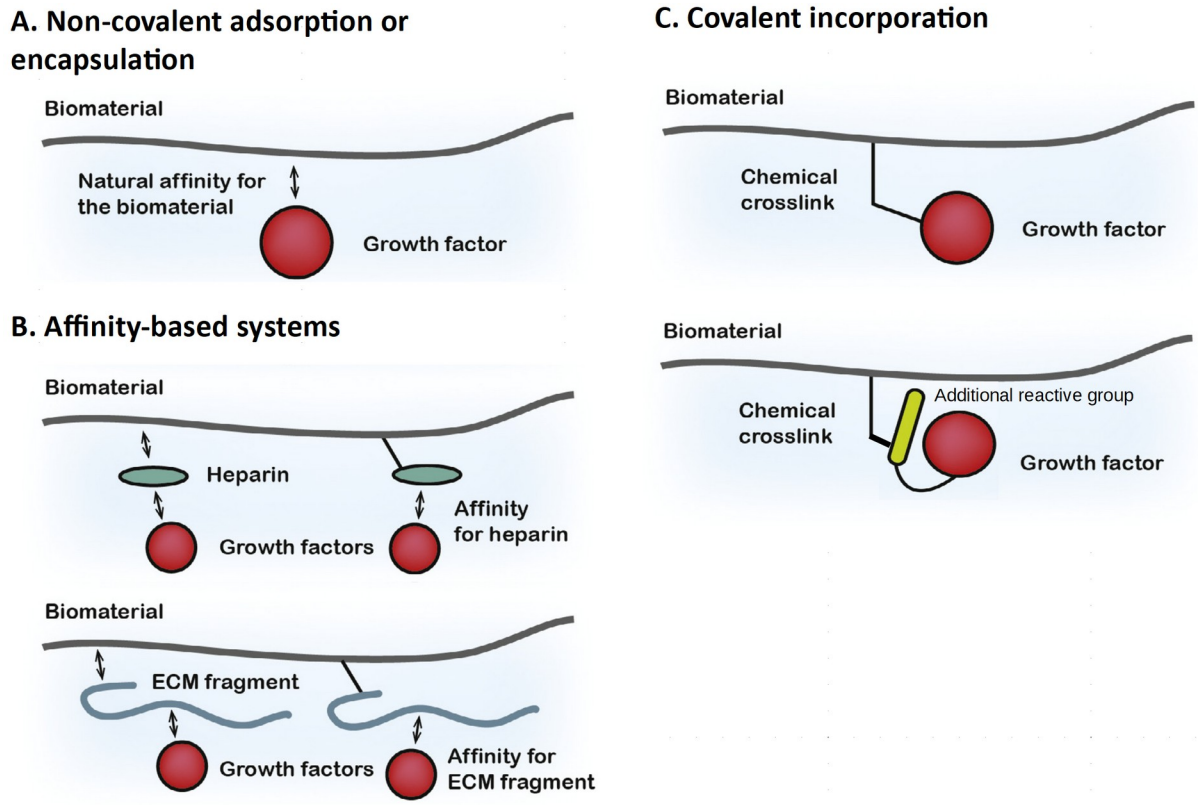

Figure 2.2. Types of material-growth factor interaction. *(A) Non-covalent interactions based on surface properties. (B) Affinity-based systems rely on natural interactions between growth factors and the extracellular matrix. (C) Covalent incorporation methods bind the growth to the material directly or through added functional groups or amino acids. Adapted and modified from (64).*

Non-covalent interactions are weaker and can be mainly hydrogen bonds (93), Van der Waals forces, ionic forces or hydrophobic interaction (94). Modifying the surface charges, charge density (95,96) or available functional groups (97) of the material result in different GF binding affinities and release profiles. For example, increasing the surface hydrophobicity and decreasing the isoelectric point (pI) of PLGA microspheres resulted in an increase in the

amount of rhBMP-2 adsorbed, whereas changes in PLGA molecular weight did not significantly change BMP-2 adsorption (98). Functionalizing the material surface or the polymer chains with amino (89), alkyl (89,99) or oxygen-terminated groups (100) can increase the adsorption of rhBMP-2 and result in a longer release time. The interaction with the functional groups will also depend on the pI of the GF, and thus each GF will have specific release profiles when incorporated in the same material based on this approach (101).

A special case in non-covalent interactions is the use of GF-binding domains from ECM molecules. These strategies are generally classified as affinity-based, as the affinity of certain GFs for these domains is significantly higher and more specific than for single chemical groups or surface charges (102). An example of these affinity-based domains are heparin or heparan sulphate, which have been extensively used for the delivery of specific GFs such as NGF or BMP-2 (103,104). Fibronectin (105) and fibrinogen (106) GF-binding domains, which bind to several GFs from the PDGF, VEGF and FGF families and some from the TGF-β family, have also been used to functionalize scaffolds. The use of affinity-based systems has been extensively studied and reported in the literature (107), and the resulting release profile, which is significantly more sustained than for other non-covalent incorporation methods, positioned them as one of the most successful GF incorporation approaches to date. However, the strategies are limited to the release of GFs that display natural affinity for these domains, and the release profile differs between different GFs due to their distinct affinities with the system. In order to further improve the therapeutic effects, some studies have engineered GF containing ECM binding domains. Genetically engineered IGF-1 including the heparin-binding (HB) domain of HB-EGF was able to interact with specific GAGs in cartilage matrix after injection to the knee (108). Through similar techniques, collagen-binding domains were added to NGF (109) or BDNF (15), promoting their interaction with collagen scaffolds (110) and the retention of the GF at the wound site.

The release profile for delivery systems that use non-covalent incorporation is generally characterized by an initial burst release (111). The observed burst release profile has been suggested to have a role in early post-implantation complications (112,113). In order to reduce or eliminate the burst release, protein immobilization to the matrix through covalent incorporation has been extensively studied (92). It has been reported that the release of GFs conjugated to the biomaterial is then dependent on the materials' degradation profile. Moreover, it is possible to have further precise control over the GF release profile by adding features such as protease-cleavable sequences to the material (114) or to the material-GF

linkage (115). Aside from improved control over the GF release profile, presentation of covalently bound GFs to cells can result in a differentiated response in comparison to soluble GFs by inhibiting the internalization of the GF-receptor complex (116). Covalent incorporation can also be used for patterning GF (117), including the formation of gradients in a material. Several GFs have been covalently incorporated in biomaterials for different applications, leading to improved functions such as endothelial cell proliferation (118), osteoblast adhesion to titanium implants (119) and even bone formation *in vivo* (120). Common reactions for GF immobilization include carbodiimide coupling (121), photo-polymerization methods such as phenyl azide-based (120) or acrylate-based (117), and also click chemistry (122,123). One of the main limitations of these approaches is poor control over the exact reaction site of the GF, which can lead to disruption of the receptor-binding domain (92). In order to improve the therapeutic effects of covalently incorporated GFs, some studies have engineered growth factors containing functional groups (124) or amino acids (125) at specific sites that do not overlap with the receptor-binding domain.

2.1.3.3. Delivery Vehicles for GF Administration

The biomaterials used for GF delivery can be fabricated into different types of vehicles, such as particles or scaffolds. Each delivery vehicle poses favourable characteristics and is adaptable to specific therapeutic strategies or administration procedures. A list of different GF delivery vehicles is tabulated in Table 2.2 below.

2.1.3.3.1. Particle Systems

Particle systems, which can be in the range of <1 μm for nanoparticles or <1000 μm for microparticles, have been used to deliver GF for TERM applications (184). The particle size affects the rate of GF release due to different surface-to-volume ratios and intracellular uptake (185).

2.1.3.3.1.1. Nanoparticles

Nanoparticles (NPs) can infiltrate deeper into tissue via capillaries and epithelial lining due to their small sizes, improving the transport properties and pharmacokinetic prolife of drugs *in vivo*. They are generally highly soluble and display low immunogenicity (186). Targeted delivery of GFs to specific tissues can be achieved using surface functionalized NPs or using electromagnetic fields (143). Surface functionalization can also enable NPs to cross the

blood-brain barrier (BBB), which is not possible for other delivery systems without invasive procedures (187). NPs can be classified into polymeric, lipidic and inorganic depending on their composition.

Polymeric NPs can be fabricated as nanospheres, nanocapsules, micelles and dendrimers, all of which have been studied for GF delivery. PLGA is the most studied material to form nanospheres and nanocapsules, and it has been used for IGF-I (127), VEGF (126) and BMP-2 release (128). Functionalization of PLGA nanoparticles with different concentrations of heparin has also been used to form an affinity-based system, where increasing the heparin concentration resulted in longer term release (126). Using this method, it is possible to achieve long-term release: a heparin-conjugated Tetronic®-PCL micellar system was used for bFGF delivery, showing long-term delivery up to 2 months (133,134). This type of particles have also been combined with other techniques to promote their penetration into tissues: Low frequency ultrasound was combined with bFGF-loaded PLGA NPs to increase microvessel permeability for targeted skeletal muscle angiogenic therapy (188). Apolipoprotein E (ApoE) was adsorbed to poly(butylcyanoacrylate) (PBCA) NPs in order to cross the BBB through an ApoE receptor-mediated response. NGF was adsorbed to the PBCA NP surface and then delivered to rats by intraperitoneal injection. Symptoms of scopolamine-induced amnesia were reduced after the administration, indicating targeted delivery to the brain (131).

Table 2.2. GF delivery vehicles fabricated using biomaterials

Delivery vehicle/Fabrication method	Biomaterials	GFs
Particles	PLGA	IGF-1,VEGF, BMP-2 (126–128)
	PCL-PEG-PCL	bFGF (129,130)
	PBCA	NGF (131)
	PEG-PLGA	bFGF (132)
	Tetronic®-PCL (Heparin)	bFGF (133,134)
	PAMAM	EGF,VEGF (135,136)
	Liposomes with magnetite particles	BMP-2, TGF-β-1 (137,138)
	DSPE-PEG-NHS	NGF (139)
	Pluronic® F127 with nanolipid	VEGF (140)
	SLN	NGF (141)
	Poloxamer 188/HSPC/cholesterol	bFGF (142)
	MSN	BMP-2,FGF (143)
	Magnetic oxide nanoparticles	bFGF (144)
	SPION	EGF, BDNF (145,146)
	QD	BDNF,NGF (147,148)
Scaffolds	Collagen	BMP-2, BMP-7 (3)
	PLA	BDNF (149)
	PLGA	FGF, BMP-2 (150,151)
	Chitosan-glycerophosphate	BMP-2, Insulin (152,153)
	Fibrin	FGF-2, VEGF-A (154)
	PEGDA-Heparin	bFGF, TGF-β, KGF, Ang1, PDGF (155,156)
	PEG	FGF-2, PlGF-2 (106)
	GelMA	BMP-2 (157,158)
	PEG-PLLA-PEG	TGF-β1 (159)
	B-TCP	PDGF, GDF-5, BMP-2, hGH (160–163)
	Bioglass	VEGF, BMP-2 (164,165)
	CPC	BMP-7,VEGF (166)
	Titanium	TGF-β1, BMP-2, VEGF (167–169)
Particles incorporated in another material	OPF	TGF-β1 (170)
	PLGA, Gelatin, PPF	BMP-2 (171)
	PLGA, PEG	CNTF, NT-2 (172)
	Gelatin, OPF	TGF-β1, IGF-1 (173,174)
	PLA, alginate	BMP-2, VEGF (175)
	PLA, chitosan	IGF-1, BMP-2 (176)
	PHBV, chitosan	BMP-2,BMP-7 (177)
Core-shell	Gelatin, PPF	BMP-2, VEGF (178)
	PLLA,PLGA	BMP2-,FGF (179)
Layer by layer	Gelatin	BMP-2 IGF-1 (180)
	OPF	BMP-2,IGF-1 (181)

Lipid based NPs that have been used for GF delivery are mostly liposomes and solid lipid nanoparticles (SLNs) (189). The main advantages of these formulations are their inherent low toxicity and scalable production methods (190). Liposomes are vesicles formed by bilayers of hydrated phospholipids which enclose an aqueous core (191). Their empty core allows easily loading GFs and other nanoparticle systems, providing flexibility in their application. Phosphatidylcholine liposomes loaded with magnetite particles were used for bone and cartilage regeneration after loading with BMP-2 (137) or TGF-β1 (138), where the magnetite particles could be directed to the injury site using a magnetic field. Despite their flexibility, liposome nanoparticles display low GF loading capacity and low stability due to enzymatic degradation, leading to a short term release (143). Other types of lipid NPs with different conformations have been used in order to overcome these issues. For example, a lecithin anionic nanolipid core was loaded with VEGF and covered by a Pluronic F-127 shell. The system showed increased stability in comparison to liposome systems, and a sustained release of VEGF for more than 30 days. The release period was extended by increasing the lecithin/Pluronic F-127 ratio, presumably due to changes in the ionic charge that enabled stronger interactions with VEGF (140). Recently, another SLN system has been conjugated with heparin and loaded with NGF for neuronal differentiation. The release could be tuned by changing the composition of the solid core, where using stearylamine resulted in a faster release than using esterquat, and increasing the amount of cholesterol resulted in slower release (141).

Inorganic nanoparticles such as mesoporous silica NPs (MSNs), quantum dots (QDs) or metallic NPs have been also applied to GF delivery. In general terms, inorganic nanoparticles excel due to their easy handling and their physical properties. MSNs are used due to their high surface area and porosity (192). A good example of their application is the study by Zhou et al., where BMP-2 was covalently grafted to the MSNs surface through an aminosaline linker, while dexamethasone was loaded in the nanopores to form a dual delivery system. The combination resulted in synergistic induction of bone formation in an *in vivo* ectopic model (193). It has also been shown that the release kinetics can be tuned by controlling the porosity of the nanoparticles, where increased porosity leads to faster release (194), or by coating them with PEG, resulting in increased release time (195). Magnetite NPs have been combined with other types of NPs, including MSNs (196) and liposomes (137,138), to provide them with magnetic properties that enable guided targeting using an external magnetic field. Other magnetic NPs can also be directly incorporated with GFs, such

as superparamagnetic iron oxide nanoparticles (SPIONs), which enabled targeting specific areas of the brain using a magnetic field after adsorption of BDNF to their surface (145). The main drawbacks of metal-based nanoparticles are their poor degradability and tissue accumulation. Thus, their long-term toxicology should be further evaluated (192). QDs have fluorescent properties that can be used to track conjugated molecules. Conjugation of BDNF (148) and NGF (147) with QDs enabled tracking of the GF after internalization by neurons and PC12 cells respectively, which enabled monitoring of the receptor internalization dynamics. In the field of bone regeneration, calcium phosphate nanoparticles have also been studied due to their high biocompatibility and bioactivity (197).

Overall, NP delivery systems represent a promising approach for GF delivery. One of the most important advantages of NP systems is the possibility of intravenous administration, which positions them as the least invasive GF delivery method. Another unique feature of NP systems is the ability to cross the BBB, enabling access of GFs to the central nervous system. The specific properties of different NPs provide great advantages such as targeted delivery, enhanced MRI contrast or tracking of the NPs. Other systems such as MSNs can be used as a sequential delivery system, and complex NPs can be synthesized in order to combine the advantages of different nanostructured materials. On the other hand, aspects such as long-term toxicity and tissue accumulation of NPs should be further investigated before advancing to the clinical field.

2.1.3.3.1.2. Microparticles

The use of microparticles (MPs) generally results in a lower cellular uptake and tissue penetration in comparison to NPs due to their larger sizes (185). On the other hand, their increased volume results in higher drug loading capacity, slower release and ease of production. These characteristics enable a longer-term release, which can be extended by increasing the particle size (198). The materials used to generate MPs for GF release include naturally derived polymers such as gelatin (199), alginate (200) and chitosan (201), as well as synthetic polymers such as PLGA (202). As MPs adaptability to intravenous administration is low in comparison to NPs, most of the applications require the formation of a scaffold through microsphere fusion (203) or being incorporated in a solid scaffold (204) or an injectable hydrogel (205). Thus, section 2.3.3.3. ‘Combined approaches in growth factor delivery’ will cover more of the applications of microparticles.

2.1.3.3.2. Scaffold Systems

Biomaterial scaffolds can be incorporated with GFs and implanted into the damaged area to achieve local release (91). Scaffold systems can be classified as solid scaffolds or hydrogels depending on their composition.

Solid scaffolds are typically porous matrices fabricated by techniques such as solvent casting, gas foaming, particulate leaching, electrospinning or rapid prototyping (90). These systems can be classified as organic or inorganic.

Solid organic scaffolds are mainly polymeric, and have been extensively studied for GF delivery. Homo- and copolymers of lactide and glycolide (like PLGA or PLLA) have been widely used due to their degradation into lactide and glycolide, which can enter physiological metabolic pathways (206). The physical properties of these polymers can be altered by varying the ratio of lactide/glycolide, molecular weight or crystallinity (207), which can directly influence the release profile of GFs. For example, PLA scaffolds have been loaded with BDNF by entrapment for spinal cord injury applications (149) while PLGA has been loaded with BMP-2 for bone regeneration (151). Affinity-based systems have also been generated by conjugating heparin to the surface of PLGA scaffolds. FGF was adsorbed onto these scaffolds, resulting prolonged release and stimulation of vascularization *in vivo* (150).

Due to their mechanical properties and inherent tissue compatibility, **solid inorganic** scaffolds such as ceramic, bioglass or titanium play an important role in regenerative medicine (208). Calcium phosphate-based systems excel due to their compositional similarities to the native bone ECM, and they have been extensively studied for GF delivery (197). Most commonly used calcium phosphate materials include hydroxyapatite and TCP scaffolds with different porosities, which have been used for BMP-2 delivery resulting in positive effects (160–162). The incorporation of GFs within TCP to treat bone defects has resulted in different commercially available products. Therapeutic goods administration (TGA, Australia) and Health Canada have approved the safety of utilization of tricalcium phosphate (TCP) as scaffold to deliver PDGF (Augment™ Bone Graft; Biomimetyics, Franklin, TN). Different clinical trials have concluded that PDGF-BB (209–213) and FGF-2 (214) loaded in β-TCP resulted in improved bone regeneration in periodontal osseous defects (70). Clinical trials using β-TCP as scaffold to deliver GDF-5 for sinus lift augmentation in 2010 (163) and for periodontal defects in 2012 (215) also yielded positive results. Other

calcium phosphates have also been studied for GF delivery. Mesoporous bioglass scaffolds have been fabricated to load VEGF, and the addition of pores resulted in more than 90% loading efficacy and extended release profile while retaining VEGF bioactivity (165). Sumner et al employed a titanium scaffold to deliver TGF-β1 and BMP-2 in a dog humerus model, resulting in improved integration (168). In another study, VEGF and antibacterial peptides were bound to titanium scaffolds, resulting in increased cell attachment and reduced bacterial growth (169).

Hydrogel scaffolds are one of the most successful and versatile GF delivery approaches, and the major proof of that are the commercially available products (3). A collagen hydrogel loaded with BMP-2 (INFUSE®-BMP-2; Medtronic, Minneapolis, MN) has been approved by the FDA for treatment of lumbar fusion. Another similar design using type I collagen matrix to encapsulate BMP-7 (OP-1™ Putty; Olympus Biotech Corporation, Hopkinton, MA) is also approved for fractures of long bones and lumbar fusion procedures. Furthermore, PDGF impregnated in a hydrogel (REGRANEX®, BioMimetic) has been approved for diabetic ulcer treatment. However, an increased rate of mortality secondary to malignancy was detected in patients treated with high amounts of REGRANEX® (13) and other adverse effects such as heterotopic ossification were reported in patients treated with INFUSE (270), which clearly shows the need for optimized controlled delivery systems. Hydrogel scaffolds can be classified according to the origin of their polymeric component, which can be synthetic or naturally-derived.

Synthetic hydrogels such as poly(vinyl alcohol) (PVA) and poly(ethylene glycol) (PEG) are biologically inert, but have well-controlled and reproducible physical and chemical properties and no risk of disease transmission. These characteristics are of special interest for clinical translation and mass production. A good example of their application is the study by Tong et al., where PEG has been crosslinked using thiol-ene chemistry (216). This combination enabled high control over the mesh size and the degradation time, where decreased mesh size and increased degradation time led to longer-term release for up to 60 days. **Naturally-derived hydrogels** have higher batch-to-batch variation, but they hold the potential to interact with cells and undergo cell-mediated degradation. Most widely used naturally-derived hydrogels include fibrin, collagen, gelatin, chitosan, alginate and hyaluronic acid. As an example, tyraminated hyaluronic acid crosslinked using horseradish peroxidase (HRP) has been studied as an injectable system for protein delivery, showing increased release time by

increasing the crosslinking density through changes in HRP concentration (217). Fibrin sealants have been used for controlled release of FGF-2 and VEGF-A, enhancing blood reperfusion after myocardium infarction and limb ischemia (154).

Different strategies have been designed to obtain the benefits of synthetic and natural polymers in the same scaffold. In a comprehensive study, gelatin or heparin were crosslinked to PEG diacrylate (PEGDA) and the composites were used for incorporation of bFGF, TGFβ, KGF, angiopoietin-1 (Ang1) and PDGF. In general, the heparin conjugated PEGDA had a longer GF release profile, which was different for each GFs due to differences in their interaction with heparin (155,156). In another study, the GF-binding domain of fibrin was incorporated in a PEG hydrogel. Co-delivery of FGF-2 and PlGF-2 using these gels enhanced skin wound healing (106). On the other hand, modification of naturally-derived polymers with functional groups that enable controlled crosslinking is also a generalized strategy. These modifications enable tailorability of the crosslinking density and mesh size, providing higher control over the release profile. As an example, gelatin undergoes gelation at temperatures under 35°C. This process is not adequate for applications requiring high control over the network characteristics. Thus, gelatin functionalised with methacryloyl groups (GelMA) has been used for different applications that require high control over the crosslinking density (218), including the generation of scaffolds for BMP-2 encapsulation (157,158). Increasing the degree of functionalization of GelMA results in decreased mesh sizes, increasing the release time of GFs such as BMP-2 (219).

Both hydrogels and solid scaffolds are the most successful platforms for GF delivery, as shown by the amount of commercially available products and clinical trials performed to date. The ability to spatially deliver GFs at the wound site by implantation of the scaffold, or injection followed by *in situ* crosslinking, is the most important advantage of these platforms.

2.1.3.3.3. Combined Approaches in Growth Factor Delivery

The combination of different materials and platforms allows several advantages in GF delivery applications. Firstly, it enables coordinated delivery of GFs by incorporating them in different materials or through different methods (10). Secondly, combining different materials that can be independently modified increases the tailorability of the release profile. Furthermore, these materials can have other favourable characteristics for the targeted therapeutic application, such as high stiffness for load-bearing tissues or bioactive properties.

Multiple incorporation strategies can be used in the same material in order to deliver different GFs with independent release profiles. For example, encapsulation of PDGF in PLGA microspheres, followed by surface adsorption of VEGF and generation of a scaffold by gas foaming-particulate leaching resulted in a burst release of VEGF and a prolonged PDGF release (220). In a different study, BMP-2 was covalently grafted to the surface of MSNs through an aminosaline linker while dexamethasone (DEX) was incorporated in the nanopores, obtaining short-term DEX release profile and a longer-term BMP-2 release profile (Figure 2.3A) (193).

MPs or NPs can be incorporated into a tissue engineering scaffold (Figure 2.3B) to further control the GF release profile. TGF-β1 loaded gelatin particles have been immobilized in oligo poly(ethylene glycol) fumarate (OPF) and resulted in a reduction of the burst release. The release time can be further increased by increasing the molecular weight and the crosslinking time of the OPF hydrogel (170). Encapsulation of NT-3 in PLGA MPs, and inclusion of these MPs in a ciliary-neurotrophic factor (CNTF) loaded hybrid hydrogel resulted in a rapid CNTF release and a more sustained NT-3 release. Increasing the crosslinking density of the hydrogel phase resulted in increased release time from weeks to months (172). Gelatin MPs encapsulated in OPF have been used for coordinated and tailorable delivery of TGF-β1 and IGF-1 with the aim of cartilage regeneration (173,174). Further examples include BMP-2-loaded PLA microspheres incorporated in VEGF-loaded alginate hydrogels (175) and IGF-1 encapsulated in gelatin microspheres loaded into chitosan scaffolds containing BMP-2 (176), both resulting in enhanced bone regeneration.

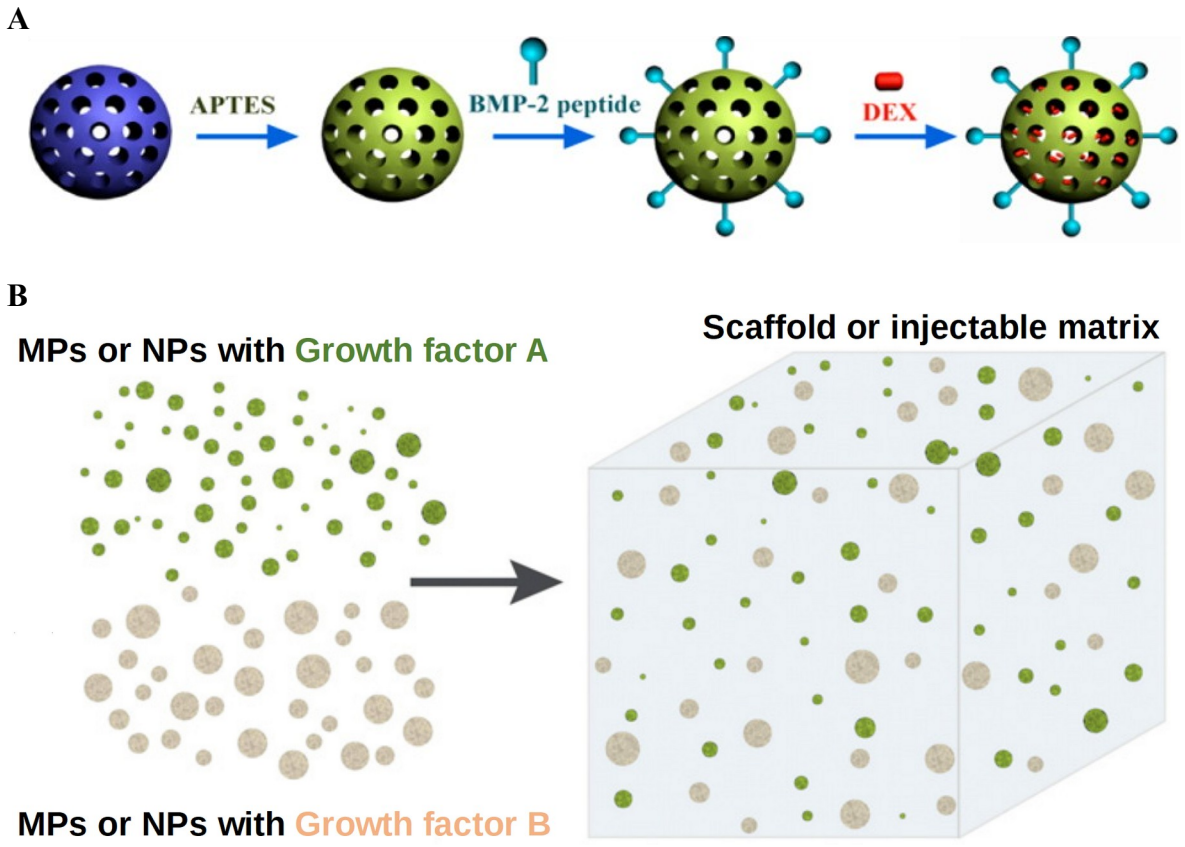

Figure 2.3. Combined approaches in growth factor delivery. *(A) Mesoporous silica nanoparticles incorporated with two different bioactive components through different incorporation strategies. Firstly, MSNs were functionalised with an amino group by treatment with APTES. BMP-2 was covalently linked to the amino groups through carbodiimide chemistry, and Dexamethasone was incorporated into the MSN pores by surface adsorption. Reproduced from (193). (B) Incorporation of microparticles and nanoparticles into scaffolds. Materials with different release characteristics are used to generate MPs or NPs, enabling high control over the release profile of one or more growth factors. These particles can be incorporated into a matrix in order to generate a scaffold or an injectable composite material. Adapted from (10).*

2.2. Generation of In Vitro Vascularised Tissues

2.2.1. Introduction and Main Strategies

The generation of engineered constructs of clinically relevant size is one of the biggest challenges in tissue engineering (221). One of the main tissue engineering strategies to avoid the formation of a necrotic core within the construct is to generate a vessel network throughout the scaffold that provides a steady supply of oxygen and nutrients, mimicking the blood vessels present in native tissues and organs. Within tissues, the main blood vessels are arterioles, venules and capillaries, which differ in their size and general structure. Arterioles and venules range from 5 to 100 μm in diameter and include a tunica intima (endothelial cell monolayer), a tunica media (smooth muscle layer) and a tunica adventitia composed mainly of collagen. Capillaries are the smallest vessels, ranging between 5 and 10 μm in diameter, and are formed by an endothelial cell layer surrounded by pericytes (222). Efforts to reproduce blood vessel networks within engineered tissues have followed two main routes: top-down strategies, which involve fabrication of pre-designed structures; and bottom-up strategies, which aim to stimulate endothelial cells to form a micro-capillary network by providing a suitable microenvironment (Figure 2.4).

2.2.2. Top-down Strategies

Top-down strategies use 3D fabrication techniques to generate a pre-designed channel network. Different fabrication techniques such as 3D plotting of a sacrificial ink can be used to generate an initial template, which is then embedded in the material of interest and washed away to leave an empty channel network. Alternatively, the materials of interest can also be directly fabricated with a designed channel network with techniques such as lithography. The channel network then needs to be endothelialised by perfusing seeding endothelial cells that attach to the surface of the channel and cover it, mimicking the tunica intima of blood vessels. The material of interest can contain encapsulated cells that will receive nutrients and oxygen from the media perfused through the channel network.

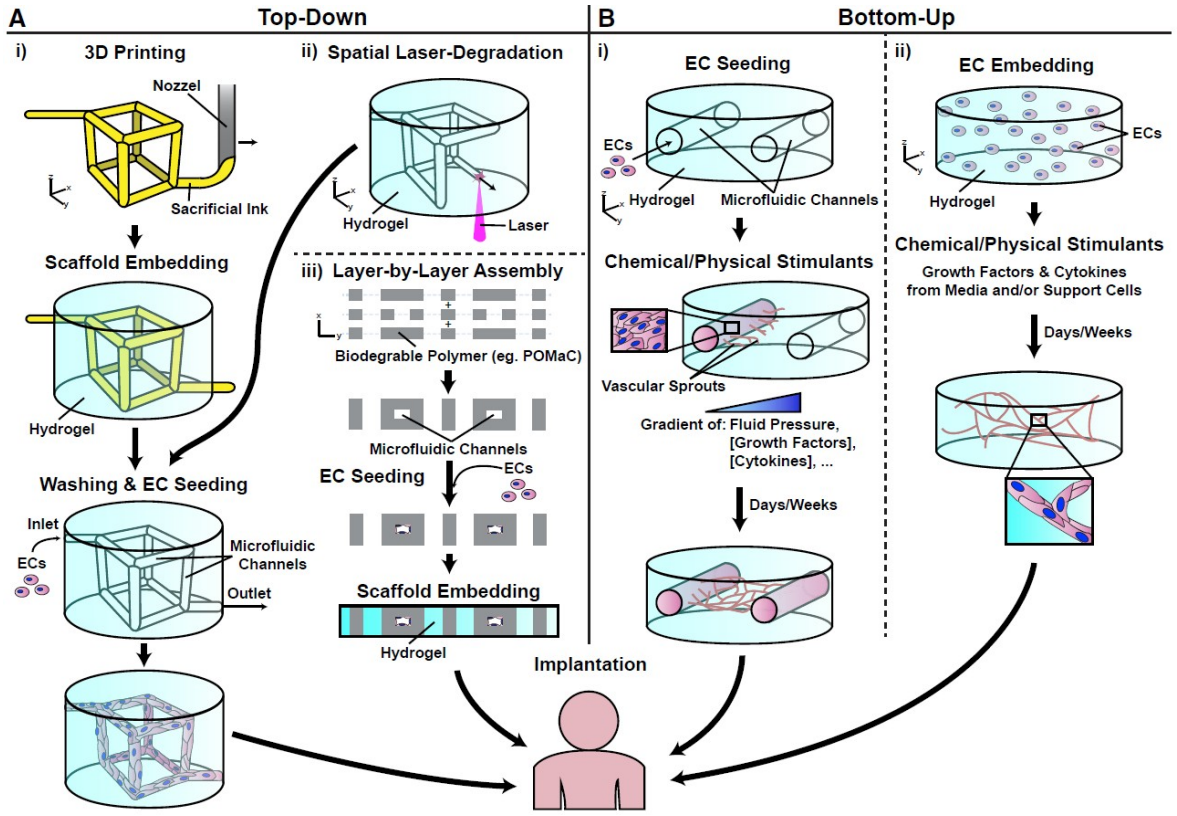

Figure 2.4. Main strategies for the fabrication of pre-vascularised tissue analogues. *Microvessels can be fabricated within tissue engineered constructs by top-down or bottom-up methods. Top-down approaches involve the 3D fabrication of a pre-designed channel structure through techniques such as 3D printing or spatial laser-degradation, which are then embedded in the scaffold material, or the direct fabrication of scaffolds with a pre-defined channel network layer-by-layer manufacturing techniques. The channels are then seeded with endothelial cells to form microvessels. Bottom-up approaches use chemical of physical stimuli to promote angiogenesis or vasculogenesis by encapsulated endothelial cells. Reproduced from (221).*

2.2.2.1. Fabrication Techniques and Biomaterials

One of the most important and limiting aspects of top-down approaches is the fabrication technique. Firstly, the resolution of the fabrication techniques used to generate the channel network determines the diameter of the channels. Secondly, the type of fabrication technique also limits the range of materials that can be used in the process, as some techniques such as 3D plotting require specific material viscosities and rheological behaviours.

The most extended technique to generate these channel networks is **3D printing of a sacrificial mould**, which is then embedded in the material of interest and washed away, leaving an empty channel network (Figure 2.4Ai). The sacrificial material needs to have specific rheological properties in order to be 3D plotted, including high viscosity and shear thinning (223). Printable, biocompatible materials such as water-soluble sugars (224),

agarose (225), alginate (226), gelatin (227), Pluronic F-127 (228) or polyester-based thermoplastics (229) have been used in this step. The main advantage of this technique is its flexibility and accessibility, as it only requires the usage of a 3D printer in a sterile environment. The resolution of the channels generated using this technique is reported to be between 150 (224) and 1000 μm (229). Additionally, the material in which the channels are generated does not have many specific requirements, except it has to undergo a crosslinking process. A range of hydrogels that enable cell encapsulation such as alginate (229), gelatin (228) or fibrin (224,227) have been used in this type of approach. One of the best examples of this techniques is the work done by Kolesky et al., where they aimed to generate large tissues with a perfused channel network. They printed a structure based on Pluronic F-127 and gelatin, where the Pluronic was the sacrificial material and gelatin contained mesenchymal stem cells (MSCs). This structure was then embedded in gelatin, which was crosslinked using a fibrinogen and thrombin system. The Pluronic was removed to generate the channel network, which was then endothelialised and used to provide media to the encapsulated cells (228). The co-printing of two different materials with different roles in the construct, followed by embedding on a third cell-free material, is a good demonstration of the flexibility of this technique.

Laser degradation is another 3D fabrication technique that enables selectively degrading certain regions of a bulk material to generate a channel network (Figure 2.4Aii). The limitation of this technique is that the bulk material needs to be photodegradable, restricting the range of materials that can be applied (230,231). Poly(ethylene glycol) diacrylate (PEGDA) crosslinked with 1-vinyl-2-pyrrolidone (230) or cyclooctyne-terminated PEG crosslinked using an azide crosslinker (231) have been previously applied to selective laser degradation. Heintz et al. fabricated channels with a resolution as small as 3 μm using this technique. However, the minimum channel diameter that could be endothelialised was 50 μm due to the need to perfuse cells (230). The most interesting advantage of this technique is the possibility of generating complex three-dimensional designs with intertwined channels, which they used to reproduce the microvascular network of a mouse brain (230).

Alternatively, the material of interest can be directly 3D fabricated in a layer-by-layer fashion with a pore network in it using **lithography** (Figure 2.4Aiii). This technique has allowed materials such as collagen (232,233) or poly-(octamethylene maleate (anhydride) citrate) (POMaC) (234) to be fabricated with a controlled channel network and encapsulated cells. In

these studies, separate layers were crosslinked with the desired shapes using poly(dimethylsiloxane) (PDMS) moulds, and the layers were then bonded together to create the channel networks (232–234). This technology has shown resolutions of around 150 μm. However, it seems difficult to scale up to the generation of larger constructs due to the separate fabrication process and bonding of the layers.

2.2.2.2. Endothelialisation Process

The endothelialisation step is a necessary process in top-down approaches regardless of the fabrication technique used to generate the channel network. It is done through the perfusion of endothelial cells together with cell culture media into the fabricated channels. HUVECs are generally used for the endothelialisation step because they are already differentiated into cells from the tunica intima of larger vessels (227–229,233,234), but embryonic stem cell-derived endothelial cells have also been reported (232). Depending on the materials used for fabrication of the constructs, the channels can be coated with ECM-derived molecules such as gelatin prior to the perfusion of endothelial cells to facilitate cell attachment and the formation of a monolayer (234).

It has been shown that the formation of this endothelial cell monolayer changes the diffusion characteristics of the channels, making them more similar to native vessels (228,234,235). Most importantly, it reduces the attachment of platelets from circulating blood, reducing blood clotting (232) an therefore making endothelialisation an essential step towards translation of these vascularised tissues.

2.2.2.3. Encapsulated Cells

The fabrication of channels within the constructs aims to avoid the lack of oxygen and nutrient diffusion towards the encapsulated cells. These techniques have allowed the generation of different types of tissue analogues, each of them involving different types of encapsulated cells. For example, Kolesky et al. encapsulated MSCs into their gelatin scaffolds and demonstrated that the fabrication of channels allowed diffusion of oxygen, nutrients and osteogenic signals, resulting in improved differentiation of the encapsulated MSCs into the osteogenic lineage as compared to samples without channels (228). Most importantly, the fabricated tissues were larger than 1 cm in all dimensions, demonstrating the advantages that these techniques offer towards translation into a clinical setting. Other cell types such as fibroblasts (224), human brain vascular pericytes (233) and human umbilical

arterial smooth muscle cells (233) have also been encapsulated in the fabricated materials, demonstrating the ability to migrate towards the endothelialised channels and interact with the endothelial cells in a similar way to pericytes. Encapsulating cells that show this type of behaviour could be useful to further stabilise the endothelial cell monolayer and mimic the vessels in native tissues. A study done by Zhang et al. demonstrated the potential of this type of vascularised setup to provide nutrient diffusion to different cell types. They fabricated collagen scaffolds using lithography and encapsulated either rat primary hepatocytes co-cultured with fibroblasts or human embryonic stem cell (hESC)-derived hepatocytes co-cultured with MSCs to generate liver tissue analogues. These constructs showed the ability to metabolise drugs *in vitro* and also secreted urea, demonstrating adequate diffusion through the channel system. The study continued by encapsulating hESC-derived cardiomyocytes and MSCs in the construct, which resulted in cell alignment and synchronous macroscopic contractions after 5 days of culture (234). These studies show that the generation of adequately vascularised tissue analogues could be applied to a large variety of tissue engineering applications, enabling the fabrication of larger tissue analogues that are needed for clinical translation.

Presently, the most important limitation of top-down approaches is their inability to reproduce blood vessels below 50 μm in diameter. More systematic measurements of oxygen and nutrient diffusion and their impact on encapsulated cells would be key to determine the maximum separation that should be designed between channels. Furthermore, technologies to evaluate the quality of the endothelialised channels would be really important for adequate comparison and optimisation of cell types, fabrication techniques and biomaterials.

2.2.3. Bottom-up Strategies

Bottom-up approaches rely on the self-organisation of encapsulated cells to form a micro-capillary network by reproducing the natural processes of angiogenesis and vasculogenesis Figure 2.4B).

Angiogenesis has been reproduced *in vitro* by generating endothelialised channels, which are then stimulated using fluid shear stress or gradients of growth factors to promote endothelial cell sprouting (236,237) (Figure 2.4Bi). While these techniques are really useful as a model of the angiogenesis process, the difficulties in scalability make them hard to translate to the generation of large, vascularised tissues.

Reproducing vasculogenesis has been achieved *in vitro* by encapsulating endothelial cells (238) or stem cells (239) together with support cells such as fibroblasts (240) or mesenchymal stem cells (241) (Figure 2.4Bii). The process generally starts with clustering of the endothelial cells and formation of a lumen, followed by sprouting and formation of interconnected luminal structures (242). Support cells have shown to surround these endothelial cell structures and stabilise them, resulting in improved vessel formation (240).

2.2.3.1. Endothelial Cells

The endothelial cells in the co-cultures are the cell type that forms network structures and develops vacuoles that fuse into a vascular lumen (243). While endothelial cells are still able to form these structures without the need of support cells (244), support cells are generally co-cultured with them to accelerate self-assembly and stabilize the resulting micro-capillary network (236,238,245).

The most widely used endothelial cell types in pre-vascularisation studies are HUVECs (227,241,242,246,247) as they are easy to obtain and have been extensively studied. However, other cell types have also been studied that could potentially result in improved vascularisation. One of the arguments against HUVECs is that they are differentiated into endothelial cells from the tunica intima of large vessels, potentially making them less adequate for the formation of micro-capillaries. For example, it has been shown that Human adipose-derived microvascular endothelial cells (HAMECs) are able to develop more mature micro-capillary networks as compared to HUVECs in a co-culture setting (241,248), which was hypothesized to be due to the fact that HAMECs originate from microvessels. Furthermore, HAMECs could be obtained from each specific patient in case of clinical translation, bypassing immune rejection. Other cell types that could be readily available from the patient before treatment are stem cells such as endothelial colony forming cells (ECFCs), which have also shown the ability to form micro-capillaries under co-culture conditions and are growing in popularity (249–252). Finally iPSC-derived endothelial cells have also demonstrated the ability to form micro-capillaries (239,253). In fact, Wimmer et al. demonstrated the possibility to obtain both endothelial cells and pericytes from the same original iPSC culture after a multi-step maturation process (239). The obtained vascular organoids, which had also developed a collagen IV basement membrane, were used to model diabetic vasculopathy. The vessels showed responses that were similar to native vessels when exposed to hyperglycaemia and a range of pharmacological treatments (239). While the

dedifferentiation and differentiation processes seemed long and convoluted for clinical translation, the resulting vessel models were very similar to native vessels in ways that had not been demonstrated previously, which is a significant step forward to understand how to reproduce the vascular complexity in tissues and organs.

2.2.3.2. Support Cells

The support cells in the co-cultures accelerate and stabilize the assembly of endothelial cells into micro-capillary networks, acting as pericytes. The most commonly used support cells are fibroblasts from different origins, including human lung fibroblasts (227,249) and dermal fibroblasts (241,242,246,248). In a similar way to HUVECs, these cells are easy to obtain and have been widely studied, becoming the most commonly used cell type. However, fibroblasts are not fulfilling their native roles in these co-cultures. Other cell types that support vasculature in native tissues such as human aortic smooth muscle cells have also been used as support cells, resulting in micro-capillary formation (252). In fact, it has been reported that adipose-derived MSCs (aMSCs) could be a better support cell type as compared to fibroblasts, as shown by the formation of a higher quality micro-capillary network when co-encapsulated with HAMECs (241). Both bone marrow-derived MSCs (bmMSCs) (250,251,253) and aMSCs (241), which could also be obtainable from the patient, have shown the ability to differentiate into α-smooth muscle actin (α-SMA) expressing cells and support the micro-capillary network. This potential has been exploited to try to generate models with both microvessels and bone formation by exposing the cells to specific differentiation factors (250). Klotz et al. co-encapsulated EPCs and bmMSCs in GelMA hydrogels and exposed them to different types of culture media. It was found that exposure of the co-cultures to a 1:1 ratio of osteogenic and vasculogenic media resulted in formation of microvessels with support cells expressing α-SMA and the expression of osteogenic markers by the encapsulated cells. These results suggest that part of the MSC population differentiated to the bone lineage, while other MSCs differentiated to support the microvessel formation (250). This research shows the potential of using the right stromal cells to generate specific vascularised tissue types. As discussed in the previous section, it is also possible to obtain both endothelial cells and support cells by differentiating iPSCs (239)

2.2.3.3. Biomaterials

To promote the self-assembly of endothelial cells into micro-capillaries, hydrogels used for cell encapsulation need to provide very specific conditions. A key condition for a material to be adaptable to pre-vascularisation techniques is that it needs to be mechanically soft, generally bellow 5 kPa of compression modulus (250,251,254). In fact, it has been shown that small changes in the polymer concentration (wt%) have a significant impact on the quality of the developed micro-capillary network (244,255), highlighting how specific these conditions need to be.

The most studied materials for this application are naturally-derived ECM molecules due to their soft mechanical properties and bioactive sequences, from which fibrin stands out (227,241,242,246,248,253). Collagen (249), Matrigel/collagen mixtures (239) and Gelfoam (248) have also been used to successfully generate micro-capillaries *in vitro*. However, these soft mechanical properties have also been reproduced using chemically-modified naturally-derived polymers such as photo-crosslinked GelMA (250,251,253), which allows tailoring the hydrogel mechanical properties by changing the degree of functionalisation. Finally, synthetic polymers such as PEG have also shown the ability to promote micro-capillary formation when combined with RGD sequences (252) or with gelatin and laminin (256). The fact that a range of materials that have been successful to promote micro-capillary formation suggests that the presence of bioactive cues in the material is necessary for cell migration and self-assembly, but these cues do not need to be very specific. However, the soft mechanical properties are a key variable for success in bottom-up vascularisation techniques.

One of the present limitations of bottom-up strategies is that the scalability of pre-vascularisation techniques to generate larger tissue analogues has not been demonstrated yet. On the other hand, the need for the materials to be very soft for the formation of micro-capillaries would make the generation of large constructs a challenge due to the lack of shape fidelity of soft materials.

2.2.4. Anastomosis with the Host Vasculature

A very important feature of the vessel networks formed using top-down and bottom-up approaches is that they have the ability to anastomose with the host vessel network after implantation (232,238).

Due to the larger size of the channels in top-down fabricated constructs, the anastomosis process can require a surgical procedure to directly connect the host vessels with the construct channels (234). However, it has also been shown to happen without surgical help (232,257,258). Zheng et al. fabricated 150 μm diameter endothelialised channels in endothelial cell-laden collagen hydrogels and implanted them in infarcted rat hearts. The presence of the channels improved the overall vascularisation of the sample 5 weeks after implantation, as shown by a 6-fold greater vascular density and a 2.5-fold higher blood velocity in the sample (232). The information on how to promote this natural anastomosis process is presently very scarce. The only variable that has been repeatedly reported to have a significant impact in the integration of top-down fabricated constructs is the orientation of the fabricated channels. Improved integration when fabricating parallel channels has been reported in a model of hind limb ischaemia (257) and in liver tissue analogues (258,259) as compared other orientations. These results suggest that there could be an optimal arrangement for the fabricated channels.

The formation of a host-vessel anastomosis in bottom-up pre-vascularised tissues was reported for the first time by Levenberg et al in 2002 (260). Since then, a number of studies have reported similar findings and tried to study the nature of this anastomosis and variables affecting it. However, the information obtained to date is still very limited. Chen et al suggested that a high density of fibroblasts, which were used as support cells, helps accelerate the anastomosis process (261). Sekine et al. reported that the addition of bFGF during the *in vitro* culture helped the tissue integrate once implanted, although it was not possible to distinguish between the direct effects of the presence of the GF after implantation and the indirect effects through an improved *in vitro* micro-capillary formation (262). Ben-Shaul et al. reported improved host-vessel anastomosis when the samples had been cultured *in vitro* during two weeks versus direct implantation of co-cultures without *in vitro* maturation, remarking the importance of the pre-vascularisation process for optimal anastomosis (263).

Techniques that allow better tracking of the host-vessel anastomosis process are needed in order to study the optimal conditions for quick tissue integration. Furthermore, studies on the optimal channel diameter, density and orientation of the fabricated constructs in top-down approaches would be valuable for the field.

2.3. Combination of Growth Factor Delivery and Vascularised Tissue Engineering

In the past decade, emerging biofabrication approaches that generate complex scaffolds following a layer-by-layer automated deposition technique have been studied for vascularisation. This automated high resolution approach offers a superior level of control over the spatial distribution of the materials in each single layer, dictating the scaffold architecture. Biofabrication techniques are classified in bioprinting and bioassembly (264). While the number of studies using biofabrication approaches has been growing, only a very small number of studies combine the delivery of GFs with cell-based approaches for vascularisation purposes.

Bioprinting refers to the use of computer-aided transfer processes for patterning and assembly of living and non-living materials with a prescribed 2D or 3D organization (Figure 2.5) (264). A good example of the combination of cell and GF delivery using bioprinting is the study done by Byambaa et al., where they bioprinted a scaffold with similar architectural features as bone using bioinks consisting of GelMA with covalently conjugated VEGF. The GelMA-VEGF regions of the scaffold resulted in increased proliferation and network formation by endothelial cell (183). In a different study, VEGF-loaded GelMA MPs were fabricated with different crosslinking densities. The MPs showed longer GF release time when increasing the crosslinking density of GelMA. The MPs were bioprinted in a Matrigel/alginate bioink with encapsulated endothelial cells, showing that a more sustained VEGF release resulted in increased vessel formation. Further *in vivo* implantation showed that the presence of VEGF-releasing MPs resulted in increased vascularization of the constructs (182), demonstrating the potential of these combined therapies. However, this approach did not include an *in vitro* maturation step and did not co-encapsulate support cells for pre-vascularisation of the construct.

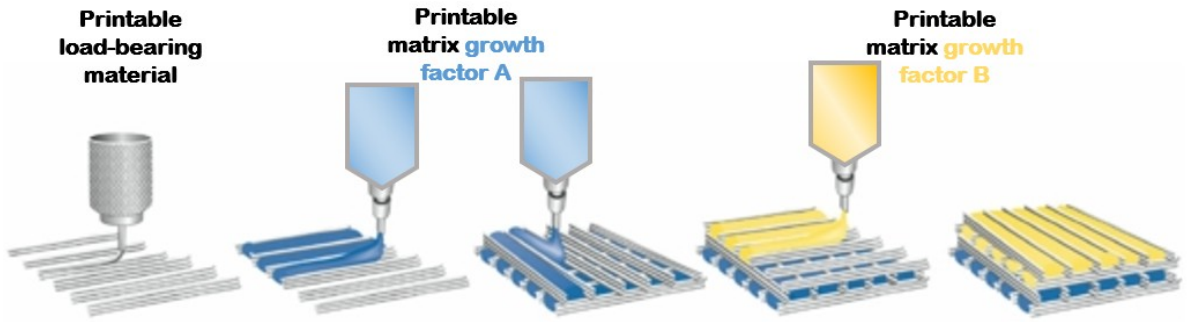

Figure 2.5. Bioprinting approaches. *Materials with different release characteristics are automatically deposited to generate scaffolds with high spatial control, enabling the generation of internal gradients and controllable 3D architectures for improved biomimicry. Adapted from* (268).

Bioassembly is based on the automated deposition of previously fabricated cell-containing building blocks, such as microspheres or microtissues, within 3D scaffolds (Figure 2.6) (269). A significant advantage of bioassembly over bioprinting is that the materials do not need to have the specific rheological properties required for 3D printing. While this technique offers high potential in terms of combining different materials and controlling the scaffold 3D architecture, it has not been applied yet to the delivery of growth factors in combination with cells for tissue vascularisation purposes.

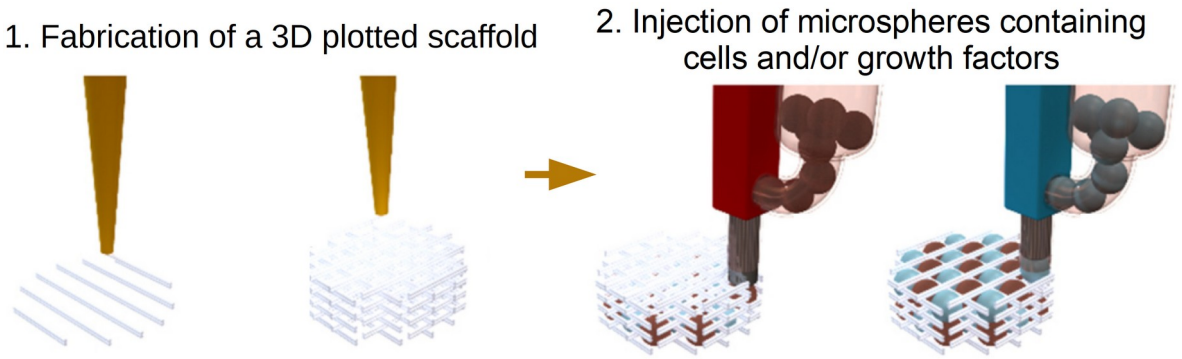

Figure 2.6. Bioassembly approaches. *Building blocks made of materials containing cells or growth factors with different release profiles are assembled into a solid scaffold, enabling the generation of internal gradients and controllable 3D architectures for improved biomimicry. Adapted from* (269).

These examples showcase the potential of biofabrication to generate complex biomimetic scaffolds that include spatially- and temporally-controlled GF release for both tissue regeneration and *in vitro* modelling. Furthermore, the small amount of studies dedicated to the combination of GF delivery and cell delivery for vascularisation highlights the need for research in this area.

2.4. Conclusions and Future Perspectives

2.4.1 Growth Factor Delivery

Although several GFs have been identified as signalling molecules that play important roles in developmental and regenerative processes, the use of GFs as therapeutics agents have yet made significant progress in the clinic. One major issue that still persist is the lack of suitable GF delivery systems to achieve optimal therapeutic effect while avoiding side effects. It was identified that the ideal GF delivery system should meet key design criteria such as being able to deliver the GF to a localized site, at the right concentration and following adequate temporal patterns. While there are signs that following the natural expression patterns of certain growth factors during the regenerative process may result in improved regeneration, more research is needed in order to establish the optimal concentrations and rates of GF needed for each specific TERM application

A number of commercially available products based on GF delivery have been released to the market, achieving some clinical success. However, the observation of potential side effects highlights the need for development of more advanced delivery systems. The spatial and temporal control over the GF release profile from these delivery systems is highly desired. Various biomaterials, incorporation methods and fabrication techniques have been developed and employed for GF delivery. Although these delivery platforms often pose desirable characteristics, they also show important limitations. Additionally, they are usually only characterised to one specific GF. In the native regenerative microenvironment, several GFs work concurrently with different expression levels and profiles to synergistically facilitate the desired cellular behaviour. With our current understanding of this biological phenomena and the limitations of the current GFs delivery vehicles, it is recommended that the field should be moving forward with combinatorial approaches.

2.4.2. Generation of In Vitro Vascularised Tissues

Top-down and bottom-up approaches have been successful at reproducing specific levels of vascularisation. While top-down approaches can only fabricate larger endothelialised channels (>50μm), bottom-up approaches can only generate micro-capillary networks. Thus, both strategies fail to closely reproduce the complex vasculature in native tissues and organs. Research is needed to try to combine both strategies, which could prove successful if the right materials are used.

Another aspect that requires further research is the generation of larger tissues using top-down or bottom-up approaches. While some studies using top-down approaches have focused on this aspect, there are no studies that use bottom-up strategies that generate tissues with more than 1mm thickness. However, generating large tissues will be essential for clinical translation.

Both bottom-up and top-down approaches have shown the ability to anastomose with the host vessel network. However, the mechanisms of this process and the variables that affect it are not well known. Studies are required to optimise the fabrication conditions for improved integration of vascularised tissues.

2.4.3. Combination of Growth Factor Delivery and Vascularised Tissue Engineering

There is a very limited number of studies that combine GF delivery with cells for vascularisation purposes. In fact, there are no studies up to date that combine bottom-up pre-vascularisation techniques with growth factor delivery. Therefore, there is a wide range of possibilities that could be explored in terms of specific GFs, release profiles, cells to deliver, and their 3D organisation within engineered scaffolds. Biofabrication techniques show great potential to combine GF delivery and cell delivery, making them a potentially useful tool for tissue vascularisation purposes.

2.5. References

1. Cohen S. Origins of growth factors: NGF and EGF. J Biol Chem [Internet]. 2008;283(49):33793–7. Available from: https://www.ncbi.nlm.nih.gov/pubmed/18697735

2. Cohen S, Levi-Montalcini R. Purification and Properties of a Nerve Growth-promoting Factor Isolated from Mouse Sarcoma 180. Cancer Res [Internet]. 1957;17(1):15–20. Available from: http://cancerres.aacrjournals.org/content/canres/17/1/15.full.pdf

3. Koria P. Delivery of Growth Factors for Tissue Regeneration and Wound Healing. BioDrugs [Internet]. 2012;26(3):163–75. Available from: https://doi.org/10.2165/11631850-000000000-00000

4. Lissenberg-Thunnissen SN, de Gorter DJJ, Sier CFM, Schipper IB. Use and efficacy of bone morphogenetic proteins in fracture healing. Int Orthop [Internet]. 2011;35(9):1271. Available from: https://doi.org/10.1007/s00264-011-1301-z

5. Hanft JR, Pollak RA, Barbul A, van Gils C, Kwon PS, Gray SM, et al. Phase I trial on the safety of topical rhVEGF on chronic neuropathic diabetic foot ulcers. J Wound Care [Internet]. 2008;17(1):30–7. Available from: https://www.magonlinelibrary.com/doi/abs/10.12968/jowc.2008.17.1.27917

6. Mulder G, Tallis AJ, Marshall VT, Mozingo D, Phillips L, Pierce GF, et al. Treatment of nonhealing diabetic foot ulcers with a platelet-derived growth factor gene-activated matrix (GAM501): Results of a Phase 1/2 trial. Wound Repair Regen [Internet]. 2009;17(6):772–9. Available from: http://dx.doi.org/10.1111/j.1524-475X.2009.00541.x

7. Wang RN, Green J, Wang Z, Deng Y, Qiao M, Peabody M, et al. Bone Morphogenetic Protein (BMP) signaling in development and human diseases. Genes Dis [Internet]. 2014;1(1):87–105. Available from: https://www.ncbi.nlm.nih.gov/pubmed/25401122

8. Tsuji K, Bandyopadhyay A, Harfe BD, Cox K, Kakar S, Gerstenfeld L, et al. BMP2 activity, although dispensable for bone formation, is required for the initiation of fracture healing. Nat Genet [Internet]. 2006;38:1424. Available from: http://dx.doi.org/

10.1038/ng1916

9. De Biase P, Capanna R. Clinical applications of BMPs. Injury [Internet]. 2005;36 Suppl 3:S43-6. Available from: https://www.ncbi.nlm.nih.gov/pubmed/16188549

10. Bayer EA, Gottardi R, Fedorchak M V, Little SR. The scope and sequence of growth factor delivery for vascularized bone tissue regeneration. J Control Release [Internet]. 2015;219:129–40. Available from: https://www.ncbi.nlm.nih.gov/pubmed/26264834

11. Theiss HD, Brenner C, Engelmann MG, Zaruba M-M, Huber B, Henschel V, et al. Safety and efficacy of SITAgliptin plus GRanulocyte-colony-stimulating factor in patients suffering from Acute Myocardial Infarction (SITAGRAMI-Trial) — Rationale, design and first interim analysis. Int J Cardiol [Internet]. 2010;145(2):282–4. Available from: http://www.sciencedirect.com/science/article/pii/S0167527309015010

12. Bing M, Da-Sheng C, Zhao-Fan X, Dao-Feng B, Wei L, Zhi-Fang C, et al. Randomized, multicenter, double-blind, and placebo-controlled trial using topical recombinant human acidic fibroblast growth factor for deep partial-thickness burns and skin graft donor site. Wound Repair Regen [Internet]. 2007;15(6):795–9. Available from: http://dx.doi.org/10.1111/j.1524-475X.2007.00307.x

13. FDA. Safety Warning on Becaplermin in Regranex. 2008.

14. Huang EJ, Reichardt LF. Neurotrophins: roles in neuronal development and function. Annu Rev Neurosci [Internet]. 2001;24:677–736. Available from: https://www.ncbi.nlm.nih.gov/pubmed/11520916

15. Han Q, Sun W, Lin H, Zhao W, Gao Y, Zhao Y, et al. Linear Ordered Collagen Scaffolds Loaded with Collagen-Binding Brain-Derived Neurotrophic Factor Improve the Recovery of Spinal Cord Injury in Rats. Tissue Eng Part A [Internet]. 2009;15(10):2927–35. Available from: https://doi.org/10.1089/ten.tea.2008.0506

16. Chan SJ, Love C, Spector M, Cool SM, Nurcombe V, Lo EH. Endogenous regeneration: Engineering growth factors for stroke. Neurochem Int [Internet]. 2017;107:57–65. Available from: https://www.ncbi.nlm.nih.gov/pubmed/28411103

17. Xian CJ. Roles of epidermal growth factor family in the regulation of postnatal somatic growth. Endocr Rev [Internet]. 2007;28(3):284–96. Available from: https://www.ncbi.nlm.nih.gov/pubmed/17322455

18. Berlanga-Acosta J, Fernandez-Montequin J, Valdes-Perez C, Savigne-Gutierrez W, Mendoza-Mari Y, Garcia-Ojalvo A, et al. Diabetic Foot Ulcers and Epidermal Growth Factor: Revisiting the Local Delivery Route for a Successful Outcome. Biomed Res Int [Internet]. 2017;2017:2923759. Available from: https://www.ncbi.nlm.nih.gov/pubmed/28904951

19. Beenken A, Mohammadi M. The FGF family: biology, pathophysiology and therapy. Nat Rev Drug Discov [Internet]. 2009;8(3):235–53. Available from: https://www.ncbi.nlm.nih.gov/pubmed/19247306

20. Itoh N, Ornitz DM. Fibroblast growth factors: from molecular evolution to roles in development, metabolism and disease. J Biochem [Internet]. 2011;149(2):121–30. Available from: https://www.ncbi.nlm.nih.gov/pubmed/20940169

21. Jau-Ching Wu, Wen-Cheng Huang, Yu-Chun Chen, Tsung-Hsi Tu, Yun-An Tsai, Shih-Fong Huang, et al. Acidic fibroblast growth factor for repair of human spinal cord injury: a clinical trial. J Neurosurg Spine [Internet]. 2011;15(3):216–27. Available from: http://thejns.org/doi/abs/10.3171/2011.4.SPINE10404

22. El Agha E, Kosanovic D, Schermuly RT, Bellusci S. Role of fibroblast growth factors in organ regeneration and repair. Semin Cell Dev Biol [Internet]. 2016;53:76–84. Available from: https://www.ncbi.nlm.nih.gov/pubmed/26459973

23. Kawaguchi H, Jingushi S, Izumi T, Fukunaga M, Matsushita T, Nakamura T, et al. Local application of recombinant human fibroblast growth factor-2 on bone repair: A dose–escalation prospective trial on patients with osteotomy. J Orthop Res [Internet]. 2007;25(4):480–7. Available from: http://dx.doi.org/10.1002/jor.20315

24. Kimura Y, Hokugo A, Takamoto T, Tabata Y, Kurosawa H. Regeneration of Anterior Cruciate Ligament by Biodegradable Scaffold Combined with Local Controlled Release of Basic Fibroblast Growth Factor and Collagen Wrapping. Tissue Eng Part C Methods [Internet]. 2008;14(1):47–57. Available from:

https://doi.org/10.1089/tec.2007.0286

25. Jansen RG, Van Kuppevelt TH, Daamen WF, Kuijpers-Jagtman AM, Von den Hoff JW. FGF-2-loaded collagen scaffolds attract cells and blood vessels in rat oral mucosa. J Oral Pathol Med [Internet]. 2009;38(8):630–8. Available from: http://dx.doi.org/10.1111/j.1600-0714.2009.00763.x

26. Tatekawa Y, Kawazoe N, Chen G, Shirasaki Y, Komuro H, Kaneko M. Tracheal defect repair using a PLGA–collagen hybrid scaffold reinforced by a copolymer stent with bFGF-impregnated gelatin hydrogel. Pediatr Surg Int [Internet]. 2010;26(6):575–80. Available from: https://doi.org/10.1007/s00383-010-2609-2

27. Kitamura M, Akamatsu M, Machigashira M, Hara Y, Sakagami R, Hirofuji T, et al. FGF-2 Stimulates Periodontal Regeneration: Results of a Multi-center Randomized Clinical Trial. J Dent Res [Internet]. 2010;90(1):35–40. Available from: https://doi.org/10.1177/0022034510384616

28. Funakoshi H, Nakamura T. Hepatocyte growth factor: from diagnosis to clinical applications. Clin Chim Acta [Internet]. 2003;327(1):1–23. Available from: http://www.sciencedirect.com/science/article/pii/S0009898102003029

29. Kishimoto Y, Hirano S, Kitani Y, Suehiro A, Umeda H, Tateya I, et al. Chronic vocal fold scar restoration with hepatocyte growth factor hydrogel. Laryngoscope [Internet]. 2010;120(1):108–13. Available from: http://dx.doi.org/10.1002/lary.20642

30. Morishita R, Makino H, Aoki M, Hashiya N, Yamasaki K, Azuma J, et al. Phase I/IIa Clinical Trial of Therapeutic Angiogenesis Using Hepatocyte Growth Factor Gene Transfer to Treat Critical Limb Ischemia. Arterioscler Thromb Vasc Biol [Internet]. 2011;31(3):713–20. Available from: http://atvb.ahajournals.org/content/atvbaha/31/3/713.full.pdf

31. Pulavendran S, Rose C, Mandal AB. Hepatocyte growth factor incorporated chitosan nanoparticles augment the differentiation of stem cell into hepatocytes for the recovery of liver cirrhosis in mice. J Nanobiotechnology [Internet]. 2011;9(1):15. Available from: https://doi.org/10.1186/1477-3155-9-15

32. Liu J-J, Wang C-Y, Wang J-G, Ruan H-J, Fan C-Y. Peripheral nerve regeneration

using composite poly(lactic acid-caprolactone)/nerve growth factor conduits prepared by coaxial electrospinning. J Biomed Mater Res Part A [Internet]. 2011;96A(1):13–20. Available from: http://dx.doi.org/10.1002/jbm.a.32946

33. Andrae J, Gallini R, Betsholtz C. Role of platelet-derived growth factors in physiology and medicine. Genes Dev [Internet]. 2008;22(10):1276–312. Available from: https://www.ncbi.nlm.nih.gov/pubmed/18483217

34. Li B, Davidson JM, Guelcher SA. The effect of the local delivery of platelet-derived growth factor from reactive two-component polyurethane scaffolds on the healing in rat skin excisional wounds. Biomaterials [Internet]. 2009;30(20):3486–94. Available from: http://www.sciencedirect.com/science/article/pii/S0142961209002737

35. Caplan AI, Correa D. PDGF in bone formation and regeneration: New insights into a novel mechanism involving MSCs. J Orthop Res [Internet]. 2011;29(12):1795–803. Available from: http://dx.doi.org/10.1002/jor.21462

36. Jayakumar A, Rajababu P, Rohini S, Butchibabu K, Naveen A, Reddy PK, et al. Multi-centre, randomized clinical trial on the efficacy and safety of recombinant human platelet-derived growth factor with β-tricalcium phosphate in human intra-osseous periodontal defects. J Clin Periodontol [Internet]. 2011;38(2):163–72. Available from: http://dx.doi.org/10.1111/j.1600-051X.2010.01639.x

37. Gary EF, Sheldon L, Luis AS, Leo BS, Samuel EL. The Role of Recombinant Human Platelet-derived Growth Factor-BB (rhPDGF-BB) in Orthopaedic Bone Repair and Regeneration. Curr Pharm Des [Internet]. 2013;19(19):3384–90. Available from: http://www.eurekaselect.com/node/109266/article

38. Ge Zhang Xiaohong Wang, Qingsong Hu, Laura J. Suggs, and Jianyi Zhang. YN. Controlled Release of Stromal Cell–Derived Factor-1alpha In Situ Increases C-kit+ Cell Homing to the Infarcted Heart. Tissue Eng. 2007;13(8):2063–71.

39. Grefte S, Kuijpers-Jagtman AM, Torensma R, Hoff JWV den. Skeletal muscle fibrosis: the effect of stromal-derived factor-1α-loaded collagen scaffolds. Regen Med [Internet]. 2010;5(5):737–47. Available from: https://www.futuremedicine.com/doi/abs/10.2217/rme.10.69

40. Shen W, Chen X, Chen J, Yin Z, Heng BC, Chen W, et al. The effect of incorporation of exogenous stromal cell-derived factor-1 alpha within a knitted silk-collagen sponge scaffold on tendon regeneration. Biomaterials [Internet]. 2010;31(28):7239–49. Available from: http://www.sciencedirect.com/science/article/pii/S0142961210006587

41. Sarkar A, Tatlidede S, Scherer SS, Orgill DP, Berthiaume F. Combination of stromal cell-derived factor-1 and collagen–glycosaminoglycan scaffold delays contraction and accelerates reepithelialization of dermal wounds in wild-type mice. Wound Repair Regen [Internet]. 2011;19(1):71–9. Available from: http://www.ncbi.nlm.nih.gov/pmc/articles/PMC3167377/

42. Lee J-Y, Kim K-H, Shin S-Y, Rhyu I-C, Lee Y-M, Park Y-J, et al. Enhanced bone formation by transforming growth factor-β1-releasing collagen/chitosan microgranules. J Biomed Mater Res Part A [Internet]. 2006;76A(3):530–9. Available from: http://dx.doi.org/10.1002/jbm.a.30434

43. Park JS, Park K, Woo DG, Yang HN, Chung H-M, Park K-H. PLGA Microsphere Construct Coated with TGF-β 3 Loaded Nanoparticles for Neocartilage Formation. Biomacromolecules [Internet]. 2008;9(8):2162–9. Available from: http://dx.doi.org/10.1021/bm800251x

44. Park K-H, Lee DH, Na K. Transplantation of poly(N-isopropylacrylamide-co-vinylimidazole) hydrogel constructs composed of rabbit chondrocytes and growth factor-loaded nanoparticles for neocartilage formation. Biotechnol Lett [Internet]. 2009;31(3):337–46. Available from: https://doi.org/10.1007/s10529-008-9871-6

45. Maeda H, Wada N, Tomokiyo A, Monnouchi S, Akamine A. Prospective potency of TGF-beta1 on maintenance and regeneration of periodontal tissue. Int Rev Cell Mol Biol [Internet]. 2013;304:283–367. Available from: https://www.ncbi.nlm.nih.gov/pubmed/23809439

46. Roy H, Bhardwaj S, Yla-Herttuala S. Biology of vascular endothelial growth factors. FEBS Lett [Internet]. 2006;580(12):2879–87. Available from: https://www.ncbi.nlm.nih.gov/pubmed/16631753

47. Hanzhe Z, Tatsushi K, Takeshi H, Kanji T, Kentaro D, Violeta L, et al. Gelatin-

Siloxane Hybrid Scaffolds with Vascular Endothelial Growth Factor Induces Brain Tissue Regeneration. Curr Neurovasc Res [Internet]. 2008;5(2):112–7. Available from: http://www.eurekaselect.com/node/66891/article

48. Yang P, Wang C, Shi Z, Huang X, Dang X, Li X, et al. rhVEGF165 delivered in a porous β-tricalcium phosphate scaffold accelerates bridging of critical-sized defects in rabbit radii. J Biomed Mater Res Part A [Internet]. 2010;92A(2):626–40. Available from: http://dx.doi.org/10.1002/jbm.a.32403

49. Ye L, Zhang W, Su L-P, Haider HK, Poh K-K, Galupo MJ, et al. Nanoparticle based delivery of hypoxia-regulated VEGF transgene system combined with myoblast engraftment for myocardial repair. Biomaterials [Internet]. 2011;32(9):2424–31. Available from: http://www.sciencedirect.com/science/article/pii/S0142961210015450

50. Hu K, Olsen BR. The roles of vascular endothelial growth factor in bone repair and regeneration. Bone [Internet]. 2016;91:30–8. Available from: https://www.ncbi.nlm.nih.gov/pubmed/27353702

51. Lau TT, Wang DA. Stromal cell-derived factor-1 (SDF-1): homing factor for engineered regenerative medicine. Expert Opin Biol Ther [Internet]. 2011;11(2):189–97. Available from: https://www.ncbi.nlm.nih.gov/pubmed/21219236

52. Vanden Berg-Foels WS. In Situ Tissue Regeneration: Chemoattractants for Endogenous Stem Cell Recruitment. Tissue Eng Part B Rev [Internet]. 2013;20(1):28–39. Available from: https://doi.org/10.1089/ten.teb.2013.0100

53. Ashikari-Hada S, Habuchi H, Kariya Y, Itoh N, Reddi AH, Kimata K. Characterization of growth factor-binding structures in heparin/heparan sulfate using an octasaccharide library. J Biol Chem [Internet]. 2004;279(13):12346–54. Available from: https://www.ncbi.nlm.nih.gov/pubmed/14707131

54. Tufvesson E, Westergren-Thorsson G. Tumour necrosis factor-α interacts with biglycan and decorin. FEBS Lett [Internet]. 2002;530(1–3):124–8. Available from: http://dx.doi.org/10.1016/S0014-5793(02)03439-7

55. Vilchis-Landeros MM, Montiel JL, Mendoza V, Mendoza-Hernandez G, Lopez-Casillas F. Recombinant soluble betaglycan is a potent and isoform-selective

transforming growth factor-β neutralizing agent. Biochem J [Internet]. 2001;355(1):215–22. Available from: http://www.biochemj.org/content/ppbiochemj/355/1/215.full.pdf

56. Hirose J, Kawashima H, Yoshie O, Tashiro K, Miyasaka M. Versican interacts with chemokines and modulates cellular responses. J Biol Chem [Internet]. 2001;276(7):5228–34. Available from: https://www.ncbi.nlm.nih.gov/pubmed/11083865

57. Martino MM, Hubbell JA. The 12th–14th type III repeats of fibronectin function as a highly promiscuous growth factor-binding domain. FASEB J [Internet]. 2010;24(12):4711–21. Available from: http://www.fasebj.org/content/24/12/4711.abstract

58. Schuppan D, Schmid M, Somasundaram R, Ackermann R, Ruehl M, Nakamura T, et al. Collagens in the liver extracellular matrix bind hepatocyte growth factor. Gastroenterology [Internet]. 1998;114(1):139–52. Available from: http://dx.doi.org/10.1016/S0016-5085(98)70642-0

59. Upton Z, Cuttle L, Noble A, Kempf M, Topping G, Malda J, et al. Vitronectin: Growth Factor Complexes Hold Potential as a Wound Therapy Approach. J Invest Dermatol [Internet]. 2008;128(6):1535–44. Available from: http://www.sciencedirect.com/science/article/pii/S0022202X15339142

60. Brekken RA, Sage EH. SPARC, a matricellular protein: at the crossroads of cell–matrix communication: [Matrix Biology (2000) 569–580]. Matrix Biol [Internet]. 2001;19(8):815–27. Available from: http://www.sciencedirect.com/science/article/pii/S0945053X00001335

61. De Laporte L, Rice JJ, Tortelli F, Hubbell JA. Tenascin C Promiscuously Binds Growth Factors via Its Fifth Fibronectin Type III-Like Domain. PLoS One [Internet]. 2013;8(4):e62076. Available from: https://doi.org/10.1371/journal.pone.0062076

62. Wells A, Nuschke A, Yates CC. Skin tissue repair: Matrix microenvironmental influences. Matrix Biol [Internet]. 2016;49:25–36. Available from: https://www.ncbi.nlm.nih.gov/pubmed/26278492

63. Frangogiannis NG. The extracellular matrix in myocardial injury, repair, and remodeling. J Clin Invest [Internet]. 2017;127(5):1600–12. Available from: https://www.ncbi.nlm.nih.gov/pubmed/28459429

64. Mitchell AC, Briquez PS, Hubbell JA, Cochran JR. Engineering growth factors for regenerative medicine applications. Acta Biomater [Internet]. 2016;30:1–12. Available from: https://www.ncbi.nlm.nih.gov/pubmed/26555377

65. Barnard JA, Daniel Beauchamp R, Russell WE, Dubois RN, Coffey RJ. Epidermal growth factor-related peptides and their relevance to gastrointestinal pathophysiology. Gastroenterology [Internet]. 1995;108(2):564–80. Available from: http://dx.doi.org/10.1016/0016-5085(95)90087-X

66. Kenney NJ, Bowman A, Korach KS, Carl Barrett J, Salomon DS. Effect of Exogenous Epidermal-Like Growth Factors on Mammary Gland Development and Differentiation in the Estrogen Receptor-Alpha Knockout (ERKO) Mouse. Breast Cancer Res Treat [Internet]. 2003;79(2):161–73. Available from: https://doi.org/10.1023/A:1023938510508

67. Chan SY, Wong RW. Expression of epidermal growth factor in transgenic mice causes growth retardation. J Biol Chem [Internet]. 2000;275(49):38693–8. Available from: https://www.ncbi.nlm.nih.gov/pubmed/11001946

68. Hankinson SE, Willett WC, Colditz GA, Hunter DJ, Michaud DS, Deroo B, et al. Circulating concentrations of insulin-like growth factor I and risk of breast cancer. Lancet. 1998;351(9113):1393–6.

69. Witsch E, Sela M, Yarden Y. Roles for growth factors in cancer progression. Physiol [Internet]. 2010;25(2):85–101. Available from: https://www.ncbi.nlm.nih.gov/pubmed/20430953

70. Li F, Yu F, Xu X, Li C, Huang D, Zhou X, et al. Evaluation of Recombinant Human FGF-2 and PDGF-BB in Periodontal Regeneration: A Systematic Review and Meta-Analysis. Sci Rep [Internet]. 2017;7(1):65. Available from: https://doi.org/10.1038/s41598-017-00113-y

71. Hyzy SL, Olivares-Navarrete R, Schwartz Z, Boyan BD. BMP2 induces osteoblast

apoptosis in a maturation state and noggin-dependent manner. J Cell Biochem [Internet]. 2012;113(10):3236–45. Available from: http://dx.doi.org/10.1002/jcb.24201

72. Kim HKW, Oxendine I, Kamiya N. High-concentration of BMP2 reduces cell proliferation and increases apoptosis via DKK1 and SOST in human primary periosteal cells. Bone [Internet]. 2013;54(1):141–50. Available from: http://www.sciencedirect.com/science/article/pii/S8756328213000483

73. Ozawa CR, Banfi A, Glazer NL, Thurston G, Springer ML, Kraft PE, et al. Microenvironmental VEGF concentration, not total dose, determines a threshold between normal and aberrant angiogenesis. J Clin Invest [Internet]. 2004;113(4):516–27. Available from: https://doi.org/10.1172/JCI18420

74. Perrimon N, Pitsouli C, Shilo BZ. Signaling mechanisms controlling cell fate and embryonic patterning. Cold Spring Harb Perspect Biol [Internet]. 2012;4(8):a005975. Available from: https://www.ncbi.nlm.nih.gov/pubmed/22855721

75. Bier E, De Robertis EM. Embryo Development. BMP gradients: A paradigm for morphogen-mediated developmental patterning. Science (80-) [Internet]. 2015;348(6242):aaa5838. Available from: https://www.ncbi.nlm.nih.gov/pubmed/26113727

76. Bao P, Kodra A, Tomic-Canic M, Golinko MS, Ehrlich HP, Brem H. The role of vascular endothelial growth factor in wound healing. J Surg Res [Internet]. 2009;153(2):347–58. Available from: https://www.ncbi.nlm.nih.gov/pubmed/19027922

77. Sharma M, Afrin F, Satija N, Tripathi RP, Gangenahalli GU. Stromal-derived factor-1/ CXCR4 signaling: indispensable role in homing and engraftment of hematopoietic stem cells in bone marrow. Stem Cells Dev [Internet]. 2011;20(6):933–46. Available from: https://www.ncbi.nlm.nih.gov/pubmed/21186999

78. Walchli T, Wacker A, Frei K, Regli L, Schwab ME, Hoerstrup SP, et al. Wiring the Vascular Network with Neural Cues: A CNS Perspective. Neuron [Internet]. 2015;87(2):271–96. Available from: https://www.ncbi.nlm.nih.gov/pubmed/26182414

79. de Boer WI, Schuller AG, Vermey M, van der Kwast TH. Expression of growth

factors and receptors during specific phases in regenerating urothelium after acute injury in vivo. Am J Pathol [Internet]. 1994;145(5):1199–207. Available from: http://www.ncbi.nlm.nih.gov/pmc/articles/PMC1887427/

80. Marsell R, Einhorn TA. The biology of fracture healing. Injury [Internet]. 2011;42(6):551–5. Available from: https://www.ncbi.nlm.nih.gov/pubmed/21489527

81. Marsell R, Einhorn TA. The role of endogenous bone morphogenetic proteins in normal skeletal repair. Injury [Internet]. 2009;40:S4–7. Available from: http://www.sciencedirect.com/science/article/pii/S0020138309700038

82. Seeherman H, Li R, Bouxsein M, Kim H, Li XJ, Smith-Adaline EA, et al. rhBMP-2/calcium phosphate matrix accelerates osteotomy-site healing in a nonhuman primate model at multiple treatment times and concentrations. J Bone Jt Surg - Ser A. 2006 Jan;88(1):144–60.

83. Betz OB, Betz VM, Nazarian A, Egermann M, Gerstenfeld LC, Einhorn TA, et al. Delayed administration of adenoviral BMP-2 vector improves the formation of bone in osseous defects. Gene Ther [Internet]. 2007;14:1039. Available from: http://dx.doi.org/10.1038/sj.gt.3302956

84. Jeon O, Song SJ, Yang HS, Bhang SH, Kang SW, Sung MA, et al. Long-term delivery enhances in vivo osteogenic efficacy of bone morphogenetic protein-2 compared to short-term delivery. Biochem Biophys Res Commun [Internet]. 2008;369(2):774–80. Available from: https://www.ncbi.nlm.nih.gov/pubmed/18313401

85. King WJ, Krebsbach PH. Growth factor delivery: how surface interactions modulate release in vitro and in vivo. Adv Drug Deliv Rev [Internet]. 2012;64(12):1239–56. Available from: https://www.ncbi.nlm.nih.gov/pubmed/22433783

86. Duggirala SS, Mehta RC, Deluca PP. Interaction of Recombinant Human Bone Morphogenetic Protein-2 with Poly (d,l Lactide-co-glycolide) Microspheres. Pharm Dev Technol [Internet]. 1996;1(1):11–9. Available from: https://doi.org/10.3109/10837459609031413

87. Zhang H, Migneco F, Lin C-Y, Hollister SJ. Chemically-Conjugated Bone Morphogenetic Protein-2 on Three-Dimensional Polycaprolactone Scaffolds

Stimulates Osteogenic Activity in Bone Marrow Stromal Cells. Tissue Eng Part A [Internet]. 2010;16(11):3441–8. Available from: https://doi.org/10.1089/ten.tea.2010.0132

88. Rechendorff K, Hovgaard MB, Foss M, Zhdanov VP, Besenbacher F. Enhancement of Protein Adsorption Induced by Surface Roughness. Langmuir [Internet]. 2006;22(26):10885–8. Available from: http://dx.doi.org/10.1021/la0621923

89. Ehlert N, Hoffmann A, Luessenhop T, Gross G, Mueller PP, Stieve M, et al. Amino-modified silica surfaces efficiently immobilize bone morphogenetic protein 2 (BMP2) for medical purposes. Acta Biomater [Internet]. 2011;7(4):1772–9. Available from: http://www.sciencedirect.com/science/article/pii/S1742706110005921

90. Lanza Langer, R. S., Vacanti, J. RP. Principles of Tissue Engineering. Amsterdam, The Netherlands: Elsevier Academic Press; 2007.

91. Lee K, Silva EA, Mooney DJ. Growth factor delivery-based tissue engineering: general approaches and a review of recent developments. J R Soc Interface [Internet]. 2011;8(55):153–70. Available from: https://www.ncbi.nlm.nih.gov/pubmed/20719768

92. Masters KS. Covalent Growth Factor Immobilization Strategies for Tissue Repair and Regeneration. Macromol Biosci [Internet]. 2011;11(9):1149–63. Available from: http://dx.doi.org/10.1002/mabi.201000505

93. Dong X, Wang Q, Wu T, Pan H. Understanding Adsorption-Desorption Dynamics of BMP-2 on Hydroxyapatite (001) Surface. Biophys J [Internet]. 2007;93(3):750–9. Available from: http://www.ncbi.nlm.nih.gov/pmc/articles/PMC1913162/

94. Dee KC, Puleo DA, Bizios R. Biomaterials. In: An Introduction To Tissue-Biomaterial Interactions [Internet]. John Wiley & Sons, Inc.; 2003. p. 1–13. Available from: http://dx.doi.org/10.1002/0471270598.ch1

95. Gessner A, Lieske A, Paulke BR, Müller RH. Influence of surface charge density on protein adsorption on polymeric nanoparticles: analysis by two-dimensional electrophoresis. Eur J Pharm Biopharm [Internet]. 2002;54(2):165–70. Available from: http://www.sciencedirect.com/science/article/pii/S0939641102000814

96. Arima Y, Iwata H. Effect of wettability and surface functional groups on protein adsorption and cell adhesion using well-defined mixed self-assembled monolayers. Biomaterials [Internet]. 2007;28(20):3074–82. Available from: http://www.sciencedirect.com/science/article/pii/S0142961207002323

97. Gessner A, Lieske A, Paulke B-R, Müller RH. Functional groups on polystyrene model nanoparticles: Influence on protein adsorption. J Biomed Mater Res Part A [Internet]. 2003;65A(3):319–26. Available from: http://dx.doi.org/10.1002/jbm.a.10371

98. Schrier JA, DeLuca PP. Porous bone morphogenetic protein-2 microspheres: Polymer binding and in vitro release. AAPS PharmSciTech [Internet]. 2001;2(3):66–72. Available from: http://www.ncbi.nlm.nih.gov/pmc/articles/PMC2750582/

99. Chatzinikolaidou M, Laub M, Rumpf H, Jennissen HP. Biocoating of Electropolished and Ultra-Hydrophilic Titanium and Cobalt Chromium Molybdenum Alloy Surfaces with Proteins. Materwiss Werksttech [Internet]. 2002;33(12):720–7. Available from: http://dx.doi.org/10.1002/mawe.200290002

100. Steinmüller-Nethl D, Kloss FR, Najam-Ul-Haq M, Rainer M, Larsson K, Linsmeier C, et al. Strong binding of bioactive BMP-2 to nanocrystalline diamond by physisorption. Biomaterials [Internet]. 2006;27(26):4547–56. Available from: http://www.sciencedirect.com/science/article/pii/S0142961206003905

101. Patterson J, Siew R, Herring SW, Lin ASP, Guldberg R, Stayton PS. Hyaluronic acid hydrogels with controlled degradation properties for oriented bone regeneration. Biomaterials [Internet]. 2010;31(26):6772–81. Available from: http://www.sciencedirect.com/science/article/pii/S0142961210006654

102. Morgan AW, Chan LL, Sendemir-Urkmez A, Cunningham BT, Jamison RD. Detection of growth factor binding to gelatin and heparin using a photonic crystal optical biosensor. Mater Sci Eng C [Internet]. 2010;30(5):686–90. Available from: http://www.sciencedirect.com/science/article/pii/S0928493110000512

103. Sakiyama-Elbert SE, Hubbell JA. Controlled release of nerve growth factor from a heparin-containing fibrin-based cell ingrowth matrix. J Control Release [Internet].

2000;69(1):149–58. Available from: http://www.sciencedirect.com/science/article/pii/S0168365900002960

104. Yang HS, La W-G, Cho Y-M, Shin W, Yeo G-D, Kim B-S. Comparison between heparin-conjugated fibrin and collagen sponge as bone morphogenetic protein-2 carriers for bone regeneration. Exp &Amp; Mol Med [Internet]. 2012;44:350. Available from: http://dx.doi.org/10.3858/emm.2012.44.5.039

105. Martino MM, Tortelli F, Mochizuki M, Traub S, Ben-David D, Kuhn GA, et al. Engineering the Growth Factor Microenvironment with Fibronectin Domains to Promote Wound and Bone Tissue Healing. Sci Transl Med [Internet]. 2011;3(100):100ra89-100ra89. Available from: http://stm.sciencemag.org/content/scitransmed/3/100/100ra89.full.pdf

106. Martino MM, Briquez PS, Ranga A, Lutolf MP, Hubbell JA. Heparin-binding domain of fibrin(ogen) binds growth factors and promotes tissue repair when incorporated within a synthetic matrix. Proc Natl Acad Sci [Internet]. 2013;110(12):4563–8. Available from: http://www.pnas.org/content/110/12/4563.abstract

107. Vulic K, Shoichet MS. Affinity-Based Drug Delivery Systems for Tissue Repair and Regeneration. Biomacromolecules [Internet]. 2014;15(11):3867–80. Available from: http://dx.doi.org/10.1021/bm501084u

108. Miller RE, Grodzinsky AJ, Cummings K, Plaas AHK, Cole AA, Lee RT, et al. Intraarticular injection of heparin-binding insulin-like growth factor 1 sustains delivery of insulin-like growth factor 1 to cartilage through binding to chondroitin sulfate. Arthritis Rheum [Internet]. 2010;62(12):3686–94. Available from: http://dx.doi.org/10.1002/art.27709

109. Sun W, Lin H, Chen B, Zhao W, Zhao Y, Xiao Z, et al. Collagen scaffolds loaded with collagen-binding NGF-β accelerate ulcer healing. J Biomed Mater Res - Part A [Internet]. 2010;92(3):887–95. Available from: https://www.scopus.com/inward/record.uri?eid=2-s2.0-75749155054&doi=10.1002%2Fjbm.a.32445&partnerID=40&md5=53a33fbfd711a0a4aa9fc083114d6c51

110. Sun W, Sun C, Lin H, Zhao H, Wang J, Ma H, et al. The effect of collagen-binding NGF-β on the promotion of sciatic nerve regeneration in a rat sciatic nerve crush injury model. Biomaterials [Internet]. 2009;30(27):4649–56. Available from: http://www.sciencedirect.com/science/article/pii/S0142961209005420

111. Huang X, Brazel CS. On the importance and mechanisms of burst release in matrix-controlled drug delivery systems. J Control Release [Internet]. 2001;73(2):121–36. Available from: http://www.sciencedirect.com/science/article/pii/S0168365901002486

112. Toth JM, Boden SD, Burkus JK, Badura JM, Peckham SM, McKay WF. Short-term Osteoclastic Activity Induced by Locally High Concentrations of Recombinant Human Bone Morphogenetic Protein–2 in a Cancellous Bone Environment. Spine (Phila Pa 1976) [Internet]. 2009;34(6):539–50. Available from: http://journals.lww.com/spinejournal/Fulltext/2009/03150/Short_term_Osteoclastic_Activity_Induced_by.3.aspx

113. Carragee EJ, Hurwitz EL, Weiner BK. A critical review of recombinant human bone morphogenetic protein-2 trials in spinal surgery: emerging safety concerns and lessons learned. Spine J [Internet]. 2011;11(6):471–91. Available from: http://www.sciencedirect.com/science/article/pii/S1529943011002993

114. García JR, Clark AY, García AJ. Integrin-specific hydrogels functionalized with VEGF for vascularization and bone regeneration of critical-size bone defects. J Biomed Mater Res Part A [Internet]. 2016;104(4):889–900. Available from: http://dx.doi.org/10.1002/jbm.a.35626

115. Ehrbar M, Metters A, Zammaretti P, Hubbell JA, Zisch AH. Endothelial cell proliferation and progenitor maturation by fibrin-bound VEGF variants with differential susceptibilities to local cellular activity. J Control Release [Internet]. 2005;101(1):93–109. Available from: http://www.sciencedirect.com/science/article/pii/S016836590400330X

116. Ito Y. Covalently immobilized biosignal molecule materials for tissue engineering. Soft Matter [Internet]. 2008;4(1):46–56. Available from: http://dx.doi.org/10.1039/B708359A

117. Leslie-Barbick JE, Shen C, Chen C, West JL. Micron-Scale Spatially Patterned, Covalently Immobilized Vascular Endothelial Growth Factor on Hydrogels Accelerates Endothelial Tubulogenesis and Increases Cellular Angiogenic Responses. Tissue Eng Part A [Internet]. 2010;17(1–2):221–9. Available from: https://doi.org/10.1089/ten.tea.2010.0202

118. Chiu LLY, Weisel RD, Li R-K, Radisic M. Defining conditions for covalent immobilization of angiogenic growth factors onto scaffolds for tissue engineering. J Tissue Eng Regen Med [Internet]. 2011;5(1):69–84. Available from: http://dx.doi.org/10.1002/term.292

119. Shi Z, Neoh KG, Kang ET, Poh CK, Wang W. Surface Functionalization of Titanium with Carboxymethyl Chitosan and Immobilized Bone Morphogenetic Protein-2 for Enhanced Osseointegration. Biomacromolecules [Internet]. 2009;10(6):1603–11. Available from: http://dx.doi.org/10.1021/bm900203w

120. Yamachika E, Tsujigiwa H, Shirasu N, Ueno T, Sakata Y, Fukunaga J, et al. Immobilized recombinant human bone morphogenetic protein-2 enhances the phosphorylation of receptor-activated Smads. J Biomed Mater Res Part A [Internet]. 2009;88A(3):599–607. Available from: http://dx.doi.org/10.1002/jbm.a.31833

121. Liu L, Deng D, Xing Y, Li S, Yuan B, Chen J, et al. Activity analysis of the carbodiimide-mediated amine coupling reaction on self-assembled monolayers by cyclic voltammetry. Electrochim Acta [Internet]. 2013;89:616–22. Available from: http://www.sciencedirect.com/science/article/pii/S0013468612018683

122. Moore NM, Lin NJ, Gallant ND, Becker ML. The use of immobilized osteogenic growth peptide on gradient substrates synthesized via click chemistry to enhance MC3T3-E1 osteoblast proliferation. Biomaterials [Internet]. 2010;31(7):1604–11. Available from: http://www.sciencedirect.com/science/article/pii/S014296120901223X

123. Lee HJ, Fernandes-Cunha GM, Putra I, Koh W-G, Myung D. Tethering Growth Factors to Collagen Surfaces Using Copper-Free Click Chemistry: Surface Characterization and in Vitro Biological Response. ACS Appl Mater Interfaces [Internet]. 2017;9(28):23389–99. Available from:

http://dx.doi.org/10.1021/acsami.7b05262

124. Ogiwara K, Nagaoka M, Cho C-S, Akaike T. Effect of photo-immobilization of epidermal growth factor on the cellular behaviors. Biochem Biophys Res Commun [Internet]. 2006;345(1):255–9. Available from: http://www.sciencedirect.com/science/article/pii/S0006291X06007856

125. Swiderska KW, Szlachcic A, Czyrek A, Zakrzewska M, Otlewski J. Site-specific conjugation of fibroblast growth factor 2 (FGF2) based on incorporation of alkyne-reactive unnatural amino acid. Bioorg Med Chem [Internet]. 2017;25(14):3685–93. Available from: http://www.sciencedirect.com/science/article/pii/S0968089617301670

126. Chung Y-I, Tae G, Hong Yuk S. A facile method to prepare heparin-functionalized nanoparticles for controlled release of growth factors. Biomaterials [Internet]. 2006;27(12):2621–6. Available from: http://www.sciencedirect.com/science/article/pii/S0142961205010926

127. Eley JG, Mathew P. Preparation and release characteristics of insulin and insulin-like growth factor-one from polymer nanoparticles. J Microencapsul [Internet]. 2007;24(3):225–34. Available from: https://doi.org/10.1080/02652040601162335

128. Wei G, Jin Q, Giannobile W V, Ma PX. The enhancement of osteogenesis by nano-fibrous scaffolds incorporating rhBMP-7 nanospheres. Biomaterials [Internet]. 2007;28(12):2087–96. Available from: http://www.ncbi.nlm.nih.gov/pmc/articles/PMC2048538/

129. Gou ML, Huang MJ, Gou ML, Huang MJ, Qian ZY, Gou ML, et al. Preparation of anionic poly(ε-caprolactone)-poly(ethylene glycol)-poly(ε-caprolactone) copolymeric nanoparticles as basic protein antigen carrier. Growth Factors [Internet]. 2007;25(3):202–8. Available from: https://doi.org/10.1080/08977190701671613

130. Gou M, Dai M, Gu Y, Li X, Wen Y, Yang L, et al. Basic Fibroblast Growth Factor Loaded Biodegradable PCL-PEG-PCL Copolymeric Nanoparticles: Preparation, In Vitro Release and Immunogenicity Study. J Nanosci Nanotechnol [Internet]. 2008;8(5):2357–61. Available from: http://www.ingentaconnect.com/content/asp/jnn/2008/00000008/00000005/art00020

131. Kurakhmaeva KB, Voronina TA, Kapica IG, Kreuter J, Nerobkova LN, Seredenin SB, et al. Antiparkinsonian effect of nerve growth factor adsorbed on polybutylcyanoacrylate nanoparticles coated with polysorbate-80. Bull Exp Biol Med [Internet]. 2008;145(2):259–62. Available from: https://doi.org/10.1007/s10517-008-0065-y

132. Zhang C, Chen J, Feng C, Shao X, Liu Q, Zhang Q, et al. Intranasal nanoparticles of basic fibroblast growth factor for brain delivery to treat Alzheimer's disease. Int J Pharm [Internet]. 2014;461(1):192–202. Available from: http://www.sciencedirect.com/science/article/pii/S0378517313010430

133. Lee JS, Go DH, Bae JW, Lee SJ, Park KD. Heparin conjugated polymeric micelle for long-term delivery of basic fibroblast growth factor. J Control Release [Internet]. 2007;117(2):204–9. Available from: http://europepmc.org/abstract/MED/17196698

134. Lee JS, Bae JW, Joung YK, Lee SJ, Han DK, Park KD. Controlled dual release of basic fibroblast growth factor and indomethacin from heparin-conjugated polymeric micelle. Int J Pharm [Internet]. 2008;346(1–2):57–63. Available from: http://europepmc.org/abstract/MED/17689210

135. Backer M V, Gaynutdinov TI, Patel V, Bandyopadhyaya AK, Thirumamagal BTS, Tjarks W, et al. Vascular endothelial growth factor selectively targets boronated dendrimers to tumor vasculature. Mol Cancer Ther [Internet]. 2005;4(9):1423–9. Available from: http://mct.aacrjournals.org/content/molcanther/4/9/1423.full.pdf

136. Thomas TP, Shukla R, Kotlyar A, Liang B, Ye JY, Norris TB, et al. Dendrimer−Epidermal Growth Factor Conjugate Displays Superagonist Activity. Biomacromolecules [Internet]. 2008;9(2):603–9. Available from: http://dx.doi.org/10.1021/bm701185p

137. Matsuo T, Sugita T, Kubo T, Yasunaga Y, Ochi M, Murakami T. Injectable magnetic liposomes as a novel carrier of recombinant human BMP-2 for bone formation in a rat bone-defect model. J Biomed Mater Res Part A [Internet]. 2003;66A(4):747–54. Available from: http://dx.doi.org/10.1002/jbm.a.10002

138. Tanaka H, Sugita T, Yasunaga Y, Shimose S, Deie M, Kubo T, et al. Efficiency of

magnetic liposomal transforming growth factor-beta 1 in the repair of articular cartilage defects in a rabbit model. J Biomed Mater Res Part A [Internet]. 2005;73A(3):255–63. Available from: http://dx.doi.org/10.1002/jbm.a.30187

139. Xie Y, Ye L, Zhang X, Cui W, Lou J, Nagai T, et al. Transport of nerve growth factor encapsulated into liposomes across the blood–brain barrier: In vitro and in vivo studies. J Control Release [Internet]. 2005;105(1):106–19. Available from: http://www.sciencedirect.com/science/article/pii/S0168365905001070

140. Oh KS, Han SK, Lee HS, Koo HM, Kim RS, Lee KE, et al. Core/Shell Nanoparticles with Lecithin Lipid Cores for Protein Delivery. Biomacromolecules [Internet]. 2006;7(8):2362–7. Available from: http://dx.doi.org/10.1021/bm060362k

141. Kuo Y-C, Rajesh R. Nerve growth factor-loaded heparinized cationic solid lipid nanoparticles for regulating membrane charge of induced pluripotent stem cells during differentiation. Mater Sci Eng C [Internet]. 2017;77:680–9. Available from: http://www.sciencedirect.com/science/article/pii/S0928493117310391

142. Zhao Y-Z, Li X, Lu C-T, Lin M, Chen L-J, Xiang Q, et al. Gelatin nanostructured lipid carriers-mediated intranasal delivery of basic fibroblast growth factor enhances functional recovery in hemiparkinsonian rats. Nanomedicine Nanotechnology, Biol Med [Internet]. 2014;10(4):755–64. Available from: http://www.sciencedirect.com/science/article/pii/S1549963413005856

143. Zhang S, Uludağ H. Nanoparticulate Systems for Growth Factor Delivery. Pharm Res [Internet]. 2009;26(7):1561. Available from: https://doi.org/10.1007/s11095-009-9897-z

144. Skaat H, Ziv-Polat O, Shahar A, Margel S. Enhancement of the Growth and Differentiation of Nasal Olfactory Mucosa Cells by the Conjugation of Growth Factors to Functional Nanoparticles. Bioconjug Chem [Internet]. 2011 Dec 21;22(12):2600–10. Available from: https://doi.org/10.1021/bc200454k

145. Pilakka-Kanthikeel S, Atluri VSR, Sagar V, Saxena SK, Nair M. Targeted Brain Derived Neurotropic Factors (BDNF) Delivery across the Blood-Brain Barrier for Neuro-Protection Using Magnetic Nano Carriers: An In-Vitro Study. PLoS One

[Internet]. 2013 Apr 30;8(4):e62241. Available from: https://doi.org/10.1371/journal.pone.0062241

146. Shevtsov MA, Nikolaev BP, Yakovleva LY, Marchenko YY, Dobrodumov A V, Mikhrina AL, et al. Superparamagnetic iron oxide nanoparticles conjugated with epidermal growth factor (SPION-EGF) for targeting brain tumors. Int J Nanomedicine [Internet]. 2014/01/03. 2014;9:273–87. Available from: https://www.ncbi.nlm.nih.gov/pubmed/24421639

147. Rajan SS, Liu HY, Vu TQ. Ligand-Bound Quantum Dot Probes for Studying the Molecular Scale Dynamics of Receptor Endocytic Trafficking in Live Cells. ACS Nano [Internet]. 2008;2(6):1153–66. Available from: http://dx.doi.org/10.1021/nn700399e

148. Xie W, Zhang K, Cui B. Functional characterization and axonal transport of quantum dot labeled BDNF. Integr Biol [Internet]. 2012;4(8):953–60. Available from: http://dx.doi.org/10.1039/C2IB20062G

149. Patist CM, Mulder MB, Gautier SE, Maquet V, Jérôme R, Oudega M. Freeze-dried poly(d,l-lactic acid) macroporous guidance scaffolds impregnated with brain-derived neurotrophic factor in the transected adult rat thoracic spinal cord. Biomaterials [Internet]. 2004;25(9):1569–82. Available from: http://www.sciencedirect.com/science/article/pii/S0142961203005039

150. Yoon JJ, Chung HJ, Lee HJ, Park TG. Heparin-immobilized biodegradable scaffolds for local and sustained release of angiogenic growth factor. J Biomed Mater Res Part A [Internet]. 2006 Dec 15;79A(4):934–42. Available from: https://doi.org/10.1002/jbm.a.30843

151. Fu Y-C, Nie H, Ho M-L, Wang C-K, Wang C-H. Optimized bone regeneration based on sustained release from three-dimensional fibrous PLGA/HAp composite scaffolds loaded with BMP-2. Biotechnol Bioeng [Internet]. 2008 Mar 1;99(4):996–1006. Available from: https://doi.org/10.1002/bit.21648

152. Chenite A, Chaput C, Wang D, Combes C, Buschmann MD, Hoemann CD, et al. Novel injectable neutral solutions of chitosan form biodegradable gels in situ.

Biomaterials [Internet]. 2000;21(21):2155–61. Available from: http://www.sciencedirect.com/science/article/pii/S0142961200001162

153. Shi W, Ji Y, Zhang X, Shu S, Wu Z. Characterization of ph- and thermosensitive hydrogel as a vehicle for controlled protein delivery. J Pharm Sci [Internet]. 2011;100(3):886–95. Available from: http://dx.doi.org/10.1002/jps.22328

154. Zisch AH, Lutolf MP, Hubbell JA. Biopolymeric delivery matrices for angiogenic growth factors. Cardiovasc Pathol [Internet]. 2003;12(6):295–310. Available from: http://www.sciencedirect.com/science/article/pii/S1054880703000899

155. Pike DB, Cai S, Pomraning KR, Firpo MA, Fisher RJ, Shu XZ, et al. Heparin-regulated release of growth factors in vitro and angiogenic response in vivo to implanted hyaluronan hydrogels containing VEGF and bFGF. Biomaterials [Internet]. 2006;27(30):5242–51. Available from: http://www.sciencedirect.com/science/article/pii/S014296120600456X

156. Peattie RA, Pike DB, Yu B, Cai S, Shu XZ, Prestwich GD, et al. Effect of Gelatin on Heparin Regulation of Cytokine Release from Hyaluronan-Based Hydrogels. Drug Deliv [Internet]. 2008;15(6):389–97. Available from: https://doi.org/10.1080/10717540802035442

157. Barati D, Shariati SRP, Moeinzadeh S, Melero-Martin JM, Khademhosseini A, Jabbari E. Spatiotemporal release of BMP-2 and VEGF enhances osteogenic and vasculogenic differentiation of human mesenchymal stem cells and endothelial colony-forming cells co-encapsulated in a patterned hydrogel. J Control Release [Internet]. 2016;223:126–36. Available from: http://www.sciencedirect.com/science/article/pii/S0168365915302807

158. Samorezov JE, Headley EB, Everett CR, Alsberg E. Sustained presentation of BMP-2 enhances osteogenic differentiation of human adipose-derived stem cells in gelatin hydrogels. J Biomed Mater Res Part A [Internet]. 2016;104(6):1387–97. Available from: http://dx.doi.org/10.1002/jbm.a.35668

159. Lee P-Y, Li Z, Huang L. Thermosensitive Hydrogel as a Tgf-β1 Gene Delivery Vehicle Enhances Diabetic Wound Healing. Pharm Res [Internet]. 2003;20(12):1995–

2000. Available from: https://doi.org/10.1023/B:PHAM.0000008048.58777.da

160. Guicheux J, Gauthier O, Aguado E, Pilet P, Couillaud S, Jegou D, et al. Human Growth Hormone Locally Released in Bone Sites by Calcium-Phosphate Biomaterial Stimulates Ceramic Bone Substitution Without Systemic Effects: A Rabbit Study. J Bone Miner Res [Internet]. 1998;13(4):739–48. Available from: http://dx.doi.org/10.1359/jbmr.1998.13.4.739

161. Koempel JA, Patt BS, O'Grady K, Wozney J, Toriumi DM. The effect of recombinant human bone morphogenetic protein-2 on the integration of porous hydroxyapatite implants with bone. J Biomed Mater Res [Internet]. 1998;41(3):359–63. Available from: http://dx.doi.org/10.1002/(SICI)1097-4636(19980905)41:3%3C359::AID-JBM3%3E3.0.CO;2-B

162. Toshiyuki Takahashi, Teiji Tominaga, Noriaki Watabe, A. Toshimitu Yokobori J, Hiroshi Sasada, Takashi Yoshimoto. Use of porous hydroxyapatite graft containing recombinant human bone morphogenetic protein-2 for cervical fusion in a caprine model. J Neurosurg Spine [Internet]. 1999;90(2):224–30. Available from: http://thejns.org/doi/abs/10.3171/spi.1999.90.2.0224

163. Koch FP, Becker J, Terheyden H, Capsius B, Wagner W, on behalf of the research group of this multicenter clinical trial. A prospective, randomized pilot study on the safety and efficacy of recombinant human growth and differentiation factor-5 coated onto β-tricalcium phosphate for sinus lift augmentation. Clin Oral Implants Res [Internet]. 2010;21(11):1301–8. Available from: http://dx.doi.org/10.1111/j.1600-0501.2010.01949.x

164. Dai C, Guo H, Lu J, Shi J, Wei J, Liu C. Osteogenic evaluation of calcium/magnesium-doped mesoporous silica scaffold with incorporation of rhBMP-2 by synchrotron radiation-based μCT. Biomaterials [Internet]. 2011;32(33):8506–17. Available from: http://www.sciencedirect.com/science/article/pii/S0142961211008878

165. Wu C, Fan W, Chang J, Xiao Y. Mesoporous bioactive glass scaffolds for efficient delivery of vascular endothelial growth factor. J Biomater Appl [Internet]. 2013;28(3):367–74. Available from: http://journals.sagepub.com/doi/abs/10.1177/0885328212453635

166. Roldán JC, Detsch R, Schaefer S, Chang E, Kelantan M, Waiss W, et al. Bone formation and degradation of a highly porous biphasic calcium phosphate ceramic in presence of BMP-7, VEGF and mesenchymal stem cells in an ectopic mouse model. J Cranio-Maxillofacial Surg [Internet]. 2010;38(6):423–30. Available from: http://www.sciencedirect.com/science/article/pii/S1010518210000156

167. Sachse A, Wagner A, Keller M, Wagner O, Wetzel WD, Layher F, et al. Osteointegration of hydroxyapatite-titanium implants coated with nonglycosylated recombinant human bone morphogenetic protein-2 (BMP-2) in aged sheep. Bone [Internet]. 2005;37(5):699–710. Available from: http://www.sciencedirect.com/science/article/pii/S8756328205002735

168. Sumner DR, Turner TM, Urban RM, Virdi AS, Inoue N. Additive Enhancement of Implant Fixation Following Combined Treatment with rhTGF-β2 and rhBMP-2 in a Canine Model. JBJS [Internet]. 2006;88(4):806–17. Available from: https://journals.lww.com/jbjsjournal/Fulltext/2006/04000/ADDITIVE_ENHANCEMENT_OF_IMPLANT_FIXATION_FOLLOWING.16.aspx

169. Tan XW, Lakshminarayanan R, Liu SP, Goh E, Tan D, Beuerman RW, et al. Dual functionalization of titanium with vascular endothelial growth factor and β-defensin analog for potential application in keratoprosthesis. J Biomed Mater Res Part B Appl Biomater [Internet]. 2012;100B(8):2090–100. Available from: http://dx.doi.org/10.1002/jbm.b.32774

170. Holland T, Tabata Y, Mikos A. In vitro release of transforming growth factor-β1 from gelatin microparticles encapsulated in biodegradable, injectable oligo(poly(ethylene glycol) fumarate) hydrogels. J Control Release [Internet]. 2003;91(3):299–313. Available from: http://www.sciencedirect.com/science/article/pii/S016836590300258X

171. Kempen DH, Lu L, Hefferan TE, Creemers LB, Maran A, Classic KL, et al. Retention of in vitro and in vivo BMP-2 bioactivities in sustained delivery vehicles for bone tissue engineering. Biomaterials [Internet]. 2008;29(22):3245–52. Available from: https://www.ncbi.nlm.nih.gov/pubmed/18472153

172. Burdick JA, Ward M, Liang E, Young MJ, Langer R. Stimulation of neurite outgrowth

by neurotrophins delivered from degradable hydrogels. Biomaterials [Internet]. 2006;27(3):452–9. Available from: http://www.sciencedirect.com/science/article/pii/S0142961205006265

173. Holland TA, Tabata Y, Mikos AG. Dual growth factor delivery from degradable oligo(poly(ethylene glycol) fumarate) hydrogel scaffolds for cartilage tissue engineering. J Control Release [Internet]. 2005;101(1):111–25. Available from: http://www.sciencedirect.com/science/article/pii/S016836590400313X

174. Holland TA, Bodde EWH, Cuijpers VMJI, Baggett LS, Tabata Y, Mikos AG, et al. Degradable hydrogel scaffolds for in vivo delivery of single and dual growth factors in cartilage repair. Osteoarthr Cartil [Internet]. 2007;15(2):187–97. Available from: http://www.sciencedirect.com/science/article/pii/S1063458406002317

175. Kanczler JM, Ginty PJ, White L, Clarke NMP, Howdle SM, Shakesheff KM, et al. The effect of the delivery of vascular endothelial growth factor and bone morphogenic protein-2 to osteoprogenitor cell populations on bone formation. Biomaterials [Internet]. 2010;31(6):1242–50. Available from: http://www.sciencedirect.com/science/article/pii/S0142961209011806

176. Kim S, Kang Y, Krueger CA, Sen M, Holcomb JB, Chen D, et al. Sequential delivery of BMP-2 and IGF-1 using a chitosan gel with gelatin microspheres enhances early osteoblastic differentiation. Acta Biomater [Internet]. 2012;8(5):1768–77. Available from: http://www.sciencedirect.com/science/article/pii/S1742706112000165

177. Shah NJ, Macdonald ML, Beben YM, Padera RF, Samuel RE, Hammond PT. Tunable dual growth factor delivery from polyelectrolyte multilayer films. Biomaterials [Internet]. 2011;32(26):6183–93. Available from: http://www.sciencedirect.com/science/article/pii/S0142961211004431

178. Kempen DHR, Lu L, Heijink A, Hefferan TE, Creemers LB, Maran A, et al. Effect of local sequential VEGF and BMP-2 delivery on ectopic and orthotopic bone regeneration. Biomaterials [Internet]. 2009;30(14):2816–25. Available from: http://www.sciencedirect.com/science/article/pii/S0142961209000520

179. Wang S, Ju W, Shang P, Lei L, Nie H. Core-shell microspheres delivering FGF-2 and

BMP-2 in different release patterns for bone regeneration. J Mater Chem B [Internet]. 2015;3(9):1907–20. Available from: http://dx.doi.org/10.1039/C4TB01876A

180. Raiche AT, Puleo DA. In vitro effects of combined and sequential delivery of two bone growth factors. Biomaterials [Internet]. 2004;25(4):677–85. Available from: http://www.sciencedirect.com/science/article/pii/S0142961203005647

181. Lu S, Lam J, Trachtenberg JE, Lee EJ, Seyednejad H, van den Beucken JJJP, et al. Dual growth factor delivery from bilayered, biodegradable hydrogel composites for spatially-guided osteochondral tissue repair. Biomaterials [Internet]. 2014;35(31):8829–39. Available from: http://www.sciencedirect.com/science/article/pii/S0142961214007881

182. Poldervaart MT, Gremmels H, van Deventer K, Fledderus JO, Öner FC, Verhaar MC, et al. Prolonged presence of VEGF promotes vascularization in 3D bioprinted scaffolds with defined architecture. J Control Release [Internet]. 2014;184:58–66. Available from: http://www.sciencedirect.com/science/article/pii/S0168365914002119

183. Byambaa B, Annabi N, Yue K, Trujillo-de Santiago G, Alvarez MM, Jia W, et al. Bioprinted Osteogenic and Vasculogenic Patterns for Engineering 3D Bone Tissue. Adv Healthc Mater [Internet]. 2017;6(16):1700015-n/a. Available from: http://dx.doi.org/10.1002/adhm.201700015

184. Moshfeghi AA, Peyman GA. Micro- and nanoparticulates. Adv Drug Deliv Rev [Internet]. 2005;57(14):2047–52. Available from: http://www.sciencedirect.com/science/article/pii/S0169409X05001663

185. Panyam J, Labhasetwar V. Biodegradable nanoparticles for drug and gene delivery to cells and tissue. Adv Drug Deliv Rev [Internet]. 2003;55(3):329–47. Available from: http://www.sciencedirect.com/science/article/pii/S0169409X02002284

186. Lauzon MA, Daviau A, Marcos B, Faucheux N. Nanoparticle-mediated growth factor delivery systems: A new way to treat Alzheimer's disease. J Control Release [Internet]. 2015;206:187–205. Available from: https://www.ncbi.nlm.nih.gov/pubmed/25804873

187. Faustino C, Rijo P, Reis CP. Nanotechnological strategies for nerve growth factor

delivery: Therapeutic implications in Alzheimer's disease. Pharmacol Res [Internet]. 2017;120:68–87. Available from: http://www.sciencedirect.com/science/article/pii/S1043661816311094

188. Chappell JC, Song J, Burke CW, Klibanov AL, Price RJ. Targeted Delivery of Nanoparticles Bearing Fibroblast Growth Factor-2 by Ultrasonic Microbubble Destruction for Therapeutic Arteriogenesis. Small [Internet]. 2008;4(10):1769–77. Available from: http://dx.doi.org/10.1002/smll.200800806

189. Béduneau A, Saulnier P, Benoit J-P. Active targeting of brain tumors using nanocarriers. Biomaterials [Internet]. 2007;28(33):4947–67. Available from: http://www.sciencedirect.com/science/article/pii/S0142961207004656

190. Blasi P, Giovagnoli S, Schoubben A, Ricci M, Rossi C. Solid lipid nanoparticles for targeted brain drug delivery. Adv Drug Deliv Rev [Internet]. 2007;59(6):454–77. Available from: http://www.sciencedirect.com/science/article/pii/S0169409X07000427

191. Copland MJ, Rades T, Davies NM, Baird MA. Lipid based particulate formulations for the delivery of antigen. Immunol Cell Biol [Internet]. 2005;83:97. Available from: http://dx.doi.org/10.1111/j.1440-1711.2005.01315.x

192. Wang Z, Wang Z, Lu WW, Zhen W, Yang D, Peng S. Novel biomaterial strategies for controlled growth factor delivery for biomedical applications. Npg Asia Mater [Internet]. 2017;9:e435. Available from: http://dx.doi.org/10.1038/am.2017.171

193. Zhou X, Feng W, Qiu K, Chen L, Wang W, Nie W, et al. BMP-2 Derived Peptide and Dexamethasone Incorporated Mesoporous Silica Nanoparticles for Enhanced Osteogenic Differentiation of Bone Mesenchymal Stem Cells. ACS Appl Mater Interfaces [Internet]. 2015;7(29):15777–89. Available from: http://dx.doi.org/10.1021/acsami.5b02636

194. Horcajada P, Rámila A, Pérez-Pariente J, Vallet R, x, M. Influence of pore size of MCM-41 matrices on drug delivery rate. Microporous Mesoporous Mater [Internet]. 2004;68(1):105–9. Available from: http://www.sciencedirect.com/science/article/pii/S1387181103007054

195. Bhattacharyya S, Wang H, Ducheyne P. Polymer-coated mesoporous silica nanoparticles for the controlled release of macromolecules. Acta Biomater [Internet]. 2012;8(9):3429–35. Available from: http://www.sciencedirect.com/science/article/pii/S1742706112002516

196. Wu Q, Liu C, Fan L, Shi J, Liu Z, Li R, et al. Heparinized magnetic mesoporous silica nanoparticles as multifunctional growth factor delivery carriers. Nanotechnology. 2012 Nov 6;23:485703.

197. Bose S, Tarafder S. Calcium phosphate ceramic systems in growth factor and drug delivery for bone tissue engineering: A review. Acta Biomater [Internet]. 2012;8(4):1401–21. Available from: http://www.sciencedirect.com/science/article/pii/S1742706111005046

198. Chen W, Palazzo A, Hennink WE, Kok RJ. Effect of Particle Size on Drug Loading and Release Kinetics of Gefitinib-Loaded PLGA Microspheres. Mol Pharm [Internet]. 2017;14(2):459–67. Available from: http://dx.doi.org/10.1021/acs.molpharmaceut.6b00896

199. Park CJ, Clark SG, Lichtensteiger CA, Jamison RD, Johnson AJW. Accelerated wound closure of pressure ulcers in aged mice by chitosan scaffolds with and without bFGF. Acta Biomater [Internet]. 2009;5(6):1926–36. Available from: http://www.sciencedirect.com/science/article/pii/S1742706109000993

200. Liu Q, Huang Y, Lan Y, Zuo Q, Li C, Zhang Y, et al. Acceleration of skin regeneration in full-thickness burns by incorporation of bFGF-loaded alginate microspheres into a CMCS–PVA hydrogel. J Tissue Eng Regen Med [Internet]. 2017;11(5):1562–73. Available from: http://dx.doi.org/10.1002/term.2057

201. Ribeiro MP, Morgado PI, Miguel SP, Coutinho P, Correia IJ. Dextran-based hydrogel containing chitosan microparticles loaded with growth factors to be used in wound healing. Mater Sci Eng C [Internet]. 2013;33(5):2958–66. Available from: http://www.sciencedirect.com/science/article/pii/S0928493113001872

202. Ruhe PQ, Hedberg EL, Padron NT, Spauwen PHM, Jansen JA, Mikos AG. rhBMP-2 Release from Injectable Poly(DL-Lactic-co-glycolic Acid)/ Calcium-Phosphate

Cement Composites. J Bone Jt Surgery, Am Vol [Internet]. 2003;85:75. Available from: http://search.ebscohost.com/login.aspx?direct=true&db=a9h&AN=10374380&site=ehost-live&scope=site

203. Nof M, Shea LD. Drug-releasing scaffolds fabricated from drug-loaded microspheres. J Biomed Mater Res [Internet]. 2002;59(2):349–56. Available from: http://dx.doi.org/10.1002/jbm.1251

204. Ennett AB, Kaigler D, Mooney DJ. Temporally regulated delivery of VEGF in vitro and in vivo. J Biomed Mater Res Part A [Internet]. 2006;79A(1):176–84. Available from: http://dx.doi.org/10.1002/jbm.a.30771

205. Davoodi P, Ng WC, Yan WC, Srinivasan MP, Wang C-H. Double-Walled Microparticles-Embedded Self-Cross-Linked, Injectable, and Antibacterial Hydrogel for Controlled and Sustained Release of Chemotherapeutic Agents. ACS Appl Mater Interfaces [Internet]. 2016;8(35):22785–800. Available from: http://dx.doi.org/10.1021/acsami.6b03041

206. Hua N, Sun J. Body distribution of poly(d,l-lactide-co-glycolide) copolymer degradation products in rats. J Mater Sci Mater Med [Internet]. 2008;19(10):3243–8. Available from: https://doi.org/10.1007/s10856-008-3460-z

207. Sinha VR, Trehan A. Biodegradable microspheres for protein delivery. J Control Release [Internet]. 2003;90(3):261–80. Available from: http://www.sciencedirect.com/science/article/pii/S0168365903001949

208. Lee SH, Shin H. Matrices and scaffolds for delivery of bioactive molecules in bone and cartilage tissue engineering. Adv Drug Deliv Rev [Internet]. 2007;59(4):339–59. Available from: http://www.sciencedirect.com/science/article/pii/S0169409X07000324

209. Nevins M, Giannobile W V, McGuire MK, Kao RT, Mellonig JT, Hinrichs JE, et al. Platelet-Derived Growth Factor Stimulates Bone Fill and Rate of Attachment Level Gain: Results of a Large Multicenter Randomized Controlled Trial. J Periodontol [Internet]. 2005;76(12):2205–15. Available from: http://dx.doi.org/10.1902/jop.2005.76.12.2205

210. McGuire MK, Scheyer ET, Schupbach P. Growth Factor–Mediated Treatment of Recession Defects: A Randomized Controlled Trial and Histologic and Microcomputed Tomography Examination. J Periodontol [Internet]. 2009;80(4):550–64. Available from: http://dx.doi.org/10.1902/jop.2009.080502

211. Thakare K, Deo V. Randomized controlled clinical study of rhPDGF-BB + β-TCP versus HA + β-TCP for the treatment of infrabony periodontal defects: clinical and radiographic results. Int J Periodontics Restor Dent. 2012;32(6):689–96.

212. Deshpande A, Koudale SB, Bhongade LM. A Comparative Evaluation of rhPDGF-BB + β-TCP and Subepithelial Connective Tissue Graft for the Treatment of Multiple Gingival Recession Defects in Humans. Periodontics Restor Dentristy. 2014;34(2):241–9.

213. Maroo S, Murthy KR. Treatment of Periodontal Intrabony Defects Using β-TCP Alone or in Combination with rhPDGF-BB: A Randomized Controlled Clinical and Radiographic Study. Periodontics Restor Dentristy. 2014;34(6):841–7.

214. Cochran DL, Oh TJ, Mills MP, Clem DS, McClain PK, Schallhorn RA, et al. A Randomized Clinical Trial Evaluating rh-FGF-2/β-TCP in Periodontal Defects. J Dent Res [Internet]. 2016;95(5):523–30. Available from: https://doi.org/10.1177/0022034516632497

215. Windisch P, Stavropoulos A, Molnár B, Szendröi-Kiss D, Szilágyi E, Rosta P, et al. A phase IIa randomized controlled pilot study evaluating the safety and clinical outcomes following the use of rhGDF-5/β-TCP in regenerative periodontal therapy. Clin Oral Investig [Internet]. 2012;16(4):1181–9. Available from: https://doi.org/10.1007/s00784-011-0610-3

216. Tong X, Lee S, Bararpour L, Yang F. Long-Term Controlled Protein Release from Poly(Ethylene Glycol) Hydrogels by Modulating Mesh Size and Degradation. Macromol Biosci [Internet]. 2015;15(12):1679–86. Available from: https://www.ncbi.nlm.nih.gov/pubmed/26259711

217. Lee F, Chung JE, Kurisawa M. An injectable hyaluronic acid–tyramine hydrogel system for protein delivery. J Control Release [Internet]. 2009;134(3):186–93.

Available from: http://www.sciencedirect.com/science/article/pii/S0168365908007773

218. Klotz BJ, Gawlitta D, Rosenberg AJWP, Malda J, Melchels FPW. Gelatin-Methacryloyl Hydrogels: Towards Biofabrication-Based Tissue Repair. Trends Biotechnol [Internet]. 2016;34(5):394–407. Available from: http://www.sciencedirect.com/science/article/pii/S0167779916000159

219. Nguyen AH, McKinney J, Miller T, Bongiorno T, McDevitt TC. Gelatin methacrylate microspheres for controlled growth factor release. Acta Biomater [Internet]. 2015;13:101–10. Available from: http://www.sciencedirect.com/science/article/pii/S1742706114005224

220. Simmons CA, Alsberg E, Hsiong S, Kim WJ, Mooney DJ. Dual growth factor delivery and controlled scaffold degradation enhance in vivo bone formation by transplanted bone marrow stromal cells. Bone [Internet]. 2004;35(2):562–9. Available from: http://www.sciencedirect.com/science/article/pii/S8756328204000882

221. Song H-HG, Rumma RT, Ozaki CK, Edelman ER, Chen CS. Vascular Tissue Engineering: Progress, Challenges, and Clinical Promise. Cell Stem Cell [Internet]. 2018 Mar 1;22(3):340–54. Available from: https://www.ncbi.nlm.nih.gov/pubmed/29499152

222. Xu J, Shi G-P. Vascular wall extracellular matrix proteins and vascular diseases. Biochim Biophys Acta [Internet]. 2014/07/18. 2014 Nov;1842(11):2106–19. Available from: https://www.ncbi.nlm.nih.gov/pubmed/25045854

223. Melchels FPW, Domingos MAN, Klein TJ, Malda J, Bartolo PJ, Hutmacher DW. Additive manufacturing of tissues and organs. Prog Polym Sci [Internet]. 2012;37(8):1079–104. Available from: http://dx.doi.org/10.1016/j.progpolymsci.2011.11.007

224. Miller JS, Stevens KR, Yang MT, Baker BM, Nguyen D-HT, Cohen DM, et al. Rapid casting of patterned vascular networks for perfusable engineered three-dimensional tissues. Nat Mater [Internet]. 2012;11(9):768–74. Available from: https://doi.org/10.1038/nmat3357

225. Bertassoni LE, Cecconi M, Manoharan V, Nikkhah M, Hjortnaes J, Cristino AL, et al.

Hydrogel bioprinted microchannel networks for vascularization of tissue engineering constructs. Lab Chip [Internet]. 2014;14(13):2202–11. Available from: http://dx.doi.org/10.1039/C4LC00030G

226. Abaci HE, Guo Z, Coffman A, Gillette B, Lee W, Sia SK, et al. Human Skin Constructs with Spatially Controlled Vasculature Using Primary and iPSC-Derived Endothelial Cells. Adv Healthc Mater [Internet]. 2016 Jul 1;5(14):1800–7. Available from: https://doi.org/10.1002/adhm.201500936

227. Lee VK, Lanzi AM, Ngo H, Yoo SS, Vincent PA, Dai G. Generation of multi-scale vascular network system within 3D hydrogel using 3D bio-printing technology. Cell Mol Bioeng. 2014;7(3):460–72.

228. Kolesky DB, Homan KA, Skylar-Scott MA, Lewis JA. Three-dimensional bioprinting of thick vascularized tissues. Proc Natl Acad Sci [Internet]. 2016 Mar 22;113(12):3179 LP – 3184. Available from: http://www.pnas.org/content/113/12/3179.abstract

229. Justin AW, Brooks RA, Markaki AE. Multi-casting approach for vascular networks in cellularized hydrogels. J R Soc Interface. 2016;13(125).

230. Heintz KA, Bregenzer ME, Mantle JL, Lee KH, West JL, Slater JH. Fabrication of 3D Biomimetic Microfluidic Networks in Hydrogels. Adv Healthc Mater [Internet]. 2016 Sep 1;5(17):2153–60. Available from: https://doi.org/10.1002/adhm.201600351

231. Brown TE, Marozas IA, Anseth KS. Amplified Photodegradation of Cell-Laden Hydrogels via an Addition–Fragmentation Chain Transfer Reaction. Adv Mater [Internet]. 2017 Mar 1;29(11):1605001. Available from: https://doi.org/10.1002/adma.201605001

232. Redd MA, Zeinstra N, Qin W, Wei W, Martinson A, Wang Y, et al. Patterned human microvascular grafts enable rapid vascularization and increase perfusion in infarcted rat hearts. Nat Commun [Internet]. 2019;10(1). Available from: http://dx.doi.org/10.1038/s41467-019-08388-7

233. Zheng Y, Chen J, Craven M, Choi NW, Totorica S, Diaz-Santana A, et al. In vitro microvessels for the study of angiogenesis and thrombosis. Proc Natl Acad Sci U S A. 2012;109(24):9342–7.

234. Zhang B, Montgomery M, Chamberlain MD, Ogawa S, Korolj A, Pahnke A, et al. Biodegradable scaffold with built-in vasculature for organ-on-a-chip engineering and direct surgical anastomosis. Nat Mater [Internet]. 2016;15(6):669–78. Available from: https://doi.org/10.1038/nmat4570

235. Alimperti S, Mirabella T, Bajaj V, Polacheck W, Pirone DM, Duffield J, et al. Three-dimensional biomimetic vascular model reveals a RhoA, Rac1, and N-cadherin balance in mural cell–endothelial cell-regulated barrier function. Proc Natl Acad Sci [Internet]. 2017 Aug 15;114(33):8758 LP – 8763. Available from: http://www.pnas.org/content/114/33/8758.abstract

236. Kim S, Lee H, Chung M, Jeon NL. Engineering of functional, perfusable 3D microvascular networks on a chip. Lab Chip [Internet]. 2013;13(8):1489–500. Available from: http://dx.doi.org/10.1039/C3LC41320A

237. Galie PA, Nguyen D-HT, Choi CK, Cohen DM, Janmey PA, Chen CS. Fluid shear stress threshold regulates angiogenic sprouting. Proc Natl Acad Sci [Internet]. 2014 Jun 3;111(22):7968 LP – 7973. Available from: http://www.pnas.org/content/111/22/7968.abstract

238. Lesman A, Koffler J, Atlas R, Blinder YJ, Kam Z, Levenberg S. Engineering vessel-like networks within multicellular fibrin-based constructs. Biomaterials [Internet]. 2011;32(31):7856–69. Available from: http://www.sciencedirect.com/science/article/pii/S0142961211007745

239. Wimmer RA, Leopoldi A, Aichinger M, Wick N, Hantusch B, Novatchkova M, et al. Human blood vessel organoids as a model of diabetic vasculopathy. Nature [Internet]. 2019;565(7740):505–10. Available from: http://dx.doi.org/10.1038/s41586-018-0858-8

240. Chen X, Aledia AS, Ghajar CM, Griffith CK, Putnam AJ, Hughes CCW, et al. Prevascularization of a Fibrin-Based Tissue Construct Accelerates the Formation of Functional Anastomosis with Host Vasculature. Tissue Eng Part A [Internet]. 2008 Oct 24;15(6):1363–71. Available from: https://doi.org/10.1089/ten.tea.2008.0314

241. Freiman A, Shandalov Y, Rozenfeld D, Shor E, Segal S, Ben-David D, et al. Adipose-

derived endothelial and mesenchymal stem cells enhance vascular network formation on three-dimensional constructs in vitro. Stem Cell Res Ther [Internet]. 2016;7(1):5. Available from: https://doi.org/10.1186/s13287-015-0251-6

242. Blinder YJ, Freiman A, Raindel N, Mooney DJ, Levenberg S. Vasculogenic dynamics in 3D engineered tissue constructs. Sci Rep [Internet]. 2015;5:17840. Available from: https://www.ncbi.nlm.nih.gov/pubmed/26648270

243. Davis GE, Speichinger KR, Norden PR, Kim DJ, Bowers SLK. Endothelial Cell Polarization During Lumen Formation, Tubulogenesis, and Vessel Maturation in 3D Extracellular Matrices BT - Cell Polarity 1: Biological Role and Basic Mechanisms. In: Ebnet K, editor. Cham: Springer International Publishing; 2015. p. 205–20. Available from: https://doi.org/10.1007/978-3-319-14463-4_9

244. Morgan JT, Shirazi J, Comber EM, Eschenburg C, Gleghorn JP. Fabrication of centimeter-scale and geometrically arbitrary vascular networks using in vitro self-assembly. Biomaterials [Internet]. 2019;189(July 2018):37–47. Available from: https://doi.org/10.1016/j.biomaterials.2018.10.021

245. Moya ML, Hsu YH, Lee AP, Christopher CWH, George SC. In vitro perfused human capillary networks. Tissue Eng - Part C Methods. 2013;19(9):730–7.

246. Juliar BA, Keating MT, Kong YP, Botvinick EL, Putnam AJ. Sprouting angiogenesis induces significant mechanical heterogeneities and ECM stiffening across length scales in fibrin hydrogels. Biomaterials [Internet]. 2018;162:99–108. Available from: https://www.ncbi.nlm.nih.gov/pubmed/29438884

247. Gilbert-Honick J, Iyer SR, Somers SM, Lovering RM, Wagner K, Mao HQ, et al. Engineering functional and histological regeneration of vascularized skeletal muscle. Biomaterials [Internet]. 2018;164:70–9. Available from: https://doi.org/10.1016/j.biomaterials.2018.02.006

248. Landau S, Guo S, Levenberg S. Localization of Engineered Vasculature within 3D Tissue Constructs. Front Bioeng Biotechnol [Internet]. 2018;6:2. Available from: https://www.ncbi.nlm.nih.gov/pubmed/29404324

249. White SM, Pittman CR, Hingorani R, Arora R, Esipova T V, Vinogradov SA, et al.

Implanted cell-dense prevascularized tissues develop functional vasculature that supports reoxygenation after thrombosis. Tissue Eng Part A [Internet]. 2014;20(17–18):2316–28. Available from: https://www.ncbi.nlm.nih.gov/pubmed/24593148

250. Klotz BJ, Lim KS, Chang YX, Soliman BG, Pennings I, Melchels FPW, et al. Engineering of a complex bone tissue model with endothelialised channels and capillary-like networks. Eur Cell Mater [Internet]. 2018;35:335–48. Available from: https://www.ncbi.nlm.nih.gov/pubmed/29873804

251. Chen YC, Lin RZ, Qi H, Yang Y, Bae H, Melero-Martin JM, et al. Functional Human Vascular Network Generated in Photocrosslinkable Gelatin Methacrylate Hydrogels. Adv Funct Mater [Internet]. 2012;22(10):2027–39. Available from: https://www.ncbi.nlm.nih.gov/pubmed/22907987

252. Peters EB, Christoforou N, Leong KW, Truskey GA, West JL. Poly(ethylene glycol) Hydrogel Scaffolds Containing Cell-Adhesive and Protease-Sensitive Peptides Support Microvessel Formation by Endothelial Progenitor Cells. Cell Mol Bioeng [Internet]. 2015/10/20. 2016 Mar 1;9(1):38–54. Available from: https://www.ncbi.nlm.nih.gov/pubmed/27042236

253. Calderon GA, Thai P, Hsu CW, Grigoryan B, Gibson SM, Dickinson ME, et al. Tubulogenesis of co-cultured human iPS-derived endothelial cells and human mesenchymal stem cells in fibrin and gelatin methacrylate gels. Biomater Sci. 2017;5(8):1652–60.

254. Stratesteffen H, Köpf M, Kreimendahl F, Blaeser A, Jockenhoevel S, Fischer H. GelMA-collagen blends enable drop-on-demand 3D printablility and promote angiogenesis. Biofabrication [Internet]. 2017;9(4):45002. Available from: http://dx.doi.org/10.1088/1758-5090/aa857c

255. Edgar LT, Underwood CJ, Guilkey JE, Hoying JB, Weiss JA. Extracellular Matrix Density Regulates the Rate of Neovessel Growth and Branching in Sprouting Angiogenesis. PLoS One [Internet]. 2014 Jan 22;9(1):e85178. Available from: https://doi.org/10.1371/journal.pone.0085178

256. Klotz BJ, Oosterhoff LA, Utomo L, Lim KS, Vallmajo-Martin Q, Clevers H, et al. A

Versatile Biosynthetic Hydrogel Platform for Engineering of Tissue Analogues. Adv Healthc Mater [Internet]. 2019 Oct 1;8(19):1900979. Available from: https://doi.org/10.1002/adhm.201900979

257. Mirabella T, MacArthur JW, Cheng D, Ozaki CK, Woo YJ, Yang MT, et al. 3D-printed vascular networks direct therapeutic angiogenesis in ischaemia. Nat Biomed Eng [Internet]. 2017;1(6):83. Available from: https://doi.org/10.1038/s41551-017-0083

258. Stevens KR, Scull MA, Ramanan V, Fortin CL, Chaturvedi RR, Knouse KA, et al. In situ expansion of engineered human liver tissue in a mouse model of chronic liver disease. Sci Transl Med [Internet]. 2017 Jul 19;9(399):eaah5505. Available from: https://www.ncbi.nlm.nih.gov/pubmed/28724577

259. Baranski JD, Chaturvedi RR, Stevens KR, Eyckmans J, Carvalho B, Solorzano RD, et al. Geometric control of vascular networks to enhance engineered tissue integration and function. Proc Natl Acad Sci [Internet]. 2013 May 7;110(19):7586 LP – 7591. Available from: http://www.pnas.org/content/110/19/7586.abstract

260. Levenberg S, Golub JS, Amit M, Itskovitz-Eldor J, Langer R. Endothelial cells derived from human embryonic stem cells. Proc Natl Acad Sci [Internet]. 2002 Apr 2;99(7):4391 LP – 4396. Available from: http://www.pnas.org/content/99/7/4391.abstract

261. Chen X, Aledia AS, Popson SA, Him L, Hughes CCW, George SC. Rapid anastomosis of endothelial progenitor cell-derived vessels with host vasculature is promoted by a high density of cotransplanted fibroblasts. Tissue Eng Part A [Internet]. 2010 Feb;16(2):585–94. Available from: https://www.ncbi.nlm.nih.gov/pubmed/19737050

262. Sekine H, Shimizu T, Sakaguchi K, Dobashi I, Wada M, Yamato M, et al. In vitro fabrication of functional three-dimensional tissues with perfusable blood vessels. Nat Commun [Internet]. 2013;4(1):1399. Available from: https://doi.org/10.1038/ncomms2406

263. Ben-Shaul S, Landau S, Merdler U, Levenberg S. Mature vessel networks in engineered tissue promote graft–host anastomosis and prevent graft thrombosis. Proc

Natl Acad Sci [Internet]. 2019 Feb 19;116(8):2955 LP – 2960. Available from: http://www.pnas.org/content/116/8/2955.abstract

264. Groll J, Boland T, Blunk T, Burdick JA, Cho D-W, Dalton PD, et al. Biofabrication: reappraising the definition of an evolving field. Biofabrication [Internet]. 2016;8(1):13001. Available from: http://dx.doi.org/10.1088/1758-5090/8/1/013001

265. Kundu J, Shim J-H, Jang J, Kim S-W, Cho D-W. An additive manufacturing-based PCL–alginate–chondrocyte bioprinted scaffold for cartilage tissue engineering. J Tissue Eng Regen Med [Internet]. 2015 Nov 1;9(11):1286–97. Available from: https://doi.org/10.1002/term.1682

266. Shim J-H, Jang K-M, Hahn SK, Park JY, Jung H, Oh K, et al. Three-dimensional bioprinting of multilayered constructs containing human mesenchymal stromal cells for osteochondral tissue regeneration in the rabbit knee joint. Biofabrication [Internet]. 2016;8(1):14102. Available from: http://dx.doi.org/10.1088/1758-5090/8/1/014102

267. Cornock R, Beirne S, Thompson B, Wallace GG. Coaxial additive manufacture of biomaterial composite scaffolds for tissue engineering. Biofabrication [Internet]. 2014;6(2):25002. Available from: http://stacks.iop.org/1758-5090/6/i=2/a=025002

268. Schuurman W, Khristov V, Pot MW, van Weeren PR, Dhert WJA, Malda J. Bioprinting of hybrid tissue constructs with tailorable mechanical properties. Biofabrication [Internet]. 2011;3(2):21001. Available from: http://dx.doi.org/10.1088/1758-5082/3/2/021001

269. Mekhileri N V, Lim K, Brown GCJ, Mutreja I, Schon BS, Hooper GJ, et al. Automated 3D bioassembly of micro-tissues for biofabrication of hybrid tissue engineered constructs. Biofabrication [Internet]. 2017; Available from: https://www.ncbi.nlm.nih.gov/pubmed/29199637

270. Epstein NE. Complications due to the use of BMP/INFUSE in spine surgery: The evidence continues to mount. Surg Neurol Int. 2013;

Chapter 3. Visible Light Mediated PVA-Tyramine Hydrogels for Covalent Incorporation and Controlled Release of Functional Growth Factors

3.1. Introduction

Growth factors (GFs) play critical roles in the development, function and repair of native tissues such a skin, bone and cartilage, which has made them attractive therapeutic agents for regenerative medicine applications. Specifically, GFs such as vascular endothelial growth factor (VEGF), basic fibroblast growth factor (bFGF) and brain-derived growth factor (BDNF) have undergone pre-clinical and clinical trials for a range of applications including treatment of diabetic foot ulcers (1), skin burns (2), bone fractures (3) and strokes (4). Direct injection or application of GFs into the targeted area either results in limited therapeutic effects or requires very high dosage, resulting in risk of side effects such as oncogenesis (5,6) or local edema (7). This is due to their short half-life in the physiological environment, which can last from minutes to a few hours (2,8). Using biomaterials as delivery vehicles widens the release time frame and protects GFs from the physiological environment, increasing their half-life (9). Several biomaterials have been investigated as GF delivery vehicles, from which collagen and calcium phosphate-based scaffolds have had some clinical success due to their biocompatibility and inherent bioactivity (10,11). Albeit some of these products have reached the market, there is still a need to optimise GF delivery methods to achieve improved bioactivity and reduce the risk of side effects caused by GFs.

Achieving controlled delivery of GFs in a way that resembles their natural expression patterns has shown potential to further improve their effectiveness (12–15). Achieving this level of control over the release profile has, however, proven to be a complicated task, especially when targeting long-term release. This is due to the current unmet limitations in methods to incorporate GFs into biomaterials. Adsorption and entrapment are simple methods but result in burst release profiles and inefficient incorporation (16,17). On the other hand,

stable covalent incorporation provides a more tailorable, longer term release profile, but generally requires prior chemical modification of the GFs, reducing their bioactivity with unnecessary complications (18). Other methods relying on bioaffinity are driven by the ability of specific GFs to bind molecules such as heparin to achieve longer term release, but depend on GF specificity to binding complexes (19). Thus, the ideal incorporation method should be simple to lower the production costs and facilitate clinical translation, but still result in controllable long-term release for the adaptation to different regenerative therapies without relying on highly specific interactions that limit their applicability.

With inspiration drawn from naturally-occurring di-tyrosine cross-links, different hydrogel systems have been developed and used for tissue engineering and regenerative medicine applications (20). Tyraminated hyaluronic acid (HA-Tyr) cross-linked with horseradish peroxidase (HRP) has been applied for rheumatoid arthritis (21) and bone regeneration (22). Tyraminated dextran (Dex-Tyr), also cross-linked using HRP, has been studied for cartilage regeneration (23). A distinct characteristic of these formulations is their ability to form bi-phenol cross-links with native tyrosine groups present in proteins, resulting in enhanced tissue adhesion (24,25). Lim *et al*. have previously shown that tyraminated poly-vinyl-alcohol (PVA-Tyr) is able to covalently incorporate native gelatin and sericin during the cross-linking process, improving cell survival, attachment and proliferation of encapsulated cells (26,27). The presence of ester bonds in PVA-Tyr results in a hydrolytically degradable hydrogel (28), and a visible light initiating reaction consisting of Ruthenium (Ru) and sodium persulfate (SPS) enables the formation of bi-phenol cross-links in a rapid and controllable manner (28,29). It is therefore hypothesised that this PVA-Tyr system could enable covalent incorporation of GFs through their native tyrosine moieties without the need of additional chemical modification. GFs will then be released through hydrolytic degradation of the hydrogel network following a tailorable degradation profile. The combination of these characteristics result in a delivery system that facilitates a simple and rapid covalent incorporation of GFs without the need of prior chemical modification into a hydrogel system, where the subsequent release profile can be tailored depending on the degradation profile of the base hydrogel network.

In the present study, the potential of the PVA-Tyr system as a GF delivery platform is systematically evaluated. Mass loss studies are used to explore the range of degradation profiles that can be obtained by changing the cross-linking conditions of PVA-Tyr. A range of GFs are then incorporated within PVA-Tyr hydrogels and study their release profile.

Finally, *in vitro* studies are used to determine the functionality of released growth factors on endothelial cells and mesenchymal stem cells.

3.2. Materials and Methods

3.2.1. Materials

PVA (13–23 kDa, 98% hydrolyzed), Dimethyl sulfoxide, succinic anhydride (SA), triethylamine (TEA), 1,3-Dicyclohexylcarbodiimide (DCC), N-hydroxysuccinimide (NHS), Tyramine, sodium persulphate (SPS), 1,1-carbonyldiimidazole, tris(2,2-bipyridyl)dichlororuthenium(II) hexahydrate (Ru), molecular sieves (4 A °) and Phosphate buffered saline (PBS), dialysis tubing (10 kDa molecular weight cutoff), were purchased from Sigma-Aldrich and used as received. BSA-Texas Red conjugate was purchased from Invitrogen. rhVEGF-165 was purchased from Gibco (PHC9394). bFGF and was purchased from R&D Systems (P09038). BDNF was purchased from Peprotech (540-02). Human umbilical vein endothelial cells (HUVEC), vascular cell basal medium, endothelial cell growth kit-VEGF, trypsin for primary cells and trypsin neutralizing solution were purchased from ATCC. Human bone marrow-derived mesenchymal stem cells (MSCs) were purchased from RoosterBio. Alpha-MEM, Fetal bovine serum (FBS), Trypsin and Penicillin/streptomycin were purchased from Gibco.

3.2.2. Methods

3.2.2.1. Synthesis of PVA-Tyr

PVA-Tyr was synthesised according to a two-step reaction previously published (26). Briefly, carboxyl groups were conjugated onto the PVA backbone using SA and TEA in DMSO. To modify the degree of carboxylation, the reaction was performed at different ratios of SA to PVA (Figure 3.2A) while maintaining the ratio of TEA to SA at 0.73 mL/g. Tyr moieties were then conjugated to the carboxylated PVA (PVA-COOH) using a carbodiimide-coupling reaction. DCC, NHS and Tyramine were added to the reaction at three times the molar concentration of the targeted carboxyl groups from PVA-COOH. The by-product (dicyclohexylurea) formed during the reaction was removed using vacuum filtration. The resulting PVA-Tyr solution was further purified by dialysis against water and freeze-dried. The resulting amounts of carboxyl groups in PVA-COOH and tyramine groups in PVA-Tyr were quantified using ^{1}H NMR.

3.2.2.2. Hydrogel Fabrication

Dried PVA-Tyr was dissolved in PBS at 80 °C. Upon complete dissolution, the polymer solution was cooled to room temperature (RT) and mixed with Ru and SPS stock solutions to a final concentration of 5 to 20 PVA-Tyr wt% and 0.5/5 to 2/20 mM Ru/SPS. BSA or growth factor solutions were mixed with the PVA-Tyr solution prior to the addition of Ru and SPS. BSA hydrogels were obtained by mixing a 10 wt% BSA solution with Ru and SPS stock solutions to a final concentration of 2/20 mM Ru/SPS. All samples were photo-cross-linked using visible light (OmniCure® S1500, Excelitas Technologies with a Rosco IR/UV filter 400 – 450nm, 3min, 30 mW cm^{-2}) in cylindrical moulds (h = 1 mm, Ø = 6 mm) in an open environment.

3.2.2.3. Swelling and Mass Loss Assays

After cross-linking, each hydrogel (35 µL) was weighed ($m_{initial,t0}$), out of which three samples per hydrogel composition were directly freeze-dried to record their initial dry weights ($m_{dry,t0}$) and determine the actual macromer weight fraction, which is reported as the ratio of the initial dry weight to the initial weight. To determine the initial dry weight of the remaining samples, the factor of the actual macromer fraction and individual initial weight was used (Eq. 1).

$$Actual macromer fraction = \frac{m_{dry,t0}}{m_{initial}} \quad (1)$$

The remaining samples were allowed to swell in PBS at 37 °C until up to 1d or longer time points to determine the mass loss. Swollen hydrogel samples were collected to record wet weight ($m_{swollen}$), then freeze-dried to obtain the freeze dried weight (m_{dry}) to calculate the mass loss and mass swelling ratio (q) according to equations 2, 3 and 4:

$$m_{dry,t0} = m_{initial}\, x actual macromer fraction \quad (2)$$

$$Mass loss = \frac{m_{dry,t0} - m_{dry}}{m_{dry,t0}}\, x\, 100 \quad (3)$$

$$q = \frac{m_{swollen}}{m_{dry}} \quad (4)$$

The sol fraction of the hydrogels is defined as percent macromers that are not cross-linked into the hydrogel network, and determined as the mass loss after equilibrium swelling (t = 1 d).

3.2.2.4. Proteinase K Degradation Assays

PVA-Tyr hydrogels (35 μL) with or without incorporated BSA were left in a 1 mL solution of either PBS or Proteinase K 1 mg/mL in PBS as previously described (30), then incubated at 37 °C. The PBS or Proteinase K solutions were discarded every 48h and fresh solution was added for continuous exposure to functional enzyme. Mass loss and swelling ratios were calculated using equations 1-4. Pure BSA hydrogel controls were generated by cross-linking a 10wt% BSA solution in PBS with 2/20 mM Ru/SPS.

3.2.2.5. Protein and Growth Factor Retention and Release Assays

rhVEGF-165, bFGF and BDNF were labelled using Alexa Fluor 594 carboxylic acid, succinimidyl ester (ThermoFisher) (31,32) following the manufacturer's instructions. Unreacted dye was separated using 3 kDa MWCO centrifuge filter units. During hydrogel fabrication, labelled growth factors were mixed with the macromer solution before cross-linking. Fabricated hydrogels (25 μL) were incubated in 1 mL of basal endothelial cell media supplemented with 1% P/S. All the media was collected at selected time points and fresh media was added, until total hydrogel degradation. Fluorescence in the media was measured by fluorescence spectroscopy (Thermo Scientific Varioskan Flash, Darmstadt, Germany). Release media from plain PVA-Tyr hydrogels was used as a control for background fluorescence subtraction. Release was calculated relative to the total fluorescence detected during the degradation process. Retention was calculated as the % of growth factor left in the hydrogel after 24h of incubation.

Table 3.1. *GF concentrations used for functionality experiments. Concentrations are expressed as ng of GF per mL of macromer solution before light exposure.*

	VEGF	bFGF	BDNF
Metabolic activity assays	10, 20, 50, 250, 500	10, 20, 50, 250	50, 250, 500, 1000
Migration assays	500	250	1000
3D network formation	500	250	1000

3.2.2.6. Hydrogel Preparation for Bioactivity Assays

Different amounts of unlabelled rhVEGF 165, bFGF or BDNF (Table 3.1) were incorporated in the PVA-Tyr macromere solution (5wt% PVA-7Tyr cross-linked using 0.5/5mM Ru/SPS) before the addition of Ru/SPS and photocrosslinking following the procedure described in section 3.2.2.2. For the cell migration assay, the fabricated GFs incorporated PVA-Tyr hydrogels were incubated in assay media, where the supernatant after 1 day was collected (initial release), and the supernatant was again collected when the samples are completely degraded (degradation products) (Figure 1A). For the cell proliferation assay, similarly, the GFs incorporated PVA-Tyr hydrogels were firstly incubated in assay media. The supernatant after 1 day (initial release) was collected, followed by the samples transferred to a transwell culture (Figure 1B). For the tube-formation assay, all samples were transferred directly to a transwell culture after fabrication (Figure 1C). For HUVECs, the assay media composed of vascular endothelial cell basal media supplemented with 1% P/S, 2% FBS, 50 µg/mL ascorbic acid, 1 µg/mL hydrocortisone hemisuccinate, 0.75 units/mL heparin sulfate and 10 mM L-glutamine. For MSCs, the assay media composed of α-MEM supplemented with 2% FBS, 20 mM ascorbic acid and 1% PS for MSC assays.

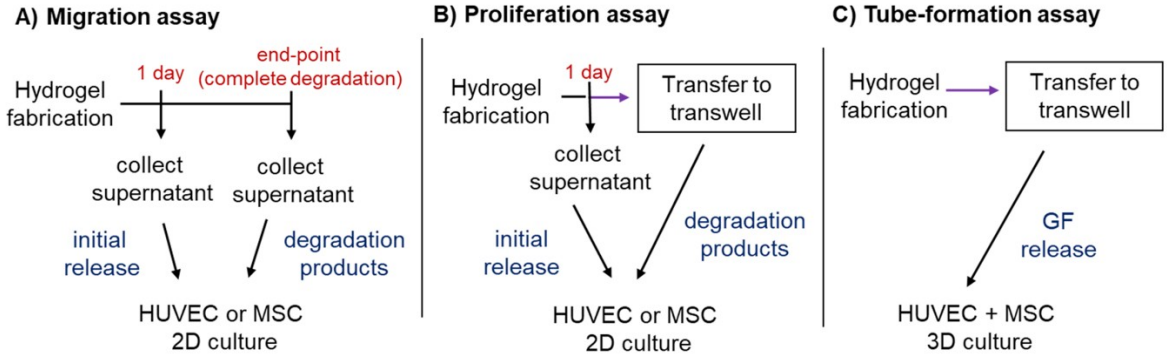

Figure 3.1. Schematic of the experimental workflow in sample preparation for the migration, proliferation and tube-formation assays.

3.2.2.7. Metabolic Activity Assays

Passage 3 to 4 HUVECs or MSCs were cultured in growth media (Endothelial Basal Media supplemented with ATCC endothelial Cell Growth Kit-VEGF for HUVEC, or α-MEM supplemented with 10% FBS, Ascorbic acid 20 mM, bFGF 5 ng/mL and 1% P/S for MSC), trypsinised, seeded in 96 well plates at a density of 500 cells/mm^2 and starved for 24h in assay media. After that, the assay media was discarded and cells were exposed during 48h to

assay media with soluble GF or initial release from PVA-Tyr hydrogels (250 µL). Alternatively, for exposure to the degradation products, fresh assay media (250 µL) was added to the cells and they were exposed to PVA-Tyr hydrogels (from which the initial release had been separated) through an 8 µm pore size transwell for 48h. After exposure, AlamarBlue® was used to measure the metabolic activity of cells. Briefly, each sample was incubated for 5h with 350 µL media containing 10% of AlamarBlue® solution, diluted according to manufacturer's instructions. The reduction of AlamarBlue® in the solution was determined by reading absorbance at wavelengths of 570 nm and 600 nm using a spectrophotometer (Thermo Scientific Varioskan Flash, Darmstadt, Germany) followed by data processing according to manufacturer's instructions.

3.2.2.8. Migration Assays

Passage 3 to 4 HUVECs or MSCs were trypsinised, seeded in a 48 well-plate at a density of 1.500 cells/mm^2. Cells were then starved overnight in assay media, and linear scratches were generated using a 1mL pipette tip. Cells were then washed with PBS to discard any floating cells or cell debris and pictures of the wound area (t_0) were taken. Cells were then exposed to 250 µL of either assay media with soluble GF, initial release or full degradation products from PVA-Tyr or PVA-Tyr-GF hydrogels for either 8h (HUVECs) or 24h (MSCs). Pictures of the wound area (t_f) were taken after the exposure. Wound closure (%) was calculated following eq. 6:

$$Woundclosure(\%) = \frac{woundarea_{t0} - woundarea_{tf}}{woundarea_{t0}} x\,100 \quad (6)$$

3.2.2.9. 3D Endothelial Cell-Pericyte Coculture Assays

Passage 2 HUVECs and passage 3 MSCs were incubated in growth media, trypsinised and resuspended in Cultrex Stem Cell Qualified RGF Basement Membrane Extract (R&D Systems 3434-001-02) at a concentration of 5 million HUVEC and 1 million MSCs per 1 mL. Gels were left to physically cross-link for 45 min at 37°C and 5% CO_2. After that, gels were exposed to 250 µL of growth media (positive control), assay media with soluble GF, or assay media and PVA-Tyr hydrogels through a transwell. Media was fully changed on days 1, 3 and 5. For immunofluorescence examination, samples were collected on day 7, washed in PBS and fixed in 4% formaldehyde for 45 minutes at RT. Samples were then blocked with 2% BSA for 1h at RT and permeabilised using a 0.2% Triton-X solution. Samples were then

washed in PBS, and blocking buffer including mouse anti-CD-31 primary antibody at 1:100 dilution was added for an O/N incubation at 4°C . Samples were washed three times in blocking buffer for 30 min each and followed by an incubation with Goat-anti-mouse (Alexa fluor 488) secondary antibody diluted in blocking buffer (1:500) for 30 min at 37°C. Samples were then washed 3 times in PBS during 30 min, incubated in a DAPI (1:1000) solution for 2 min and washed three times in PBS. Image stacks (100 μm thickness) were captured in 3 different areas of each sample using a Zeiss Axioimager Z1 fluorescence microscope (Carl Zeiss Microscopy, Jena, Germany) and their maximum intensity projection was extracted. Total vessel length and junctions density were quantified using AngioTool software.

3.2.2.10.Statistical Analysis

Data are presented as mean ± standard deviation. All samples were prepared in triplicates and each experiment was repeated 3 times to study variability between experiments (N=3). Individual differences between groups and time points were assessed using one or two-way ANOVA and Holm-Sidak post hoc analysis (GraphPad Prism 7). Statistical significance was accepted at $p<0.05$.

3.3. Results and Discussion

3.3.1. Tailoring the Degradation Profile of PVA-Tyr Hydrogels

Different tissue engineering applications require specific GF release profiles. When using a biomaterial vehicle, tailoring the release profile to specific time frames is a major challenge, especially for long term release of over 4 weeks. The initial goal of this study was to demonstrate the possibility of tailoring the degradation profile of PVA-Tyr hydrogels so that they can be adaptable to a range of applications. Therefore, the effects of three main parameters on the physico-chemical properties and degradation profile of PVA-Tyr hydrogels were studied: the degree of tyramination, the macromer concentration, and the photo-initiators (Ru/SPS) concentrations.

A

	4Tyr	7Tyr	10Tyr
SA/hydroxyl ratio (mol/mol)	0.011	0.019	0.027
Average COOH per PVA chain	5.4	7.1	9.7
Average Tyr per PVA chain	4.3	7.0	10.0

B

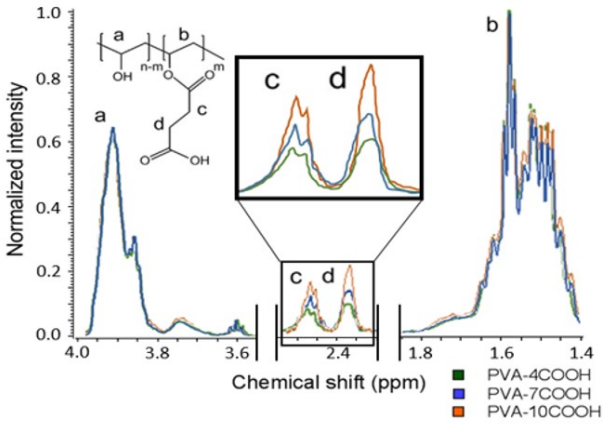

C

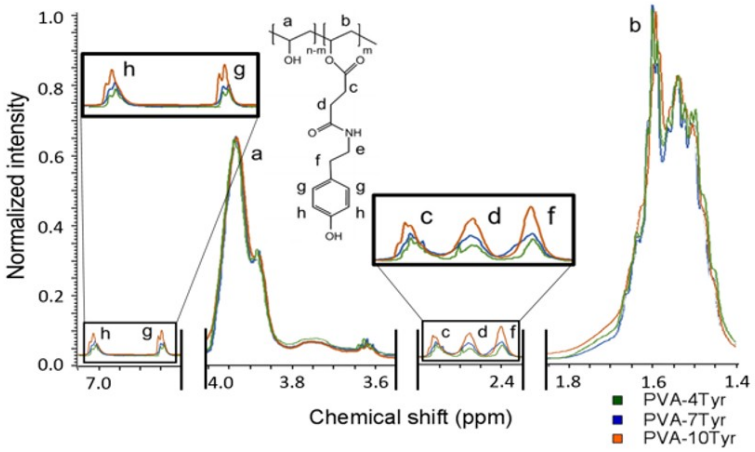

Figure 3.2. Synthesis of PVA-Tyr of different degrees of tyramination. *(A) Ratios of SA to hydroxyl groups (mol/mol) used during carboxylation of PVA and quantified degrees of carboxylation and tyramination of PVA. ^{1}H NMR profiles of (B) PVA-COOH of different degrees of carboxylation and (C) PVA-Tyr of different degrees of tyramination. All experiments were repeated three times with three technical replicates each (N=3).*

PVA-Tyr was successfully synthesised as previously published (26,33). Firstly, carboxyl groups are grafted on to the hydroxyl groups of PVA, forming PVA-COOH (Figure 3.2A-B). These carboxyl groups are subsequently substituted by tyramine groups, forming PVA-Tyr (Figure 3.2A and 3.2C). By adjusting the SA:OH ratio during the carboxylation reaction and then fully substituting these carboxyl groups with tyramine groups, it was possible to obtain PVA-Tyr of average 4, 7 and 10 tyramine groups per PVA chain as confirmed by H^1 NMR (Figure 3.2A). It was hypothesised that, by varying the degree of tyramination, it is possible to construct a library of PVA-Tyr hydrogels of different physico-chemical properties and degradation rates.

Sol fraction analysis showed that at low Ru/SPS concentration (0.5mM/5mM), higher degree of tyramination supported higher crosslinking efficiency, where 5wt% PVA-4Tyr hydrogels showed significantly higher sol fraction values when compared to both 5wt% PVA-7Tyr and PVA-10Tyr gels (Figure 3.3A, Supplementary Tables 3.1-3). This result was expected as an increased availability of tyramine groups would result in more efficient cross-linking. However, this phenomena was not observed when higher Ru/SPS concentrations (2mm/20mM) were utilised. Regardless, all the 5wt% PVA-Tyr hydrogels of different degree of tyramination and Ru/SPS concentrations yielded good crosslinking efficiency evidenced by relatively low sol fraction values (20-30%). The mass swelling ratios follow the same trend of the sol fraction analysis, where formulations of higher sol fraction values also have higher mass swelling ratios (Figure 3.3B, Supplementary Tables S3.4-6). This trend was expected, as hydrogels that retain a smaller amount of macromer after cross-linking have a less dense network that can imbibe more water.

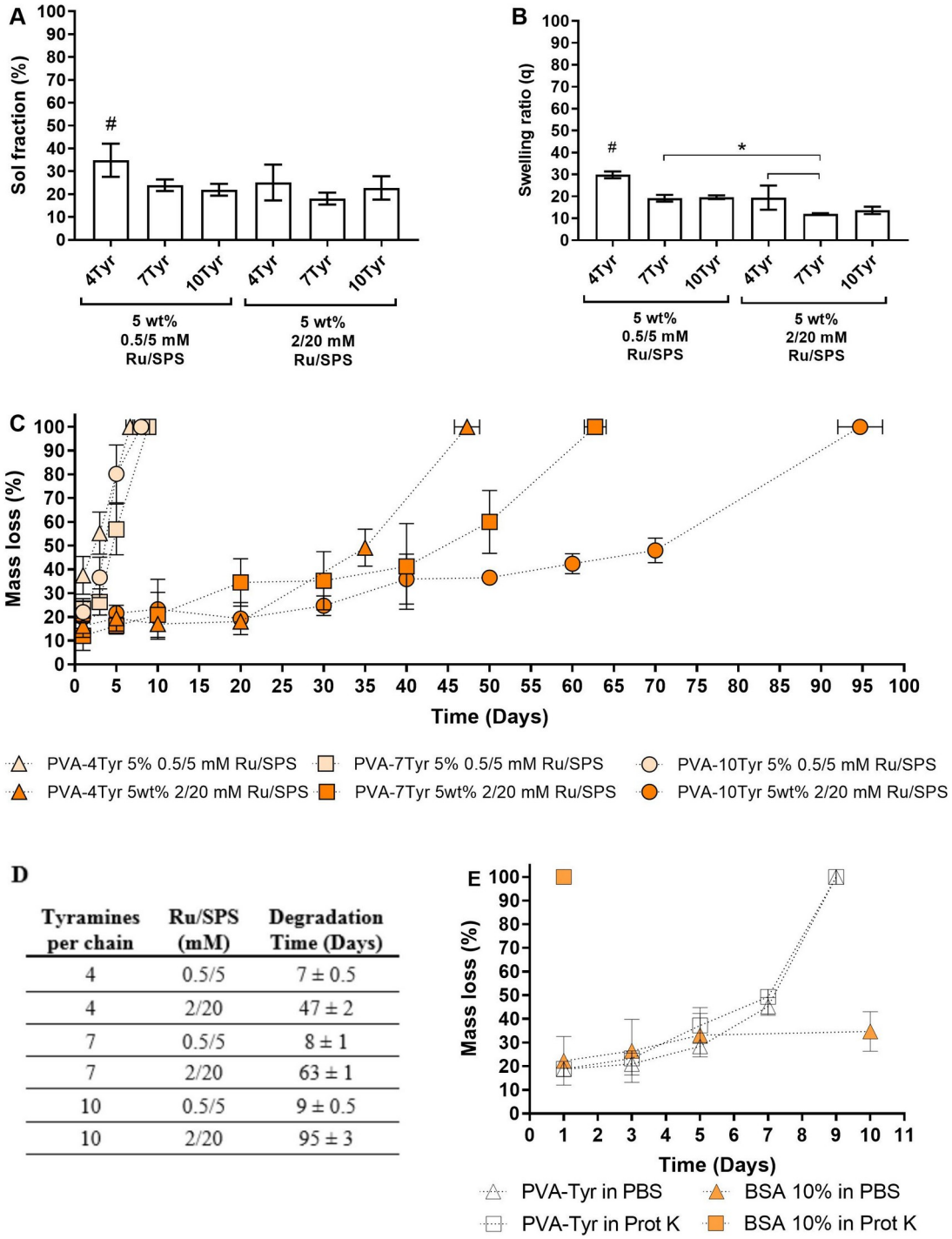

D

Tyramines per chain	Ru/SPS (mM)	Degradation Time (Days)
4	0.5/5	7 ± 0.5
4	2/20	47 ± 2
7	0.5/5	8 ± 1
7	2/20	63 ± 1
10	0.5/5	9 ± 0.5
10	2/20	95 ± 3

Figure 3.3. Tailoring the degradation profile of PVA-Tyr hydrogels. *(A) Sol fraction and (B) swelling ratio of hydrogels fabricated using PVA-Tyr of different degrees of tyramination and Ru/SPS concentrations. (C) Mass loss profile and (D) Degradation time of PVA-Tyr 5wt% with different degrees of Tyramination, cross-linked at either 0.5/5 or 2/20 mM Ru/SPS. (E) Mass loss profile of PVA-Tyr (7Tyr, 5wt% PVA-Tyr, 0.5/5 mM Ru/SPS) and BSA (10wt%, 2/20 mM Ru/SPS) exposed to either PBS or proteinase K (Prot K). *: Significant difference between groups ($p<0.05$). #: Significant difference as compared to all other groups ($p<0.05$). All experiments were repeated three times with three technical replicates each (N=3).*

The long term degradation profile of the fabricated PVA-Tyr hydrogels was further evaluated (Figure 3.3C). The degradation period of the hydrogels increased with the degree of tyramination, where PVA-10Tyr gels take longer to degrade, followed by PVA-7Tyr then PVA-4Tyr when cross-linked using the same Ru/SPS concentrations. A potential explanation for these differences is that the increased availability of tyramine groups resulted in the formation of more crosslinks, delaying the degradation of the network. Our result is in agreement with previous research on tyraminated dextran (34), which showed that increasing the degree of substitution from 5% to 10% to 15% resulted in increased crosslinking density indicated by increase in storage modulus under the same cross-linking conditions. Similarly, research on HA-Tyr showed that increasing the degree of tyramination from 6 to 12.5 mol% results in increased cross-linking density from 3 to 5.8 mol% (21). Another factor that possibly influenced the degradation time is the increase in hydrophobicity of the network caused by the increased presence of tyramine moieties.

To demonstrate that the physico-chemical properties and degradation profile of PVA-Tyr hydrogels can be finely tailored, a library of degradation profiles was generated by systematically varying the photo-initiators concentrations, degree of tyramination and macromer concentration (Supplementary Figures S3.1-4). Increasing photo-initiator concentrations significantly prolonged the total time required to achieve complete degradation regardless of the degree of tyramination or the macromer concentration (Figure 3.3C, Supplementary Figures S3.1-2). These results are in agreement with previous research on degradation of PVA-Tyr hydrogels (28). Increasing the macromer concentration generally resulted in shorter degradation times (Supplementary Figures S3.3-4). This tendency was attributed to a reduction in the ratio of free radicals to tyramine groups, resulting in a less efficient cross-linking.

Another key aspect for the clinical translation of this PVA-Tyr system would be to model and understand its potential degradation profile *in vivo.* Exposure to physiological environment generally results in an *in vitro* and *in vivo* mismatch of degradation behaviour of biomaterials, generally caused by the uncontrolled presence of proteases and other components that can influence the swelling behaviour of the material (35). Theoretically, PVA-Tyr hydrogels degrade exclusively through hydrolysis of the ester bonds part of the crosslinked network, and hence should not be influenced by enzymatic degradation. As such, PVA-Tyr hydrogels

(5wt%, 0.5/5 mM Ru/SPS) were exposed to proteinase K, a broad-spectrum protease known to non-specifically degrade a number of proteins that has been widely applied for investigation of enzymatic degradation (Figure 3.3E) (36). It was observed that PVA-Tyr hydrogels in either PBS or proteinase K had identical degradation profile, confirming that this synthetic hydrogel network is not susceptible to enzymatic degradation. In contrast, pure 10wt% BSA hydrogels cross-linked using 2/20 mM Ru/SPS were fully degraded after overnight exposure in proteinase K due to the enzymatic proteolysis.

Overall, these results demonstrate that the degradation profiles of PVA-Tyr hydrogels can be tailored from 7 (short-term) to 95 days (long-term), just by changing the degree of tyramination, photo-initiator and macromer concentrations, where the primary degradation mechanism is through hydrolysis. Furthermore, our library of degradation profiles shows that the exact degradation time that is needed for any application can be achieved by tuning these cross-linking parameters (Supplementary Figure S3.1-4). These results highlight that the PVA-Tyr platform could be adapted to tissue engineering applications that require short term or long term release, such as tissue vascularisation or bone and cartilage regeneration.

3.3.2. Tailoring the Incorporation and Release of Proteins in PVA-Tyr Hydrogels

PVA-Tyr has pendant tyramine moieties that can form covalent bi-phenol bonds with naturally occurring tyrosine groups of proteins when using the photo-initiating system employed in this study. It was sought to evaluate the efficiency of protein incorporation into PVA-Tyr hydrogels using BSA as a model protein. PVA-Tyr hydrogels with incorporated BSA fabricated under different cross-linking conditions were subjected to a mass loss, swelling and release study. Our initial results indicated that the BSA incorporated into 5wt% PVA-7Tyr hydrogels crosslinked using 0.5/5 mM Ru/SPS had low retention (<20%, Figure 3.4A). Increasing the degree of tyramination did not affect the BSA retention, where both 5wt % PVA-7Tyr and PVA-10Tyr hydrogels crosslinked at the same Ru/SPS concentration had equally low BSA retention. However, it was observed that increasing the Ru/SPS concentration significantly enhanced the retention of BSA within the hydrogel to 50% and 80% in 5wt% PVA-7Tyr crosslinked using 1/10 and 2/20 mM Ru/SPS, respectively. Interestingly, when using a similar Ru/SPS concentration (2/20 mM Ru/SPS), it was observed that the BSA retention was significantly lower in hydrogels of higher macromer concentration, where 20wt% PVA-Tyr hydrogel resulted in 65% BSA retention as compared

to 5wt% PVA-Tyr gels (80% retention). These results were attributed to the higher cross-linking efficiency caused by the higher ratio of free radical to tyrosine group in hydrogels with lower macromer concentration, which also results in longer degradation times (Supplementary Figure S3.1-2). Interestingly, the differences between groups in terms of BSA retention were more marked than the differences in sol fraction, which was 10-20% in all groups, or swelling ratio, which did not show significant changes when increasing the Ru/SPS concentrations from 1/10 to 2/20 mM (Supplementary Figures S3.5A-B). These results demonstrate that modifying the cross-linking conditions allows us to control the incorporation efficiency of proteins into our PVA-Tyr hydrogels.

Incorporating covalently bound proteins in the polymer network could potentially alter the rate of hydrolytic degradation of the hydrogels or make them sensitive to proteolytic degradation, modifying their degradation and release profiles in an unwanted manner. These hypotheses were tested by exposing PVA-Tyr hydrogels (5wt%, 0.5/5 mM Ru/SPS) incorporated with BSA 10 ng/mL to PBS or Proteinase K. In PBS, it was found that the addition of 0.05 mg/mL BSA did not change the degradation time of the hydrogels. However, increasing the BSA concentration to 10 mg/mL resulted in increased degradation time from 8 to 12 days (Supplementary Figure S3.6A-B). At this concentration, it is possible that the large size and increased presence of BSA results in molecular entanglements that cause steric hindrance to the hydrolysis of the ester bonds. Exposure to proteinase K did not result in significant differences in the mass loss or swelling profile of PVA-Tyr with incorporated BSA (Figure 3.4B and Supplementary Figure S3.6C), whereas plain 10wt% BSA hydrogels were fully degraded after overnight exposure. In addition, the release profile of fluorescently-labelled BSA (0.05mg/ml) from the hydrogels was measured, showing that the release profile was not significantly affected when incubated in proteinase K (Supplementary Figure S3.6D). These results suggest that the PVA-Tyr network can protect the incorporated proteins from the action of proteases, which is very important not only to maintain the degradation and release processes driven exclusively by hydrolysis, but also to protect incorporated GFs from degradation in the physiological environment.

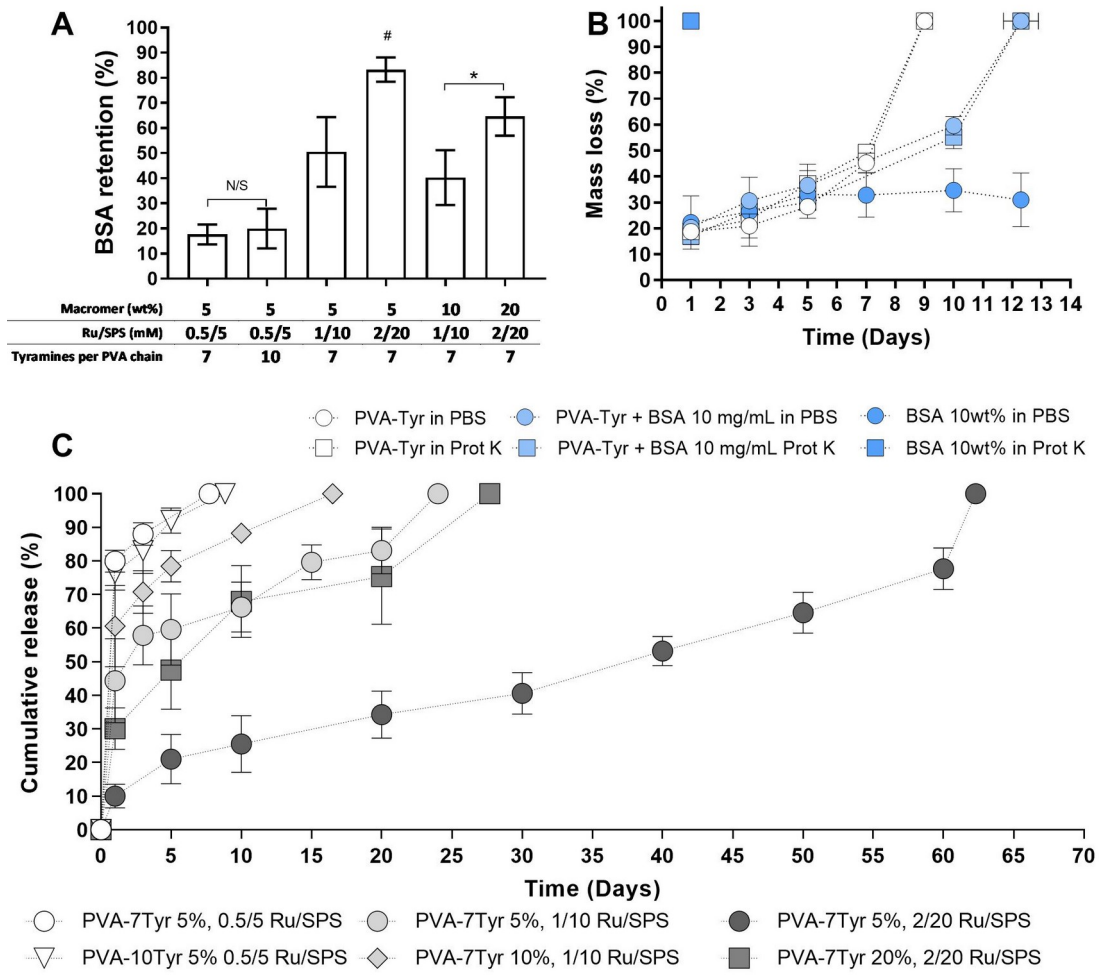

Figure 3.4. Controllable incorporation and release of BSA from PVA-Tyr hydrogels. *(A) Effects of proteinase K exposure on the mass loss profile of PVA-Tyr with incorporated BSA hydrogels. (B) BSA retention and (C) BSA release profile of PVA-Tyr hydrogels generated with different degrees of tyramination, macromer and Ru/SPS concentrations. *: Significant difference between groups ($p<0.05$). #: Significant difference to all other groups ($p<0.05$). N/S: no significant differences between groups ($p>0.05$).* ***Experiments*** *were repeated 3 times with 3 technical repeats each (N=3).*

Long-term BSA release measurements revealed that the release time matched the hydrogel degradation time for all cross-linking conditions (Figure 3.4C and Supplementary Figure S3.7A-B). These results demonstrate that the timespan of the release profile by can be tailored modifying the formulation and cross-linking conditions of our PVA-Tyr hydrogels. Furthermore, after the initial 24h of release of non-incorporated proteins, all release profiles displayed linear tendencies up until total degradation of the hydrogel (Supplementary Figure S3.8), with a minimum R^2 of 0.936 in 20wt% PVA-Tyr hydrogels (crosslinked with 2/20 mM Ru/SPS) to a maximum of 0.986 in 5wt% PVA-Tyr hydrogels (crosslinked with 0.5/5 mM

Ru/SPS) (Supplementary Table S3.7). This indicates that the released protein concentration is consistent during the degradation process, which would result in constant promotion of the desired changes in cell behaviour.

3.3.3. Covalent Incorporation and Release of Different Growth Factors in PVA-Tyr Hydrogels

After studying the general incorporation and release dynamics of the system using BSA as a model protein, this system was further evaluated using clinically relevant GFs, specifically VEGF, bFGF and BDNF. Properties like the isoelectric point (37), the hydrodynamic size (38) or the presence of certain amino acid sequences (39) in GFs heavily influence their release profile when they are directly adsorbed or incorporated into biomaterials. Using covalent incorporation, the major factors determining the release are the efficiency of the covalent incorporation and the rate of hydrolytic degradation of the PVA-GF bonds, and thus different GFs would be released at the same rates. It was hypothesized that the release profiles of different GFs could then potentially be determined by the presence and availability of tyrosine groups in the GFs, which would dictate the amount of bi-phenol bonds formed between GFs and PVA-Tyr during the cross-linking process.

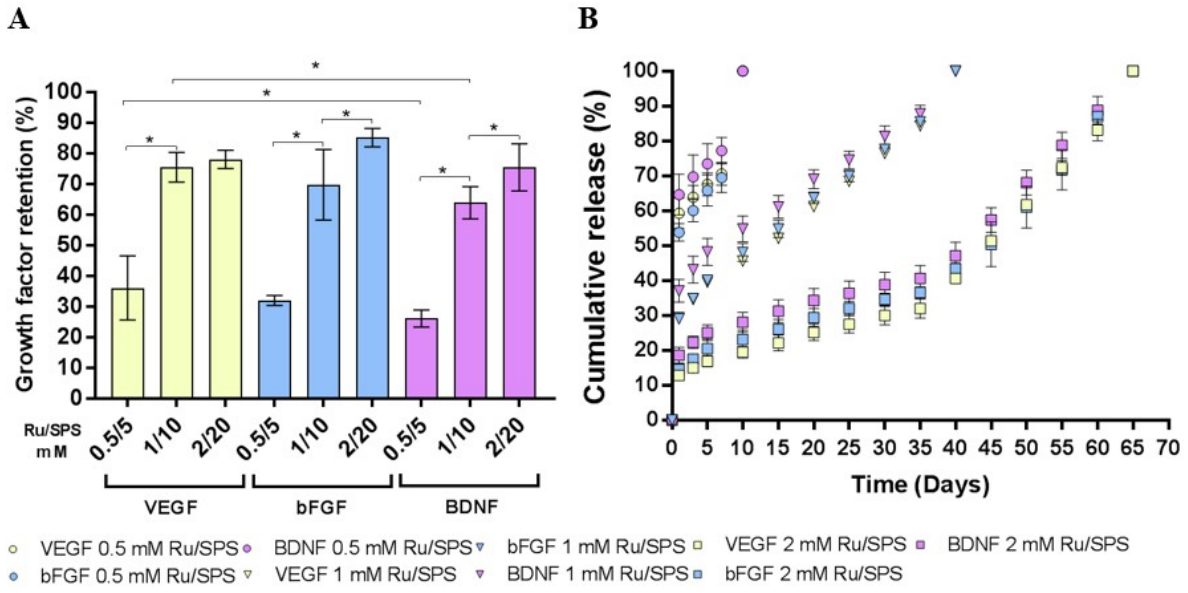

Figure 3.5. Incorporation and release of growth factors in PVA-Tyr hydrogels. *(A) Growth factor retention and (B) release profile from PVA-7Tyr 5wt% hydrogels cross-linked at a range of Ru/SPS concentrations.*: significant difference between groups ($p<0.05$). Experiments were repeated 3 times with 3 technical repeats each (N=3).*

Initial mass loss and swelling studies showed that the incorporation of different GFs (VEGF, bFGF or BDNF) at a range of different concentrations did not result in changes in the sol

fraction values or swelling ratio of the resultant hydrogels (Supplementary Figures S3.9-10). The retention of GFs on day 1 was then studied (Figure 3.5A). When incorporated in PVA-Tyr crosslinked with 0.5/5 mM Ru/SPS, the retention values were between 25% and 35% for those three GFs. A potential explanation for the lower retention of GFs as compared to the cross-linking efficiency of PVA-Tyr is an overall lower availability of tyrosine groups per GF molecule. For example, PVA-7Tyr macromers contain an average of 7 tyramines per polymer chain with a linear conformation, which results in the tyramines being accessible for bi-phenol bond formation. On the other hand, the availability of tyrosine moieties in the incorporated GFs depends on their different structural conformation, which results in only a fraction of the tyrosine groups being available to participate in the cross-linking reaction (Supplementary Table S3.8) (40–43). This lower availability results in decreased formation of bi-phenol bonds between PVA-Tyr and GFs, resulting in lower retention. In a similar way to BSA, increasing the Ru/SPS concentration improved GF retention, reaching 75-85% for samples crosslinked using 2/20 mM Ru/SPS with no significant differences between GFs. Interestingly, VEGF showed small but significant differences in the retention rate as compared to BDNF when incorporated using 0.5/5 and 1/10 mM Ru/SPS, demonstrating the possibility of GF-dependent incorporation efficiency. As both VEGF and BDNF have similar number of tyrosine residues in their sequence (Supplementary Table S3.8), this result suggests that the availability of tyrosine groups is not the only factor determining the incorporation efficiency and release profiles.

In a similar way to the incorporation efficiency, the release profile of encapsulated GFs could change depending on their tyrosine content and other characteristics of the proteins that determine surface interactions and diffusion rates. Results showed that VEGF, bFGF and BDNF had a release time matching the degradation time of the hydrogels (Figure 3.5B), similarly to BSA. Interestingly, the release profiles were comparable between VEGF, bFGF and BDNF under all cross-linking conditions. Furthermore, the release profiles fit linear trends when PVA-Tyr was cross-linked at 1/10 and 2/20 mM Ru/SPS, with R^2 values around 0.9 for all GFs (Supplementary Table S3.9). Overall, these results demonstrate that PVA-Tyr can incorporate and release a range of different GFs, that the release time span and incorporation rate can be modulated by changing the hydrogel cross-linking conditions and that the differences between GFs in terms of retention and release are small. These aspects

are key for the adaptation of PVA-Tyr hydrogels to different regenerative medicine applications that require any protein to be delivered in a specific time frame.

3.3.4. Evaluating the Bioactivity of Growth Factors Released from PVA-Tyr Hydrogels

During photo-crosslinking, GFs in the system are exposed to oxidative damage. Although previous studies showed that gelatin is able to retain its ability to promote cell attachment and proliferation after cross-linking (26), these properties come mostly from the presence of short amino acid sequences like RGD, which do not rely so much on the 3D conformation of the protein. Receptor-binding domains in GFs have a higher specificity and complexity, and therefore their binding affinity is more sensitive to oxidative damage, modification of certain amino acid residues or changes in tertiary structure. Previous studies showed that photo-crosslinking and exposure to UV light can reduce the bioactivity of GFs and enzymes in a dose-dependent manner (44,45). For example, Gu *et al.* showed that VEGF bioactivity is reduced after exposure to UV alone or to UV-activated photoinitiator (DMPA) in a dose-dependent manner, and this reduction is affected by other factors such as the presence of albumin or the macromer molecular weight (44). It has also been shown that the photoinitiator system used can also influence these changes in functionality (45). Although the activation of our system through the more clinically friendly visible light (450 nm wavelength) could be a potential advantage to maintain GF bioactivity during this process, it remains inevitable that the GFs are subjected to radical-based oxidative damage. Additionally, the chemical modification that remains in some tyrosine groups after release could further affect their receptor-binding affinity, especially if those tyrosine residues are localised in the receptor-binding domain. During our initial bioactivity studies, the aim was trying to determine that GFs retain bioactivity even after covalent incorporation into the network and formation of bi-phenol groups. To do that, the initial 24h of release (initial release) was separated from the rest of the release profile (degradation products). It was assumed that the initial release contains mostly GFs that were not incorporated in the matrix, and therefore would be mostly affected by oxidative damage. In the degradation products group, most of the GF has been incorporated in the network and posteriorly released, and therefore it was exposed to both oxidative damage and the chemical modifications associated to covalent incorporation.

In a similar way to the retention and release dynamics, the effects of covalent incorporation on GF bioactivity could differ between GFs depending on their susceptibility to oxidative damage or the stability of their receptor-binding domains. VEGF (46), bFGF (47) and BDNF (48) have been widely studied as vascularisation promoters. Based on that information, vascularisation *in vitro* models were chosen to study their bioactivity, which allowed a more reliable comparison of how the incorporation and release processes affect the bioactivity of these three GFs. 5wt% PVA-7Tyr cross-linked using 0.5/5mM Ru/SPS, a short-term degradation formulation (7-9 days), was chosen for the bioactivity studies as vascularisation happens during the first 1-2 weeks of tissue regeneration (49). Metabolic activity and migration assays were performed to evaluate the bioactivity of GFs right after being released from PVA-Tyr, whereas 3D vascularisation assays were performed to evaluate the bioactivity of the overall release profile in a longer term assay.

3.3.4.1. Effects of Released Growth Factors on the Metabolic Activity of HUVECs and MSCs

VEGF, bFGF and BDNF were incorporated into PVA-Tyr and both HUVECs and MSCs were exposed to the resulting initial release and degradation products (Figure 3.6A-F). Released VEGF from both the initial release and the degradation products induced an increase in metabolic activity in HUVECs (Figure 3.6A) and MSCs (Figure 3.6B).When comparing free VEGF to VEGF released from hydrogels that were initially loaded with equivalent VEGF concentrations, the free control resulted in higher metabolic activity in both HUVECs and MSCs. Part of these differences could be explained by the lower effective concentration caused by the separation of the release in two phases. However, we attribute most of the differences to the effects of oxidative stress of VEGF. Similar tendencies were found with bFGF, where both the initial release and the degradation products were able to induce an increase in metabolic activity in both cell types (Figures 3.6C-D). At the highest concentration tested, the released bFGF was able to induce an increase in metabolic activity in HUVECs at rates that were equivalent to its free bFGF control. BDNF did not increase HUVEC metabolic activity in its free form (Figure 3.6E), which is in accordance to previous reports where BDNF pose no effect on the proliferative capacity of HUVECs (50). It did, however, induce an increase in metabolic activity in MSCs (Figure 3.6F). Interestingly, exposure to both the initial release and the degradation products of BDNF resulted in increased MSC metabolic activity at rates that were comparable to their free BDNF controls.

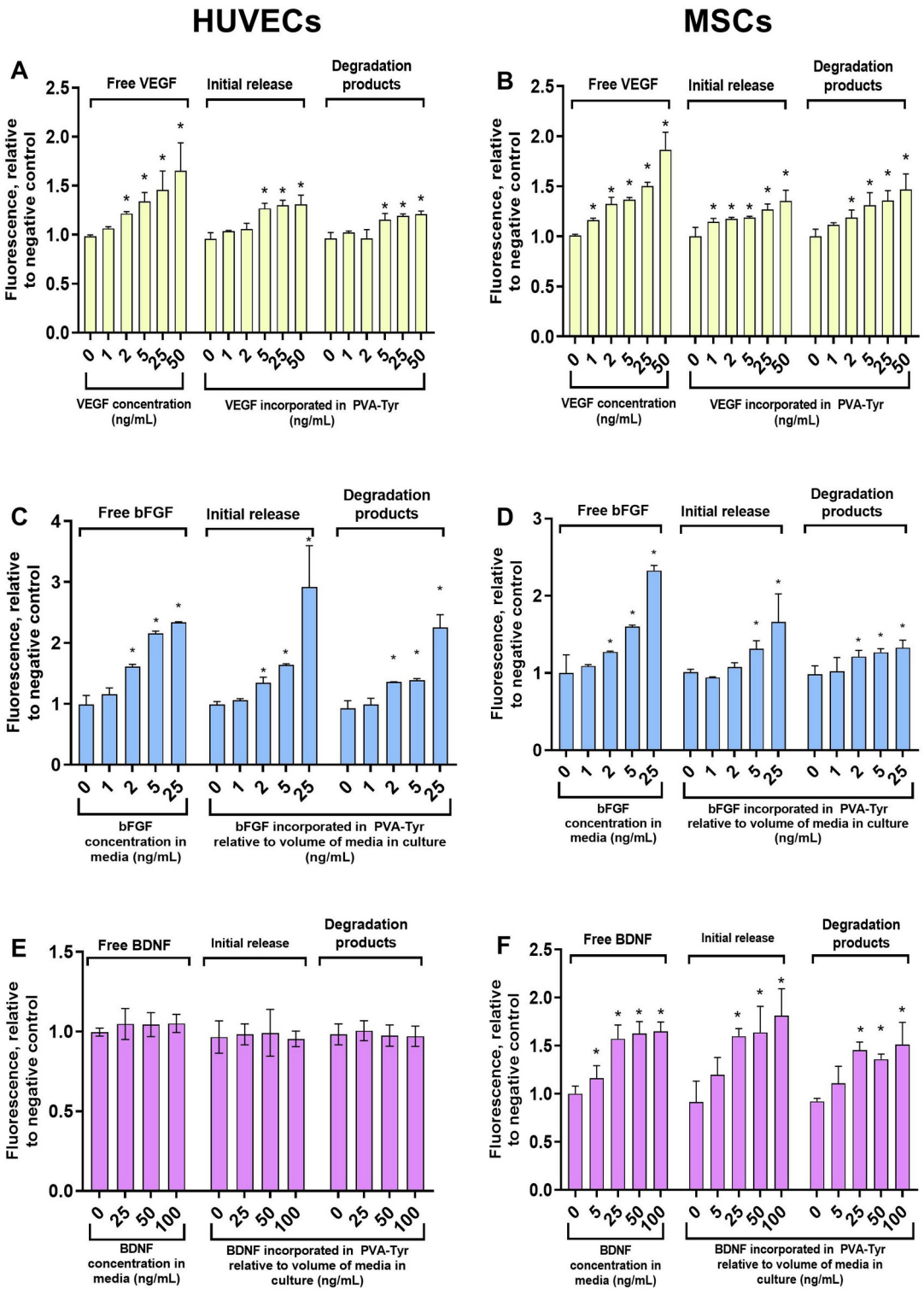

Figure 3.6. Effects of released growth factors on the metabolic activity of HUVECs and MSCs. *Stimulation of HUVEC (A, C, E) and MSCs (B, D, F) by VEGF (A, B), bFGF (C, D) and BDNF (E, F) released from PVA-Tyr hydrogels (7Tyr, 5wt%, 0.5/5 mM Ru/SPS) during 48h. *: Significant difference ($p<0.05$) as compared to its corresponding negative control (0 ng/mL). Experiments were repeated 3 times with 3 technical repeats each (N=3).*

Overall, these results show that the tested GFs are able to withstand the oxidative stress and the chemical modifications associated to covalent incorporation, maintaining at least part of their ability to promote HUVEC and MSC metabolic activity. Furthermore, they show that the sensitivity to changes in their receptor-binding domains can differ between specific GFs. Specifically, bFGF and BDNF are potentially more resistant to these changes as compared to VEGF. Therefore, any new GF that is to be incorporated into PVA-Tyr will need to be tested in a similar way.

3.3.5. Effects of released growth factors on the migration of HUVECs and MSCs

The overall functionality of GFs is the result of binding to a combination of different receptors. Therefore, it is important to evaluate GF bioactivity with multiple assays that recapitulate their different effects. In a regenerative medicine context, a migration assay provides information about the ability of the GF to recruit cells from the surrounding environment to promote tissue regeneration. Scratch assays were performed on both HUVECs and MSCs by exposing them to the separated initial release or degradation products (fully degraded hydrogel) (Figure 3.7A-D). Results showed that VEGF, bFGF and BDNF were able to induce cell migration regardless of the cell type, the exposure to oxidative stress or the presence of bi-phenol groups. . These findings are consistent with previous reports where VEGF, bFGF and BDNF induced migration of HUVECs (50–53) and MSCs (54–56). Interestingly, the rates of migration induced by both the initial release and the degradation products were similar to their free GF counterparts, which is in contrast with the results seen in metabolic activity assays for VEGF and bFGF. This disparity between results could be caused by changes in the GF that only affect the binding affinity with some of these receptors.

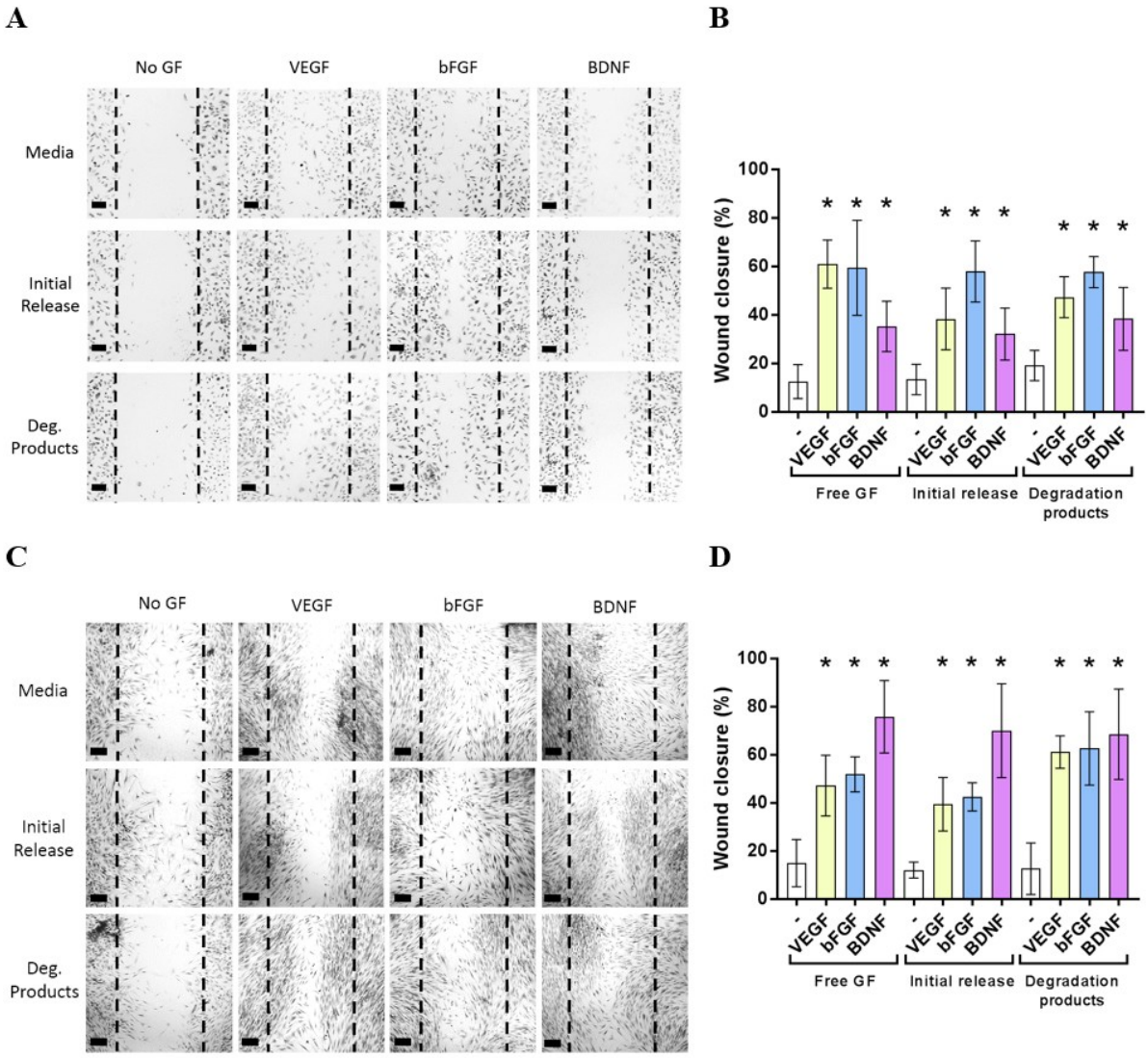

Figure 3.7. Effects of released growth factors on the migration HUVECs and MSCs. *(A) Representative pictures of HUVEC migration, (B) HUVEC wound closure assay quantification after 8h of exposure, (C) Representative pictures of MSC migration and (D) MSC wound closure quantification after 24h of exposure. PVA-7Tyr was cross-linked at 5wt%, 0.5/5 mM Ru/SPS. Scale bar: 200 µm. *: Significant difference ($p<0.05$) as compared to its respective negative (-) control. Experiments were repeated 3 times with 3 technical repeats each (N=3).*

3.3.4.3. Effects of released growth factors on 3D network formation by HUVEC/MSC co-cultures

To demonstrate the capability of the PVA-Tyr-GF system to stimulate cell response in a more complex setup and during a longer time span, an established 3D HUVEC/MSC co-culture system (57–59) was exposed to PVA-Tyr hydrogels with incorporated GFs through a transwell system. Immunofluorescence at day 7 (Figure 3.8A) showed that VEGF, bFGF and BDNF were able to promote an increase in junctions density (Figure 3.8B) both as free GF in media or released from PVA-Tyr. VEGF and bFGF also induced an increase in total vessel length (Figure 3.8C). These results agree with HUVEC metabolic activity and migration results, demonstrating that the GFs still retain bioactivity after covalent incorporation. Moreover, released GFs displayed an ability to promote network formation that was comparable to the free GF controls despite the fact that fresh GFs were added in every media change in the latter groups. This result suggests that the hydrogel system protects the GFs from the microenvironment, which agrees with previous reports on biomaterial-based GF delivery (Kempen et al., 2008; Tong, Lee, Bararpour, & Yang, 2015). Another interesting observation is that BDNF was able to promote 3D vessel formation despite not promoting HUVEC metabolic activity. These results are also supported by previous literature (48,50), and suggest that the effects of BDNF on angiogenesis are triggered mostly by the interaction with MSCs.

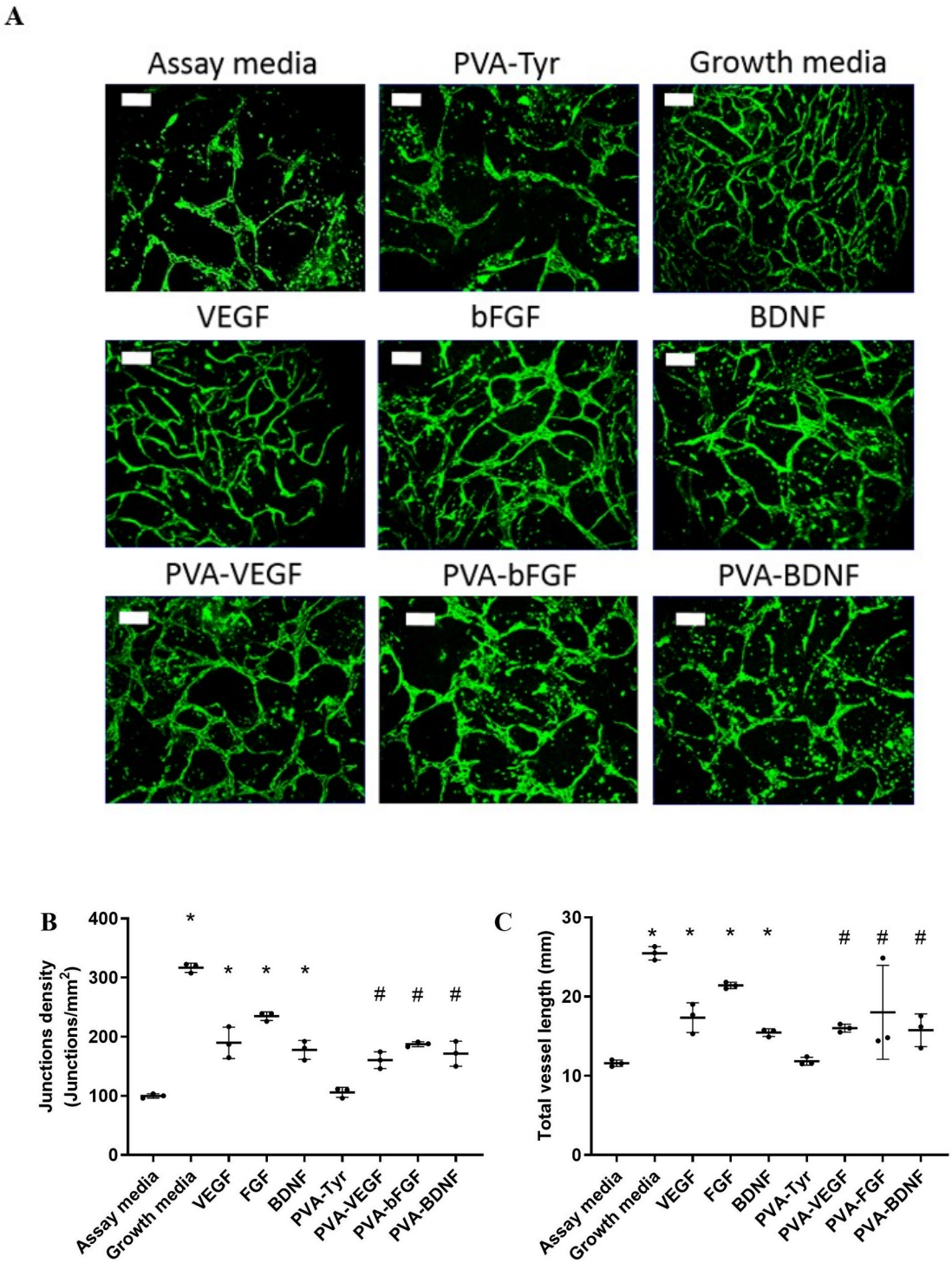

Figure 3.8. Effects of released growth factors on 3D network formation by HUVEC/MSC co-cultures. *(A) Representative images of the CD-31 immunostaining (green) showing the 3D network formation in ECM hydrogels after continuous exposure to either soluble GF or release from PVA-Tyr hydrogels (5wt%, 0.5/5 mM Ru/SPS) after 7 days. (B) Junctions density and (C) total vessel length extracted from Angiotool network analysis. Scale bars: 200 µm. *: Significant difference ($p<0.05$) as compared to assay media. #: Significant difference ($p<0.05$) as compared to PVA-Tyr. Experiments were repeated 3 times with 3 technical repeats each (N=3).*

Overall, bioactivity studies show that it is possible to incorporate GFs in PVA-Tyr hydrogels while retaining their functionality. Results suggest that different GFs could have different sensitivities to the effects of oxidative stress and the chemical modifications associated to covalent incorporation, as shown by metabolic activity studies when comparing VEGF to bFGF or BDNF. Furthermore, these effects could potentially modify the binding affinities of GFs to each of their receptors in different ways. A question remaining to be answered is how increasing the Ru/SPS concentrations will affect GF bioactivity, as previous studies have shown that the loss of functionality depends on the photoinitiator concentration (44,45). A potential strategy to reduce oxidative stress could be the addition of albumin or other proteins with radical-quenching properties to the hydrogels (44). Our results have shown that the protein concentration in the hydrogels can be increased without inducing changes in their degradation profile, which makes this strategy feasible for future research.

3.4. Conclusions

In the present study, the potential of PVA-Tyr/Ru/SPS as a growth factor delivery system has been investigated. It has been demonstrated that, by changing the degree of tyramination, macromer concentration and Ru/SPS concentration, hydrogels with highly tailorable degradation profiles from seven days to up to three months can be obtained. The release of covalently incorporated BSA and GFs from different PVA-Tyr formulations consistently showed a linear tendency that lasted until total degradation of the hydrogel, demonstrating potential for long term continuous release applications. It has been shown that the encapsulation of VEGF, bFGF or BDNF in PVA-Tyr does not result in relevant differences in the incorporation rate or release profile of the system, which facilitates its translation to the delivery of different GFs and even coordinated delivery. Furthermore, proteinase K has been used as a model to show that the degradation of PVA-Tyr hydrogels is driven by hydrolysis even after the covalent incorporation of a high protein concentration. Finally, 2D and 3D *in vitro* models were used to prove that VEGF, bFGF and BDNF still retain functionality after exposure to oxidative stress and to the chemical modifications associated with covalent incorporation. To our knowledge, no other GF delivery system has shown to provide such level of control over the release profiles in combination with the ability to covalently incorporate a wide range of native proteins.

There are some aspects of the system that still need to be further investigated. Studies on the effects of increased Ru/SPS concentration in GF bioactivity should be performed, together with potential strategies to reduce oxidative stress such as the addition of protective proteins in the hydrogel. However, evidence has been provided showing that the process of covalent incorporation does not inactivate the studied GFs and, therefore, that this type of cross-linking is a viable strategy for long term GF delivery. Another key aspect for future study is the degradation profile of PVA-Tyr hydrogels in an *in vivo* environment.

Overall, the present study provides sufficient evidence to demonstrate the potential of PVA-Tyr as a highly tailorable GF delivery system due to its controllable degradation profiles, its long-term linear release and its ability to incorporate and release a wide range of native proteins in a simple manner while retaining functionality.

3.5. Supplementary information

Supplementary Table S3.1. *Sol fraction values for PVA-4Tyr hydrogels cross-linked at different macromer and Ru/SPS concentration.*

PVA-4T	5wt%	10wt%	15wt%	20wt%
0.5/5 mM Ru/SPS	34.9 ± 7.3			
1/10 mM Ru/SPS	34.1 ± 11.0	53.6 ± 5.9		
1.5/15 mM Ru/SPS	34.2 ± 4.8	44.8 ± 1.7	73.0 ± 2.9	
2/20 mM Ru/SPS	25.2 ± 9.9	45.3 ± 3.6	63.9 ± 1.4	73.5 ± 5.5

Supplementary Table S3.2. *Sol fraction values for PVA-7Tyr hydrogels cross-linked at different macromer and Ru/SPS concentration.*

PVA-7T	5wt%	10wt%	15wt%	20wt%
0.5/5 mM Ru/SPS	23.7 ± 3.6			
1/10 mM Ru/SPS	14.0 ± 8.0	18.2 ± 2.7		
1.5/15 mM Ru/SPS	11.8 ± 2.7	18.6 ± 5.2	20.5 ± 2.3	
2/20 mM Ru/SPS	13.9 ± 5.9	14.2 ± 6.9	24.5 ± 5.2	26.4 ± 9.7

Supplementary Table S3.3. *Sol fraction values for PVA-10Tyr hydrogels cross-linked at different macromer and Ru/SPS concentration.*

PVA-10T	5wt%	10wt%	15wt%	20wt%
0.5/5 mM Ru/SPS	22 ± 4.5			
1/10 mM Ru/SPS	9.2 ± 5.2	19.3 ± 6.2		
1.5/15 mM Ru/SPS	7.8 ± 3.0	14.1 ± 5.4	17.6 ± 2.8	
2/20 mM Ru/SPS	22.6 ± 6.7	17.4 ± 2.6	20.6 ± 6.7	32.6 ± 9.7

Supplementary Table S3.4. *Swelling ratio values for PVA-4Tyr hydrogels cross-linked at different macromer and Ru/SPS concentration.*

PVA-4T	5wt%	10wt%	15wt%	20wt%
0.5/5 mM Ru/SPS	30.6 ± 9.0			
1/10 mM Ru/SPS	26.4 ± 3.9	31.0 ± 1.0		
1.5/15 mM Ru/SPS	21.6 ± 1.6	18.7 ± 1.5	29.0 ± 5.5	
2/20 mM Ru/SPS	19.5 ± 6.4	16.7 ± 1.3	21.2 ± 2.3	22.25 ± 5.3

Supplementary Table S3.5. *Swelling ratio values for PVA-7Tyr hydrogels cross-linked at different macromer and Ru/SPS concentration.*

PVA-7T	5wt%	10wt%	15wt%	20wt%
0.5/5 mM Ru/SPS	19.2 ± 1.7			
1/10 mM Ru/SPS	12.9 ± 1.6	12.3 ± 1.1		
1.5/15 mM Ru/SPS	11.8 ± 0.5	10.9 ± 1.0	11.0 ± 0.8	
2/20 mM Ru/SPS	11.9 ± 0.4	10.1 ± 0.8	10.5 ± 0.8	11.0 ± 0.8

Supplementary Table S3.6. *Swelling ratio values for PVA-10Tyr hydrogels cross-linked at different macromer and Ru/SPS concentration.*

PVA-10T	5wt%	10wt%	15wt%	20wt%
0.5/5 mM Ru/SPS	19.7 ± 1.0			
1/10 mM Ru/SPS	15.0 ± 1.8	14.0 ± 1.2		
1.5/15 mM Ru/SPS	13.0 ± 2.0	9.7 ± 0.2	11.3 ± 0.8	
2/20 mM Ru/SPS	12.3 ± 1.6	10.9 ± 1.0	10.5 ± 1.2	10.2 ± 2.0

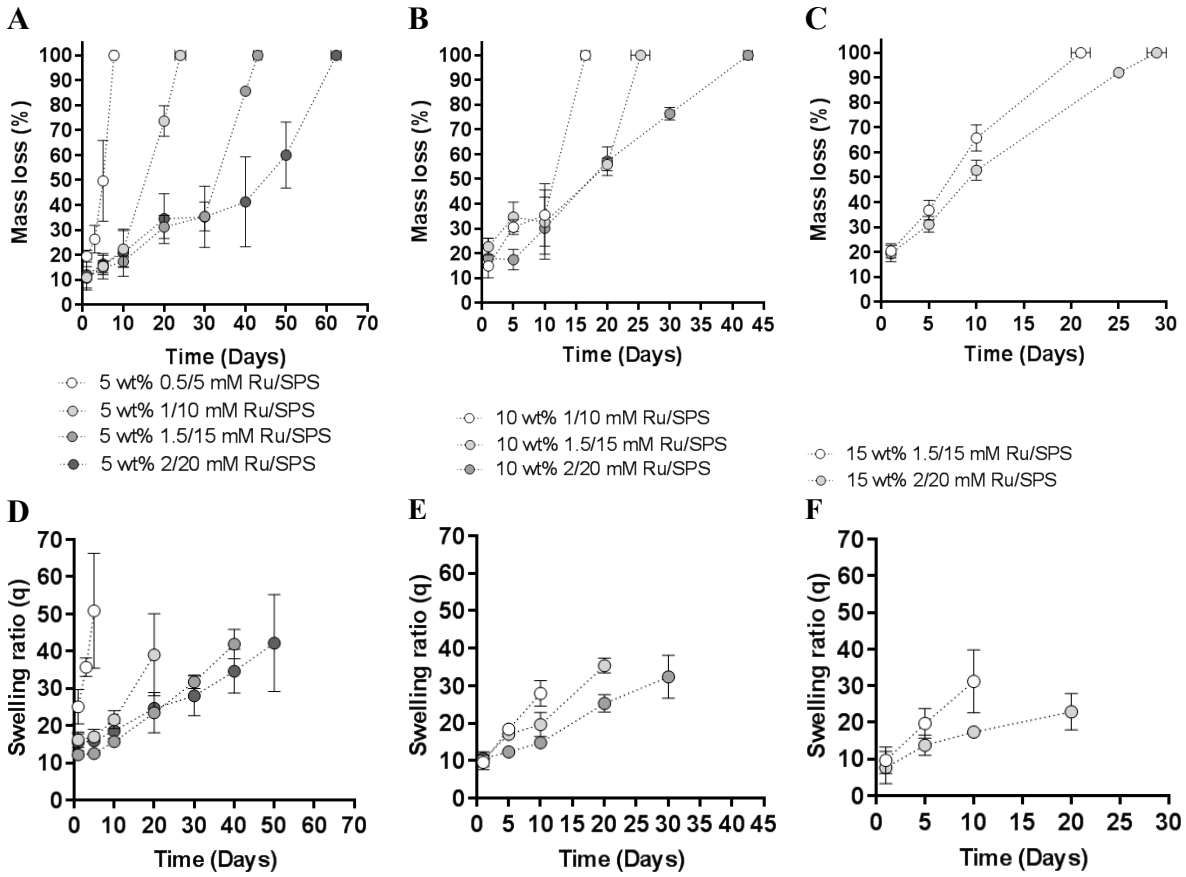

Supplementary Figure S3.1. Degradation of PVA-7Tyr hydrogels with varying Ru/SPS concentrations. *(A-C) Mass loss and (D-F) swelling ratio of PVA-7Tyr hydrogels cross-linked using increasing Ru/SPS concentrations (0.5/5-2/20 mM) at different macromer concentrations (5-15wt%).*

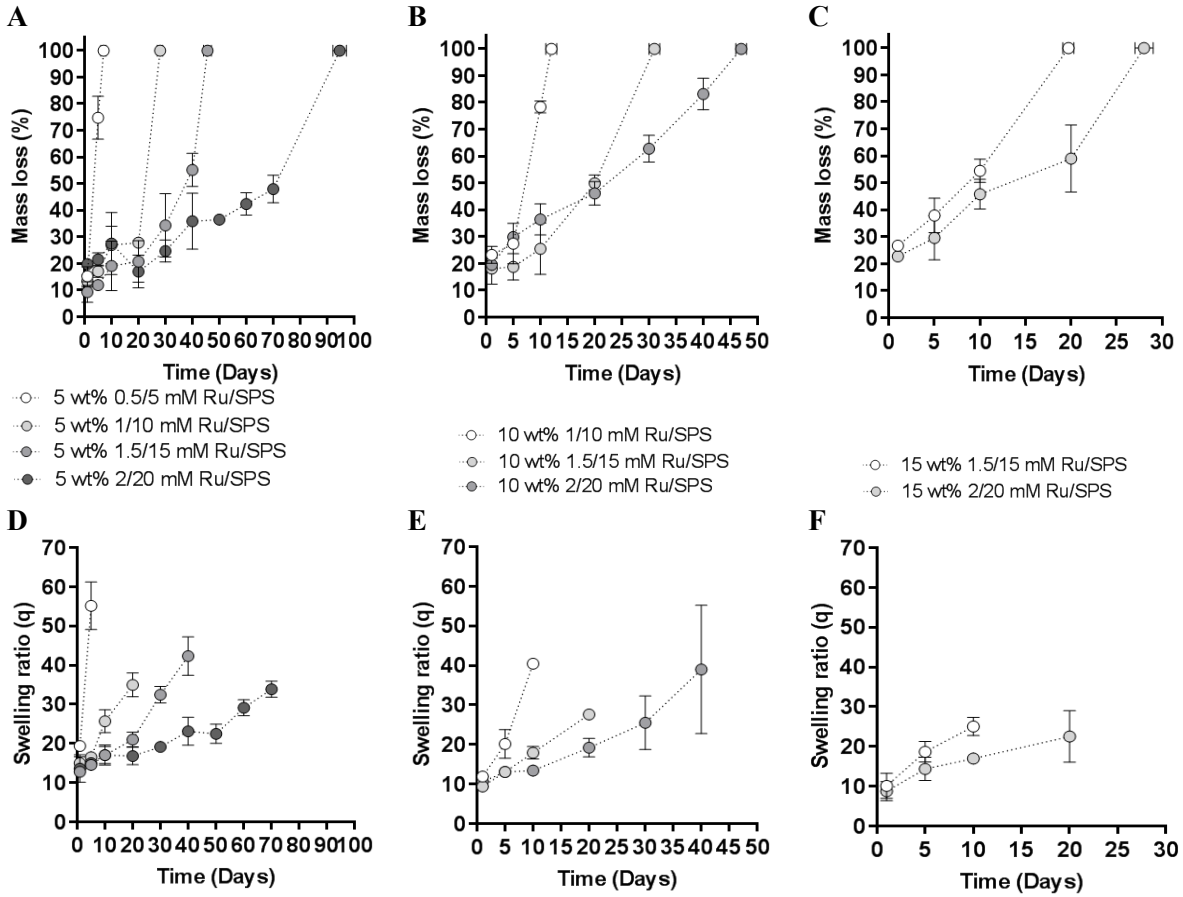

Supplementary Figure S3.2. Degradation of PVA-10Tyr hydrogels with varying Ru/SPS concentrations. *(A-C) Mass loss and (D-F) swelling ratio of PVA-10Tyr hydrogels cross-linked using increasing Ru/SPS concentrations (0.5/5-2/20 mM) at different macromer concentrations (5-15wt%).*

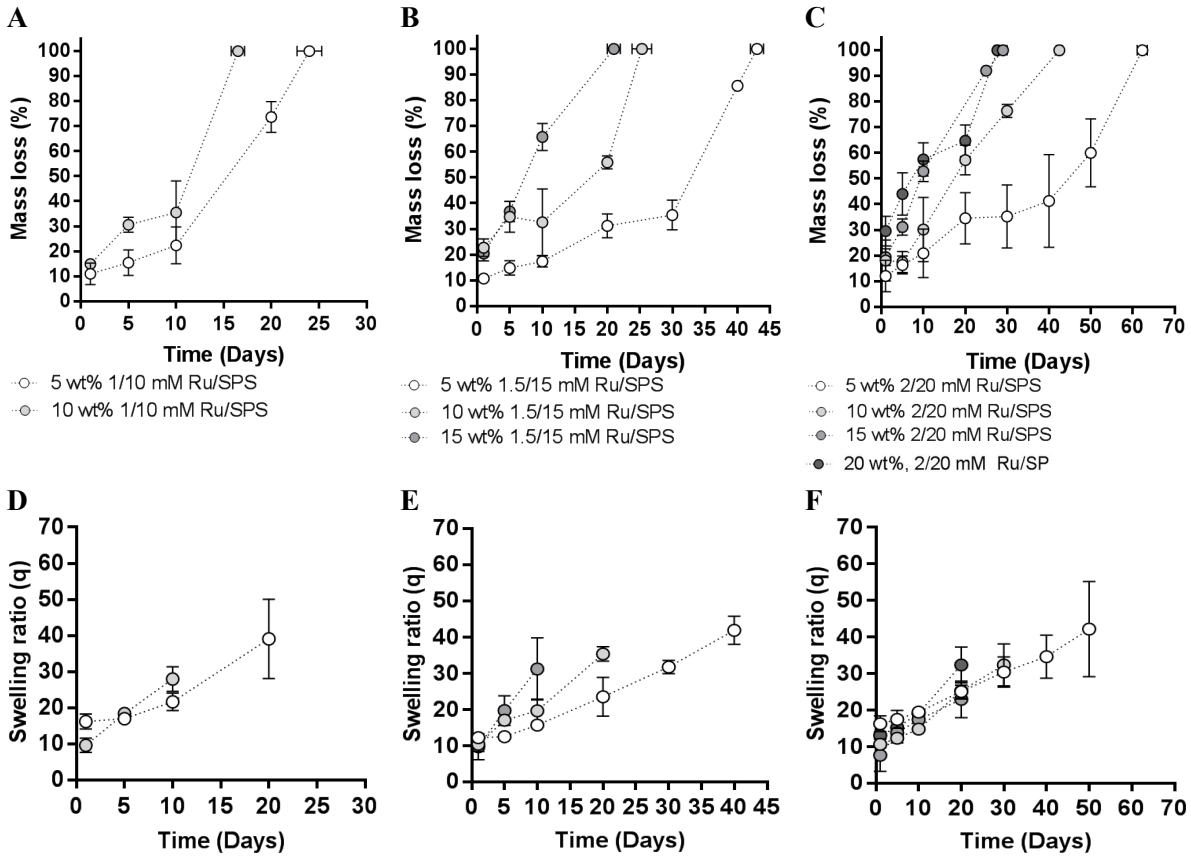

Supplementary Figure S3.3. Degradation of PVA-7Tyr hydrogels with varying macromer concentration. *(A-C) Mass loss and (D-F) swelling ratio of PVA-7Tyr hydrogels cross-linked using increasing macromer concentrations (5-20wt%) and a range photoinitiator concentrations (1/10-2/20 mM).*

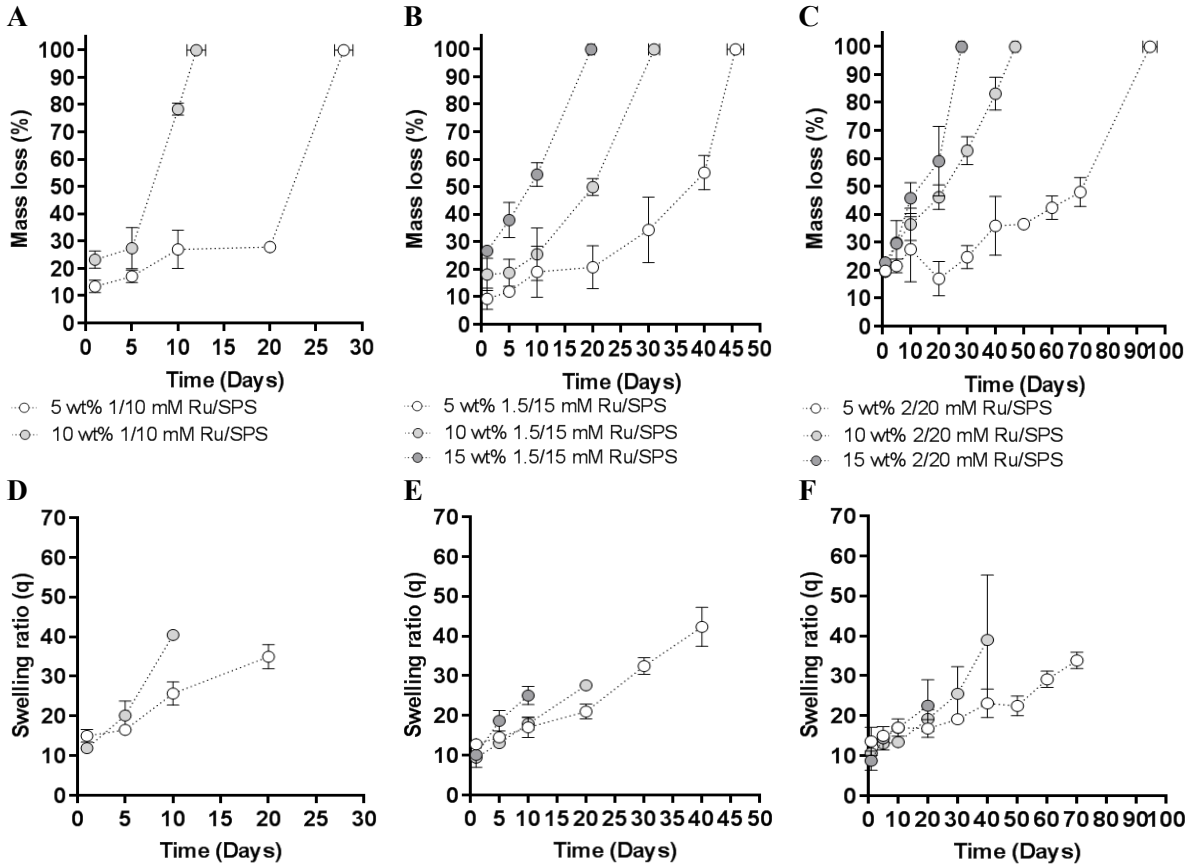

Supplementary Figure S3.4. Degradation of PVA-10Tyr hydrogels with varying macromer concentration. *(A-C) Mass loss and (D-F) swelling ratio of PVA-10Tyr hydrogels cross-linked using increasing macromer concentrations (5-15wt%) and a range photoinitiator concentrations (1/10-2/20 mM).*

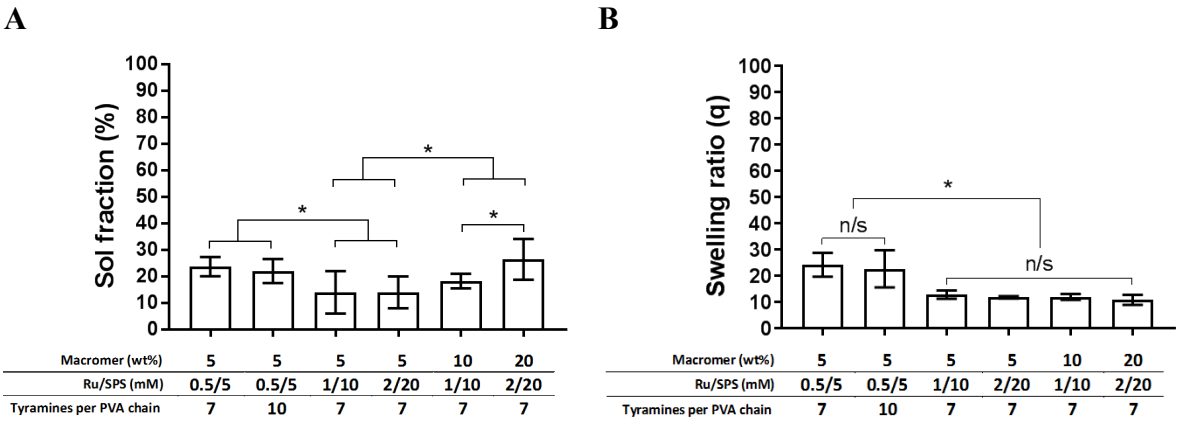

Supplementary Figure S3.5. Physico-chemical properties of PVA-Tyr hydrogels with incorporated BSA. *(A) Sol fraction and (B) day 1 swelling ratio, of PVA-Tyr hydrogels with incorporated BSA cross-linked at different conditions.*

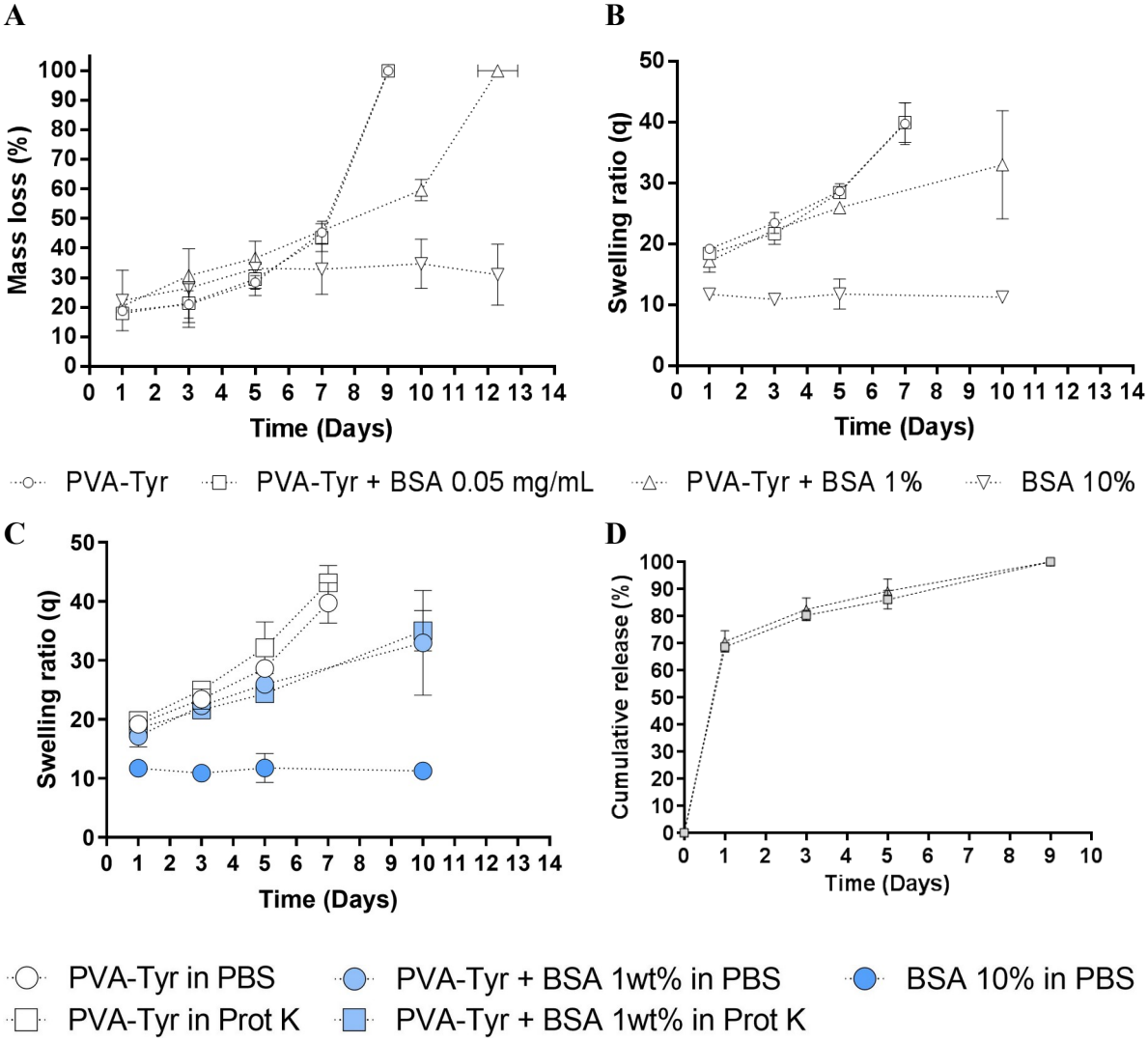

Supplementary Figure S3.6. Degradation of PVA-Tyr hydrogels with incorporated BSA under proteinase K exposure. *(A) Mass loss and (B) Swelling ratio of PVA-Tyr hydrogels with incorporated BSA. (C) Swelling ratio and (D) BSA release of PVA-Tyr hydrogels with incorporated BSA exposed to Proteinase K.*

A

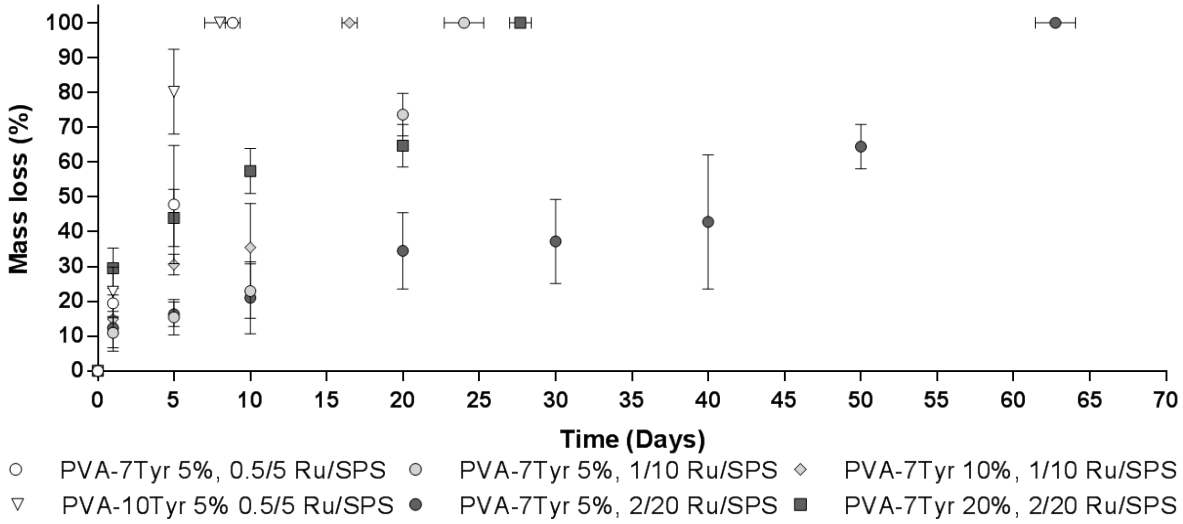

B

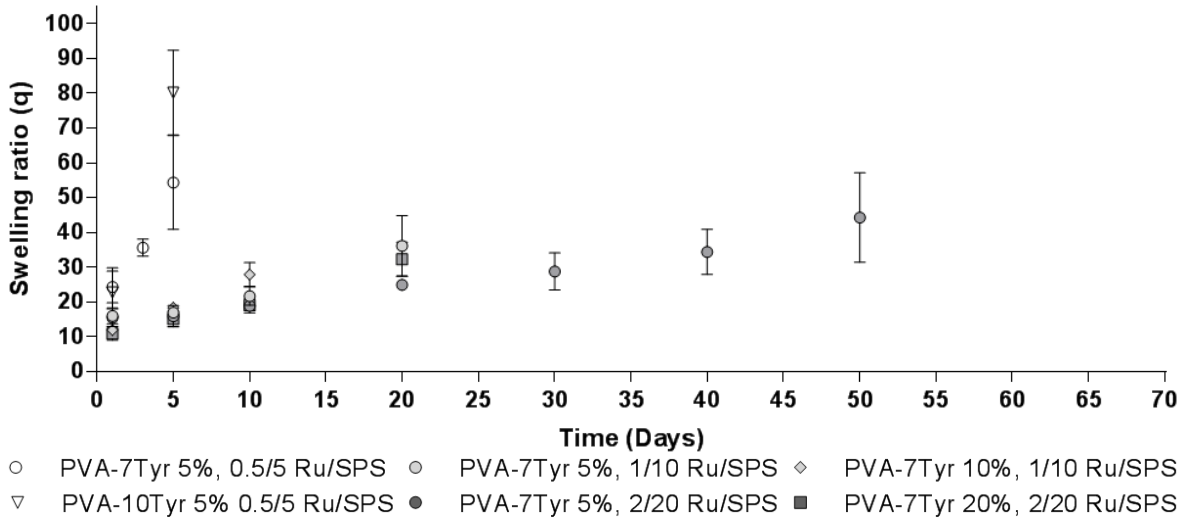

Supplementary figure S3.7. Degradation profile of PVA-Tyr hydrogels with incorporated BSA crosslinked using different photoinitiator and macromer concentrations. *(A) Mass loss profile and (B) swelling ratio profile of PVA-Tyr hydrogels with incorporated BSA cross-linked under different conditions.*

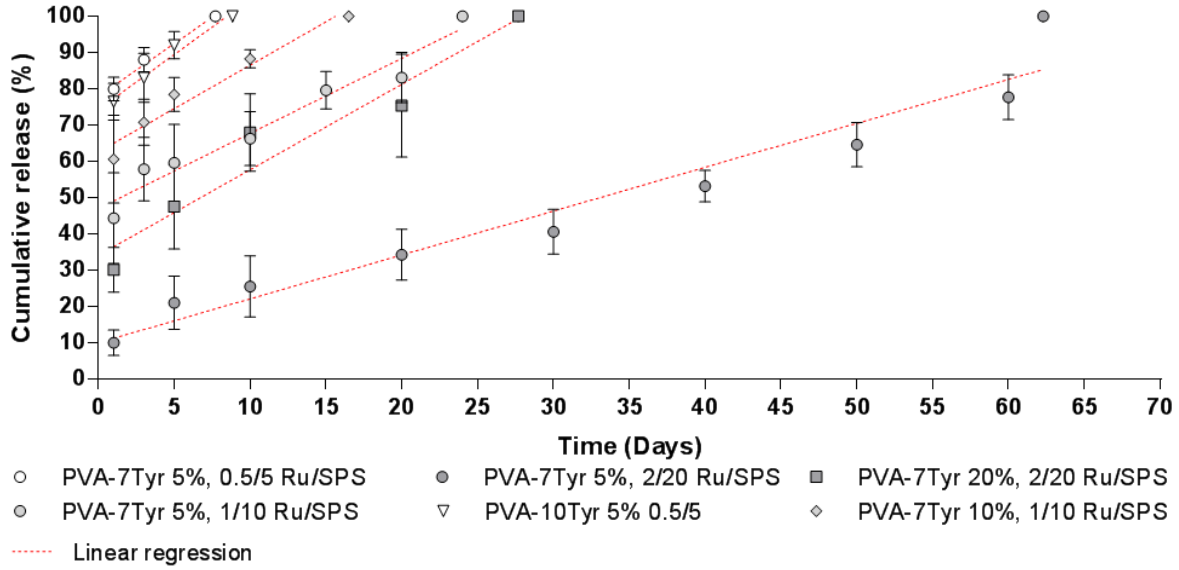

Supplementary Figure S3.8. Linear regression of BSA release profiles from PVA-Tyr hydrogels crosslinked using different photoinitiator and macromer concentrations.

Supplementary Table S3.7. *R^2 of the BSA release linear regression for different PVA-Tyr formulations and cross-linking conditions.*

	PVA-7Tyr 5 wt% 0.5/5 mM	**PVA-7Tyr 5 wt% 1/10 mM**	**PVA-7Tyr 5 wt% 2/20 mM**	**PVA-10Tyr 5 wt% 0.5/5 mM**	**PVA-7Tyr 10 wt% 1/10 mM**	**PVA-7Tyr 20 wt% 2/20 mM**
R^2	0.9861	0.9560	0.9458	0.9724	0.9541	0.9361

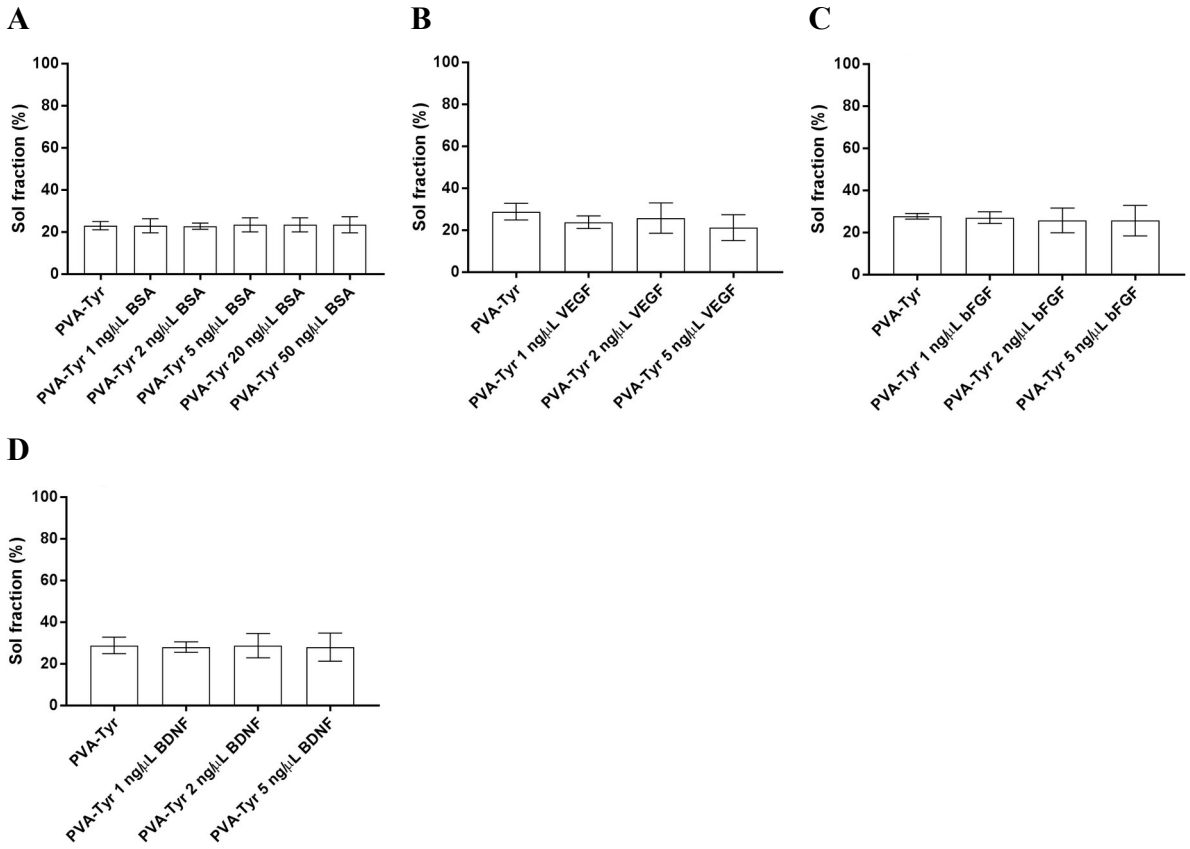

Supplementary Figure S3.9. Sol fraction of PVA-Tyr hydrogels with incorproated growth factors. *Sol fraction of PVA-7Tyr hydrogels cross-linked at 5 wt%, 0.5/5 mM Ru/SPS incorporated with different concentrations of (A) BSA, (B) VEGF, (C) bFGF and (D) BDNF. Protein concentrations are expressed as protein weight per volume of the macromer solution before cross-linking. No significant differences were found between groups (p>0.05)*

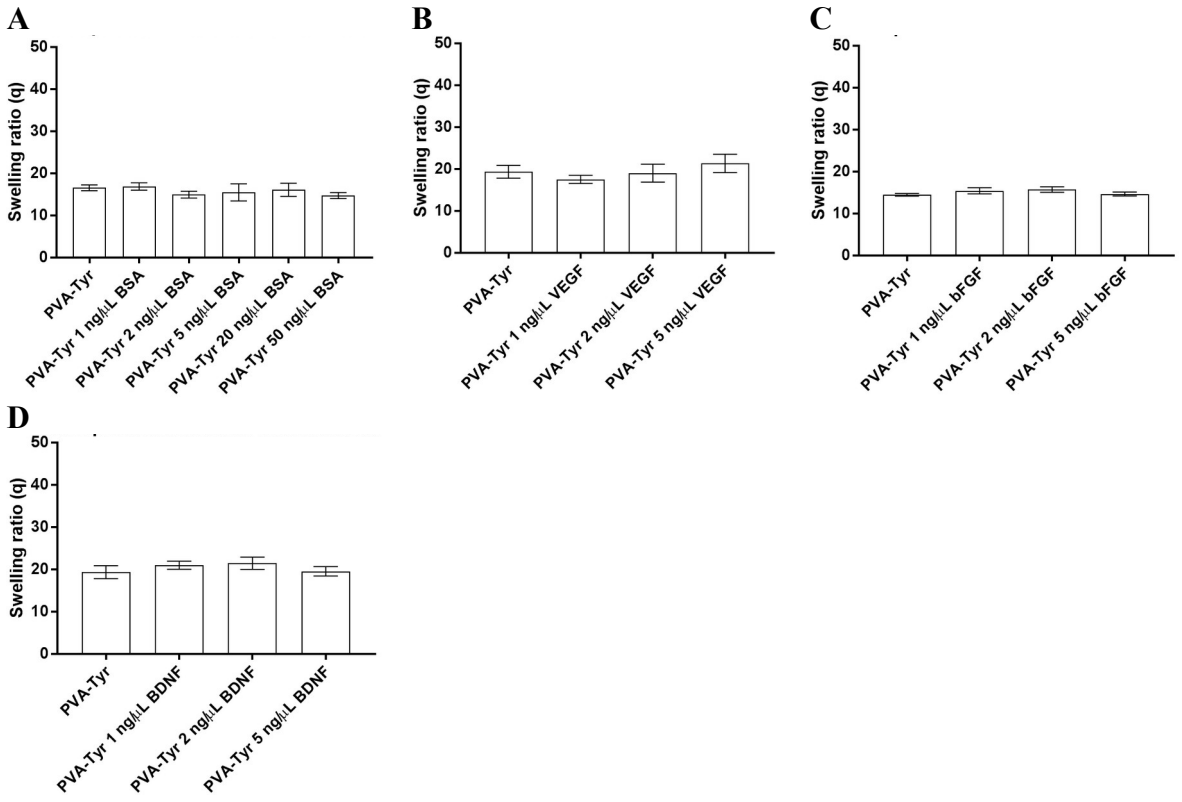

Supplementary Figure S3.10. Swelling ratio of PVA-Tyr hydrogels with incorproated growth factors. *Swelling ratio of PVA-7Tyr hydrogels cross-linked at 5 wt%, 0.5/5 mM Ru/SPS incorporated with different concentrations of (A) BSA, (B) VEGF, (C) bFGF and (D) BDNF. Protein concentrations are expressed as protein weight per volume of the macromer solution before cross-linking. No significant differences were found between groups (p>0.05)*

Supplementary Table S3.8. *Tyrosine and tyramine residues present and surface available in the incorporated growth factors. Available residues were extracted from Protein Data Bank files using Swiss-PDB Viewer at a surface availability threshold of 20%.*

	MW (Monomer)	**Number of tyrosine groups (Monomer)**	**Number of available tyrosine groups (Monomer)**
PVA-7Tyr	10 kDa	7 (Tyramine)	7 (Tyramine)
Albumin	66 kDa	18	3 (40)
VEGF	19 kDa	4	3 (41)
bFGF	9.9 kDa	10	1 (42)
BDNF	13.6 kDa	4	3 (43)

Supplementary Table S3.9. *R^2 of the linear regression of the VEGF, bFGF and BDNF release profiles for different PVA-Tyr cross-linking conditions.*

	VEGF 0.5/5 mM	**bFGF 0.5/5 mM**	**BDNF 0.5/5 mM**	**VEGF 1/10 mM**	**bFGF 1/10 mM**	**BDNF 1/10 mM**	**VEGF 2/20 mM**	**bFGF 2/20 mM**	**BDNF 2/20 mM**
R^2	0.696	0.7552	0.6492	0.9148	0.9116	0.8467	0.9084	0.9194	0.9172

3.6. References

1. Hanft JR, Pollak RA, Barbul A, van Gils C, Kwon PS, Gray SM, et al. Phase I trial on the safety of topical rhVEGF on chronic neuropathic diabetic foot ulcers. J Wound Care [Internet]. 2008;17(1):30–7. Available from: https://www.magonlinelibrary.com/doi/abs/10.12968/jowc.2008.17.1.27917

2. Bing M, Da-Sheng C, Zhao-Fan X, Dao-Feng B, Wei L, Zhi-Fang C, et al. Randomized, multicenter, double-blind, and placebo-controlled trial using topical recombinant human acidic fibroblast growth factor for deep partial-thickness burns and skin graft donor site. Wound Repair Regen [Internet]. 2007;15(6):795–9. Available from: http://dx.doi.org/10.1111/j.1524-475X.2007.00307.x

3. Kawaguchi H, Jingushi S, Izumi T, Fukunaga M, Matsushita T, Nakamura T, et al. Local application of recombinant human fibroblast growth factor-2 on bone repair: A dose–escalation prospective trial on patients with osteotomy. J Orthop Res [Internet]. 2007;25(4):480–7. Available from: http://dx.doi.org/10.1002/jor.20315

4. Chan SJ, Love C, Spector M, Cool SM, Nurcombe V, Lo EH. Endogenous regeneration: Engineering growth factors for stroke. Neurochem Int [Internet]. 2017;107:57–65. Available from: https://www.ncbi.nlm.nih.gov/pubmed/28411103

5. FDA. Safety Warning on Becaplermin in Regranex. 2008.

6. Carragee EJ, Chu G, Rohatgi R, Hurwitz EL, Weiner BK, Yoon ST, et al. Cancer Risk After Use of Recombinant Bone Morphogenetic Protein-2 for Spinal Arthrodesis. JBJS [Internet]. 2013;95(17). Available from: https://journals.lww.com/jbjsjournal/Fulltext/2013/09040/Cancer_Risk_After_Use_of_Recombinant_Bone.1.aspx

7. Simons M, Ware JA. Therapeutic angiogenesis in cardiovascular disease. Nat Rev Drug Discov [Internet]. 2003;2(11):863–72. Available from: https://doi.org/10.1038/nrd1226

8. Theiss HD, Brenner C, Engelmann MG, Zaruba M-M, Huber B, Henschel V, et al. Safety and efficacy of SITAgliptin plus GRanulocyte-colony-stimulating factor in patients suffering from Acute Myocardial Infarction (SITAGRAMI-Trial) —

Rationale, design and first interim analysis. Int J Cardiol [Internet]. 2010;145(2):282–4. Available from: http://www.sciencedirect.com/science/article/pii/S0167527309015010

9. Wang Z, Wang Z, Lu WW, Zhen W, Yang D, Peng S. Novel biomaterial strategies for controlled growth factor delivery for biomedical applications. Npg Asia Mater [Internet]. 2017;9:e435. Available from: http://dx.doi.org/10.1038/am.2017.171

10. Bose S, Tarafder S. Calcium phosphate ceramic systems in growth factor and drug delivery for bone tissue engineering: A review. Acta Biomater [Internet]. 2012;8(4):1401–21. Available from: http://www.sciencedirect.com/science/article/pii/S1742706111005046

11. Koria P. Delivery of Growth Factors for Tissue Regeneration and Wound Healing. BioDrugs [Internet]. 2012;26(3):163–75. Available from: https://doi.org/10.2165/11631850-000000000-00000

12. Jeon O, Song SJ, Yang HS, Bhang SH, Kang SW, Sung MA, et al. Long-term delivery enhances in vivo osteogenic efficacy of bone morphogenetic protein-2 compared to short-term delivery. Biochem Biophys Res Commun [Internet]. 2008;369(2):774–80. Available from: https://www.ncbi.nlm.nih.gov/pubmed/18313401

13. Betz OB, Betz VM, Nazarian A, Egermann M, Gerstenfeld LC, Einhorn TA, et al. Delayed administration of adenoviral BMP-2 vector improves the formation of bone in osseous defects. Gene Ther [Internet]. 2007;14:1039. Available from: http://dx.doi.org/10.1038/sj.gt.3302956

14. Seeherman H, Li R, Bouxsein M, Kim H, Li XJ, Smith-Adaline EA, et al. rhBMP-2/calcium phosphate matrix accelerates osteotomy-site healing in a nonhuman primate model at multiple treatment times and concentrations. J Bone Jt Surg - Ser A. 2006 Jan;88(1):144–60.

15. Kanczler JM, Ginty PJ, White L, Clarke NMP, Howdle SM, Shakesheff KM, et al. The effect of the delivery of vascular endothelial growth factor and bone morphogenic protein-2 to osteoprogenitor cell populations on bone formation. Biomaterials [Internet]. 2010;31(6):1242–50. Available from:

http://www.sciencedirect.com/science/article/pii/S0142961209011806

16. Toth JM, Boden SD, Burkus JK, Badura JM, Peckham SM, McKay WF. Short-term Osteoclastic Activity Induced by Locally High Concentrations of Recombinant Human Bone Morphogenetic Protein–2 in a Cancellous Bone Environment. Spine (Phila Pa 1976) [Internet]. 2009;34(6):539–50. Available from: http://journals.lww.com/spinejournal/Fulltext/2009/03150/Short_term_Osteoclastic_Activity_Induced_by.3.aspx

17. Carragee EJ, Hurwitz EL, Weiner BK. A critical review of recombinant human bone morphogenetic protein-2 trials in spinal surgery: emerging safety concerns and lessons learned. Spine J [Internet]. 2011;11(6):471–91. Available from: http://www.sciencedirect.com/science/article/pii/S1529943011002993

18. Masters KS. Covalent Growth Factor Immobilization Strategies for Tissue Repair and Regeneration. Macromol Biosci [Internet]. 2011;11(9):1149–63. Available from: http://dx.doi.org/10.1002/mabi.201000505

19. Vulic K, Shoichet MS. Affinity-Based Drug Delivery Systems for Tissue Repair and Regeneration. Biomacromolecules [Internet]. 2014;15(11):3867–80. Available from: http://dx.doi.org/10.1021/bm501084u

20. Partlow BP, Applegate MB, Omenetto FG, Kaplan DL. Dityrosine Cross-Linking in Designing Biomaterials. ACS Biomater Sci Eng. 2016;2(12):2108–21.

21. Kim KS, Park SJ, Yang JA, Jeon JH, Bhang SH, Kim BS, et al. Injectable hyaluronic acid–tyramine hydrogels for the treatment of rheumatoid arthritis. Acta Biomater [Internet]. 2011;7(2):666–74. Available from: http://www.sciencedirect.com/science/article/pii/S174270611000440X

22. Shona Pek Y, Kurisawa M, Gao S, Chung JE, Ying JY. The development of a nanocrystalline apatite reinforced crosslinked hyaluronic acid-tyramine composite as an injectable bone cement. Biomaterials [Internet]. 2009;30(5):822–8. Available from: http://dx.doi.org/10.1016/j.biomaterials.2008.10.053

23. Jin R, Moreira Teixeira LS, Dijkstra PJ, Zhong Z, van Blitterswijk CA, Karperien M,

et al. Enzymatically Crosslinked Dextran-Tyramine Hydrogels as Injectable Scaffolds for Cartilage Tissue Engineering. Tissue Eng Part A. 2010;16(8):2429–40.

24. Kim SH, Lee SH, Lee JE, Park SJ, Kim K, Kim IS, et al. Tissue adhesive, rapid forming, and sprayable ECM hydrogel via recombinant tyrosinase crosslinking. Biomaterials [Internet]. 2018;178:401–12. Available from: https://doi.org/10.1016/j.biomaterials.2018.04.057

25. Moreira Teixeira LS, Bijl S, Pully V V., Otto C, Jin R, Feijen J, et al. Self-attaching and cell-attracting in-situ forming dextran-tyramine conjugates hydrogels for arthroscopic cartilage repair. Biomaterials [Internet]. 2012;33(11):3164–74. Available from: http://dx.doi.org/10.1016/j.biomaterials.2012.01.001

26. Lim KS, Alves MH, Poole-Warren LA, Martens PJ. Covalent incorporation of non-chemically modified gelatin into degradable PVA-tyramine hydrogels. Biomaterials [Internet]. 2013;34(29):7097–105. Available from: http://dx.doi.org/10.1016/j.biomaterials.2013.06.005

27. Lim KS, Ramaswamy Y, Roberts JJ, Alves M-H, Poole-Warren LA, Martens PJ. Promoting Cell Survival and Proliferation in Degradable Poly(vinyl alcohol)–Tyramine Hydrogels. Macromol Biosci [Internet]. 2015;15(10):1423–32. Available from: https://onlinelibrary.wiley.com/doi/abs/10.1002/mabi.201500121

28. Lim KS, Roberts JJ, Alves M, Poole-Warren LA, Martens PJ. Understanding and tailoring the degradation of PVA-tyramine hydrogels. J Appl Polym Sci [Internet]. 2015;132(26). Available from: https://onlinelibrary.wiley.com/doi/abs/10.1002/app.42142

29. Fancy DA. Chemistry for the analysis of protein-protein interactions: Rapid and efficient cross-linking triggered by long wavelength light. Proc Natl Acad Sci [Internet]. 1999;96(11):6020–4. Available from: http://www.pnas.org/cgi/content/abstract/96/11/6020

30. Ma X, Sun X, Hargrove D, Chen J, Song D, Dong Q, et al. A Biocompatible and Biodegradable Protein Hydrogel with Green and Red Autofluorescence: Preparation, Characterization and In Vivo Biodegradation Tracking and Modeling. Sci Rep

[Internet]. 2016;6:19370. Available from: https://doi.org/10.1038/srep19370

31. Bieschke J, Giese A, Schulz-Schaeffer W, Zerr I, Poser S, Eigen M, et al. Ultrasensitive detection of pathological prion protein aggregates by dual-color scanning for intensely fluorescent targets. Proc Natl Acad Sci [Internet]. 2000 May 9;97(10):5468 LP – 5473. Available from: http://www.pnas.org/content/97/10/5468.abstract

32. Striemer CC, Gaborski TR, McGrath JL, Fauchet PM. Charge- and size-based separation of macromolecules using ultrathin silicon membranes. Nature [Internet]. 2007;445(7129):749–53. Available from: https://doi.org/10.1038/nature05532

33. Aregueta-Robles UA, Martens PJ, Poole-Warren LA, Green RA. Tissue engineered hydrogels supporting 3D neural networks. Acta Biomater [Internet]. 2019;95:269–84. Available from: http://www.sciencedirect.com/science/article/pii/S1742706118307074

34. Jin R, Moreira Teixeira LS, Dijkstra PJ, Zhong Z, van Blitterswijk CA, Karperien M, et al. Enzymatically Crosslinked Dextran-Tyramine Hydrogels as Injectable Scaffolds for Cartilage Tissue Engineering. Tissue Eng Part A [Internet]. 2010;16(8):2429–40. Available from: https://www.liebertpub.com/doi/abs/10.1089/ten.tea.2009.0764

35. Artzi N, Oliva N, Puron C, Shitreet S, Artzi S, bon Ramos A, et al. In vivo and in vitro tracking of erosion in biodegradable materials using non-invasive fluorescence imaging. Nat Mater [Internet]. 2011;10(9):890. Available from: https://doi.org/10.1038/nmat3095

36. Brömme D, Peters K, Fink S, Fittkau S. Enzyme-substrate interactions in the hydrolysis of peptide substrates by thermitase, subtilisin BPN′, and proteinase K. Arch Biochem Biophys. 1986;244(2):439–46.

37. Patterson J, Siew R, Herring SW, Lin ASP, Guldberg R, Stayton PS. Hyaluronic acid hydrogels with controlled degradation properties for oriented bone regeneration. Biomaterials [Internet]. 2010;31(26):6772–81. Available from: http://www.sciencedirect.com/science/article/pii/S0142961210006654

38. Davis HE, Leach JK. Designing bioactive delivery systems for tissue regeneration.

Ann Biomed Eng [Internet]. 2010/07/30. 2011 Jan;39(1):1–13. Available from: https://www.ncbi.nlm.nih.gov/pubmed/20676773

39. Miller RE, Grodzinsky AJ, Cummings K, Plaas AHK, Cole AA, Lee RT, et al. Intraarticular injection of heparin-binding insulin-like growth factor 1 sustains delivery of insulin-like growth factor 1 to cartilage through binding to chondroitin sulfate. Arthritis Rheum [Internet]. 2010;62(12):3686–94. Available from: http://dx.doi.org/10.1002/art.27709

40. Bujacz A. Structures of bovine, equine and leporine serum albumin. Acta Crystallogr Sect D [Internet]. 2012 Oct;68(10):1278–89. Available from: https://doi.org/10.1107/S0907444912027047

41. Muller YA, Li B, Christinger HW, Wells JA, Cunningham BC, de Vos AM. Vascular endothelial growth factor: Crystal structure and functional mapping of the kinase domain receptor binding site. Proc Natl Acad Sci [Internet]. 1997 Jul 8;94(14):7192 LP – 7197. Available from: http://www.pnas.org/content/94/14/7192.abstract

42. Zhu X, Komiya H, Chirino A, Faham S, Fox GM, Arakawa T, et al. Three-dimensional structures of acidic and basic fibroblast growth factors. Science (80-) [Internet]. 1991;251(4989):90–3. Available from: https://science.sciencemag.org/content/251/4989/90

43. Robinson RC, Radziejewski C, Spraggon G, Greenwald J, Kostura MR, Burtnick LD, et al. The structures of the neurotrophin 4 homodimer and the brain-derived neurotrophic factor/neurotrophin 4 heterodimer reveal a common Trk-binding site. Protein Sci [Internet]. 1999 Dec;8(12):2589–97. Available from: https://www.ncbi.nlm.nih.gov/pubmed/10631974

44. Gu F, Neufeld R, Amsden B. Maintenance of vascular endothelial growth factor and potentially other therapeutic proteins bioactivity during a photo-initiated free radical cross-linking reaction forming biodegradable elastomers. Eur J Pharm Biopharm [Internet]. 2007;66(1):21–7. Available from: http://www.sciencedirect.com/science/article/pii/S0939641106002232

45. Lin C-C, Sawicki SM, Metters AT. Free-Radical-Mediated Protein Inactivation and

Recovery during Protein Photoencapsulation. Biomacromolecules [Internet]. 2008;9(1):75–83. Available from: https://doi.org/10.1021/bm700782c

46. Hoeben A, Landuyt B, Highley MS, Wildiers H, Van Oosterom AT, De Bruijn EA. Vascular Endothelial Growth Factor and Angiogenesis. Pharmacol Rev [Internet]. 2004 Dec 1;56(4):549 LP – 580. Available from: http://pharmrev.aspetjournals.org/content/56/4/549.abstract

47. Cross MJ, Claesson-Welsh L. FGF and VEGF function in angiogenesis: signalling pathways, biological responses and therapeutic inhibition. Trends Pharmacol Sci [Internet]. 2001;22(4):201–7. Available from: http://www.sciencedirect.com/science/article/pii/S016561470001676X

48. Kermani P, Hempstead B. Brain-derived neurotrophic factor: a newly described mediator of angiogenesis. Trends Cardiovasc Med [Internet]. 2007 May;17(4):140–3. Available from: https://www.ncbi.nlm.nih.gov/pubmed/17482097

49. Eming SA, Martin P, Tomic-Canic M. Wound repair and regeneration: Mechanisms, signaling, and translation. Sci Transl Med [Internet]. 2014 Dec 3;6(265):265sr6 LP-265sr6. Available from: http://stm.sciencemag.org/content/6/265/265sr6.abstract

50. Sun C, Hu Y, Chu Z, Huang J, Zhang L. The effect of brain-derived neurotrophic factor on angiogenesis. J Huazhong Univ Sci Technol [Medical Sci [Internet]. 2009;29(2):139–43. Available from: https://doi.org/10.1007/s11596-009-0201-6

51. Maretzky T, Evers A, Zhou W, Swendeman SL, Wong P-M, Rafii S, et al. Migration of growth factor-stimulated epithelial and endothelial cells depends on EGFR transactivation by ADAM17. Nat Commun [Internet]. 2011;2(1):229. Available from: https://doi.org/10.1038/ncomms1232

52. Oommen S, Gupta SK, Vlahakis NE. Vascular Endothelial Growth Factor A (VEGF-A) Induces Endothelial and Cancer Cell Migration through Direct Binding to Integrin α9β1: IDENTIFICATION OF A SPECIFIC α9β1 BINDING SITE . J Biol Chem [Internet]. 2011 Jan 14;286(2):1083–92. Available from: http://www.jbc.org/content/286/2/1083.abstract

53. Nakashio A, Fujita N, Tsuruo T. Topotecan inhibits VEGF- and bFGF-induced vascular endothelial cell migration via downregulation of the PI3K-Akt signaling pathway. Int J Cancer [Internet]. 2002 Mar 1;98(1):36–41. Available from: https://doi.org/10.1002/ijc.10166

54. Schichor C, Birnbaum T, Etminan N, Schnell O, Grau S, Miebach S, et al. Vascular endothelial growth factor A contributes to glioma-induced migration of human marrow stromal cells (hMSC). Exp Neurol [Internet]. 2006;199(2):301–10. Available from: http://www.sciencedirect.com/science/article/pii/S0014488605004255

55. Naaldijk Y, Johnson AA, Ishak S, Meisel HJ, Hohaus C, Stolzing A. Migrational changes of mesenchymal stem cells in response to cytokines, growth factors, hypoxia, and aging. Exp Cell Res [Internet]. 2015;338(1):97–104. Available from: http://www.sciencedirect.com/science/article/pii/S0014482715300823

56. He S, Shen L, Wu Y, Li L, Chen W, Hou C, et al. Effect of Brain-Derived Neurotrophic Factor on Mesenchymal Stem Cell-Seeded Electrospinning Biomaterial for Treating Ischemic Diabetic Ulcers via Milieu-Dependent Differentiation Mechanism. Tissue Eng Part A [Internet]. 2014 Oct 15;21(5–6):928–38. Available from: https://doi.org/10.1089/ten.tea.2014.0113

57. Stratman AN, Davis GE. Endothelial Cell-Pericyte Interactions Stimulate Basement Membrane Matrix Assembly: Influence on Vascular Tube Remodeling, Maturation, and Stabilization. Microsc Microanal [Internet]. 2011/12/14. 2012;18(1):68–80. Available from: https://www.cambridge.org/core/article/endothelial-cellpericyte-interactions-stimulate-basement-membrane-matrix-assembly-influence-on-vascular-tube-remodeling-maturation-and-stabilization/187247E0DA9E579D6A539874E1E8A421

58. Saunders WB, Bohnsack BL, Faske JB, Anthis NJ, Bayless KJ, Hirschi KK, et al. Coregulation of vascular tube stabilization by endothelial cell TIMP-2 and pericyte TIMP-3 . J Cell Biol [Internet]. 2006 Oct 9;175(1):179–91. Available from: https://doi.org/10.1083/jcb.200603176

59. Hua L, Simone K, Brenda L. NOTCH3 Expression Is Induced in Mural Cells Through an Autoregulatory Loop That Requires Endothelial-Expressed JAGGED1. Circ Res

[Internet]. 2009 Feb 27;104(4):466–75. Available from: https://doi.org/10.1161/CIRCRESAHA.108.184846

60. Kempen DH, Lu L, Hefferan TE, Creemers LB, Maran A, Classic KL, et al. Retention of in vitro and in vivo BMP-2 bioactivities in sustained delivery vehicles for bone tissue engineering. Biomaterials [Internet]. 2008;29(22):3245–52. Available from: https://www.ncbi.nlm.nih.gov/pubmed/18472153

61. Tong X, Lee S, Bararpour L, Yang F. Long-Term Controlled Protein Release from Poly(Ethylene Glycol) Hydrogels by Modulating Mesh Size and Degradation. Macromol Biosci [Internet]. 2015;15(12):1679–86. Available from: https://www.ncbi.nlm.nih.gov/pubmed/26259711

Chapter 4. Adaptation the PVA-Tyr Growth Factor Delivery System for the Treatment of Perthes Disease

4.1. Introduction

Legg-Calve-Perthes disease (Also known as LCPD or Perthes disease) is an idiopathic avascular necrosis of the femoral head (Figure 4.1) (1). It is considered a rare disease, with an incidence ranging from 0.4/100,000 to 29/100,000 children below 15 years of age according to epidemiological studies in different countries (2). The causes of the ischaemic episodes in the femoral head are not well known, and it has been hypothesized that instances of micro-trauma (3) and environmental factors such as low-socioeconomic status (4) and passive smoking (5) could be involved.

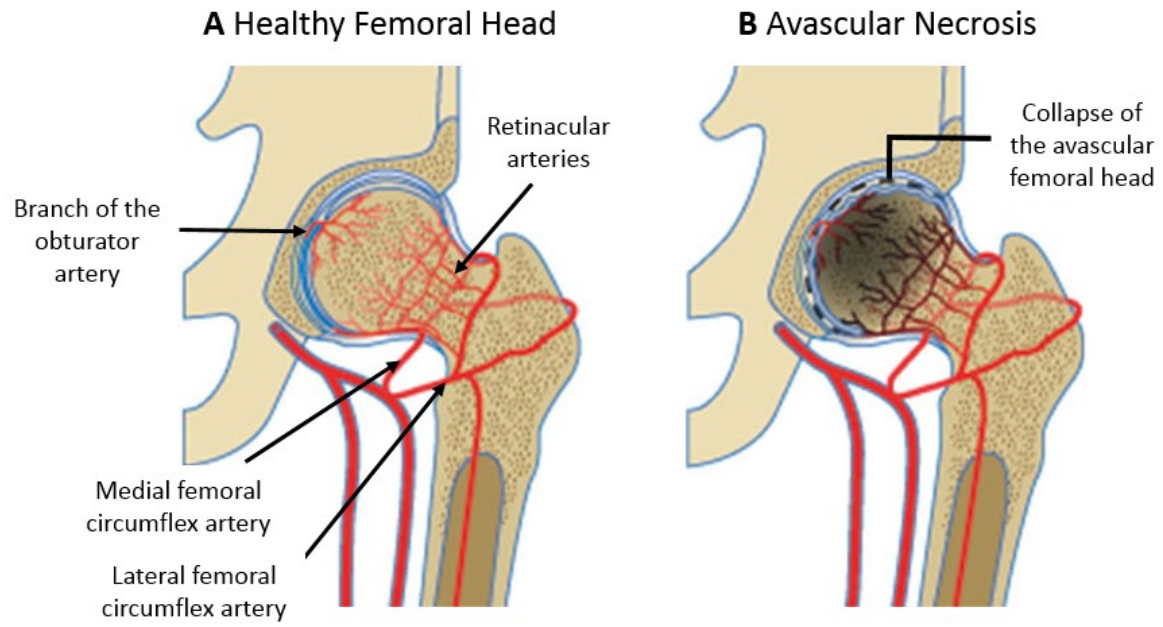

Figure 4.1. Schematic view of avascular necrosis of the femoral head. *(A) Blood supply to the femoral head mainly comes from the retinacular arteries and a branch of the obturator artery. (B) Disruption of the blood vessel supply results in necrosis and collapse of the femoral head. Adapted from (6).*

In Perthes disease, tissue necrosis causes the femoral head to deform under the physiological loading forces across the hip joint. The resulting symptoms include pain, restricted range of movement and reduced functional ability (7). Early intervention is often performed in

children to allow regrowth of healthy bone tissue. The most common intervention is core decompression, which consists in drilling a small hole in the necrotic bone to decrease the intraosseous pressure (8). Despite early intervention, the progression of the disease results in collapse of the femoral head (Figure 4.1B). If collapse happens, the long-term prognosis is poor (9–12), resulting in pain, joint stiffness, leg length inequality, limping and osteoarthritis (13). At this stage, early hip arthroplasty is necessary for pain relief and improvement in daily function (14). However, this procedure has increased complications in patients with Perthes disease (15). It therefore seems imperative to treat this condition accurately and successfully at its onset.

The underlying pathological condition in Perthes disease is the lack of blood supply in the femoral head. Therefore, a rational early treatment could aim to restore this blood supply, thus providing oxygen and nutrients to the area and promoting the formation of new, healthy bone. Delivering growth factors (GFs) is one of the most promising approaches to promote angiogenesis (16). VEGF is one of the most studied angiogenesis-promoting GFs (17–20) and plays an important role in bone repair and regeneration (21), which has inspired several research studies on the use of VEGF to promote bone vascularisation and regeneration (22–25). For example, Kaigler et al. delivered VEGF into rat critical-sized bone defects either by bolus administration or loaded into an alginate hydrogel. Their study showed that delivering VEGF using the alginate hydrogel resulted in improved blood vessel density 4 weeks after implantation and improved bone density 8 weeks after implantation as compared to negative controls without delivered VEGF and the bolus delivery group (25). These results show not only that VEGF could be a promising treatment for the promotion of revascularisation of the femoral head and the subsequent formation of new bone, but also that its release needs to be controlled using vehicles such as biomaterials. In fact, VEGF has also been used specifically for cases of avascular necrosis of the femoral head (54), but these studies did not focus on controlling the GF release and the degradation of the materials in a way that coordinates with tissue regeneration. In order to deliver VEGF to promote revascularisation of the femoral head, it is crucial to use a delivery system that can be adapted to releasing VEGF in a controlled manner during the vascularisation process. In Chapter 3, PVA-Tyr was studied as a GF delivery system that excelled due to its highly controllable degradation and release kinetics. Furthermore, the feasibility of the system was tested *in vitro*, demonstrating the bioactivity of released VEGF, which was evidenced by its ability to promote endothelial cell

proliferation, migration and network formation. These characteristics make the PVA-Tyr system a solid candidate for its application in Perthes disease.

Another important aspect to consider when designing a delivery system that aims to promote vascularisation is its interaction with cells. Newly formed vessels branching from the host vasculature need to penetrate into the necrotic area during the early stages of regeneration (26), making materials with cell-adhesive properties that facilitate cell migration and ECM remodelling highly desirable for this application. However, one of the limitations of PVA as a delivery system is its lack of biological recognition sites for interaction with cells (27). es.

In this chapter, a potential application of the PVA-Tyr system is demonstrated by tailoring it to deliver VEGF for the treatment of Perthes disease. The first aim of the chapter was to study the possibility of combining PVA-Tyr hydrogels with gelatin and investigate the effects of this combination on the interaction of the gels with endothelial cells, their degradation properties and their GF release profile. The second aim of the chapter was to develop a strategy to inject these hydrogels into the femoral head, specifically in a piglet model of avascular necrosis. While my personal involvement was exclusively in the materials related aspects of the study, preliminary results of the *in vivo* experiment to evaluate the potential of these VEGF loaded PVA-Tyr hydrogels are also provided in the chapter.

4.2. Materials and Methods

4.2.1. Hydrogel Fabrication

Dried PVA-Tyr was dissolved in PBS at 80 °C. Upon complete dissolution, the polymer solution was cooled to room temperature (RT) and mixed with Ru and SPS stock solutions to a final concentration of 5wt% PVA-Tyr and 0.5/5 mM Ru/SPS. Gelatin or growth factor stock solutions were mixed with the PVA-Tyr solution prior to the addition of Ru and SPS. BSA hydrogels were obtained by mixing a 10wt% BSA solution with Ru and SPS stock solutions to a final concentration of 2/20 mM Ru/SPS. All samples were photo-crosslinked using visible light (OmniCure® S1500, Excelitas Technologies with a Rosco IR/UV filter 400 – 450nm, 3min, 300 mW cm^{-2}) in cylindrical moulds (h = 2 mm, Ø = 6 mm) in an open environment.

4.2.2. Swelling and Mass Loss Assays

After crosslinking, each hydrogel (35 µL) was weighed ($m_{initial,t0}$), out of which three samples per hydrogel composition were directly freeze-dried to record their initial dry weights ($m_{dry,t0}$) and determine the actual macromer weight fraction, which is reported as the ratio of the initial dry weight to the initial weight. To determine the initial dry weight of the remaining samples, the factor of the actual macromer fraction and individual initial weight was used (Eq. 1).

$$Actual macromer fraction = \frac{m_{dry,t0}}{m_{initial}} \quad (1)$$

The remaining samples were allowed to swell in PBS at 37 °C until up to 1d or longer time points to determine the mass loss. Swollen hydrogel samples were collected to record wet weight ($m_{swollen}$), then freeze-dried to obtain the freeze dried weight (m_{dry}) to calculate the mass loss and mass swelling ratio (q) according to equations 2 and 3:

$$m_{dry,t0} = m_{initial} x actual macromer fraction \quad (2)$$

$$Mass loss = \frac{m_{dry,t0} - m_{dry}}{m_{dry,t0}} x 100 \quad (3)$$

$$q = \frac{m_{swollen}}{m_{dry}} \quad (4)$$

The sol fraction of the hydrogels is defined as percent macromers that are not crosslinked into the hydrogel network, and determined as the mass loss after equilibrium swelling (t = 1 d).

4.2.3. Cell Attachment Assays

PVA-Tyr hydrogels were fabricated directly in the cell culture wells of a 24 well-plate using a silicon mould (6mm diameter, 1mm depth) and allowed to swell overnight in Vascular Basal Media (ATCC) supplemented with Endothelial Cell Growth Kit-VEGF (ATCC) and Penicillin/Streptomycin (Referred to as endothelial growth media, EGM). Green fluorescent protein-labelled human umbilical vein endothelial cells (GFP-HUVECs, obtained from Cellworks) were cultured in EGM up to passage 3 to 4, trypsinized and seeded on the hydrogels at a density of 1.000 cells/mm2. After 6h, hydrogels were washed two times using EGM and imaged using a Zeiss Axioimager Z1 fluorescence microscope (Carl Zeiss Microscopy, Jena, Germany).

4.2.4. Effect of Proteinase Exposure on Degradation Profile

PVA-Tyr and hydrogels were left in either PBS or PBS with additional Proteinase K 1 mg/mL as previously described (38), then incubated at 37°C. The PBS solutions with our without Proteinase K were discarded every 48h and fresh solution was added for continuous exposure to functional enzyme. Mass loss and swelling ratios were calculated using equations 1-4.

4.2.5. Preparation of PVA-Gelatin-VEGF Hydrogels for the In Vivo Study

For each individual sample, 500 µL of a PVA-Tyr (5wt%, functionalised with 7 tyramines per chain) and Gelatin (1wt%) solution with or without 250 ng of VEGF-165 were mixed with Ru/SPS (1/10 mM final concentration) and crosslinked using visible light (OmniCure® S1500, Excelitas Technologies with a Rosco IR/UV filter 400 – 450nm, 3min, 300 mW cm^{-2}) in a transparent syringe.

4.2.6. In Vivo Surgical Procedure

To perform a pilot study to evaluate the effectiveness and feasibility of the system in an *in vivo* setting, a previously validated piglet model of avascular necrosis was used (39–41) under ethics approval from the University of Otago Animal Ethics Committee (AEC 2017-43). Briefly, large white/landrace cross piglets were anesthetised using 2% isoflurane. The limbs and pelvic area were sterilised using 2% chlorhexidine/70%isopropyl alcohol and a

longitudinal incision was made over the hip. Gluteus and hip abductor muscles overlying the hip joint were identified and separated using retractors. The hip joint capsule was partially incised to expose the lateral aspect of the femoral head and neck. The ligamentum teres was visualized by subluxing the femoral head and resected using a curved scissor. A 1.0 nylon suture was then passed around the femoral neck and tied tightly to ensure obstruction of the retinacular vessels. After vessel disruption, a hole was drilled with the entry point at the anterolateral proximal femur, penetrating across the centre of the growth plate into the core of the femoral head. PVA-Tyr hydrogels (500 µL, 5% PVA-Tyr, 1% Gelatin, 0.5/5 Ru/SPS) with or without VEGF (500 ng/mL) were then delivered through this hole using a Jamshidi needle. Experimental groups included a group where no vessels were disrupted (No operation, n=2), a group with disrupted vessels (Vessels disrupted, n=4), a group with a drilled hole but no material delivered (Sham, n=4), a group where PVA-Gelatin was delivered (PVA-Gel, n=8) and a group where PVA-Gelatin with incorporated VEGF was delivered (PVA-Gel-VEGF, n=8). The treatments were randomly distributed between piglets.

4.2.7. Histological Analysis and Imaging

Animals were sacrificed 15 weeks after the surgical procedure and the proximal part of the femur was harvested. Samples were examined grossly, dissected and CT imaged. The samples were then fixed in 10% buffered formalin, decalcified, embedded in paraffin and sectioned. For general histological analysis, the sections were stained with hematoxylin and eosin staining.

4.2.8. Statistical Analysis

All samples were prepared in triplicates and each experiment was repeated three times to study variability between experiments (N=3) except for the *in vivo* study. Individual differences between groups and time points were assessed using one or two-way ANOVA and Holm-Sidak post hoc analysis (GraphPad Prism 7). Statistical significance was accepted at $p<0.05$.

4.3. Results and Discussion

There has been extensive research on imparting synthetic polymers such as PVA with the ability to directly interact with cells through different strategies (28). The most extended strategy to improve cell interaction with the material is to directly bind or incorporate either natural ECM molecules or their bioactive sequences to the material. A good example of this strategy is the extensive study by Anderson et al., where the effects of surface functionalisation of PVA with collagen, laminin, fibronectin or peptides formed by the bioactive sequences of these ECM molecules (GFPGER, YIGSR and RGD respectively) were evaluated. Their study demonstrated that all of these modifications promoted the attachment of endothelial colony forming cells to the material (29). While most strategies to improve the cell-adhesive properties of synthetic materials require additional fabrication techniques (30) or chemical modification of the material (29,31–33), PVA-Tyr allows the incorporation of functional proteins without these additional steps (34,35). Gelatin has been widely used in tissue engineering as it allows and promotes cell adhesion, migration and proliferation while being a cheap, easy to handle, non-immunogenic biopolymer (36,37). These characteristics make it a reasonable candidate to be incorporated into the PVA-Tyr GF delivery system to improve its cell-adhesive capabilities.

It was hypothesized that it would be possible to determine a concentration of gelatin that promotes endothelial cell attachment while not having a significant impact on the degradation of PVA-Tyr hydrogels and GF release profiles from the resulting hydrogels. Other aspects such as the mechanical properties of the hydrogels could be altered by the encapsulation of gelatin. However, these were not analysed in this chapteer as we focused in the material's capabilities as a delivery vehicle.

4.3.1. Effects of Gelatin Incorporation on Endothelial Cell Attachment

The initial hypothesis to prove was that incorporation of gelatin would improve the cell-attachment properties of PVA-Tyr hydrogels. Human umbilical vein endothelial cells (HUVECs) were chosen as a model for cell attachment studies, as the aim of the incorporation of gelatin was to improve the interactions of the material with cells from invading blood vessels after implantation. To evaluate these interactions, PVA-Tyr hydrogels with different concentrations of incorporated gelatin (0 to 5wt%) were fabricated, followed

by seeding endothelial cells onto the hydrogel surface (Figure 4.2A), and the amount of cells able to attach to it were quantified (Figure 4.2B).

As expected, plain PVA-Tyr hydrogels resulted in low cell attachment due to the lack of cell-interactive features, where only an average of 3 cells/mm^2 remained in the surface after incubation. The incorporation of gelatin at 0.01 or 0.1wt% resulted in a tendency towards increasing endothelial cell attachment (9 and 22 cells/mm^2 respectively) but showed no significant differences as compared to plain PVA-Tyr hydrogels. When the concentration of incorporated gelatin was increased to 1wt%, there was a significant increase in cell attachment to an average of 125 cells/mm^2. Further increasing the gelatin concentration to 5wt% resulted in an increase in cell attachment up to 560 cells/mm^2. These results differ from previous research, where the incorporation of 0.01wt% gelatin already resulted in significant increases in fibroblast attachment (35). The morphology of attached endothelial cells remained round regardless of the incorporated gelatin concentrations (Figure 4.2A), which is another difference as compared to previous work (35). A potential explanation of these differences in cell attachment is the cell type used, as Lim et al. used L929 fibroblasts instead of HUVECs (35). Previous studies have reported that endothelial cells have lower cell attachment on various biomaterial surfaces as compared to fibroblasts (42,43), which supports these observations. Another potential explanation is differences in the physico-chemical properties between the PVA-Tyr hydrogels used in both studies. While Lim et al. used 20wt% PVA-Tyr, 2/20 mM Ru/SPS, the present study used 5wt% PVA-Tyr, 0.5/5mM Ru/SPS, where both formulations resulted in different swelling ratios and sol fraction values (35). Several studies have shown that the physico-chemical properties of the material determine the attachment and morphology of endothelial cells, making it a potential explanation of the diverging results (44,45).

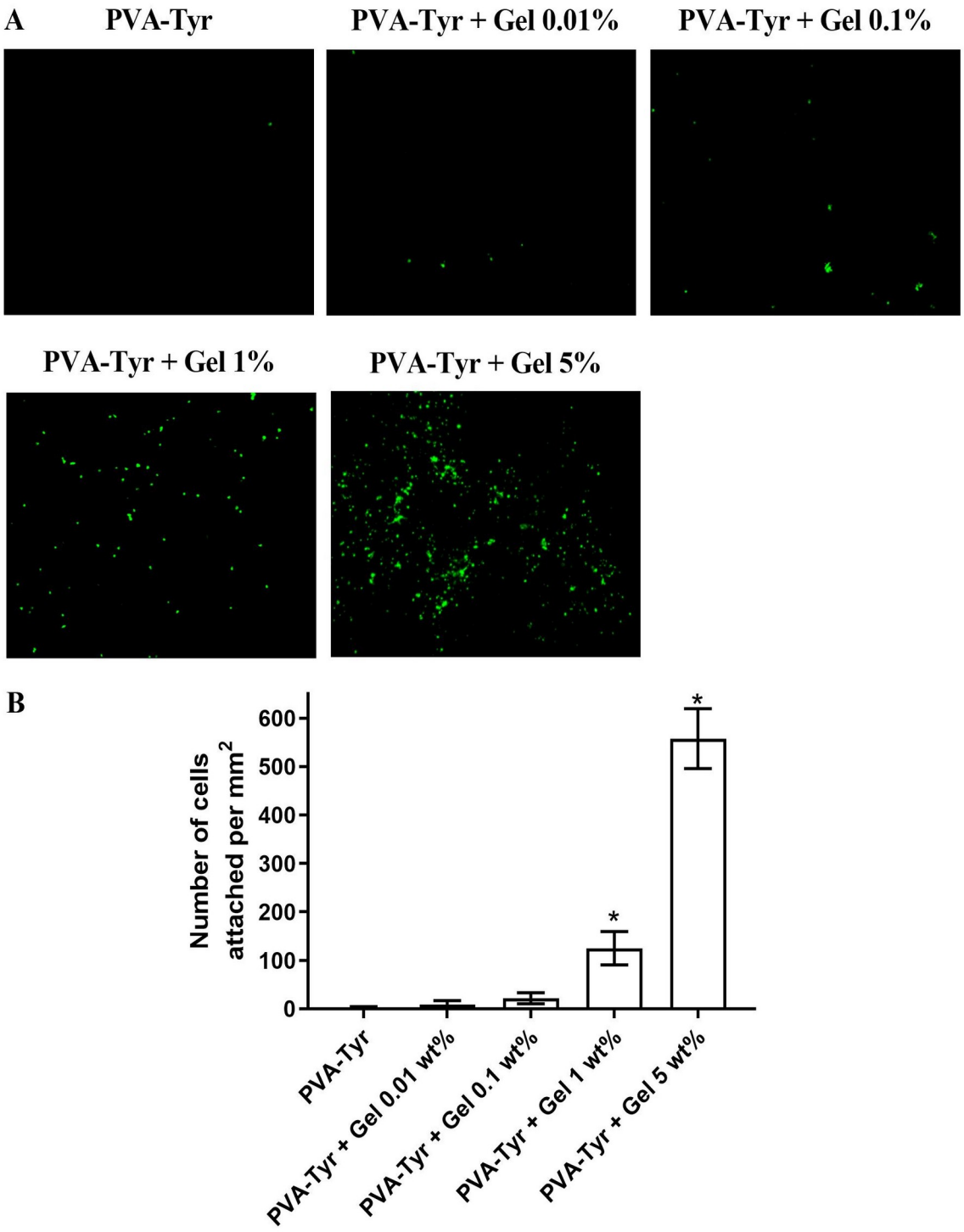

Figure 4.2. Effects of gelatin incorporation on the attachment of endothelial cells seeded on PVA-Tyr hydrogels. *(A) Representative fluorescence pictures and (B) quantification of GFP-labelled human umbilical vein endothelial cells (HUVECs) attached on PVA-Tyr hydrogels with incorporated gelatin (Gel) 6h after cell seeding.*: Significantly higher ($p<0.05$) as compared to groups with lower gelatin concentrations. Experiments were repeated 3 times with 3 technical repeats each (N=3).*

4.3.2. Effects of Gelatin Incorporation on the Physico-Chemical Properties and Degradation Profile of PVA-Tyr Hydrogels

The covalent incorporation of gelatin into PVA-Tyr hydrogels could alter the physico-chemical properties of the base PVA-Tyr network which further affects the degradation profile. These changes are not desirable for the clinical translation of PVA-Tyr as a GF delivery system, since they would potentially result in changes in the GF release kinetics as compared to previous testing that was done in pure PVA-Tyr hydrogels. To systematically evaluate the effects of gelatin incorporation on the degradation properties of PVA-Tyr gels, a range of gelatin concentrations from 0.01 to 5wt% were incorporated into PVA-Tyr hydrogels and mass loss studies were performed. Mass loss studies revealed that the initial sol fraction (Figure 4.3A) and day 1 swelling ratio (Figure 4.3B) of the hydrogels was not altered by the incorporation of 0.01 to 1wt% of gelatin, yielding sol fraction values around 20% in all cases. However, when a gelatin concentration of 5wt% was incorporated, the sol fraction increased from 20 to 80% and the swelling ratio was doubled from 20 to 40.

Longer-term mass loss and swelling profiles (Figure 4.3C-D) revealed similar tendencies, where the incorporation of gelatin concentrations between 0.01 and 1wt% did not alter the degradation time (8 days) or the mass loss and swelling values at any time point. On the other hand, further increasing gelatin concentration to 5 wt% significantly enhanced the degradation rate of the PVA-Tyr hydrogels to2 or 3 days after fabrication. These results agree with previous research, where the incorporation of gelatin into 20wt% PVA-Tyr hydrogels at concentrations up to 1wt% resulted in no differences in the physico-chemical properties of the hydrogels or their degradation profile (35). A remarkable aspect of these results is how they differ from the effects of albumin incorporation into PVA-Tyr hydrogels in Section 3.3.2, where the incorporation of 1wt% albumin resulted in longer degradation time of the gels. A potential explanation of these differences is the disparity between the properties of gelatin and albumin. While albumin is a 66 kDa protein containing 18 tyrosine residues per molecule (46), gelatin is a polydisperse solution of polypeptides with a highly variable molecular weight and number of tyrosine residues per molecule (47). These differences could result in a less homogeneous crosslinking, where the incorporation of a high enough concentration of gelatin destabilizes the network and results in lower crosslinking efficiency and faster degradation. In contrast, the incorporation of albumin results in higher crosslinking

density and lower swelling ratio, making di-tyrosine bonds less accessible for hydrolytic degradation and extending the degradation time of the hydrogels.

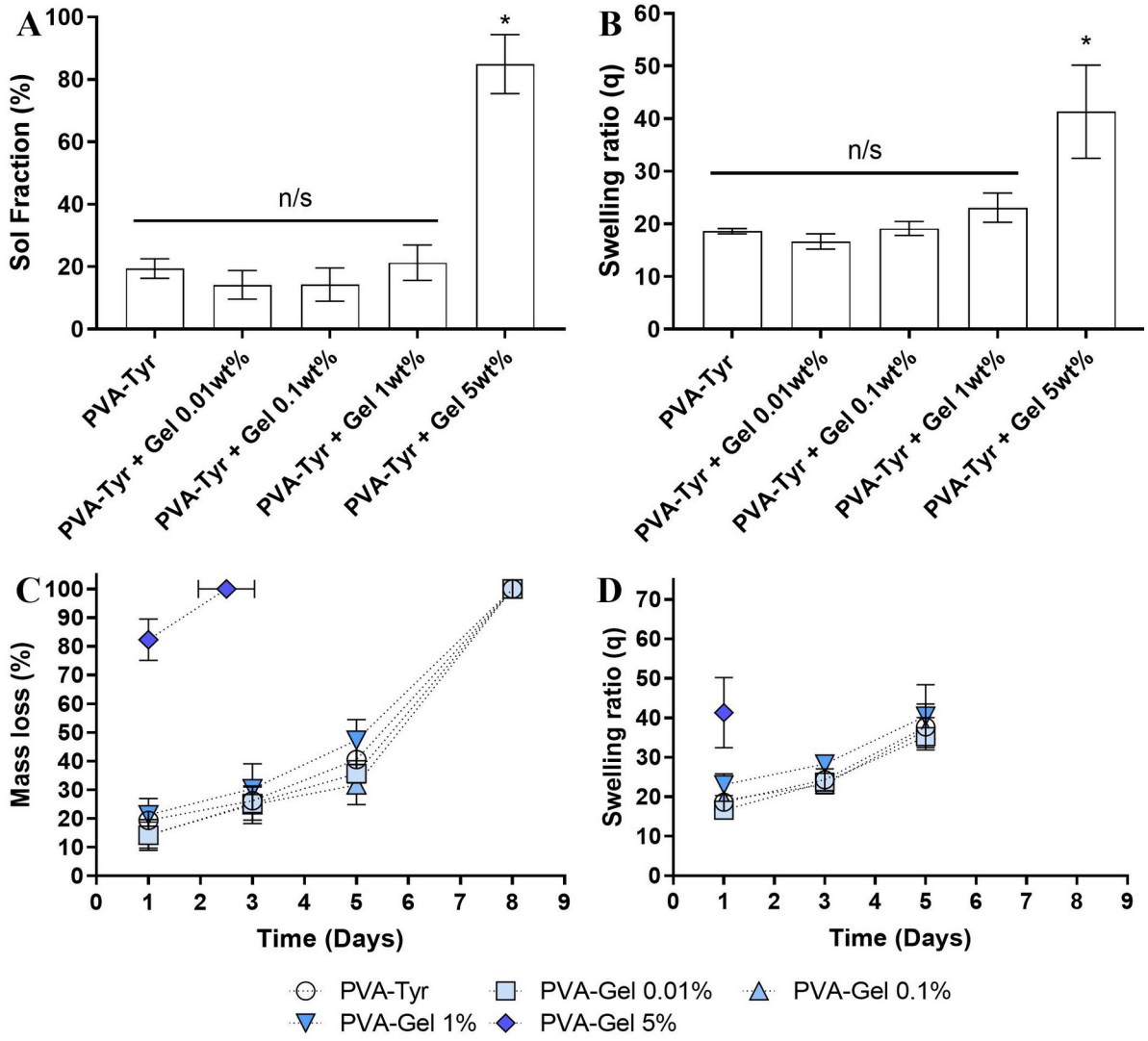

Figure 4.3. Effects of gelatin incorporation on the physico-chemical properties of PVA-Tyr hydrogels. *(A) Sol fraction, (B) swelling ratio, (C) Mass loss profile and (D) Swelling profile of PVA-Tyr hydrogels crosslinked at 5wt%, 0.5/5 mM Ru/SPS with a range of incorporated gelatin (Gel) concentrations. *: Significant difference ($p<0.05$) as compared to PVA-Tyr control. Experiments were repeated 3 times with 3 technical repeats each (N=3).*

These initial results show that a minimum of 1wt% incorporated gelatin is required to enhance endothelial cell attachment. On the other hand, the incorporation of up to 1wt% gelatin into PVA-Tyr hydrogels results in no changes in its swelling and degradation profile, while the incorporation of higher concentrations of gelatin drastically altered these properties.

Therefore, 1wt% gelatin was selected as the most adequate concentration for further experiments.

4.3.3. Effects of Gelatin Incorporation on Protease-Catalysed Degradation of PVA-Tyr Hydrogels

In Chapter 3, it was demonstrated that PVA-Tyr hydrogels are not susceptible to Proteinase K degradation. Furthermore, the incorporation of up to 1wt% albumin into PVA-Tyr hydrogels did not change these properties, demonstrating that PVA-Tyr was protecting the incorporated albumin from protease degradation. Thus, it would be expected that the incorporation of gelatin at 1wt% would not alter the sensitivity of PVA-Tyr hydrogels to protease K degradation. However, it is possible that the different properties of albumin and gelatin result in diverging sensitivities to protease degradation. In section 4.3.2, it was observed that incorporating 1wt% gelatin did not alter the physico-chemical properties of PVA-Tyr hydrogels, while incorporating 1wt% albumin into PVA-Tyr hydrogels significantly impacted the swelling and degradation behaviour of the gels (Section 3.3.2). Knowing that the incorporation of gelatin and albumin can result in diverging tendencies in the degradation and swelling profiles of PVA-Tyr hydrogels, it was hypothesized that incorporating gelatin into PVA-Tyr hydrogels could alter their susceptibility to protease degradation.

To confirm this, mass loss studies were performed on PVA-Tyr hydrogels with or without 1wt% gelatin in proteinase K (Figure 4.4). Initial mass loss (Figure 4.4A) and swelling ratio (Figure 4.4B) measurements revealed that exposure to proteinase K did not result in significant differences in sol fraction or day 1 swelling ratio, which agrees with our previous results using albumin. As seen in Chapter 3, pure BSA hydrogel controls were susceptible to degradation by proteinase K and were completely degraded after 24h.

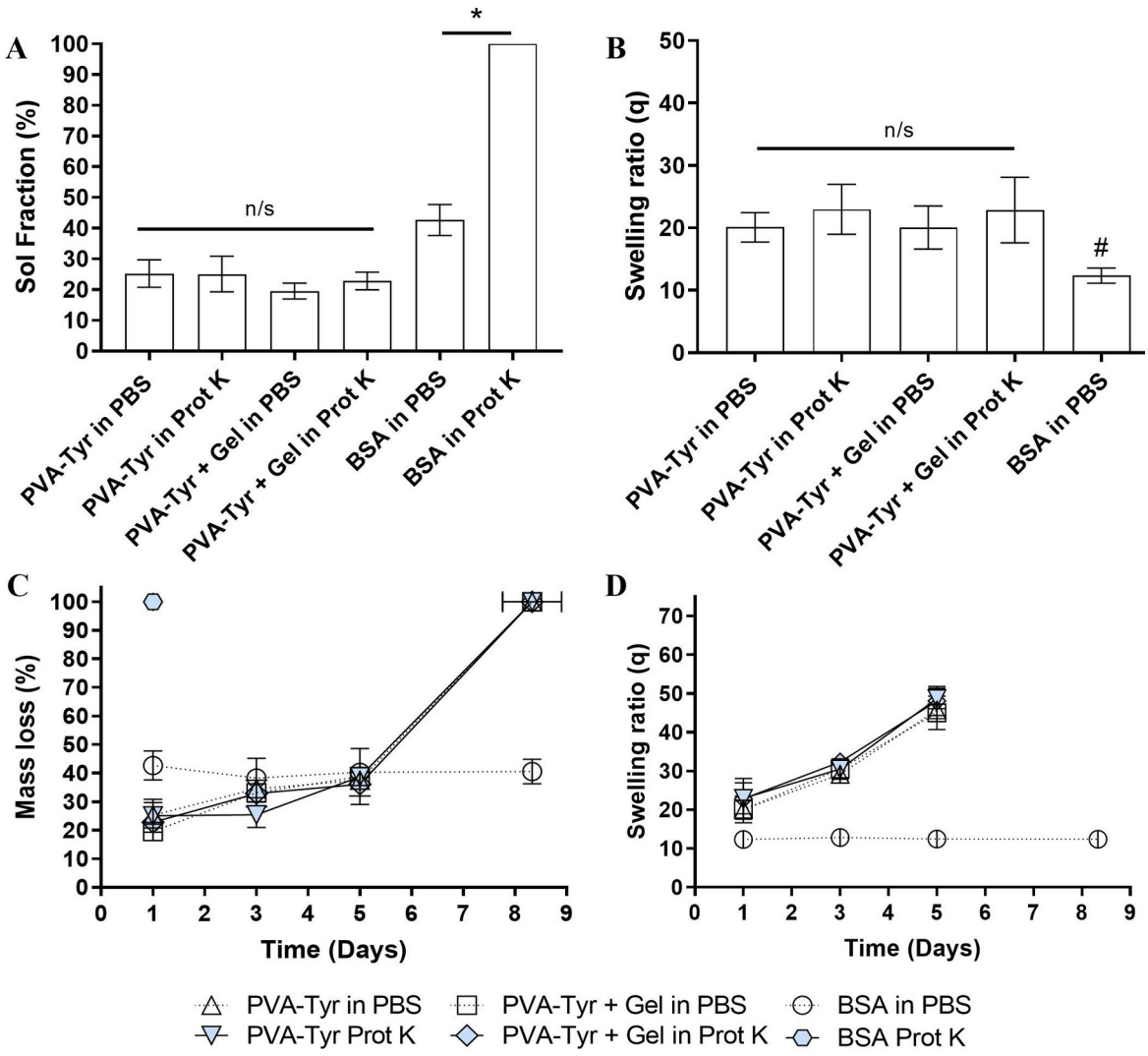

Figure 4.4. Effects of gelatin incorporation on protease-catalysed degradation of PVA-Tyr hydrogels. *(A) Sol fraction, (B) Swelling ratio at day 1, (C) Mass loss profile and (D) swelling ratio profile of 5wt% PVA-Tyr or 5wt% PVA-Tyr with incorporated 1wt% gelatin, crosslinked at 0.5/5 mM Ru/SPS. BSA controls were crosslinked at 10wt% BSA, 2/20 mM Ru/SPS. Hydrogels were exposed to either PBS or proteinase K 1mg/mL dissolved in PBS. *: Significant difference ($p<0.05$) between groups. #: Significant difference ($p<0.05$) as compared to plain PVA-Tyr hydrogels in PBS. Experiments were repeated 3 times with 3 technical repeats each (N=3).*

Longer-term mass loss (Figure 4.C) and swelling studies (Figure 4.4D) further confirmed that proteinase K did not have an effect on the degradation and swelling ratio profiles of PVA-Tyr hydrogels regardless of the incorporation of 1wt% gelatin. All PVA-Tyr hydrogels showed comparable mass loss and swelling values in all time points, and their degradation time was between 8 and 9 days in all groups. BSA controls exposed to PBS showed stable mass loss and swelling ratio throughout the whole experiment. These results provide further

information about the changes in physico-chemical properties of PVA-Tyr hydrogels after the incorporation different types of proteins. The incorporation of 1wt% albumin initially resulted in longer hydrolytic degradation times of PVA-Tyr hydrogels when exposed to PBS, but did not alter the sensitivity of the hydrogels to proteinase K degradation (Section 3.3.2). On the other hand, the incorporation of 1wt% gelatin into PVA-Tyr hydrogels did not result in changes in degradation or swelling profiles of the gels, and also did not alter their sensitivity to proteinase K degradation (Figures 4.3 and 4.4). This suggests that the ability of PVA-Tyr hydrogels to protect incorporated proteins from protease degradation is not likely to be affected by the incorporation of different types of proteins, while the rate of hydrolytic degradation of the gels could vary depending on the incorporated proteins and their concentrations. Overall, these results further confirm that the incorporation of 1wt% gelatin into PVA-Tyr hydrogels does not have a significant effect on their degradation profile.

4.3.4. Effects of Gelatin Incorporation on Growth Factor Retention and Release

Mass loss assays have confirmed that the incorporation of gelatin does not alter the physico-chemical properties of PVA-Tyr hydrogels (Section 4.3.3). Therefore, it would be expected that the incorporation and release of GFs will not be altered either. To confirm that, fluorescently tagged VEGF, bFGF and BDNF were incorporated into PVA-Tyr and hydrogels with and without 1wt% incorporated gelatin. Release assays revealed that the retention values remain between 25 and 30% regardless of the incorporation of gelatin and independently of which GF was incorporated, with no significant differences between groups (Figure 4.5A). These results show that the incorporation of 1wt% gelatin does not alter GF retention in the studied conditions. The release profiles (Figure 4.5B) were also comparable in all groups and showed no significant differences in any of the time points.

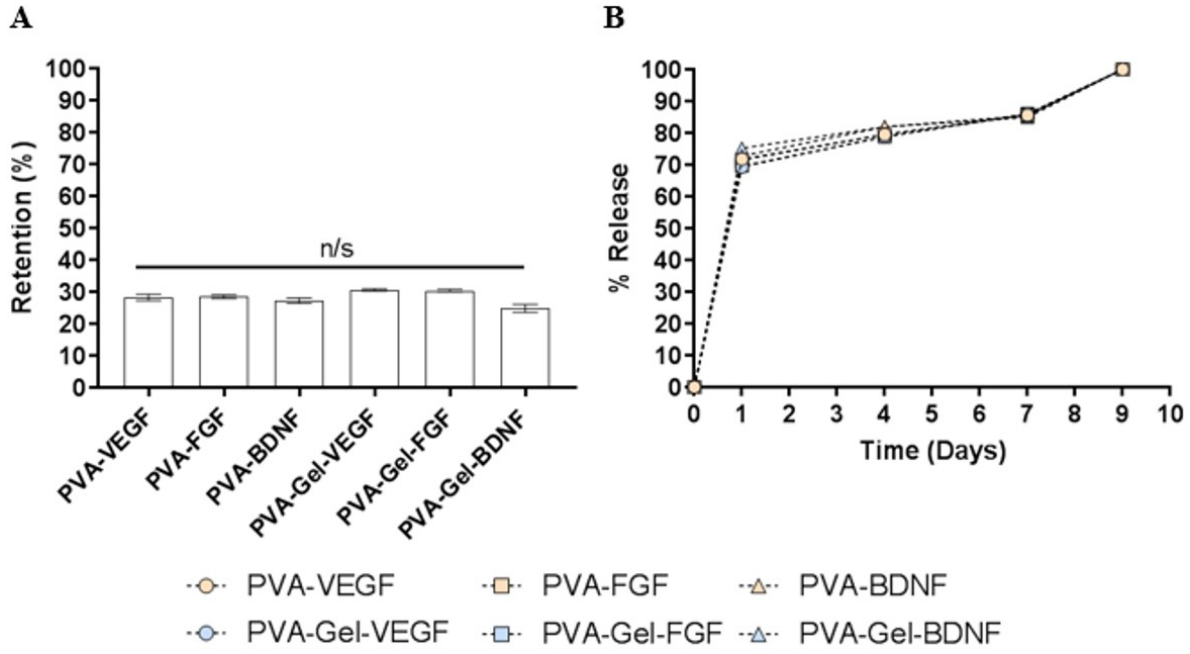

Figure 4.5. Effects of gelatin incorporation on growth factor retention and release. *(A) Retention and (B) release of VEGF, bFGF and BDNF in PVA-Tyr (5wt%, 0.5/5mM Ru/SPS) or PVA-Gel (5wt% PVA-Tyr, 1wt% gelatin, 0.5/5mM Ru/SPS) hydrogels. Experiments were repeated 3 times with 3 technical repeats each (N=3).*

These results further confirm that the incorporation of gelatin does not alter the properties of the hydrogel in terms of its GF retention and release, further demonstrating that this is a viable strategy to improve the bioactivity of the PVA-GF platform.

4.3.5. Adaptation of the PVA-Tyr Delivery System to Injection Using Surgical Tools

In sections 4.3.1-4, gelatin was covalently incorporated into PVA-Tyr hydrogels to improve their interaction with endothelial cells. It was shown that the incorporation of gelatin improves endothelial cell attachment on PVA-Tyr hydrogels while not altering the hydrolytic degradation of the hydrogels, their susceptibility to protease degradation or the release profile of encapsulated GFs. Therefore, the incorporation of gelatin was considered to be a successful step towards the adaptation of the PVA-Tyr GF delivery system for the treatment of Perthes disease. The GF chosen for the delivery is VEGF, as it is a widely studied angiogenesis-promoting GF (17–20) that has also shown positive results in bone regeneration settings (21). The next aspect to consider for the adaptation of the system was the delivery method.

The surgical intervention to which the PVA-Tyr system needed to be adapted aimed to connect the arterial network in the body of the femur with the femoral head, providing

vascular supply to the femoral head when it is not receiving enough nutrients and oxygen. The process involved drilling a hole in the lateral side of the femur, reaching the core of the femoral head (Figure 4.6). The VEGF-loaded PVA-Tyr hydrogel was then delivered and fixated into the core of the femoral head through the drilled hole, where it would release VEGF to attract angiogenic sprouts towards it from the arterial network in the femoral body.

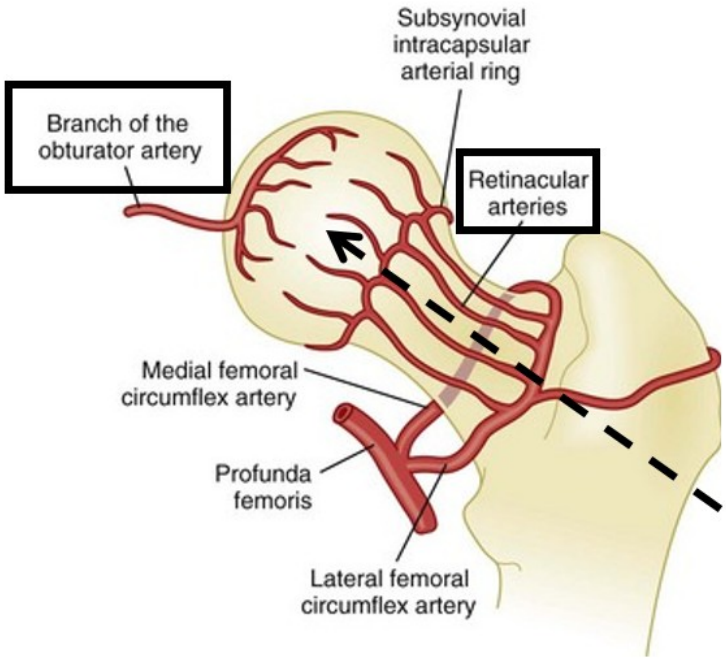

Figure 4.6. Schematic view of the vascular supply in the femoral head and important areas for the surgical intervention. *The branch of the obturator artery that provides blood supply to the medial side of the femoral head was disrupted and the retinacular arteries were blocked during the surgical procedure to generate a model of avascular necrosis. The dashed arrow indicates the point of entrance and direction of the drilled hole through which the hydrogel was delivered.*

The ideal method of delivery would then be to inject the hydrogel through the drilled hole. The approach that is generally envisioned for this type of delivery is to first inject the precursor solution into the area of need and then irradiate it with a light source for in situ crosslinking (48). However, this was not the most ideal setup for a series of reasons. Firstly, the internal environment of the bone would contain blood that cannot be easily removed during the surgical intervention, which is a significant difference compared to other areas such as cartilage (48) and could result in diffusion of the precursor solution. This diffusion would influence the crosslinking process and release GFs, macromer and photoinitiators into the body in an unwanted manner. Secondly, the PVA-Tyr and gelatin precursor solution is not highly viscous, making it more susceptible to this unwanted diffusion. Thirdly, the depth of the hole could result in uneven crosslinking of the scaffold in the deeper areas due to the

limitations in light penetration (49). Therefore, the possibility to crosslink the hydrogel before injecting it into the area of interest was explored. The precursor solution was successfully crosslinked inside a syringe and then injected into a Jamshidi needle, which enabled pushing it out into the area of interest using the internal cannula of the needle (Figure 4.7).

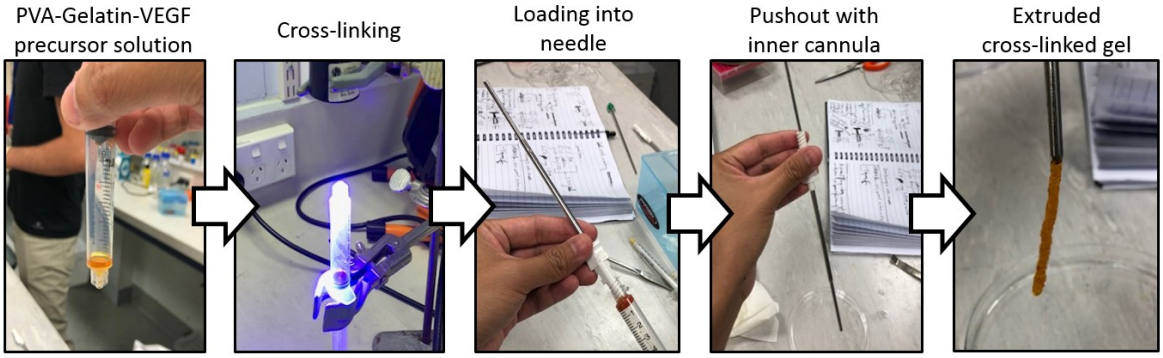

Figure 4.7. Crosslinking and injection of PVA-Tyr with gelatin and VEGF using standard surgical tools for its evaluation in a model of avascular necrosis. *The first step was to crosslink the precursor solution inside a syringe, followed by loading of the crosslinked hydrogel into a Jamshidi needle. The needle is then inserted into the area of interest and the hydrogel is pushed out using the inner cannula.*

This procedure avoids the risk of unwanted diffusion and uneven crosslinking during the surgical procedure. Furthermore, it facilitated the preparation of the samples before the intervention, as sterile syringes loaded with the crosslinked polymer could be brought to the intervention site fully prepared to load into the Jamshidi needle. This is the first instance of PVA-Tyr hydrogels being evaluated as an injectable system, which opens the door to potential clinical translation.

4.3.6. Preliminary Results of the In Vivo Study

After the system was fully adapted for its delivery into the femoral head, the surgical procedure for a pilot *in vivo* study on the effectiveness of the PVA-Tyr GF delivery system to promote revascularisation of the femoral head was performed. The proximal part of the femur was harvested 15 weeks after the surgery, samples were imaged and CT scans were taken. Figure 4.8 includes a reduced version of the results including an image for each of these groups and levels of deformity, and supplementary figures S4.1-5 include the images of all the samples in the experiment for extended information. Both types of imaging revealed that, in a high percentage of the samples where the blood flow had been disrupted, the spherical morphology of the femoral head was completely altered and in some samples the femoral head had fallen apart from the femoral body due to tissue necrosis. This level of deformation

has not been reported in previous instances of this model (39–41). An explanation for that could be the fact that both legs were operated for each piglet, which could have resulted in an unwanted weight overload of the avascular femoral heads and increased deformities as compared to other studies.

In accordance with these observations, samples were classified in three categories (Table 4.1). When the femoral head showed normal external morphology and size and its general features could be identified in the CT scans, it was classified as a 'healthy femoral head'. When the femoral head presented alterations in shape and/or size but was still identifiable in the general images or CT scans, it was classified as 'deformed femoral head'. Finally, when no structures could be identified as the femoral head through neither general imaging nor CT, the sample was classified as 'femoral head cannot be identified'. The classification revealed that 100% of the non-operated femoral heads had a healthy morphology, whereas 0% of the femoral heads in the 'vessels disrupted' group could be identified. This result demonstrates that the blood flow was successfully disrupted in the 'vessels disrupted' group and the model was executed successfully. Samples in the sham group lost the femoral head in 75% of the cases, which could be a sign that the blood vessels from the femoral body were able to migrate towards the femoral head thanks to the drilled hole. Injecting PVA-Tyr hydrogels with incorporated 1wt% gelatin (PVA-Gel) hydrogels with or without VEGF into the drilled hole further reduced the loss of femoral head to 62.5% regardless of the presence of VEGF. While there appears to be an increasing trend in the maintenance of the femoral head when drilling the hole and delivering the hydrogel, the number of samples was not high enough to provide statistical significance and the imaging should be followed up with quantitative analysis. It is possible that the excessive deformation of the femoral heads interfered with the results, making them harder to interpret.

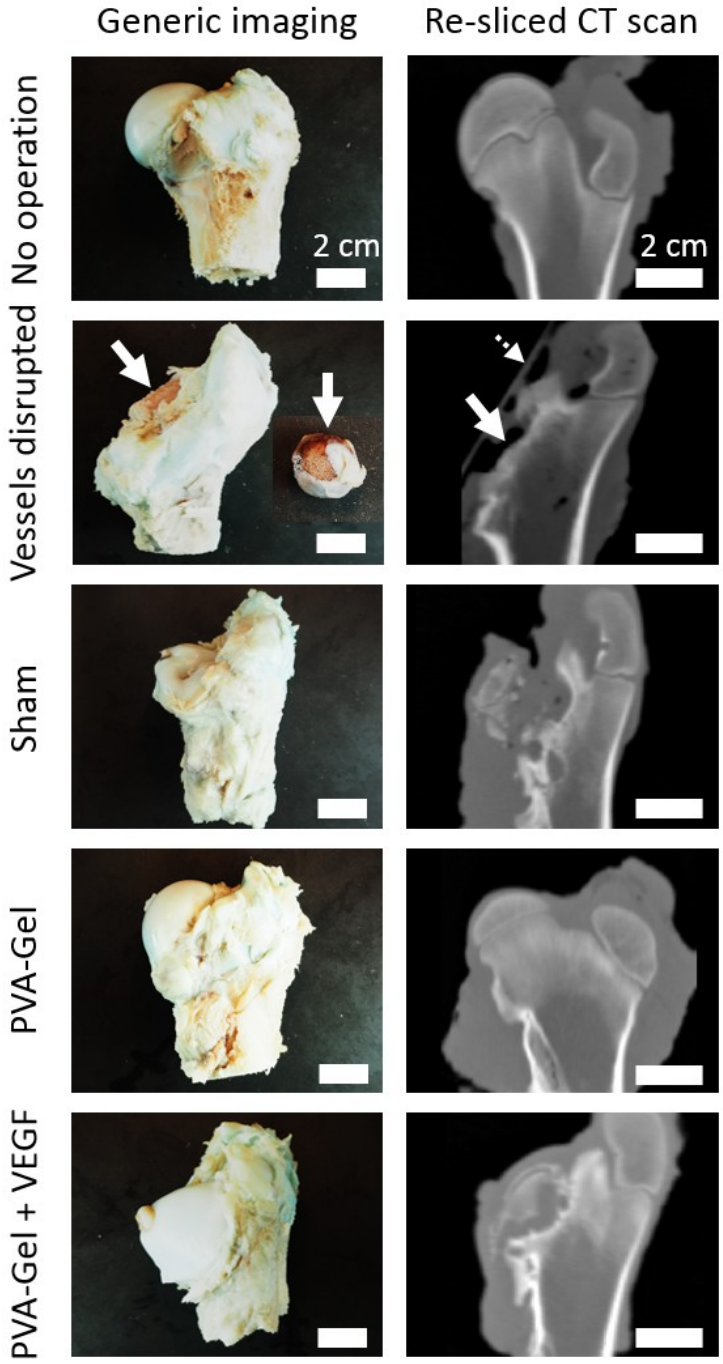

Figure 4.8. Example images of the femoral heads after the surgical intervention and treatment with PVA-Tyr hydrogels. *General images (Left row), CT images (Middle row) and hematoxylin-eosin staining of the histological sections (Right row). No operation: positive control with no surgical procedure. Vessels disrupted: The blood supply to the femoral head was disrupted. Sham: The blood supply to the femoral head was disrupted and a hole was drilled from the body to the centre of the femoral head. PVA-Gel: The blood supply was disrupted, the hole was drilled and a 5wt% PVA-Tyr + 1wt% Gelatin (PVA-Gel) hydrogel was delivered. PVA-Gel + VEGF: The blood supply was disrupted, the hole was drilled and a 5wt% PVA-Tyr + 1wt% Gelatin (PVA-Gel) + VEGF hydrogel was delivered. White and black arrows indicate the spot where the femoral head should be and the fallen necrotic femoral head. The white dashed arrow indicates the surface on which the sample was imaged.*

Table 4.1. *Scoring of the samples by general observation and CT scanning.*

	N	Healthy femoral head	Deformed femoral head	Femoral head cannot be identified	Loss of femoral head (%)
No operation	2	2	0	0	0
Vessels disrupted	4	0	0	4	100
Sham	4	0	1	3	75
PVA-Gel	8	0	3	5	62.5
PVA-Gel-VEGF	8	0	3	5	62.5

Overall, while these results do not demonstrate that delivery of PVA-Tyr with encapsulated VEGF improved the vascularisation in the femoral head, the delivery of the hydrogels resulted in an increasing trend to maintain the femoral head as compared to its negative controls. To provide detailed information on the effects of the treatments, further analysis of the vessel density and diameter will be performed in the histological images. Other characteristics of the tissue such as the quality of the cartilage in the joint and in the growth plate will also be evaluated using Safranin O staining (53), together with the presence of necrotic and fibrotic tissue in the area. If these quantifications provide evidence indicating positive effects, it will be necessary to perform follow-up experiments with an improved setup and increased number of samples to generate statistically relevant numbers. Furthermore, it will be important to determine the adequate concentration of VEGF to promoter angiogenesis while avoiding side effects such as edema.

4.4. Conclusions

In this chapter, the PVA-Tyr system was adapted to promote vascularisation in a very specific clinical setting, to revascularise the femoral head in cases of Perthes disease.

Firstly, the ability of the system to directly interact with cells in the surrounding environment was improved. The ability of PVA-Tyr to bind to any tyrosine-containing protein allowed incorporation of gelatin into the hydrogels, which promoted the attachment of endothelial cells when incorporated at a concentration of 1wt% or higher. It was demonstrated that the incorporation of 1wt% gelatin didn't affect any of the key attributes of PVA-Tyr hydrogels (degradation time, resistance to protease degradation and controlled release time frame of GFs), which shows the ability of the system to incorporate multiple proteins at the same time while still controlling the release of loaded GFs.

Secondly, the system was adapted to the specific surgical procedure and tools used by performing the photo-crosslinking prior to the injection into the site of injury, which avoided unnecessary risks such as uneven crosslinking or burst release into the body. It was demonstrated that the PVA-Tyr system can be utilised as an injectable system, easily moulded into various shapes and further administered to designated locations in the body.

Finally, PVA-Tyr hydrogels with incorporated gelatin and VEGF were applied in a large mammalian *in vivo* model of avascular necrosis. While the data is still not conclusive and needs to be further analysed, there seems to be a tendency to improve the maintenance of the femoral head after injection of the PVA-Tyr hydrogels.

4.5. Supplementary Information

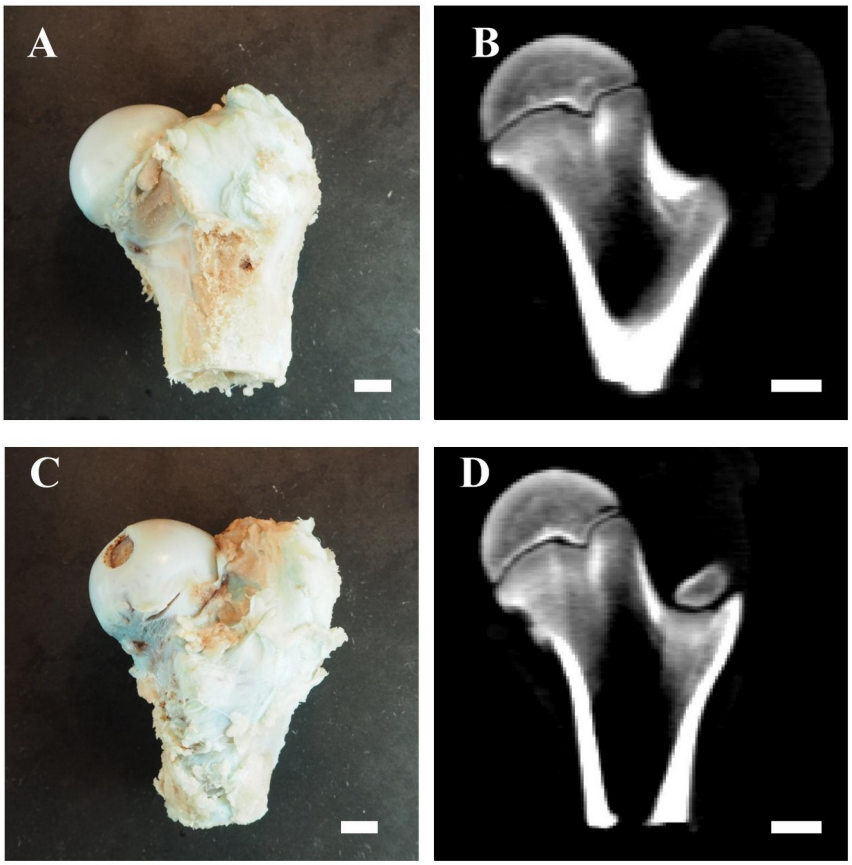

Supplementary Figure S4.1. Images of the femoral heads at the end of the experiment in the "No Operation" group. *General images (Left row) and CT images (Right row) 15 weeks after interventions. This group was the positive control with no surgical procedure.*

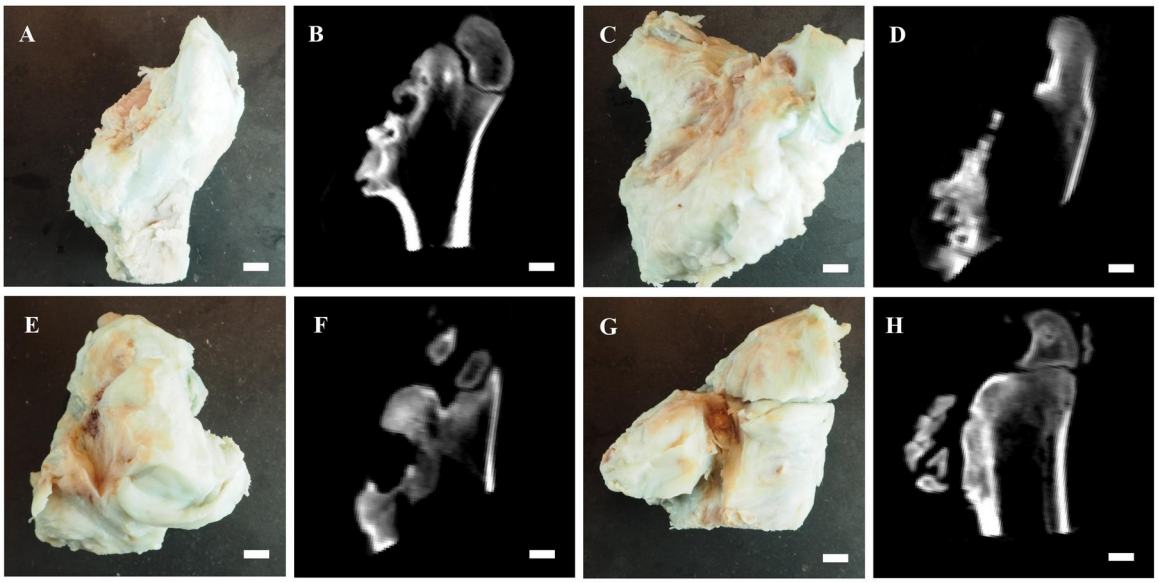

Supplementary Figure S4.2. Images of the femoral heads at the end of the experiment in the "Vessels Cut" group. *General images (Left and middle right rows) and CT images (Middle left and right rows) 15 weeks after interventions. In this group, the blood supply to the femoral head was disrupted.*

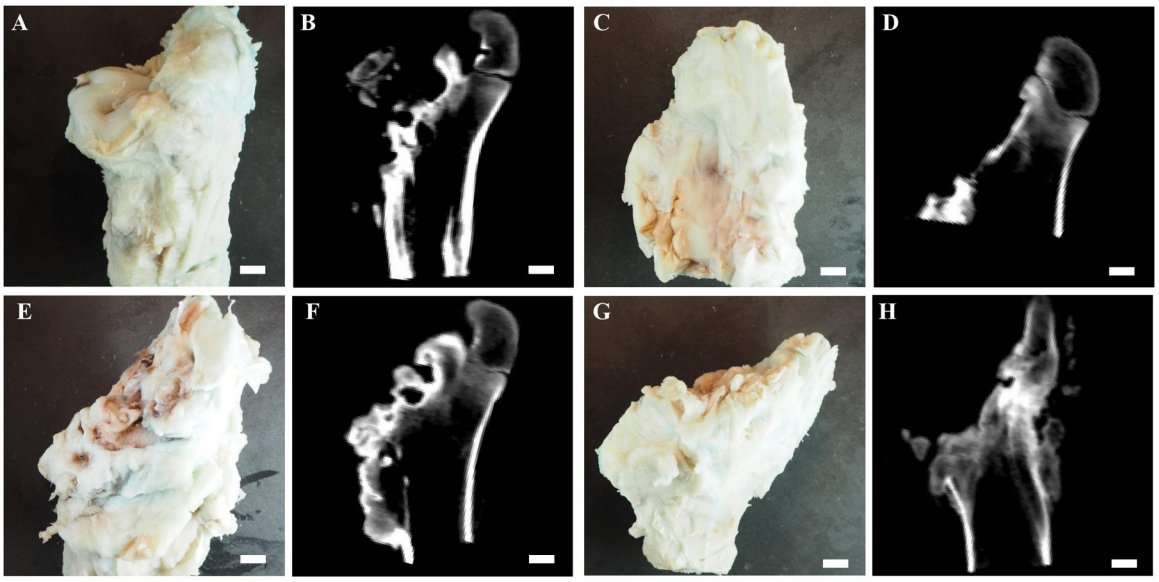

Supplementary Figure S4.3. Images of the femoral heads at the end of the experiment in the "Sham" group. *General images (Left and middle right rows) and CT images (Middle left and right rows) 15 weeks after interventions. In this group, the blood supply to the femoral head was disrupted and a hole was drilled from the body to the centre of the femoral head.*

Supplementary Figure S4.4. Images of the femoral heads at the end of the experiment in the "PVA-Gel" group. *General images (Left and middle right rows) and CT images (Middle left and right rows) 15 weeks after interventions. PVA-Gel: The blood supply was disrupted, the hole was drilled and a 5wt% PVA-Tyr + 1wt% Gelatin (PVA-Gel) hydrogel was delivered.*

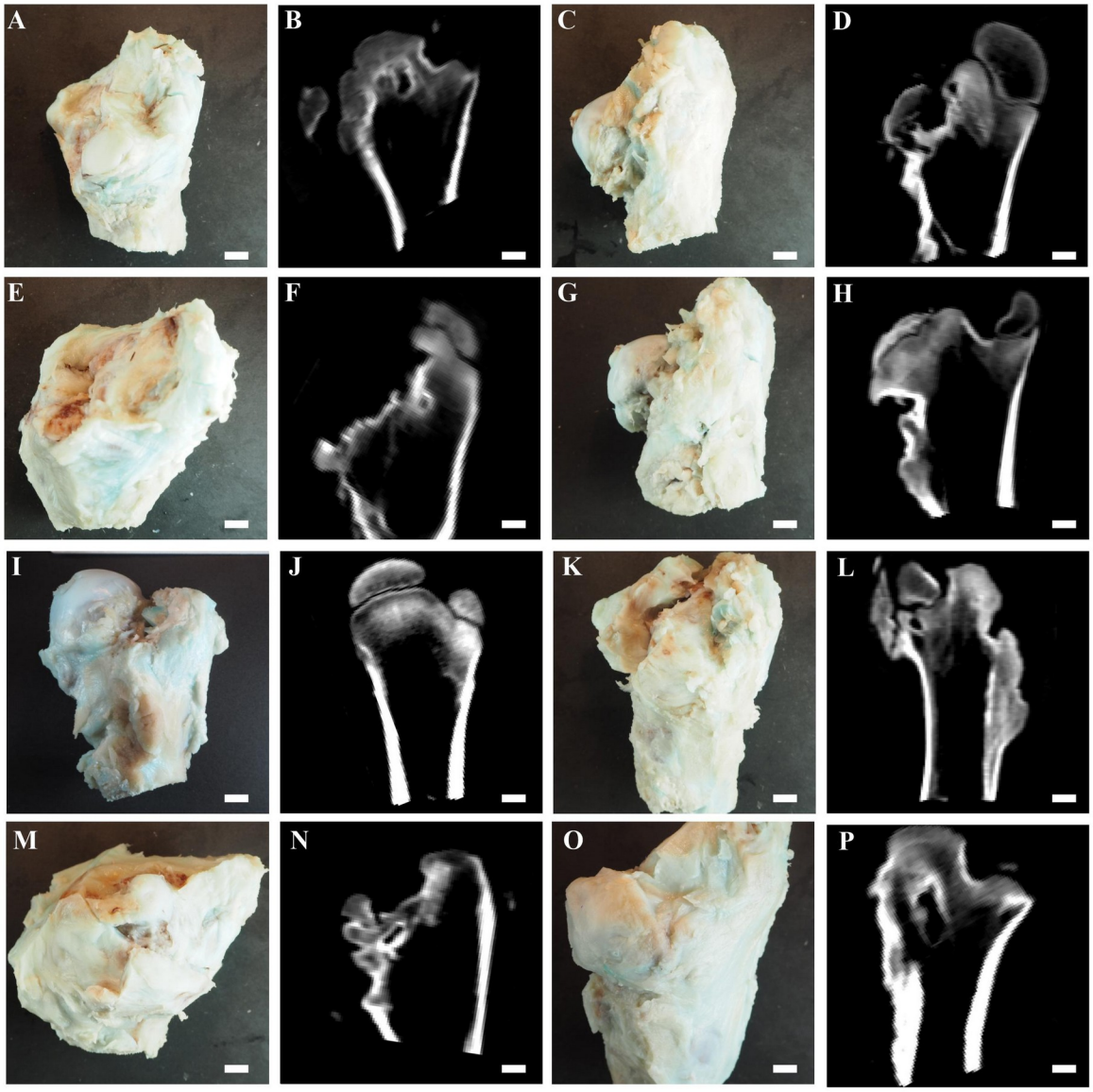

Supplementary Figure S4.5. Images of the femoral heads at the end of the experiment in the "PVA-Gel-VEGF" group. *General images (Left and middle right rows) and CT images (Middle left and right rows) 15 weeks after interventions. PVA-Gel + VEGF: The blood supply was disrupted, the hole was drilled and a 5wt% PVA-Tyr + 1wt% Gelatin (PVA-Gel) + VEGF hydrogel was delivered.*

4.6. References

1. Campbell RM. Legg-Calvé-Perthes Disease BT - Current Orthopedic diagnosis & treatment. In: Heckman JD, Schenck RC, Agarwal A, editors. London: Current Medicine Group; 2000. p. 104–5. Available from: https://doi.org/10.1007/978-1-4613-1107-2_52

2. Loder RT, Skopelja EN. The epidemiology and demographics of legg-calvé-perthes' disease. ISRN Orthop [Internet]. 2011 Sep 5;2011:504393. Available from: https://www.ncbi.nlm.nih.gov/pubmed/24977062

3. Perry DC, Pope D, Bruce CE, Dangerfield P, Hall AJ, Platt MJ. Hyperactivity and the Psychological Burden of Perthes Disease: A Case-Control Study. J Pediatr Orthop [Internet]. 2013;33(6). Available from: https://journals.lww.com/pedorthopaedics/Fulltext/2013/09000/Hyperactivity_and_the_Psychological_Burden_of.11.aspx

4. Perry DC, Bruce CE, Pope D, Dangerfield P, Platt MJ, Hall AJ. Perthes' disease of the hip: socioeconomic inequalities and the urban environment. Arch Dis Child [Internet]. 2012 Dec 1;97(12):1053 LP – 1057. Available from: http://adc.bmj.com/content/97/12/1053.abstract

5. Mata SG, Aicua EA, Ovejero AH, Grande MM. Legg-Calvé-Perthes Disease and Passive Smoking. J Pediatr Orthop [Internet]. 2000;20(3). Available from: https://journals.lww.com/pedorthopaedics/Fulltext/2000/05000/Legg_Calv__Perthes_Disease_and_Passive_Smoking.11.aspx

6. Lamb JN, Holton C, O'Connor P, Giannoudis P V. Avascular necrosis of the hip. BMJ [Internet]. 2019 May 30;365:l2178. Available from: http://www.bmj.com/content/365/bmj.l2178.abstract

7. Steppacher SD, Haefeli PC, Anwander H, Siebenrock KA, Tannast M. Traumatic Avascular Necrosis of the Femoral Head. In: Koo K-H, Mont MA, Jones LC, editors. Osteonecrosis. Berlin, Heidelberg: Springer Berlin Heidelberg.; 2014. p. 101–12.

8. Warner JJ, Philip JH, Brodsky GL, Thornhill TS. Studies of Nontraumatic Osteonecrosis. The Role of Core Decompression in the Treatment of Nontraumatic Osteonecrosis of the Femoral Head. Clin Orthop Relat Res. 1987;(225):104–27.

9. Wiig O, Terjesen T, Svenningsen S. Prognostic factors and outcome of treatment in Perthes' disease. J Bone Joint Surg Br [Internet]. 2008 Oct 1;90-B(10):1364–71. Available from: https://doi.org/10.1302/0301-620X.90B10.20649

10. Beer Y, Smorgick Y, Oron A, Mirovsky Y, Weigl D, Agar G, et al. Long-Term Results of Proximal Femoral Osteotomy in Legg-Calvé-Perthes Disease. J Pediatr Orthop [Internet]. 2008;28(8). Available from: https://journals.lww.com/pedorthopaedics/Fulltext/2008/12000/Long_Term_Results_of_Proximal_Femoral_Osteotomy_in.6.aspx

11. Myers GJC, Mathur K, O'Hara J. Valgus Osteotomy: A Solution for Late Presentation of Hinge Abduction in Legg-Calvé-Perthes Disease. J Pediatr Orthop [Internet]. 2008;28(2). Available from: https://journals.lww.com/pedorthopaedics/Fulltext/2008/03000/Valgus_Osteotomy__A_Solution_for_Late_Presentation.8.aspx

12. Rosenfeld SB, Herring JA, Chao JC. Legg-Calvé-Perthes Disease: A Review of Cases with Onset Before Six Years of Age. JBJS [Internet]. 2007;89(12). Available from: https://journals.lww.com/jbjsjournal/Fulltext/2007/12000/Legg_Calv__Perthes_Disease__A_Review_of_Cases_with.18.aspx

13. Heesakkers N, van Kempen R, Feith R, Hendriks J, Schreurs W. The long-term prognosis of Legg-Calvé-Perthes disease: a historical prospective study with a median follow-up of forty one years. Int Orthop [Internet]. 2015;39(5):859–63. Available from: https://doi.org/10.1007/s00264-014-2589-2

14. Steppacher SD, Haefeli PC, Anwander H, Siebenrock KA, Tannast M. Traumatic Avascular Necrosis of the Femoral Head BT - Osteonecrosis. In: Koo K-H, Mont MA, Jones LC, editors. Berlin, Heidelberg: Springer Berlin Heidelberg; 2014. p. 101–12. Available from: https://doi.org/10.1007/978-3-642-35767-1_14

15. Traina F, Fine M, Sudanese A, Calderoni P, Tassinari E, Toni A. Long term results of total hip replacement in patients with Legg-Calvé-Perthes disease. J Bone Joint Surg Am. 2011 Apr 1;93:e25.

16. Chu H, Wang Y. Therapeutic angiogenesis: controlled delivery of angiogenic factors. Ther Deliv [Internet]. 2012 Jun;3(6):693–714. Available from:

https://www.ncbi.nlm.nih.gov/pubmed/22838066

17. Henry L, Labied S, Fransolet M, Kirschvink N, Blacher S, Noel A, et al. Isoform 165 of vascular endothelial growth factor in collagen matrix improves ovine cryopreserved ovarian tissue revascularisation after xenotransplantation in mice. Reprod Biol Endocrinol [Internet]. 2015 Mar 7;13:12. Available from: https://www.ncbi.nlm.nih.gov/pubmed/25888918

18. Weaver JD, Headen DM, Aquart J, Johnson CT, Shea LD, Shirwan H, et al. Vasculogenic hydrogel enhances islet survival, engraftment, and function in leading extrahepatic sites. Sci Adv [Internet]. 2017 Jun 1;3(6):e1700184. Available from: http://advances.sciencemag.org/content/3/6/e1700184.abstract

19. Li S-H, Hwu Y-M, Lu C-H, Chang H-H, Hsieh C-E, Lee RK-K. VEGF and FGF2 Improve Revascularization, Survival, and Oocyte Quality of Cryopreserved, Subcutaneously-Transplanted Mouse Ovarian Tissues. Int J Mol Sci [Internet]. 2016 Jul 30;17(8):1237. Available from: https://www.ncbi.nlm.nih.gov/pubmed/27483256

20. Zhang N, Richter A, Suriawinata J, Harbaran S, Altomonte J, Cong L, et al. Elevated Vascular Endothelial Growth Factor Production in Islets Improves Islet Graft Vascularization. Diabetes [Internet]. 2004 Apr 1;53(4):963 LP – 970. Available from: http://diabetes.diabetesjournals.org/content/53/4/963.abstract

21. Hu K, Olsen BR. The roles of vascular endothelial growth factor in bone repair and regeneration. Bone [Internet]. 2016;91:30–8. Available from: https://www.ncbi.nlm.nih.gov/pubmed/27353702

22. García JR, Clark AY, García AJ. Integrin-specific hydrogels functionalized with VEGF for vascularization and bone regeneration of critical-size bone defects. J Biomed Mater Res Part A [Internet]. 2016;104(4):889–900. Available from: http://dx.doi.org/10.1002/jbm.a.35626

23. Yu H, Zeng X, Deng C, Shi C, Ai J, Leng W. Exogenous VEGF introduced by bioceramic composite materials promotes the restoration of bone defect in rabbits. Biomed Pharmacother [Internet]. 2018;98:325–32. Available from: http://www.sciencedirect.com/science/article/pii/S0753332217348163

24. Li S, Yuan H, Pan J, Fan W, Zhu L, Yan Z, et al. The treatment of femoral neck

fracture using VEGF-loaded nanographene coated internal fixation screws. PLoS One [Internet]. 2017 Nov 8;12(11):e0187447. Available from: https://doi.org/10.1371/journal.pone.0187447

25. Kaigler D, Silva EA, Mooney DJ. Guided Bone Regeneration Using Injectable Vascular Endothelial Growth Factor Delivery Gel. J Periodontol [Internet]. 2013 Feb 1;84(2):230–8. Available from: https://doi.org/10.1902/jop.2012.110684

26. Demidova-Rice TN, Durham JT, Herman IM. Wound Healing Angiogenesis: Innovations and Challenges in Acute and Chronic Wound Healing. Adv wound care [Internet]. 2012 Feb;1(1):17–22. Available from: https://www.ncbi.nlm.nih.gov/pubmed/24527273

27. Kumar A, Han SS. PVA-based hydrogels for tissue engineering: A review. Int J Polym Mater Polym Biomater [Internet]. 2017 Mar 4;66(4):159–82. Available from: https://doi.org/10.1080/00914037.2016.1190930

28. Kesireddy V, Kasper FK. Approaches for building bioactive elements into synthetic scaffolds for bone tissue engineering. J Mater Chem B [Internet]. 2016;4(42):6773–86. Available from: http://dx.doi.org/10.1039/C6TB00783J

29. Anderson DEJ, Truong KP, Hagen MW, Yim EKF, Hinds MT. Biomimetic modification of poly(vinyl alcohol): Encouraging endothelialization and preventing thrombosis with antiplatelet monotherapy. Acta Biomater [Internet]. 2019;86:291–9. Available from: http://www.sciencedirect.com/science/article/pii/S1742706119300285

30. Cutiongco MFA, Anderson DEJ, Hinds MT, Yim EKF. In vitro and ex vivo hemocompatibility of off-the-shelf modified poly(vinyl alcohol) vascular grafts. Acta Biomater [Internet]. 2015;25:97–108. Available from: http://www.sciencedirect.com/science/article/pii/S1742706115300374

31. Drozdova MG, Zaytseva-Zotova DS, Akasov RA, Golunova AS, Artyukhov AA, Udartseva OO, et al. Macroporous modified poly (vinyl alcohol) hydrogels with charged groups for tissue engineering: Preparation and in vitro evaluation. Mater Sci Eng C [Internet]. 2017;75:1075–82. Available from: http://www.sciencedirect.com/science/article/pii/S0928493116313558

32. Hartvig RA, van de Weert M, Østergaard J, Jorgensen L, Jensen H. Protein Adsorption

at Charged Surfaces: The Role of Electrostatic Interactions and Interfacial Charge Regulation. Langmuir [Internet]. 2011 Mar 15;27(6):2634–43. Available from: https://doi.org/10.1021/la104720n

33. Ino JM, Chevallier P, Letourneur D, Mantovani D, Le Visage C. Plasma functionalization of poly(vinyl alcohol) hydrogel for cell adhesion enhancement. Biomatter [Internet]. 2013/07/29. 2013;3(4):e25414. Available from: https://www.ncbi.nlm.nih.gov/pubmed/23989063

34. Lim KS, Ramaswamy Y, Roberts JJ, Alves M-H, Poole-Warren LA, Martens PJ. Promoting Cell Survival and Proliferation in Degradable Poly(vinyl alcohol)–Tyramine Hydrogels. Macromol Biosci [Internet]. 2015;15(10):1423–32. Available from: https://onlinelibrary.wiley.com/doi/abs/10.1002/mabi.201500121

35. Lim KS, Alves MH, Poole-Warren LA, Martens PJ. Covalent incorporation of non-chemically modified gelatin into degradable PVA-tyramine hydrogels. Biomaterials [Internet]. 2013;34(29):7097–105. Available from: http://dx.doi.org/10.1016/j.biomaterials.2013.06.005

36. Sachar A, Strom TA, San Miguel S, Serrano MJ, Svoboda KKH, Liu X. Cell–matrix and cell–cell interactions of human gingival fibroblasts on three-dimensional nanofibrous gelatin scaffolds. J Tissue Eng Regen Med [Internet]. 2014 Nov 1;8(11):862–73. Available from: https://doi.org/10.1002/term.1588

37. Selestina G, Vanja K. Collagen- vs. Gelatine-Based Biomaterials and Their Biocompatibility: Review and Perspectives. In: Pignatello R, editor. Biomaterials Applications for Nanomedicine. InTech; 2011.

38. Ma X, Sun X, Hargrove D, Chen J, Song D, Dong Q, et al. A Biocompatible and Biodegradable Protein Hydrogel with Green and Red Autofluorescence: Preparation, Characterization and In Vivo Biodegradation Tracking and Modeling. Sci Rep [Internet]. 2016;6:19370. Available from: https://doi.org/10.1038/srep19370

39. Zhang P, Liang Y, Kim H, Yokota H. Evaluation of a pig femoral head osteonecrosis model. J Orthop Surg Res [Internet]. 2010 Mar 6;5:15. Available from: https://www.ncbi.nlm.nih.gov/pubmed/20205927

40. Tsai A, Connolly S, Nedder A, Shapiro F. Visualization and Analysis of the

Deforming Piglet Femur and Hip Following Experimentally Induced Avascular Necrosis of the Femoral Head. IEEE Trans Biomed Eng. 2013;60(6):1742–50.

41. Shapiro F, Connolly S, Zurakowski D, Flynn E, Jaramillo D. Acetabular changes associated with avascular necrosis of the femoral head in a piglet model. Bone Joint Res [Internet]. 2014 Apr 1;3(4):130–8. Available from: https://doi.org/10.1302/2046-3758.34.2000267

42. Campillo-Fernández AJ, Unger RE, Peters K, Halstenberg S, Santos M, Sánchez MS, et al. Analysis of the Biological Response of Endothelial and Fibroblast Cells Cultured on Synthetic Scaffolds with Various Hydrophilic/Hydrophobic Ratios: Influence of Fibronectin Adsorption and Conformation. Tissue Eng Part A [Internet]. 2008 Oct 24;15(6):1331–41. Available from: https://doi.org/10.1089/ten.tea.2008.0146

43. Ziats NP, Anderson JM. Human vascular endothelial cell attachment and growth inhibition by type V collagen. J Vasc Surg [Internet]. 1993;17(4):710–8. Available from: http://www.sciencedirect.com/science/article/pii/0741521493901153

44. Jannatbabaei A, Tafazzoli-Shadpour M, Seyedjafari E, Fatouraee N. Cytoskeletal remodeling induced by substrate rigidity regulates rheological behaviors in endothelial cells. J Biomed Mater Res Part A [Internet]. 2019 Jan 1;107(1):71–80. Available from: https://doi.org/10.1002/jbm.a.36533

45. Jalali S, Tafazzoli-Shadpour M, Haghighipour N, Omidvar R, Safshekan F. Regulation of Endothelial Cell Adherence and Elastic Modulus by Substrate Stiffness. Cell Commun Adhes [Internet]. 2015 Nov 2;22(2–6):79–89. Available from: https://doi.org/10.1080/15419061.2016.1265949

46. Bujacz A. Structures of bovine, equine and leporine serum albumin. Acta Crystallogr Sect D [Internet]. 2012 Oct;68(10):1278–89. Available from: https://doi.org/10.1107/S0907444912027047

47. Gómez-Guillén MC, Giménez B, López-Caballero ME, Montero MP. Functional and bioactive properties of collagen and gelatin from alternative sources: A review. Food Hydrocoll [Internet]. 2011;25(8):1813–27. Available from: http://www.sciencedirect.com/science/article/pii/S0268005X11000427

48. Singh YP, Moses JC, Bhardwaj N, Mandal BB. Injectable hydrogels: A new paradigm

for osteochondral tissue engineering. J Mater Chem B. 2018;6(35):5499–529.

49. Lim KS, Klotz BJ, Lindberg GCJ, Melchels FPW, Hooper GJ, Malda J, et al. Visible Light Cross-Linking of Gelatin Hydrogels Offers an Enhanced Cell Microenvironment with Improved Light Penetration Depth. Macromol Biosci [Internet]. 2019 Jun 1;19(6):1900098. Available from: https://doi.org/10.1002/mabi.201900098

50. van Bruggen N, Thibodeaux H, Palmer JT, Lee WP, Fu L, Cairns B, et al. VEGF antagonism reduces edema formation and tissue damage after ischemia/reperfusion injury in the mouse brain. J Clin Invest [Internet]. 1999 Dec;104(11):1613–20. Available from: https://www.ncbi.nlm.nih.gov/pubmed/10587525

51. Infanger M, Schmidt O, Kossmehl P, Grad S, Ertel W, Grimm D. Vascular endothelial growth factor serum level is strongly enhanced after burn injury and correlated with local and general tissue edema. Burns [Internet]. 2004;30(4):305–11. Available from: http://www.sciencedirect.com/science/article/pii/S0305417903003607

52. Baumgartner I, Rauh G, Pieczek A, Wuensch D, Magner M, Kearney M, et al. Lower-Extremity Edema Associated with Gene Transfer of Naked DNA Encoding Vascular Endothelial Growth Factor. Ann Intern Med [Internet]. 2000 Jun 6;132(11):880–4. Available from: https://doi.org/10.7326/0003-4819-132-11-200006060-00005

53. Kim H, Su P, Qiu YS. Histopathologic changes in growth-plate cartilage following ischemic necrosis of the capital femoral epiphysis. An experimental investigation in immature pigs. J Bone Joint Surg Am. 2001 Jun 1;83-A:688–97.

54. Zhang HX, Zhang XP, Xiao GY, Hou Y, Cheng L, Si M, et al. In vitro and in vivo evaluation of calcium phosphate composite scaffolds containing BMP-VEGF loaded PLGA microspheres for the treatment of avascular necrosis of the femoral head. Mater Sci Eng C [Internet]. 2016;60:298–307. Available from: http://dx.doi.org/10.1016/j.msec.2015.11.055

Chapter 5. Biofabrication of Multi-Scale Vascularised Tissues with Controllable 3D Architecture

5.1. Introduction

o avoid the formation of a necrotic core within the tissue engineered constructs, it is necessary to generate a blood vessel network throughout the scaffold that provides a steady supply of oxygen and nutrients.Efforts to reproduce blood vessel networks within engineered tissues have followed two main routes: top-down strategies, which involve fabrication of pre-designed structures; and bottom-up strategies, which aim to stimulate endothelial cells to form a micro-capillary network by providing a suitable microenvironment (1).

Top-down strategies have been successful in reproducing vessel-like structures at a larger scale, generally between 100 and 800 μm in diameter (3–5). The fabrication procedure often starts by generating an initial 3D channel network using a sacrificial material, which is then embedded in the material of interest. The channel network is then perfused with culture media to remove the sacrificial material (4). Other fabrication technologies such as lithography can also be used to generate this initial channel network (5). Regardless of the fabrication method, the channels need then to be perfused with endothelial cells to form a cell monolayer covering its internal surface (4–7). This process, called endothelialisation, reduces the permeability of the channels (4) and inhibits platelet attachment (5) in a way that resembles native vessels. For example, Kolesky et al. successfully generated large engineered constructs with vascularised channels by co-printing Pluronic F127 as a sacrificial ink and a gelatin-based MSC-laden bioink (4). After removal of the sacrificial structure and endothelialisation of the channels by perfusing HUVECs, the encapsulated MSCs were able to receive oxygen, nutrients and osteogenic differentiation factors in the media that allowed for improved osteogenic differentiation as compared to a control without the fabricated microchannels. However, this type of techniques fail to reproduce the density and small diameter of capillaries in native tissues due to lack of resolution in the fabrication techniques and limitations in the diameter needed for perfusion of endothelial cells (1). Furthermore,

they generally do not provide measurements demonstrating that the oxygen and nutrients are reaching the entirety of the construct, which is the main problem targeted by vascularised tissue engineering.

Bottom-up strategies have been able to generate vessels that are more similar to capillaries in size and structure. The process involves encapsulating endothelial cells and pericyte-acting support cells in a hydrogel matrix (generally fibrin or collagen) and then stimulating them with the right combination of growth factors so that they self-assemble into micro-capillary networks (8). The resulting networks are lumenised and have a high density of micro-capillaries that present a tunica intima, pericytes and a basal membrane, mimicking native capillary networks (9,10). These networks have shown the ability to anastomose with the host vessel network post-implantation (11–13), which is promoted by *in vitro* maturation pre-implantation (14). However, the majority of studies on pre-vascularisation focus on small tissue analogues, missing a key step towards the translation to a clinical setting (10,14–17). For example, Ben-Shaul et al. studied the invasion of host vessels into fibrin hydrogels containing encapsulated endothelial cells and fibroblasts after implantation in mice (14). When comparing samples that had undergone different time periods of *in vitro* maturation (1 day or 14 days, which were considered not pre-vascularised or pre-vascularised respectively), they found that the implantation of pre-vascularised samples resulted in improved host vessel penetration and decreased clot formation as compared to samples that were not pre-vascularised. While this study generated very valuable information and demonstrated the potential of this type of approaches, the samples were discs of 1mm thickness and 6 mm diameter that only contained 7 μL of fibrin with encapsulated cells, which is very far from the size needed for translation to larger mammals. It is also worth noting that the invasion of host vessels starts at the external areas of the constructs and progresses towards the centre (14), making size and surface-volume ratio key parameters to consider when scaling up these techniques. It has been shown that the implantation and anastomosis of vascularised small tissues improves oxygen diffusion *in vivo* (13), but this advantage remains to be demonstrated for larger tissue analogues.

Thus, the translation of present technologies to the generation of large, vascularised tissues still remains a challenge. While top-down strategies are limited by the resolution of the fabrication technique and thus struggle to generate capillary-like networks, bottom-up strategies have not been demonstrated to enable the generation of larger channels and larger tissues. To generate large tissue analogues that recapitulate the different levels of

microcirculation found in native tissues, a logical step forward would be to combine both vascularisation strategies. This could be done by pre-fabricating a channel network into a material that can enable pre-vascularisation. However, materials that are adaptable to either of these strategies require very specific characteristics that are generally not overlapping. On one hand, top-down fabricated constructs need to retain their predesigned 3D architecture and their channel network (shape fidelity) during the endothelialisation process and the culture period, which requires the material to display a certain level of stiffness. The endothelialisation of the fabricated channels is also promoted by materials with higher stiffness (18,19). On the other hand, materials used in bottom-up strategies have to provide very specific conditions to endothelial cells to allow cell migration and promote their self-assembly into micro-capillaries. Hydrogels derived from extracellular matrix, like fibrin and collagen, have been the most extensively used for these strategies as they provide bioactive sequences that induce the desired cell behaviour (9,13,20). A key condition for a material to be adaptable to pre-vascularisation techniques is that it needs to be mechanically soft generally below 5 kPa of compression modulus (18,21,22), which is in contrast with the higher stiffness needed for 3D shape fidelity of the constructs. It has been shown that small changes in the polymer concentration (wt%) have a significant impact on the quality of the developed micro-capillary network (23,24), highlighting how specific these conditions need to be. Furthermore, during micro-capillary formation, the high degree of cell activity results in high ECM remodelling and the generation of forces that can result in contraction of the hydrogel (25,26). This phenomenon has been under-reported as pre-vascularisation studies generally focus on generating discs of small size. However, it has significant implications when these materials are translated to the fabrication of larger tissues with controlled architectures through top-down strategies, as it compromises shape fidelity and the required perfusion of media and endothelial cells into the sample. Thus, there is a difficult balance to be achieved, especially in terms of mechanical properties, making the combination of bottom-up and top-down techniques a challenging task.

The chemical modification of bioactive, low-cost materials such as gelatin in combination with fast and tailorable crosslinking techniques such as photo-crosslinking has been previously applied to *in vitro* pre-vascularisation approaches (18,22,27,28). For example, Chen et al. demonstrated that endothelial colony forming cells (ECFCs) and bone marrow-derived mesenchymal stem cells (MSCs) co-encapsulated in gelatin-methacryloyl (GelMA) were able to form lumenised capillary-like structures when hydrogels with very low

compressive modulus (2 kPa) were fabricated (22). However, none of these materials have been applied to the fabrication of large tissues that are pre-vascularised and also include a controllable channel network. The combination of photo-crosslinking and thiol-ene chemistry for hydrogel fabrication enables very precise tailoring of the network crosslinking density and the physico-mechanical properties of hydrogels, and has proven to be a promising strategy for biofabrication techniques that would allow fabricating channel networks and scaling up to large tissues (29).

The aim of this chapter is to generate large vascularized tissues, using both top-down fabricated endothelialised channels and bottom-up self-assembled micro-capillary networks, utilising a single material platform. A combination of Gelatin-Norbornene (Gel-NOR) with the visible-light-activated photoinitiator system Ruthenium and Sodium Persulphate (Ru/SPS) is used for hydrogel fabrication. By finely tailoring the crosslinking parameters, the possibility to enable both the formation of micro-capillary networks and the fabrication of constructs with a complex 3D architecture using a single material platform is demonstrated. Furthermore, this platform is used to investigate the effects of pore diameter and fiber diameter on the formation of micro-capillary networks, as well as endothelialisation of the fabricated channels.

5.2. Materials and Methods

5.2.1. Materials

Type A gelatin from porcine skin, sodium hydroxide, dialysis tubing (MWCO 6-8 kDa), dithiothreitiol (DTT), Tris(2,2′-bipyridyl)dichlororuthenium(II) hexahydrate (Ru), sodium persulfate (SPS), L-ascorbic acid-2-phosphate (ASAP) and Pluronic® F-127 were purchased from Sigma-Aldrich. Carbic anhydride was purchased from Acros Organics.

5.2.2. Methods

5.2.2.1. Gelatin Modification

Gelatin was dissolved in PBS (Gibco) (10wt%, 50 °C) prior to the addition of carbic anhydride up to a 20wt% concentration. 10 M NaOH was added dropwise (1 mL of NaOH per 10 mL of 10wt% gelatin) to dissolve the carbic anhydride, and pH was adjusted to 8. The reaction continued for 24 h at 50 °C and the resulting solution was centrifuged. The supernatant was dialyzed (MWCO 6-8 kDa) against deionized water. The products were freeze-dried and stored at room temperature until use. The DoM was determined to be 27% on 1H-NMR spectroscopy and fluoroaldehyde assay.

5.2.2.2. Hydrogel Fabrication

Cell-free hydrogels were prepared in PBS. A Gel-NOR precursor solution was mixed with DTT and Ru/SPS to obtain a final concentration of 5wt% Gel-NOR, functional group ratios of 1:1-1:24 (NOR:SH) and 0.1/1 to 2/20 mM of Ru/SPS. Samples were photo-crosslinked using visible light (OmniCure® S1500, Excelitas Technologies with a Rosco IR/UV filter 400 – 450nm, 3min, 300 mW cm-2) in cylindrical moulds (h = 1 mm, Ø = 5 mm) in an open environment.

5.2.2.3. Swelling and Mass Loss Assays

After crosslinking, each hydrogel was weighed (minitial,t0), out of which three samples per hydrogel composition were directly freeze-dried to record their initial dry weights (mdry,t0) and determine the actual macromer weight fraction, which is reported as the ratio of the initial dry weight to the initial weight. To determine the initial dry weight of the remaining samples, the factor of the actual macromer fraction and individual initial weight was used (Eq. 1).

$$Actual\,macromer\,fraction = \frac{m_{dry,t0}}{m_{initial}} \quad (1)$$

The remaining samples were allowed to swell in PBS at 37 ºC for up to 1d. Swollen hydrogel samples were collected to record wet weight ($m_{swollen}$). The samples were then freeze-dried to obtain the freeze dried weight (m_{dry}) and calculate the sol fraction and mass swelling ratio (q) according to equations 2, 3 and 4:

$$m_{dry,t0} = m_{initial}\, x\, actual\,macromer\,fraction \quad (2)$$

$$Mass\,loss = \frac{m_{dry,t0} - m_{dry}}{m_{dry,t0}}\, x\, 100 \quad (3)$$

$$q = \frac{m_{swollen}}{m_{dry}} \quad (4)$$

The sol fraction of the hydrogels is defined as percent macromers that are not crosslinked into the hydrogel network, and determined as the mass loss after equilibrium swelling (t = 1 d).

5.2.2.4. Mechanical Testing

The compressive modulus of the hydrogel discs was measured using an MTS Criterion® 42 mechanical testing machine equipped with a 5N load cell, at RT in an unconfined environment. The engineering stress-strain profile was obtained by uniaxial compression and the elastic modulus was calculated by obtaining the slope in the linear part of the curve, following equation 5:

$$E = \frac{\sigma_e}{\varepsilon_e} \quad (5)$$

5.2.2.5. Cell Expansion

Human umbilical vein endothelial cells (HUVECs, obtained from ATCC) were cultured in Vascular Basal Media (ATCC) supplemented with Endothelial Cell Growth Kit-VEGF (ATCC) and Penicillin/Streptomycin (Referred to as endothelial growth media, EGM). Bone marrow-derived mesenchymal stem cells (MSCs, obtained from RoosterBio) were cultured in α-MEM (Gibco) supplemented with 10% foetal calf serum (Hyclone), 1% penicillin/streptomycin, 20 mM of ASAP and 5 ng/mL basic fibroblast growth factor (R&D Systems).

5.2.2.6. Fabrication and Culture of Cell-Laden Hydrogels

Passage 2 to 3 HUVECs and passage 3 MSCs were trypsinized and encapsulated in Gel-NOR (5wt% Gel-NOR, DTT at 1:4 SH:NOR ratio, 0.2/2 to 1/10 mM Ru/SPS) or Matrigel at a concentration of 5M HUVECs and 1M MSCs/mL and cultured up to 14 days in EGM.

5.2.2.7. 3D Biofabrication of Gel-NOR Constructs with Controlled Porosity

Large Gel-NOR constructs with an interconnected porous network were biofabricated through a sacrificial templating method. Pluronic® F-127 (30wt%) was extruded through a needle at a temperature of 25°C using a BioScaffolder (SYS+ENG, Germany) and deposited onto a 30°C plate in a layer-by-layer, 0-90° orientation, with Pluronic® F-127 fibre diameter depending on needle size and printer settings (Table 5.1). Fibre spacing was adjusted to match the fibre diameter.

Table 5.1. Settings for printing Pluronic® F-127 sacrificial templates and dispensed Gel-NOR volumes.

Fibre diameter (mm)	Fibre spacing (mm)	Needle inner diameter (mm)	Print head speed (mm min^{-1})	Spindle motor speed (mm min^{-1})	Volume of Gel-NOR (µL)
0.5	0.5	0.3 (23G)	700	8	100
0.75	0.75	0.6 (21G)	500	9	110
1	1	0.9 (19G)	300	13	130

A Gel-NOR solution (5wt% Gel-NOR, 1:4 SH:NOR ratio of DTT, 0.2/2 or 0.5/5 mM Ru/SPS, $10*10^6$ HUVECs/mL, $2*10^6$ MSCs/mL) was dispensed throughout the printed construct using a pipette and photopolymerised (400 – 450nm, 3min, 300 mW cm^{-2}). Subsequently, the construct was immersed in cold EGM to dissolve the Pluronic® F-127 scaffold, after which the construct was cultured in EGM (37°C, 20% O_2, 5% CO_2) for up to 14 days. The resulting constructs had a pore diameter equal to the fiber diameter of the printed Pluronics sacrificial template, and a fiber diameter equal to the fiber spacing of the Pluronics sacrificial template.

5.2.2.8. Viability Assays

Live/dead staining was used to visualize cell viability of encapsulated cells on day 1. In brief, hydrogel samples were washed with PBS, cut in half, and were incubated with propidium iodide (1.5 μM, from Invitrogen) and calcein-AM (1 μM, from Invitrogen) in PBS for 15 min at RT. The samples were then washed with PBS and left hydrated for imaging using a fluorescent microscope (Zeiss Axioimager Z1 microscope). Live and dead cells were counted at three locations within the centre of each construct per time point using Image J (version 6.1 Fiji, National Institutes of Health). Viability was calculated using equation 6:

$$Cell\ viability\,(\%) = 100\,x\,\frac{Live\ cells}{(Live\ cells + Dead\ cells)} \tag{6}$$

5.2.2.9. DNA Quantification

Hydrogels were digested at 56° in 1 mg mL-1 proteinase K dissolved in a 10-2 M Tris-HCl and 103 M disodium EDTA solution, following a treatment with DNase-free RNase A (Thermo Fisher). Total DNA was quantified using CyQUANT Cell Proliferation Assay Kit according to manufacturer's instructions.

5.2.2.10. Metabolic Activity Assays

AlamarBlue® was used to track the cellular health of embedded cells on days 1, 4, 7, 10 and 14. Briefly, each hydrogel sample was incubated with 350 μL media containing AlamarBlue® solution, diluted according to manufacturer's instructions, for 3h. The reduction of AlamarBlue® in the solution was determined by reading absorbance at wavelengths of 570 nm and 600 nm using a spectrophotometer (Thermo Scientific Varioskan Flash, Darmstadt, Germany) followed by data processing according to manufacturer's instructions.

5.2.2.11. Immunofluorescence Examination

Cell-laden hydrogels were collected after 10 and 14 days, washed in PBS, followed by a fixation in 4% formaldehyde for 45 min at RT. Constructs were then cut in half, blocked with a solution of PBS and 2% BSA for 1h at RT and permeabilized using a 0.2% Triton-X solution. Primary anti-CD 31 and α-Smooth muscle actin (α-SMA) antibodies (R&D Systems) were diluted in blocking buffer (1:100) and applied overnight at 4°C. Samples were washed three times in 2% BSA for 30 minutes each, followed by an incubation with a goat-anti-mouse (Alexa Fluor 488, Lifetech) and donkey-anti-rabbit (Alexa Fluor 594, Abcam) secondary antibodies diluted in blocking buffer (1:500) in the dark overnight at 4°C. Samples were then washed 3 times in PBS during 30 min, incubated in a DAPI (1:1000) solution for 2 min and washed three times in PBS. Images were captured using either a Leica TCS SP5 confocal microscope (Leica camera AG, Wetzlar, Germany) or a Zeiss Axioimager Z1 fluorescence microscope (Carl Zeiss Microscopy, Jena, Germany). The stages of network development in Gel-NOR samples were described following previously reported criteria (8,20).

5.2.2.12. Endothelial Cell Network Quantification

Endothelial cell networks were quantified from the CD31 immunofluorescence images obtained on days 10 and 14. The maximum intensity projection was obtained from 100 µm Z-stacks in 3 different areas of each sample and the total vessel length and number of junctions were quantified using AngioTool software.

5.2.2.13. Statistical Analysis

All samples were prepared in triplicates and each experiment was repeated 3 times to study variability between experiments (N=3) unless stated in the specific figure. Individual differences between groups and time points were assessed using one or two-way ANOVA and Holm-Sidak post hoc analysis (GraphPad Prism 7). Statistical significance was accepted at $p<0.05$.

5.3. Results and Discussion

5.3.1. Effects of NOR:SH Ratio on the Crosslinking Efficiency of Gel-NOR Hydrogels

Using thiol-ene chemistry for hydrogel crosslinking allows the tailoring of a large number of variables in order to obtain the desired hydrogel physico-mechanical properties. Parameters such as the macromer concentration, degree of functionalisation and photoinitiator concentration, which can be modified in other crosslinking chemistries such as methacryloyl-based reactions (15), are added to parameters such as the concentration, molecular weight and degree of functionalisation of the crosslinker (29–31). Crosslinking Gel-NOR is possible using different thiol-containing molecules, including short molecules with two thiol groups such as dithiothreitol (DTT) (31) or larger molecules with a higher number of thiol groups such as modified 4-arm poly(ethylene glycol) (30–32). Munoz et al. reported that Gel-NOR crosslinked using DTT as a crosslinker resulted in lower mechanical properties than Gel-NOR crosslinked using thiolated PEG-tetra-thiol (31). Given that our aim is to generate hydrogels with low physico-mechanical properties, DTT was selected as the crosslinker. To start studying the network properties of hydrogels fabricated under different crosslinking conditions, Gel-NOR hydrogels were fabricated using different DTT concentrations using 5wt% Gel-NOR and 0.5/5 mM Ru/SPS. Mass loss and swelling studies revealed a bell-shaped pattern, where the lowest sol fraction and swelling ratio were measured in hydrogels crosslinked using 1:4 NOR:SH ratio (Figure 5.1). These results are in agreement with previous research using thiol-ene chemistry (gelatin functionalized with allyl glycidyl ether, Gel-AGE) and Ru/SPS as a photoinitiator system, which show that changing the ene:thiol ratio results in a similar bell-shaped curve of crosslinking efficiency (29). Lower sol fraction values are the result of a more efficient crosslinking reaction. When bioactive agents such as cells or drugs are encapsulated into a hydrogel, a key determinant of the encapsulation efficiency is the crosslinking efficiency, where lower crosslinking efficiency results in an increased loss of encapsulated bioactive agent (33). Therefore, subsequent characterisation was performed using the crosslinking condition that resulted in the lowest sol fraction (1:4 NOR:SH ratio).

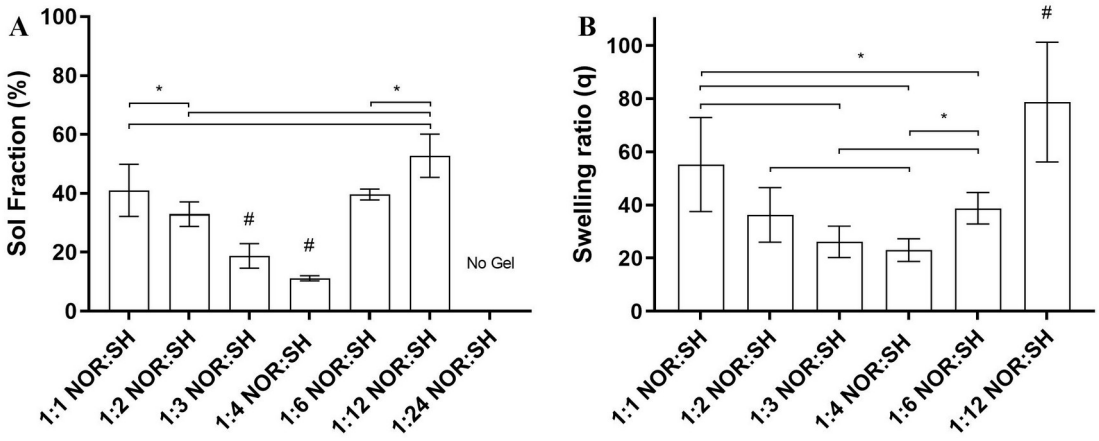

Figure 5.1. Effects of the Norbornene:Thiol ratio on the physico-chemical properties of Gel-NOR hydrogels. *(A) Sol fraction and (B) swelling ratio of 5wt% Gel-NOR hydrogels crosslinked using different Norbornene:Thiol (NOR:SH) concentrations. Ru/SPS concentrations were kept to 0.5/5 mM in all conditions. Significant differences ($p<0.05$) were found between all conditions except when comparing 1:6 with both 1:1 and 1:2 in sol fraction, and 1:2 with 1:6 in swelling ratio. *: Significant difference between groups ($p<0.05$). #: Significant difference ($p<0.05$) as compared to all other groups. Experiments were repeated 3 times with 3 technical repeats each (N=3).*

5.3.2. Effects of Ru/SPS Concentration on the Physico-Mechanical Properties of Gel-NOR Hydrogels

To study how the Ru/SPS concentration can affect the physico-mechanical properties of Gel-NOR hydrogels, Gel-NOR discs were fabricated using 5wt% Gel-NOR, 1:4 NOR:SH and a range of Ru/SPS concentrations. Their sol fraction, swelling ratio and compressive modulus were measured (Figure 5.2). Increasing the Ru/SPS concentration resulted in lower sol fraction and swelling ratio, ranging from 45% to 11% sol fraction when crosslinked using 0.1/1 and 0.5/5 mM Ru/SPS respectively. Further increasing the Ru/SPS concentration to 2/20 mM did not result in lower sol fraction. Increasing the Ru/SPS concentration also increased the compressive modulus, ranging from 4 kPa to 9 kPa when crosslinked using 0.1/1 and 1/10 mM Ru/SPS, respectively. However, further increasing the Ru/SPS concentrations resulted in a decrease in compressive modulus. Previous literature studying photo-crosslinked hydrogels for pre-vascularisation purposes have shown positive results when their compressive modulus was ≤5 kPa (18,21,22,27). Therefore, Gel-NOR hydrogels crosslinked using 0.2/2 mM Ru/SPS, which showed a compressive modulus of 5.5 kPa, were selected to continue with cell encapsulation. To study the effects of compressive modulus and Ru/SPS concentration in the pre-vascularisation process, hydrogels crosslinked using 0.5/5

and 1/10 mM Ru/SPS were also included in the experiments. Hydrogels crosslinked using 0.1/1 mM Ru/SPS were not included due to their high sol fraction, as they would result in a lower cell encapsulation efficiency.

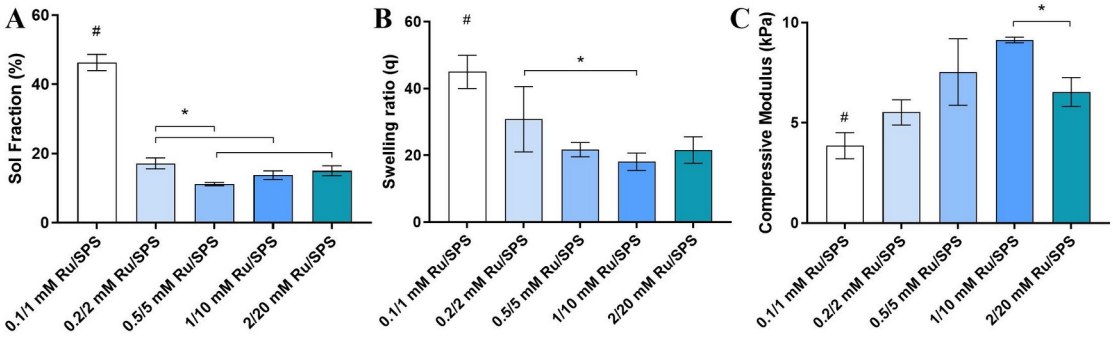

Figure 5.2. Effects of the Ru/SPS concentration on the physico-mechanical properties of Gel-NOR hydrogels. *(A) Sol fraction, (B) swelling ratio and (C) compression modulus of 5wt% Gel-NOR hydrogels crosslinked using DTT 1:4 NOR:SH ratio and a range of Ru/SPS concentrations. *: p<0.05. #: Significantly different (p<0.05) to all other groups. Experiments were repeated 3 times with 3 technical repeats each (N=3).*

5.3.3. Effects of Ru/SPS Concentration and Physico-Mechanical Properties of Gel-NOR Hydrogels on Survival and Proliferation of HUVECs and MSCs

HUVECs (5M cells/mL) and human bone marrow-derived MSCs (1M cells/mL) were co-encapsulated in either Gel-NOR using different Ru/SPS concentrations or Matrigel as a control group. Matrigel was chosen a s positive control due to its demonstrated ability to allow co-encapsulated endothelial cells and support cells to form capillarie-like structures (52). Cell viability was measured on day 1 post-encapsulation, and total DNA content and metabolic activity were measured on days 1, 4, 7, 10 and 14 of culture (Figure 5.3). It was observed that cell viability decreased from 83% to 74% when Ru/SPS concentrations were increased from 0.2/2 mM to 0.5/5 mM Ru/SPS, and cell viability further decreased to 54% when Gel-NOR hydrogels were crosslinked using 1/10 mM Ru/SPS . These results suggest that increasing the Ru/SPS concentrations results in decreased cell viability, which differs from previous research encapsulating human articular chondrocytes (HAC) in either Gel-MA/ Collagen using up to 2/20 mM Ru/SPS (34) or Gel-AGE using 1/10 mM Ru/SPS (29), where cell viability was >80%. Possible explanations of these differences are either lower gelatin concentration used in our study, which would reduce its free radical scavenging effects (35,36), or differences in sensitivity to free radical damage between cell types, which has previously been reported between MSCs and HUVECs when exposed to H_2O_2 (37). No

significant differences were found when comparing co-cultures encapsulated in Gel-NOR hydrogels crosslinked using 0.2/2 Ru/SPS with the Matrigel control.

Total DNA measurements showed a significant decrease in days 1 and 4 for all experimental groups ($p<0.05$). This result could be explained by an initial differentiation process, and has been previously reported in co-cultures of HUVECs and MSCs encapsulated in GelMA (38). Interestingly, on days 1 and 4, despite the differences in cell survival, no significant differences in total DNA were observed between Gel-NOR hydrogels crosslinked using different Ru/SPS concentrations. Total DNA content remained stable from day 4 to day 10 for all Gel-NOR groups, followed by an increase between days 10 and 14 in hydrogels crosslinked using 0.2/2 and 0.5/5 mM Ru/SPS. Total DNA in Matrigel controls showed a increasing trend at each time point between days 4 and 14. On day 14, Matrigel showed the highest total DNA content per sample (1.16 μg, $p<0.05$), followed by Gel-NOR crosslinked using 0.2/2 and 0.5/5 mM Ru/SPS with 0.73 and 0.84 μg respectively (with no significant differences between these two groups), and finally Gel-NOR crosslinked using 1/10 mM Ru/SPS with an average of 0.47 μg per sample. The fact that Matrigel is the group with the highest total DNA from day 7 onwards could be caused by the presence of bioactive components in the material such as growth factors, which could result in increased stimulation of cell proliferation (39). These results suggest that the initial differentiation phase could be followed by a slow proliferation phase, with both phases being affected by differences in mechanical properties, crosslinking density and the presence of bioactive cues in the hydrogels.

Metabolic activity measurements revealed that Gel-NOR groups maintained stable levels of metabolic activity during the culture period, except for a significant decrease in 0.2/2 Ru/SPS samples between days 1 and 4 and a significant increase in 1/10 Ru/SPS samples between days 7 and 10 ($p<0.05$). At the end of the experiment, all Gel-NOR groups showed comparable levels of metabolic activity. Matrigel groups, however, showed an increasing trend throughout the whole experiment, and had significantly higher metabolic activity than Gel-NOR groups at day 14 ($p<0.05$). After normalization to DNA, metabolic activity shows different trends depending on the experimental group. While both Matrigel and Gel-NOR 1/10 mM Ru/SPS show an increasing trend throughout the whole experiment, both Gel-NOR groups crosslinked using 0.2/2 and 0.5/5 mM Ru/SPS show a slightly decreasing tendency. On day 14, all groups showed comparable results ($p>0.05$) except for Gel-NOR 1/10 mM Ru/

SPS, which displayed significantly higher metabolic activity. These differences in metabolic activity could be explained by differences in general cell behaviour, which are further studied in section 5.3.4. An interesting observation is the fact that Matrigel samples show a lower normalised metabolic activity as compared to Gel-NOR groups, but at the same time show higher total DNA counts and overall metabolic activity. A potential explanation to that is that HUVECs and MSCs could be behaving differently within the samples. Endothelial cells in Matrigel could be differentiating more quickly during the first days of culture as compared to Gel-NOR groups, resulting in the observed drop of DNA content and the lower initial normalised metabolic activity. On the other hand, the population of MSCs in Matrigel could be proliferating at a faster rate than in Gel-NOR samples, resulting in the steady increases in total DNA and normalised metabolic activity seen in the experiment. These differences in cell behaviour could be caused by the presence of bioactive cues in Matrigel hydrogels (39).

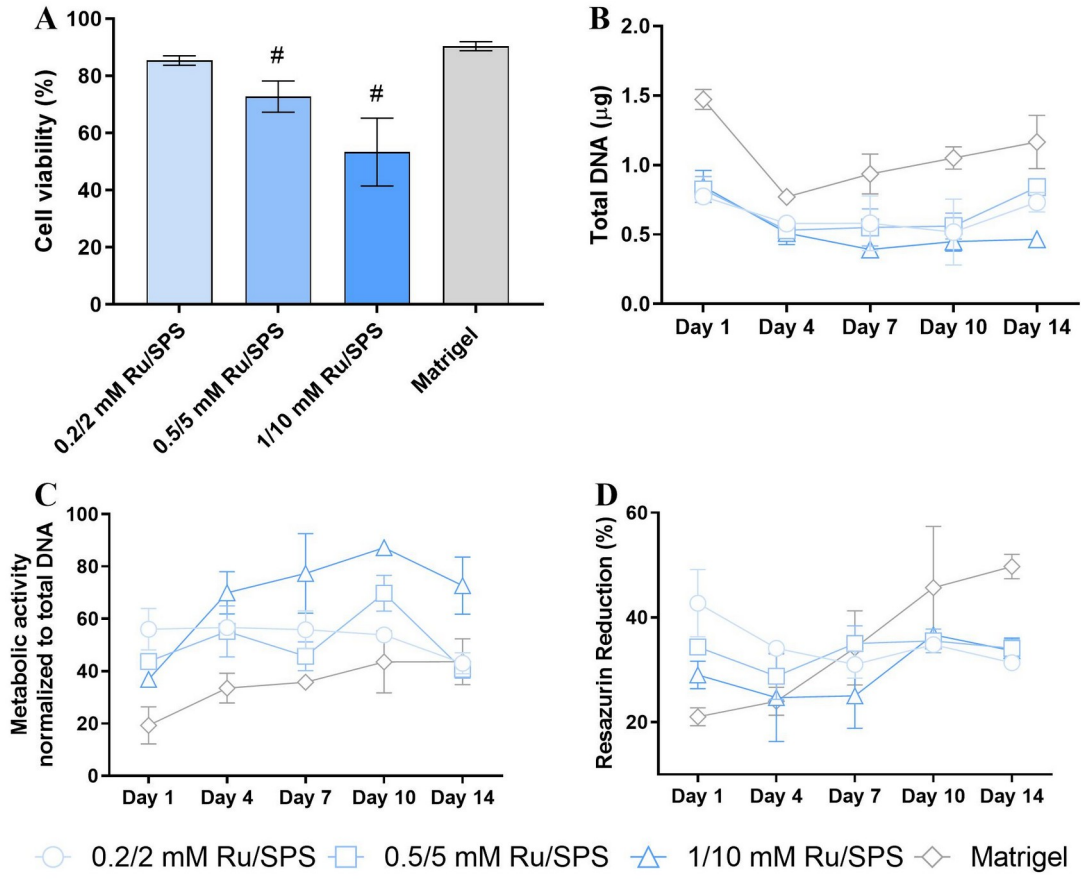

Figure 5.3. Effects of the Ru/SPS concentration on the cell survival, proliferation and metabolic activity of HUVEC/MSC co-cultures encapsulated in Gel-NOR hydrogels. *(A) Cell viability, (B) DNA quantification and (C) metabolic activity of co-encapsulated human umbilical vein endothelial cells (HUVEC) and human bone marrow-derived mesenchymal stem cells (MSCs) in either 5wt% Gel-NOR hydrogels crosslinked using DTT 1:4 NOR:SH ratio and a range of Ru/SPS concentrations or in Matrigel. #: Significantly different ($p<0.05$) to all other groups. Experiments were repeated 3 times with 3 technical repeats each (N=3).*

5.3.4. Effects of Ru/SPS Concentration and Physico-Mechanical Properties of Gel-NOR Hydrogels on Capillary-Like Network Development and Shape Fidelity

Previous studies on pre-vascularisation of hydrogels have showed micro-capillary network formation of co-encapsulated endothelial cells and support cells at days 10 (18) and 14 (10,16,17,40) of culture. Some studies have also shown improvement of the micro-capillary network when comparing samples cultured during 7 and 14 days on both fibrin (10) and photo-crosslinked PEG (17). The effects of Ru/SPS concentrations and mechanical properties of the hydrogels on the micro-capillary networks formed by the encapsulated co-cultures were studied by CD31 immunostaining of the hydrogels on days 10 and 14 of culture (Figure 5.4A). At both time points, Gel-NOR hydrogels crosslinked using 0.2/2 mM Ru/SPS and Matrigel constructs showed fully interconnected networks whereas 0.5/5 mM gels show a partially connected network. Endothelial cells on the surface of Gel-NOR 1/10 mM Ru/SPS samples didn't show a micro-capillary organisation, but were progressively endothelialising the surface. A potential explanation for these differences in endothelial cell behaviour are differences in material stiffness, which have previously been demonstrated to determine the morphology of endothelial cells seeded on the surface of photo-crosslinked gelatin-methacryloyl (GelMA) hydrogels (18). Klotz et al. seeded endothelial cells on the surface of GelMA hydrogels with compressive modulus of either 1.2 or 1.8 kPa and found that cells on softer hydrogels showed a more round morphology and were unable to form a confluent monolayer, whereas endothelial cells on stiffer gels were able to form a confluent monolayer after 10 days of culture (18). These differences in cell behaviour could also be related to the differences seen in metabolic activity in section 5.3.3., where cells encapsulated in Gel-NOR hydrogels crosslinked using 1/10 mM Ru/SPS showed increased metabolic activity as compared to other groups. It is possible that the promotion of endothelialisation on the material surface is also associated with other changes in cell behaviour such as increased cell proliferation or decreased cell differentiation when compared to the promotion of micro-capillary network formation, resulting in higher overall metabolic activity of the samples.

Analysis of the network parameters (Figure 5.4B-C) revealed diverging tendencies between groups. Gel-NOR hydrogels crosslinked using 1/10 mM Ru/SPS were not included in the analysis as endothelial cells were unable to form micro-capillary networks in that condition. Cells encapsulated in Gel-NOR hydrogels crosslinked using 0.2/2 mM Ru/SPS showed increases in both junctions density and average vessel length between day 10 and day 14, whereas cells encapsulated in Gel-NOR hydrogels crosslinked using 0.5/5 mM Ru/SPS

showed an increase in junctions density but no significant increase in average vessel length. Matrigel samples, on the other hand, show a significant decrease in both junctions density and average vessel length between days 10 and 14. A potential explanation to these results is that the micro-capillary network has reached a more mature state in Matrigel samples, where the network was fully developed on day 10 and could have be regressing due to lack of perfusion. This phenomenon has been previously reported in models of retinal angiogenesis, where lack of perfusion results in capillary regression (41,42). Gel-NOR samples, on the other hand, were still developing a fully interconnected network between days 10 and 14 regardless of the Ru/SPS concentration used for crosslinking. On days 10 and 14, the Matrigel samples showed the highest values in junctions density and average vessel length, followed by Gel-NOR 0.2/2 and 0.5/5 mM Ru/SPS. A combination of factors differ between Matrigel and Gel-NOR samples, which could explain the observed differences in cell behaviour. These factors include stiffness, which is reported to be between 10 and 50 Pa (43) in Matrigel hydrogels at the studied concentrations, and the presence of a variety of ECM molecules and growth factors that could be promoting the vascularisation process (39). The differences between Gel-NOR 0.2/2 and 0.5/5 mM Ru/SPS are most likely caused by differences in stiffness and polymer network density, as there were no significant differences between groups in both total DNA content and metabolic activity, which suggests that the initial effect of the photoinitiator concentration in cell survival was not translated to differences in longer-term cell behaviour.

The interactions between endothelial cells and HUVECs were further studied with a CD31 and α-SMA day 14 immunostaining of the Gel-NOR hydrogels crosslinked using 0.2/2 mM Ru/SPS (Figure 5.5A). Results showed that MSCs were expressing αSMA and were in close contact with the endothelial cell network, suggesting that they were developing a smooth muscle-like phenotype and acting as pericytes for the endothelial cells. Endothelial cells were starting to develop a lumen, which is a sign of maturation of the network. These results prove that the photoinitiator concentrations and stiffness of the hydrogel have highly impactful role on the endothelial cell behaviour. Additionally, the results prove that Gel-NOR hydrogels are able to provide the right microenvironment for endothelial cells to self-assemble into micro-capillary structures.

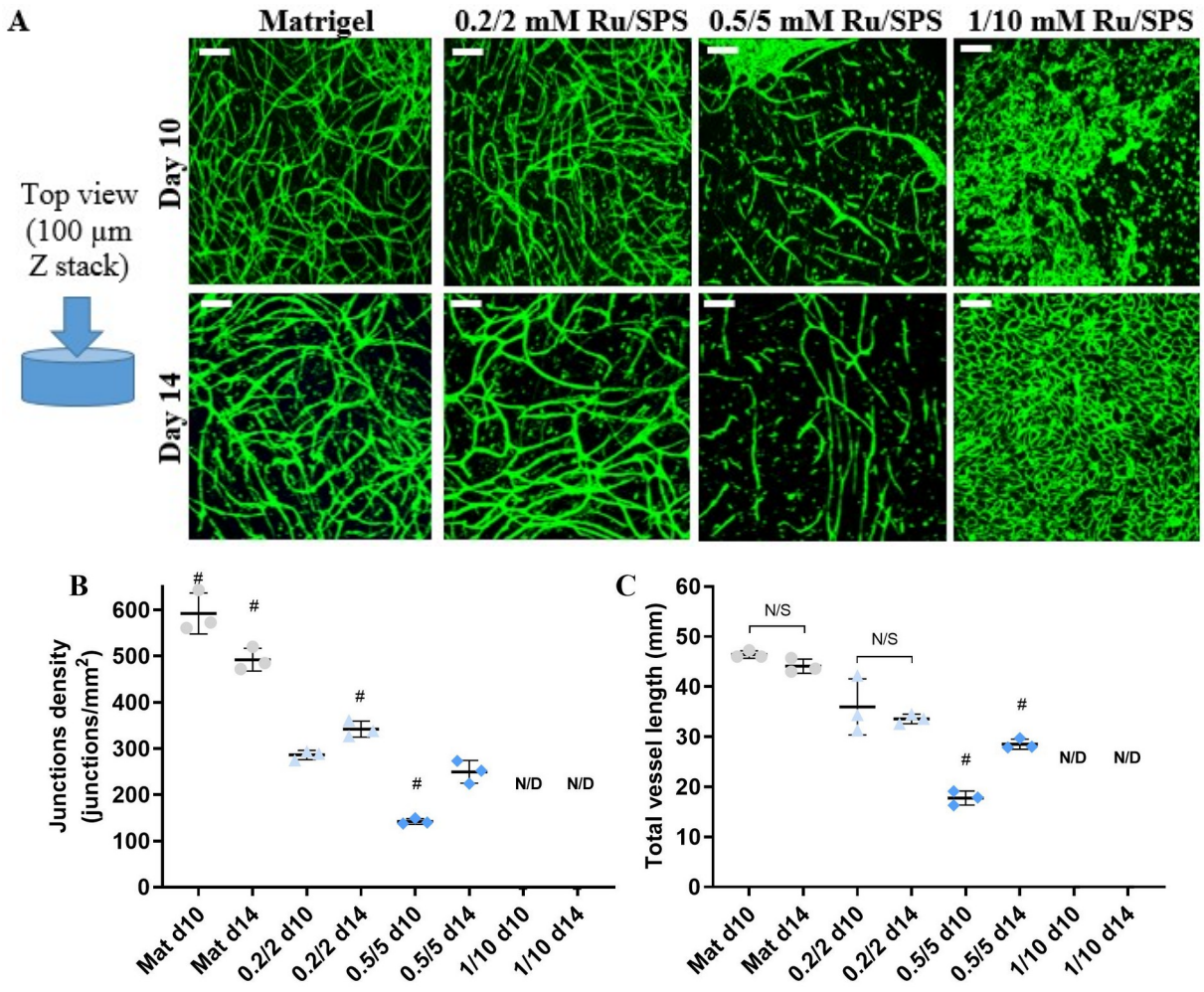

Figure 5.4. Effects of Ru/SPS Concentration and Physico-Mechanical Properties of Gel-NOR Hydrogels on Capillary-Like Network Development (Top view). *(A) Representative images and (B-C) network analysis of a CD31 immunostaining of co-encapsulated HUVECs and MSCs in Gel-NOR 5wt%, DTT 1:4 NOR:SH discs crosslinked using different Ru/SPS mM concentrations. *: Significant difference ($p<0.05$) between groups. #: Significant difference ($p<0.05$) as compared to all other groups. Scale bars: 200 µm. Mat: Matrigel® group. 0.2/2, 0.5/5 and 1/10 indicate the Ru/SPS mM concentration in Gel-NOR samples. Experiments were repeated 3 times with 3 technical repeats each (N=3).*

3D biofabrication techniques could allow the fabrication of a controlled channel network in combination with the self-assembled micro-capillary network, enabling the reproduction of the complex vascular beds in native tissues and organs. It is important for the fabricated constructs to maintain their shape after the biofabrication process so that these channels remain open during ECM remodelling and tissue maturation. To understand how different crosslinking conditions in Gel-NOR would affect shape fidelity after fabrication, the size of Gel-NOR hydrogels was monitored during the culture process (Figure 5.5B). It was found that hydrogels fabricated using higher Ru/SPS concentrations contracted significantly less, with no contraction in hydrogels fabricated using 1/10 mM Ru/SPS. Gel-NOR hydrogels

fabricated using 0.5/5 or 0.2/2 mM Ru/SPS showed significant contraction on days 14 and 10 respectively. Matrigel controls showed a significant decrease in area as early as day 4 and showed very irregular contraction patterns (Supplementary Figure S5.1). On day 14, the average area (as imaged from the top) was not significantly different between Matrigel and Gel-NOR samples crosslinked using 0.2/2 mM Ru/SPS. However, it was observed that, due to the irregular contraction, Matrigel samples with higher measured area also decreased in thickness (data not shown), suggesting that the overall volume of the samples would show a more significant decrease over time as compared to the area measurements. Our data suggests that the formation of micro-capillary structures is related to the contraction of the sample, as the only samples that did not contract were Gel-NOR hydrogels crosslinked using 1/10 mM Ru/SPS that had also showed no micro-capillary formation on the surface. Furthermore, groups that showed higher junctions density and average vessel length also showed a significant decrease in area at earlier time points and had lower measured area on day 14. These results support previous studies that demonstrate that the formation of micro-capillary networks is tightly related to ECM remodelling and the generation of mechanical forces by encapsulated cells could cause contraction of the samples (25,26). When Gel-NOR was crosslinked using 0.2/2 mM Ru/SPS, it was possible to obtain samples with a relevant degree of micro-capillary formation and with more homogeneous contraction as compared to Matrigel, making this condition a reasonable candidate for the biofabrication of larger constructs with a controllable channel network.

When generating tissue engineered constructs of relevant size for clinical translation, it is important to investigate the formation of micro-capillaries both at the surface and the deeper areas of the construct. Most studies on pre-vascularisation use samples of very small volume that do not recapitulate the oxygen and nutrient gradients of large tissue constructs, which could significantly affect micro-capillary formation *in vitro* and anastomosis with the host vessel network after implantation. Furthermore, cell behaviour at the deeper areas of the samples, which would provide more information on the effects of these gradients, is generally not clearly reported in the literature, making the information difficult to interpret (8,17). Some reports have started including analysis where the deeper areas of the constructs are studied separately, and it has been reported that the behaviour of endothelial cells and support cells can differ between cells closer to the surface and cells in deeper areas of the construct (10,16).

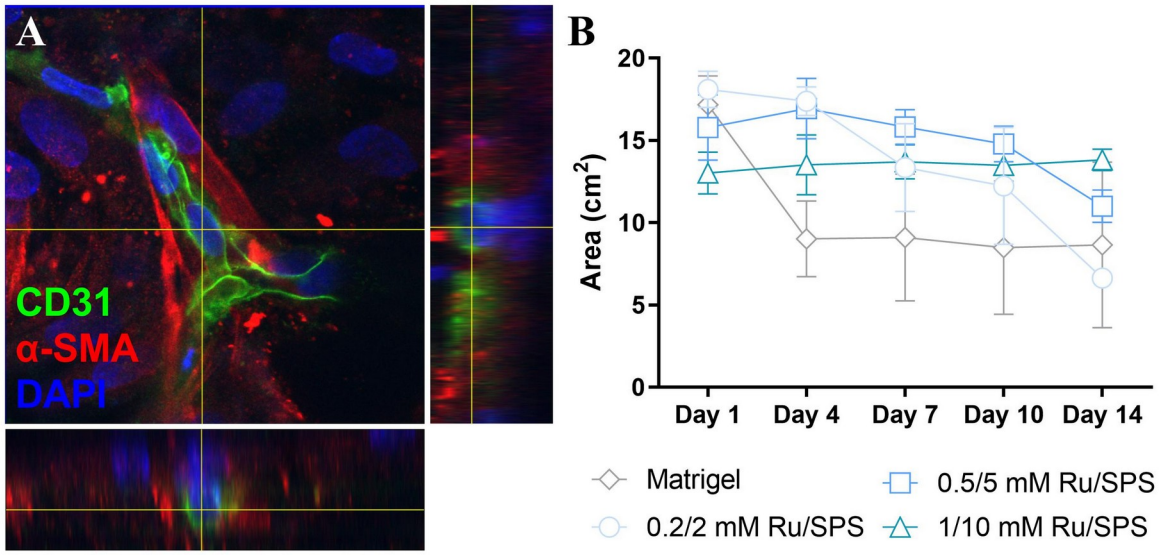

Figure 5.5. Lumen formation by endothelial cells in Gel-NOR hydrogels and effects of Ru/SPS concentration and physico-mechanical properties of Gel-NOR hydrogels on construct shape fidelity. *(A) CD31 and alpha-SMA immunostaining of co-cultures in Gel-NOR 0.2/2 mM Ru/SPS showing the interaction between endothelial cells and MSCs acting as pericytes. (B) Hydrogel size over time during culture period. Scale bars: 50 µm. Experiments were repeated 3 times with 3 technical repeats each (N=3).*

To study the formation of micro-capillaries throughout the cross-section of Gel-NOR hydrogels, CD31 and α-SMA immunostaining was performed after sectioning the fabricated discs (Supplementary Figure S5.2) and micro-capillary network formation was analysed (Figure 5.6). Due to the irregular contraction observed in Matrigel samples, it was not possible to differentiate between surface and deeper areas of the samples in a reliable and repeatable way. Thus, this group was not included in the analysis. Immunostaining on days 10 and 14 showed that endothelial cells were organising into a micro-capillary network in both Gel-NOR 0.2/2 and 0.5/5 mM Ru/SPS. However, endothelial cells in Gel-NOR hydrogels crosslinked using 1/10 mM Ru/SPS showed a round morphology (Supplementary Figure S5.2 and Figure 5.6A). These differences are most likely related to differences in stiffness, which determine cell elongation and migration inside the hydrogel (18). On the other hand, endothelial cells were directly interacting with MSCs expressing α-SMA, which showed the ability to elongate and migrate in all Gel-NOR conditions (Supplementary Figure S5.2).

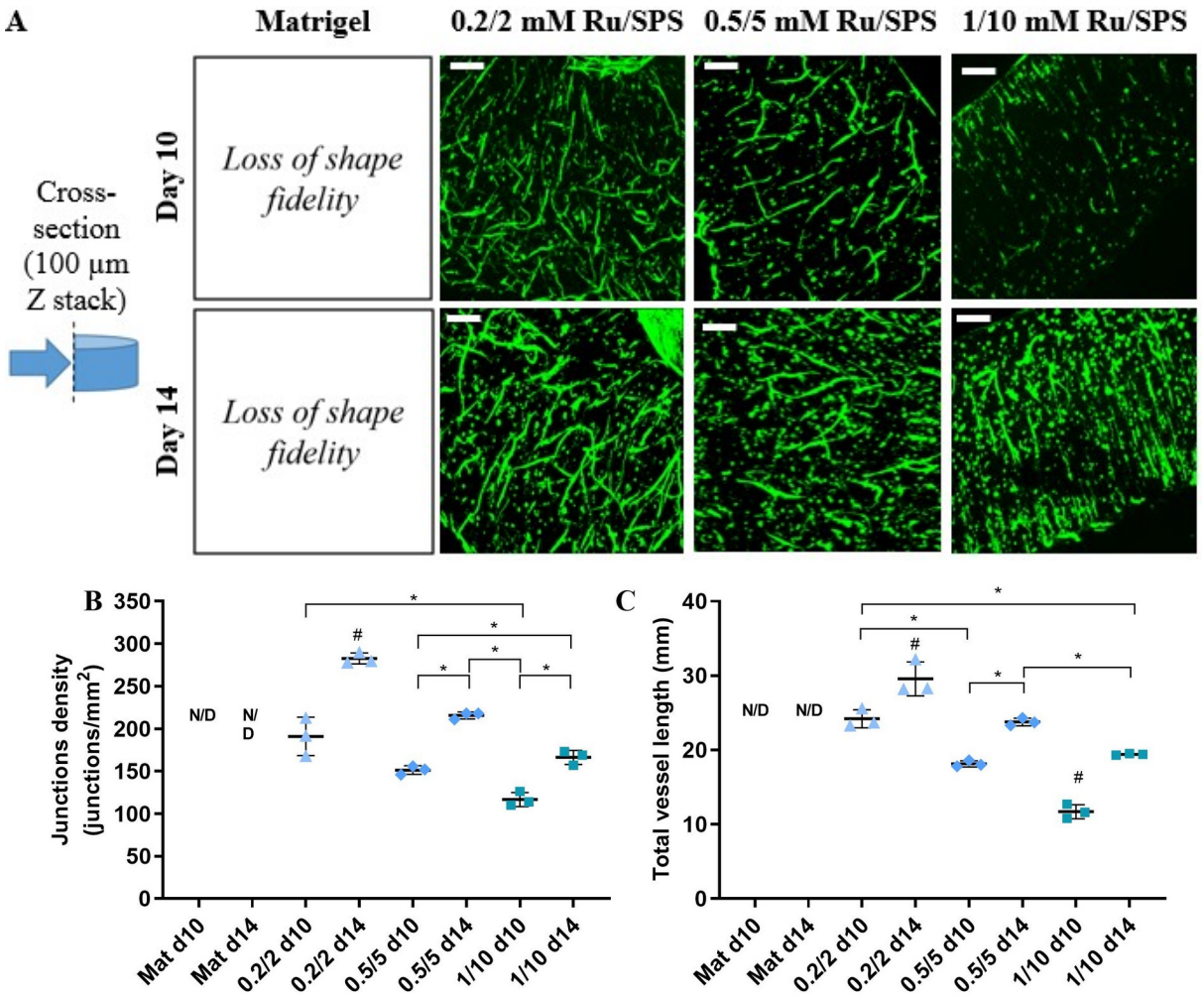

Figure 5.6. Effects of Ru/SPS concentration and physico-mechanical properties of Gel-NOR hydrogels on capillary-like network development (Cross-section). *Representative images and network analysis of CD31 immunostaining of co-encapsulated HUVECs and MSCs in Gel-NOR 5wt%, DTT 1:4 NOR:SH discs crosslinked using different Ru/SPS mM concentrations. *: Significant difference ($p<0.05$) between groups. #: Significant difference ($p<0.05$) as compared to all other groups. Scale bars: 200 µm. Mat: Matrigel® group. 0.2/2, 0.5/5 and 1/10 indicate the Ru/SPS mM concentration in Gel-NOR samples. Experiments were repeated 3 times with 3 technical repeats each (N=3).*

The network formed at the deeper areas of Gel-NOR crosslinked using 0.2/2 mM Ru/SPS was partially interconnected, which differs from its fully interconnected surface network (Figure 5.6A). Gel-NOR hydrogels crosslinked using 0.5/5 mM Ru/SPS also showed a partially interconnected network, in a similar way to its surface network. Interestingly, there seemed to be a higher number of endothelial cells with spherical shape at the deeper areas of the constructs as compared to their surface in all groups. Differences in the quality of micro-capillary networks have previously been reported in collagen-based scaffolds with co-encapsulated HUVECs and MSCs (16), where the quality of the network formed at the deeper areas of the scaffold was lower than the network formed at the surface. These results

further support the idea that cell behaviour at the deeper areas of the construct should be clearly reported in any *in vitro* pre-vascularisation studies. All Gel-NOR groups show increasing junctions density and total vessel length over time at the deeper areas of the scaffold (Figure 5.6B), which suggests that these micro-capillary networks are still being developed after two weeks of culture. In a similar way to the surface network, the network at the deeper areas of Gel-NOR discs crosslinked using 0.2/2 mM Ru/SPS hydrogels showed significantly higher junctions density and average vessel length as compared to groups crosslinked using higher Ru/SPS concentration. Taken together, these results reinforce the idea that Gel-NOR crosslinked using 0.2/2 mM Ru/SPS is a better candidate for the biofabrication of large tissue constructs with controllable channel networks.

5.3.5. 3D Biofabrication of Large Engineered Constructs with Controllable Design Parameters Using Gel-NOR Hydrogels

Pre-vascularisation techniques are highly promising due to their ability to reproduce the small diameter and high density of the capillary networks in native tissues and organs. However, the majority of studies on pre-vascularisation focus on small tissues (10,14–17). Translation to larger-sized samples could affect oxygen diffusion and the invasion of host vessels after implantation regardless of pre-vascularisation, as the invasion of vessels starts at the external areas of the constructs and progresses towards the centre (14). In this section, the Gel-NOR hydrogels studied in previous sections are biofabricated into larger constructs with a controllable pore and fiber diameter. An important factor to take into account in biofabrication is the shape fidelity of the constructs, especially when aiming to generate personalised constructs with tailored size and architecture. Due to their higher degree of vascularisation and homogeneous contraction, Gel-NOR 0.2/2 mM Ru/SPS have shown to be the group with the most potential for 3D biofabrication of large constructs with an endothelialised porous network and pre-vascularised micro-capillaries. It has been observed that contraction of the samples was directly related to micro-capillary formation in Gel-NOR hydrogels (Section 5.3.4). Therefore, it was hypothesized that Gel-NOR biofabricated constructs would undergo a certain degree of contraction. This could result in lack of shape fidelity of the fabricated porous network, reducing the diffusion of nutrients and oxygen to the core of the sample. To study how contraction affects the shape fidelity of the porous network, large samples were fabricated by 3D printing a sacrificial Pluronics 127 scaffold with controlled strand size and strand spacing, resulting in Gel-NOR constructs with different

pore and fiber diameters (Figure 5.7B). The pore diameter of Gel-NOR samples crosslinked using 0.2/2 or 0.5/5 mM Ru/SPS was tracked during a 14 day culture period (Figure 5.7C-D). Results showed that samples crosslinked using 0.5/5 mM Ru/SPS didn't undergo significant changes in pore diameter. However samples crosslinked using 0.2/2 mM Ru/SPS showed an average decrease of 40% in pore diameter. Interestingly, changes in the initial pore or fiber diameter didn't have significant effects on the average relative loss of pore diameter. These results suggest that the average final pore diameter can be predicted from the initial pore diameter, enabling targeted design regardless of the contraction of the sample. Therefore, it is possible to generate a controllable porous network that remains open during the whole culture period using Gel-NOR 0.2/2 mM Ru/SPS, enabling enhanced oxygen and nutrient diffusion. Importantly, the pores were maintained even though our culture setup did not include media perfusion throughout the network, which generates transmural pressure and helps maintain the morphology of microvessels *in vivo* (42) and *in vitro* (44).

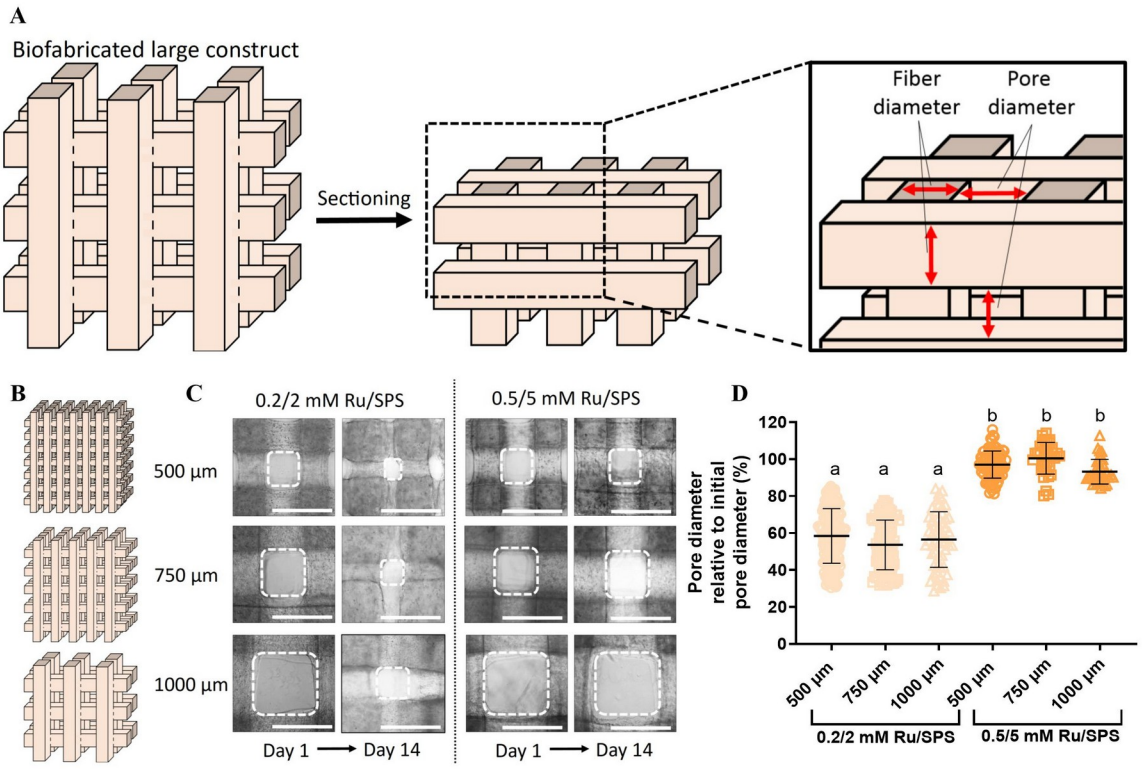

Figure 5.7. Shape fidelity of 3D biofabricated large constructs with controllable design parameters. *Constructs were biofabricated by 3D printing Pluronics as a sacrificial material and casting Gel-NOR 0.2/2 or 0.5/5 mM Ru/SPS, resulting in samples with controlled pore and fiber diameter (500, 750 or 1000 µm). Pore diameter was always designed to be equal to fiber diameter. (A) Schematic view of a biofabricated construct. (B) Design of the Gel-NOR constructs with controlled pore and fiber diameter. (C) Top view of the pore sizes on day 1 and 14 of the culture period showing the pore contraction. (D) Quantification of pore diameter on day 14 relative to day 1, each dot showing an individual diameter measurement. Scale bars: 1000 µm. a, b: Groups of statistical significance: samples in each group are not significantly different to each other ($p>0.05$) and are significantly different to all samples from other groups ($p<0.05$). Experiments were repeated 3 times with 3 technical repeats each (N=3), and in figure D all individual diameter measurements were included in the analysis to account for variation within the samples.*

5.3.6. Effects of Pore and Fiber Diameter on Endothelial Cell Morphology at the Deeper Areas of 3D Biofabricated Constructs

Aside from evaluating the shape fidelity of the constructs, it is important to evaluate cell behaviour both at the surface and the deeper areas of the constructs. An important advantage of biofabricating large constructs with controllable architectures is that it allows us to study the effects of design parameters on the behaviour of cells. To evaluate the endothelial cell morphology and behaviour in the 3D biofabricated constructs, a CD31 immunostaining was performed after sectioning of the samples and the cross-section of the fibers was imaged (Figure 5.8B-D). The general network development stage was a partially interconnected network regardless of the fiber diameter, in a similar way to the deeper areas of Gel-NOR discs. Quantification of the endothelial cell network revealed that groups with 750 and 1000 μm pore and fiber diameter had higher junctions density and average vessel length as compared to samples with 500 μm pore and fiber diameter. A potential explanation of these results is the generation of a hypoxic zone at the deeper areas of the material, which is known to stimulate angiogenesis in tissues through the activation of HIF-1 (45,46) and has been shown to promote differentiation of stem cells to the endothelial lineage (47) as well as helping the vascularisation of tissue engineered constructs (48). The general consensus for oxygen diffusion in tissue engineered constructs is that a hypoxic zone is generated at a depth of 100-200 μm (49–51). Therefore, it would be expected that the area of hypoxia in samples of 500 μm fiber diameter would be significantly smaller as compared to groups with higher fiber diameter, therefore generating lower levels of hypoxic stimulation. Interestingly, endothelial cells seemed to have covered the surface of the material in all designs.

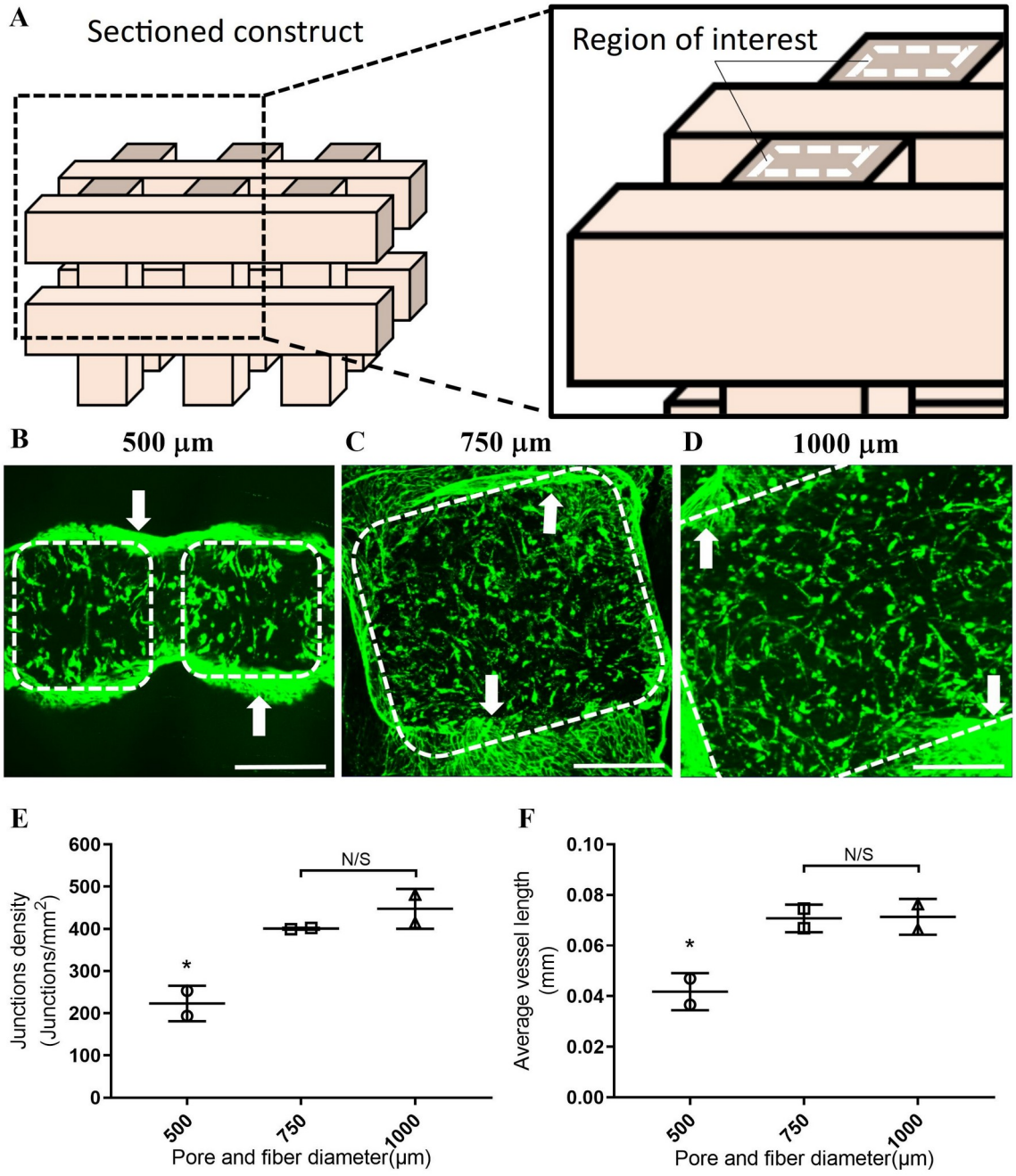

Figure 5.8. Effects of pore and fiber diameter on endothelial cell morphology at the deep areas of 3D biofabricated constructs. *(A) Schematic view of the sectioning and regions of interest for analysis of the deep areas. (B-D) CD31 immunostaining of HUVEC/ MSCs co-cultures at the deep areas of Gel-NOR constructs crosslinked using 0.2/2 mM Ru/SPS biofabricated with (B) 500, (C) 750 or (D) 1000 µm pore and fiber diameter (Day 14). Quantification of (A) junctions density and (B) average vessel length. *: significant differences ($p<0.01$) as compared to all other groups. Dashed lines indicate regions of interest for analysis. Arrows indicate endothelialisation in the internal surfaces of the pores. Scale bars: 250 µm. Experiments were repeated 2 times with at least 3 technical repeats each (N=2).*

5.3.7. Effects of Pore and Fiber Diameter on the Degree of Endothelialisation of the Porous Network

To further study the endothelialisation of the interconnected pores in biofabricated Gel-NOR samples, the surfaces of the internal pores were imaged either from perpendicular cross-section of the pore (Figure 5.9) or from a longitudinal cross-section of the pore (Figure 5.10). CD31 and α-SMA immunostaining on day 14 revealed that the internal surface of the pores was fully covered by a layer of endothelial cells and a layer of MSCs expressing α-SMA (Figure 5.B and 5.10B). These cells seemed to have migrated from the deeper areas to the surface of the material during the culture period, forming a double layer similar to the tunica intima and the tunica media of arterioles and venules (Figure 5.9A). Micro-capillary-like structures connected to the endothelialised surface were also observed, along with individual elongated endothelial cells that could be migrating to the internal surface of the pores (Figure 5.9A). During this process it would have been possible for the surface-to-volume ratio, which varied depending on pore and fiber diameter, to have resulted in changes in the degree of endothelialisation. However, the internal surface of the pores was uniformly covered by both HUVECs and MSCs independently of the pore and fiber diameter of the construct (Figure 5.9B). Interestingly, this endothelialisation was not observed in the discs of the same formulation, where endothelial cells at the surface were assembling into a micro-capillary network (Figure 5.4). A possible explanation to this phenomenon is the 3D architecture of the samples. The presence of fabricated pores allows MSCs to naturally assemble into a tube along the surface of the pores, mimicking the tunica intermedia of native vessels and potentially promoting contraction and matrix remodelling. Increased contraction would increase the mechanical properties at the surface of the samples, promoting the formation of an endothelial cell monolayer instead of a micro-capillary network as shown in Gel-NOR discs (Figure 5.4).

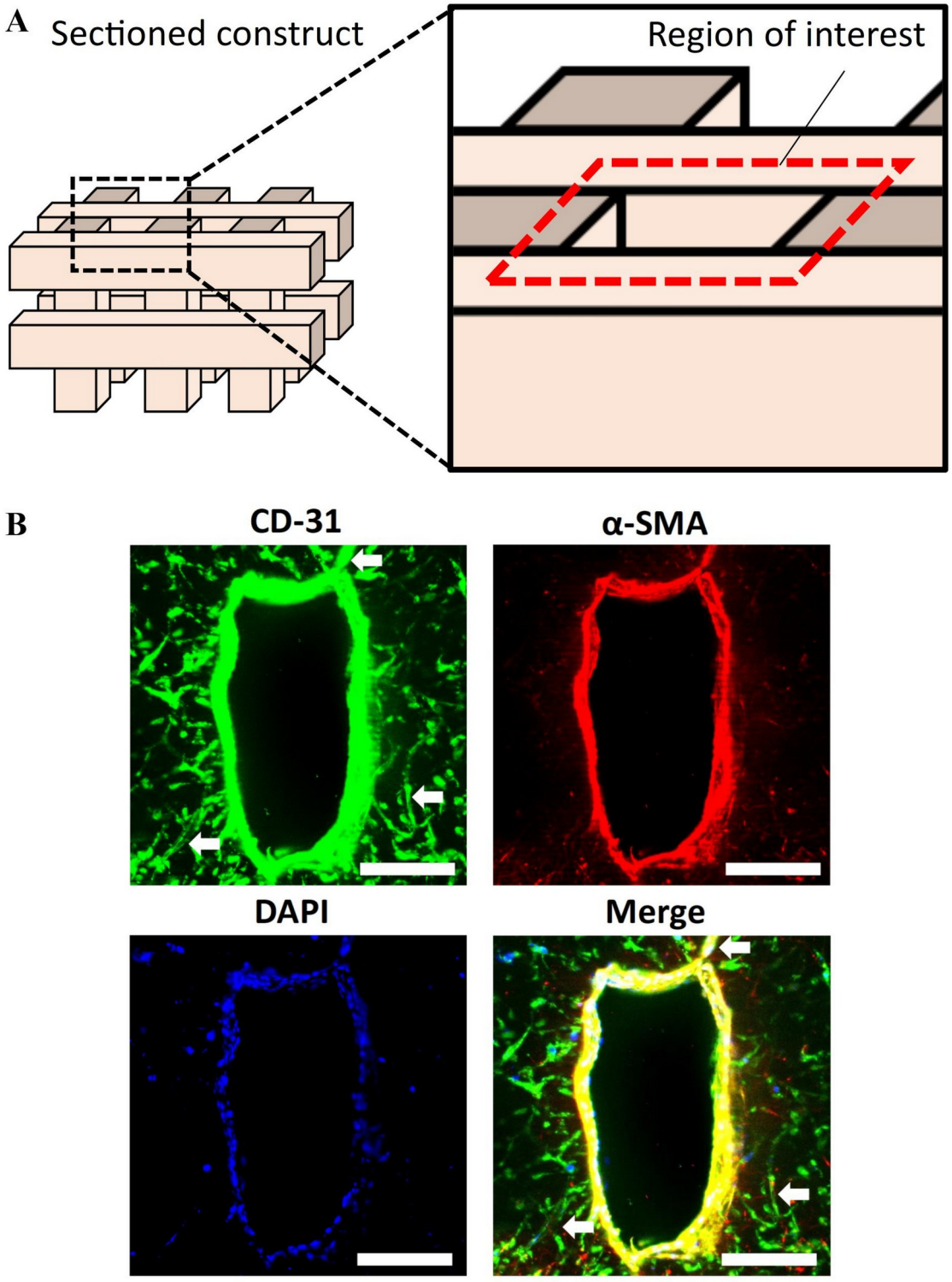

Figure 5.9. Formation of endothelialised pores within biofabricated Gel-NOR constructs (Perpendicular cross-section). *(A) Schematic view of the samples and regions of interest imaged. (B) CD31 and α-SMA immunostaining of HUVEC/MSCs co-cultures at the internal surfaces and deeper areas of Gel-NOR constructs crosslinked using 0.2/2 mM Ru/SPS biofabricated with 750 µm pore and fiber diameter (Day 14). Scale bars: 200 µm. Arrows indicate endothelial cells connecting to the endothelialised surface of the pores. Experiments were repeated 2 times with at least 3 technical repeats each (N=2).*

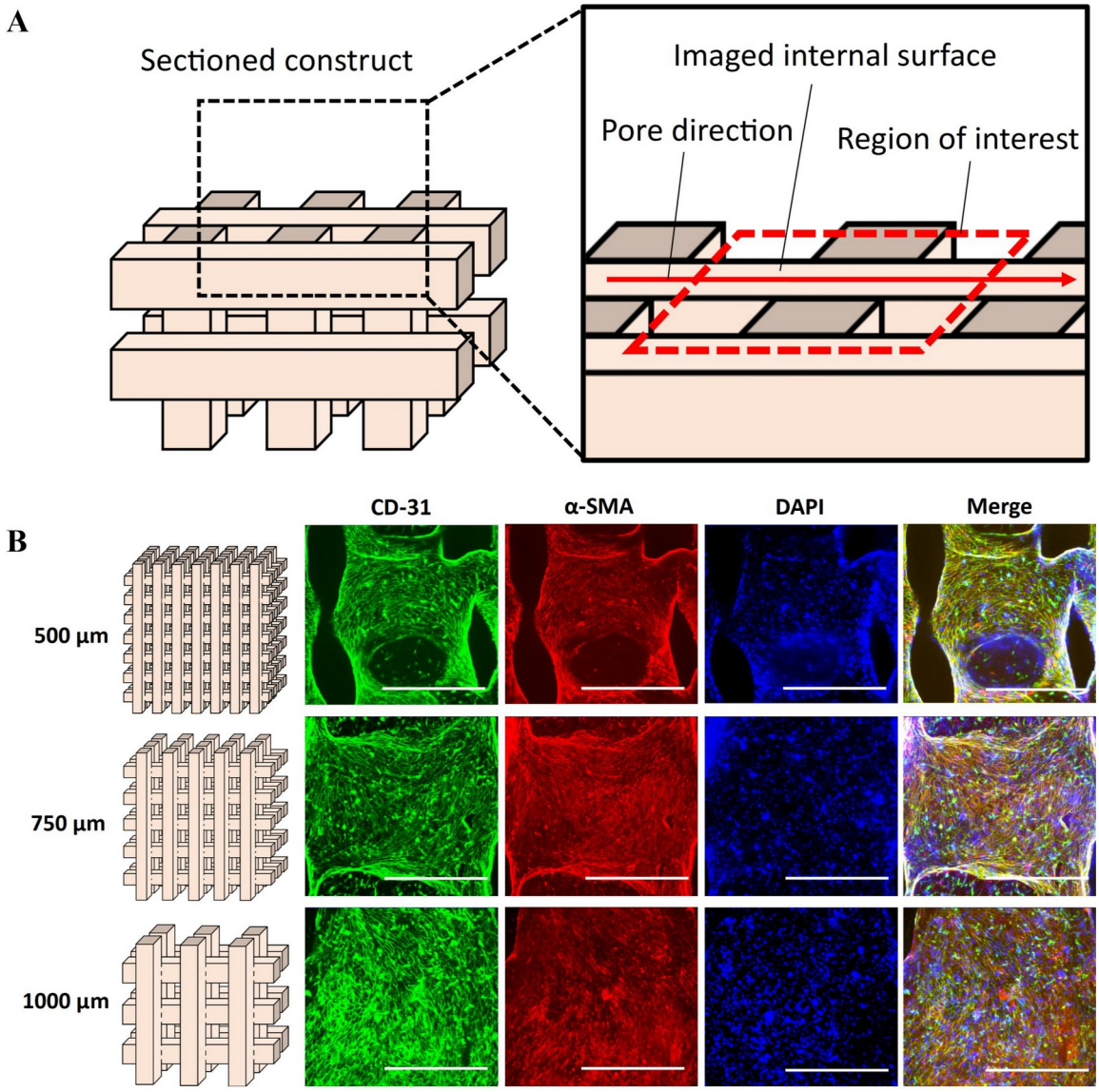

Figure 5.10. Formation of endothelialised pores within biofabricated Gel-NOR constructs (Longitudinal cross-section). *(A) Schematic view of the imaged internal surfaces in a sectioned 3D biofabricated construct. (B) CD31 and α-SMA immunostaining of HUVEC/MSCs co-cultures at the internal surfaces and deeper areas of Gel-NOR constructs crosslinked using 0.2/2 mM Ru/SPS biofabricated with 500, 750 or 1000 µm pore and fiber diameter (Day 14). Scale bars: (A) 200 µm and (B) 500 µm. Experiments were repeated 2 times with at least 3 technical repeats each (N=2).*

Taken together, these results suggest that 3D design is an important aspect to consider during the biofabrication of engineered vascularised constructs, affecting the behaviour of endothelial cells both at the surface and the deeper areas of the constructs. Firstly, the

fabrication of a controllable interconnected porous network had significant effects on the endothelial cells at the surface of the constructs, resulting in endothelialisation of the pores as opposed to the formation of a micro-capillary network that was observed in discs. Secondly, differences in the fiber diameter of the construct resulted in significant differences in network parameters of endothelial cells at the deeper areas of the construct (10-20 μm below the surface or deeper), where higher fiber diameter promoted elongation and interconnection of endothelial cells. Another important aspect of this study is that the endothelialisation of the constructs happened through migration of the encapsulated cells without the need of perfusion of endothelial cells. To our knowledge, this is the first report of this phenomenon, which could help to avoid unnecessary additional cell seeding procedures during the generation of vascularised tissue engineered constructs.

5.4. Conclusions

The formation of large vascularised tissues analogues that recapitulate the different levels of vascularisation in native tissues and organs remains one of the major challenges in tissue engineering, and efforts in this direction have taken two major routes: 3D fabrication-based top-down approaches and bottom-up approaches based on endothelial cell self-assembly. One of the major barriers for these two approaches to be combined is in the incompatibility of present material platforms to be adaptable to both 3D fabrication of channels and to promote endothelial cell self-assembly into micro-capillary networks.

In the present study, the combination of a top-down and a bottom-up approach for the biofabrication of vascularised constructs with different levels of vascularisation using a single material platform is reported. Combining thiol-ene chemistry with the Ru/SPS visible light initiated photoinitiator system enabled fine tailoring of the hydrogel mechanical properties and the obtention of constructs with micro-capillaries and homogeneous contraction. It was found that contraction of the material is tightly related to the formation of micro-capillary structures by encapsulated endothelial cells. Despite the contraction, it was possible to biofabricate large constructs with an interconnected porous network of predictable pore diameter while allowing the elongation and migration of endothelial cells at the deeper areas of the material. To our knowledge, this is the first report of the combination of both approaches without the need of support materials and perfusion of culture media and endothelial cells. This platform was then used to study the effects of 3D architecture on the behaviour of endothelial cells both at the surface of the pores and the deeper areas of the constructs. Our data suggests that the fabrication of interconnected pores stimulates endothelial cells to migrate to the surface of the pores and endothelialise them rather than forming a micro-capillary network. This resulted in full endothelialisation of the pores regardless of the pore and fiber diameters of the construct. It was also observed that increasing the fiber diameter of the constructs can affect the behaviour of endothelial cells at the deeper areas of the material, potentially by generating hypoxic conditions that stimulate micro-capillary formation. The role of hypoxia during the generation of large, pre-vascularised tissues is therefore an aspect that should be further studied as part of the efforts to translate these technologies to studies in larger mammals.

This study represents a valuable proof of concept of the combination of two major vascularisation strategies. Furthermore, we have used this platform to provide relevant

information on how 3D design can affect endothelial cell behaviour in 3D biofabricated vascularised constructs, which will be relevant for future optimisation and clinical translation of large vascularised constructs.

5.5. Supplementary Information

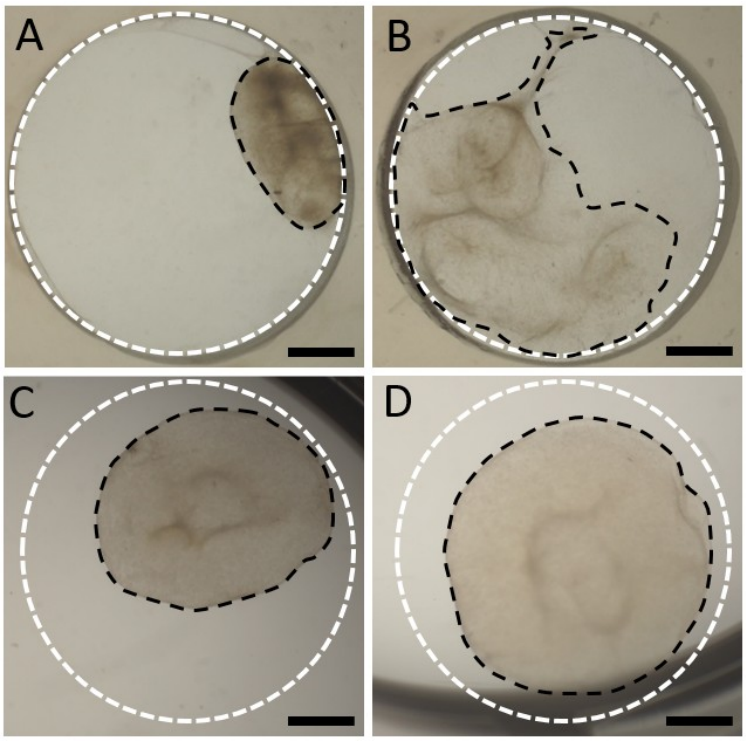

Supplementary Figure S5.1. Contraction of Gel-NOR and Matrigel hydrogels after 14 days of cultures with co-encapsulated HUVECs and MSCs. *Representative images of Matrigel (A-B), Gel-NOR 0.2/2 (C) and 0.5/5 mM Ru/SPS (D) sample size after 14 days of culture showing the variability in sample contraction. White dashed lines indicate the initial shape of the constructs. Black dashed lines indicate the final shape of the construct. Scale bars: 1 mm.*

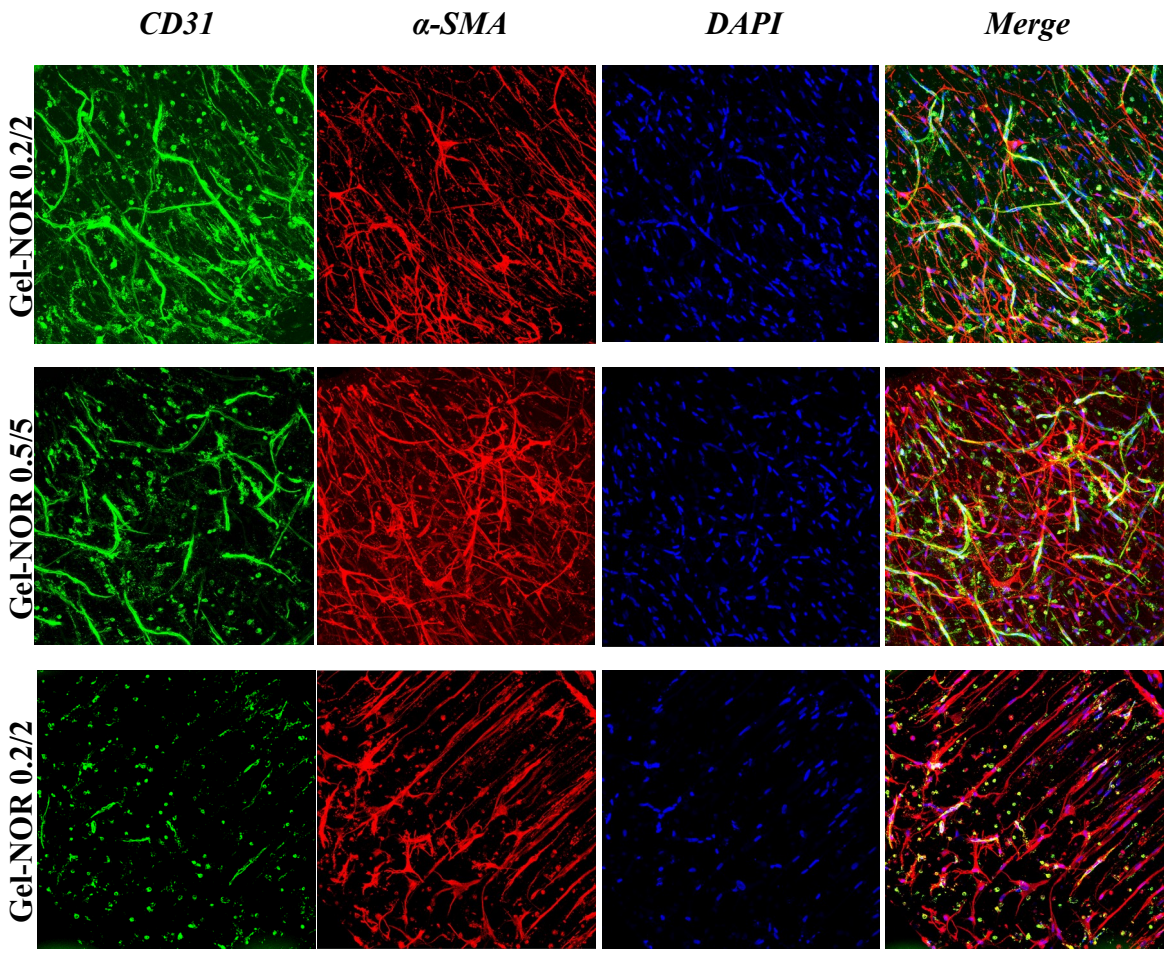

Supplementary Figure S5.2. Micro-capillary formation in Gel-NOR hydrogels with co-encapsulated HUVECs and MSCs (cross-section). *Representative images of CD31 and α-Smooth muscle actin immunostaining of co-encapsulated HUVECs and MSCs at the deeper areas of Gel-NOR 5wt%, DTT 1:4 NOR:SH discs crosslinked using 0.2/2 (Top row), 0.5/5 (Middle row) or 1/10 (bottom row) mM Ru/SPS. Scale bar: 100 µm.*

5.6. References

1. Song H-HG, Rumma RT, Ozaki CK, Edelman ER, Chen CS. Vascular Tissue Engineering: Progress, Challenges, and Clinical Promise. Cell Stem Cell [Internet]. 2018 Mar 1;22(3):340–54. Available from: https://www.ncbi.nlm.nih.gov/pubmed/29499152

2. Xu J, Shi G-P. Vascular wall extracellular matrix proteins and vascular diseases. Biochim Biophys Acta [Internet]. 2014/07/18. 2014 Nov;1842(11):2106–19. Available from: https://www.ncbi.nlm.nih.gov/pubmed/25045854

3. Justin AW, Brooks RA, Markaki AE. Multi-casting approach for vascular networks in cellularized hydrogels. J R Soc Interface. 2016;13(125).

4. Kolesky DB, Homan KA, Skylar-Scott MA, Lewis JA. Three-dimensional bioprinting of thick vascularized tissues. Proc Natl Acad Sci [Internet]. 2016 Mar 22;113(12):3179 LP – 3184. Available from: http://www.pnas.org/content/113/12/3179.abstract

5. Redd MA, Zeinstra N, Qin W, Wei W, Martinson A, Wang Y, et al. Patterned human microvascular grafts enable rapid vascularization and increase perfusion in infarcted rat hearts. Nat Commun [Internet]. 2019;10(1). Available from: http://dx.doi.org/10.1038/s41467-019-08388-7

6. Bertassoni LE, Cecconi M, Manoharan V, Nikkhah M, Hjortnaes J, Cristino AL, et al. Hydrogel bioprinted microchannel networks for vascularization of tissue engineering constructs. Lab Chip [Internet]. 2014;14(13):2202–11. Available from: http://dx.doi.org/10.1039/C4LC00030G

7. Miller JS, Stevens KR, Yang MT, Baker BM, Nguyen D-HT, Cohen DM, et al. Rapid casting of patterned vascular networks for perfusable engineered three-dimensional tissues. Nat Mater [Internet]. 2012;11(9):768–74. Available from: https://doi.org/10.1038/nmat3357

8. Lesman A, Koffler J, Atlas R, Blinder YJ, Kam Z, Levenberg S. Engineering vessel-like networks within multicellular fibrin-based constructs. Biomaterials [Internet]. 2011;32(31):7856–69. Available from: http://www.sciencedirect.com/science/article/pii/S0142961211007745

9. Wimmer RA, Leopoldi A, Aichinger M, Wick N, Hantusch B, Novatchkova M, et al.

Human blood vessel organoids as a model of diabetic vasculopathy. Nature [Internet]. 2019;565(7740):505–10. Available from: http://dx.doi.org/10.1038/s41586-018-0858-8

10. Landau S, Guo S, Levenberg S. Localization of Engineered Vasculature within 3D Tissue Constructs. Front Bioeng Biotechnol [Internet]. 2018;6:2. Available from: https://www.ncbi.nlm.nih.gov/pubmed/29404324

11. Chen X, Aledia AS, Ghajar CM, Griffith CK, Putnam AJ, Hughes CCW, et al. Prevascularization of a Fibrin-Based Tissue Construct Accelerates the Formation of Functional Anastomosis with Host Vasculature. Tissue Eng Part A [Internet]. 2008 Oct 24;15(6):1363–71. Available from: https://doi.org/10.1089/ten.tea.2008.0314

12. Chen X, Aledia AS, Popson SA, Him L, Hughes CCW, George SC. Rapid Anastomosis of Endothelial Progenitor Cell–Derived Vessels with Host Vasculature Is Promoted by a High Density of Cotransplanted Fibroblasts. Tissue Eng Part A [Internet]. 2009 Sep 8;16(2):585–94. Available from: https://doi.org/10.1089/ten.tea.2009.0491

13. White SM, Pittman CR, Hingorani R, Arora R, Esipova T V, Vinogradov SA, et al. Implanted cell-dense prevascularized tissues develop functional vasculature that supports reoxygenation after thrombosis. Tissue Eng Part A [Internet]. 2014;20(17–18):2316–28. Available from: https://www.ncbi.nlm.nih.gov/pubmed/24593148

14. Ben-Shaul S, Landau S, Merdler U, Levenberg S. Mature vessel networks in engineered tissue promote graft–host anastomosis and prevent graft thrombosis. Proc Natl Acad Sci [Internet]. 2019 Feb 19;116(8):2955 LP – 2960. Available from: http://www.pnas.org/content/116/8/2955.abstract

15. Klotz BJ, Gawlitta D, Rosenberg AJWP, Malda J, Melchels FPW. Gelatin-Methacryloyl Hydrogels: Towards Biofabrication-Based Tissue Repair. Trends Biotechnol [Internet]. 2016;34(5):394–407. Available from: http://www.sciencedirect.com/science/article/pii/S0167779916000159

16. Quade M, Knaack S, Weber D, Konig U, Paul B, Simon P, et al. Heparin modification of a biomimetic bone matrix modulates osteogenic and angiogenic cell response in vitro. Eur Cell Mater [Internet]. 2017;33:105–20. Available from: https://www.ncbi.nlm.nih.gov/pubmed/28181209

17. Peters EB, Christoforou N, Leong KW, Truskey GA, West JL. Poly(ethylene glycol) Hydrogel Scaffolds Containing Cell-Adhesive and Protease-Sensitive Peptides Support Microvessel Formation by Endothelial Progenitor Cells. Cell Mol Bioeng [Internet]. 2015/10/20. 2016 Mar 1;9(1):38–54. Available from: https://www.ncbi.nlm.nih.gov/pubmed/27042236

18. Klotz BJ, Lim KS, Chang YX, Soliman BG, Pennings I, Melchels FPW, et al. Engineering of a complex bone tissue model with endothelialised channels and capillary-like networks. Eur Cell Mater [Internet]. 2018;35:335–48. Available from: https://www.ncbi.nlm.nih.gov/pubmed/29873804

19. Jalali S, Tafazzoli-Shadpour M, Haghighipour N, Omidvar R, Safshekan F. Regulation of Endothelial Cell Adherence and Elastic Modulus by Substrate Stiffness. Cell Commun Adhes [Internet]. 2015 Nov 2;22(2–6):79–89. Available from: https://doi.org/10.1080/15419061.2016.1265949

20. Blinder YJ, Freiman A, Raindel N, Mooney DJ, Levenberg S. Vasculogenic dynamics in 3D engineered tissue constructs. Sci Rep [Internet]. 2015;5:17840. Available from: https://www.ncbi.nlm.nih.gov/pubmed/26648270

21. Stratesteffen H, Köpf M, Kreimendahl F, Blaeser A, Jockenhoevel S, Fischer H. GelMA-collagen blends enable drop-on-demand 3D printablility and promote angiogenesis. Biofabrication [Internet]. 2017;9(4):45002. Available from: http://dx.doi.org/10.1088/1758-5090/aa857c

22. Chen YC, Lin RZ, Qi H, Yang Y, Bae H, Melero-Martin JM, et al. Functional Human Vascular Network Generated in Photocrosslinkable Gelatin Methacrylate Hydrogels. Adv Funct Mater [Internet]. 2012;22(10):2027–39. Available from: https://www.ncbi.nlm.nih.gov/pubmed/22907987

23. Morgan JT, Shirazi J, Comber EM, Eschenburg C, Gleghorn JP. Fabrication of centimeter-scale and geometrically arbitrary vascular networks using in vitro self-assembly. Biomaterials [Internet]. 2019;189(July 2018):37–47. Available from: https://doi.org/10.1016/j.biomaterials.2018.10.021

24. Edgar LT, Underwood CJ, Guilkey JE, Hoying JB, Weiss JA. Extracellular Matrix Density Regulates the Rate of Neovessel Growth and Branching in Sprouting Angiogenesis. PLoS One [Internet]. 2014 Jan 22;9(1):e85178. Available from: https://

doi.org/10.1371/journal.pone.0085178

25. Mammoto A, Connor KM, Mammoto T, Yung CW, Huh D, Aderman CM, et al. A mechanosensitive transcriptional mechanism that controls angiogenesis. Nature [Internet]. 2009;457(7233):1103–8. Available from: https://www.ncbi.nlm.nih.gov/pubmed/19242469

26. Juliar BA, Keating MT, Kong YP, Botvinick EL, Putnam AJ. Sprouting angiogenesis induces significant mechanical heterogeneities and ECM stiffening across length scales in fibrin hydrogels. Biomaterials [Internet]. 2018;162:99–108. Available from: https://www.ncbi.nlm.nih.gov/pubmed/29438884

27. Loessner D, Meinert C, Kaemmerer E, Martine LC, Yue K, Levett PA, et al. Functionalization, preparation and use of cell-laden gelatin methacryloyl-based hydrogels as modular tissue culture platforms. Nat Protoc [Internet]. 2016;11(4):727–46. Available from: https://www.ncbi.nlm.nih.gov/pubmed/26985572

28. Calderon GA, Thai P, Hsu CW, Grigoryan B, Gibson SM, Dickinson ME, et al. Tubulogenesis of co-cultured human iPS-derived endothelial cells and human mesenchymal stem cells in fibrin and gelatin methacrylate gels. Biomater Sci. 2017;5(8):1652–60.

29. Bertlein S, Brown G, Lim KS, Jungst T, Boeck T, Blunk T, et al. Thiol–Ene Clickable Gelatin: A Platform Bioink for Multiple 3D Biofabrication Technologies. Adv Mater [Internet]. 2017;29(44):1703404. Available from: https://onlinelibrary.wiley.com/doi/abs/10.1002/adma.201703404

30. Greene T, Lin CC. Modular Cross-Linking of Gelatin-Based Thiol-Norbornene Hydrogels for in Vitro 3D Culture of Hepatocellular Carcinoma Cells. ACS Biomater Sci Eng. 2015;1(12):1314–23.

31. Mũnoz Z, Shih H, Lin C-C. Gelatin hydrogels formed by orthogonal thiol–norbornene photochemistry for cell encapsulation. Biomater Sci. 2014;2(8):1063–72.

32. Greene T, Lin T-Y, Andrisani OM, Lin C-C. Comparative study of visible light polymerized gelatin hydrogels for 3D culture of hepatic progenitor cells. J Appl Polym Sci. 2017;134(11).

33. Jyothi NVN, Prasanna PM, Sakarkar SN, Prabha KS, Ramaiah PS, Srawan GY.

Microencapsulation techniques, factors influencing encapsulation efficiency. J Microencapsul [Internet]. 2010 May 1;27(3):187–97. Available from: https://doi.org/10.3109/02652040903131301

34. Lim KS, Schon BS, Mekhileri N V, Brown GCJ, Chia CM, Prabakar S, et al. New Visible-Light Photoinitiating System for Improved Print Fidelity in Gelatin-Based Bioinks. ACS Biomater Sci Eng [Internet]. 2016;2(10):1752–62. Available from: https://doi.org/10.1021/acsbiomaterials.6b00149

35. Lim KS, Alves MH, Poole-Warren LA, Martens PJ. Covalent incorporation of non-chemically modified gelatin into degradable PVA-tyramine hydrogels. Biomaterials [Internet]. 2013;34(29):7097–105. Available from: http://dx.doi.org/10.1016/j.biomaterials.2013.06.005

36. Lim KS, Ramaswamy Y, Roberts JJ, Alves M-H, Poole-Warren LA, Martens PJ. Promoting Cell Survival and Proliferation in Degradable Poly(vinyl alcohol)–Tyramine Hydrogels. Macromol Biosci [Internet]. 2015;15(10):1423–32. Available from: https://onlinelibrary.wiley.com/doi/abs/10.1002/mabi.201500121

37. Abumaree MH, Hakami M, Abomaray FM, Alshabibi MA, Kalionis B, Al Jumah MA, et al. Human chorionic villous mesenchymal stem/stromal cells modify the effects of oxidative stress on endothelial cell functions. Placenta [Internet]. 2017;59:74–86. Available from: http://www.sciencedirect.com/science/article/pii/S0143400417302576

38. Barati D, Shariati SRP, Moeinzadeh S, Melero-Martin JM, Khademhosseini A, Jabbari E. Spatiotemporal release of BMP-2 and VEGF enhances osteogenic and vasculogenic differentiation of human mesenchymal stem cells and endothelial colony-forming cells co-encapsulated in a patterned hydrogel. J Control Release [Internet]. 2016;223:126–36. Available from: http://www.sciencedirect.com/science/article/pii/S0168365915302807

39. Hughes CS, Postovit LM, Lajoie GA. Matrigel: A complex protein mixture required for optimal growth of cell culture. Proteomics [Internet]. 2010 May 1;10(9):1886–90. Available from: https://doi.org/10.1002/pmic.200900758

40. Lee VK, Lanzi AM, Ngo H, Yoo SS, Vincent PA, Dai G. Generation of multi-scale vascular network system within 3D hydrogel using 3D bio-printing technology. Cell Mol Bioeng. 2014;7(3):460–72.

41. Franco CA, Jones ML, Bernabeu MO, Geudens I, Mathivet T, Rosa A, et al. Dynamic Endothelial Cell Rearrangements Drive Developmental Vessel Regression. PLOS Biol [Internet]. 2015 Apr 17;13(4):e1002125. Available from: https://doi.org/10.1371/journal.pbio.1002125

42. Watson EC, Koenig MN, Grant ZL, Whitehead L, Trounson E, Dewson G, et al. Apoptosis regulates endothelial cell number and capillary vessel diameter but not vessel regression during retinal angiogenesis. Development [Internet]. 2016 Aug 15;143(16):2973 LP – 2982. Available from: http://dev.biologists.org/content/143/16/2973.abstract

43. Slater K, Partridge J, Nandivada H. Tuning the Elastic Moduli of Corning® Matrigel® and Collagen I 3D Matrices by Varying the Protein Concentration (Application report No. CLS-AC-AN-449). Retrieved from Corning website. 2017.

44. Price GM, Wong KHK, Truslow JG, Leung AD, Acharya C, Tien J. Effect of mechanical factors on the function of engineered human blood microvessels in microfluidic collagen gels. Biomaterials [Internet]. 2010;31(24):6182–9. Available from: http://www.sciencedirect.com/science/article/pii/S0142961210005570

45. Pugh CW, Ratcliffe PJ. Regulation of angiogenesis by hypoxia: role of the HIF system. Nat Med [Internet]. 2003;9(6):677–84. Available from: https://doi.org/10.1038/nm0603-677

46. Semenza GL. Hypoxia-Inducible Factors in Physiology and Medicine. Cell [Internet]. 2012;148(3):399–408. Available from: http://www.sciencedirect.com/science/article/pii/S0092867412000876

47. Prado-Lopez S, Conesa A, Armiñán A, Martínez-Losa M, Escobedo-Lucea C, Gandia C, et al. Hypoxia Promotes Efficient Differentiation of Human Embryonic Stem Cells to Functional Endothelium. Stem Cells [Internet]. 2010 Mar 1;28(3):407–18. Available from: https://doi.org/10.1002/stem.295

48. Esser TU, Roshanbinfar K, Engel FB. Promoting vascularization for tissue engineering constructs: current strategies focusing on HIF-regulating scaffolds. Expert Opin Biol Ther [Internet]. 2019 Feb 1;19(2):105–18. Available from: https://doi.org/10.1080/14712598.2019.1561855

49. Shimizu T, Sekine H, Yang J, Isoi Y, Yamato M, Kikuchi A, et al. Polysurgery of cell sheet grafts overcomes diffusion limits to produce thick, vascularized myocardial tissues. FASEB J [Internet]. 2006 Jan 26;20(6):708–10. Available from: https://doi.org/10.1096/fj.05-4715fje

50. Radisic M, Deen W, Langer R, Vunjak-Novakovic G. Mathematical model of oxygen distribution in engineered cardiac tissue with parallel channel array perfused with culture medium containing oxygen carriers. Am J Physiol Circ Physiol [Internet]. 2005 Mar 1;288(3):H1278–89. Available from: https://doi.org/10.1152/ajpheart.00787.2004

51. Liu J, Hilderink J, Groothuis TAM, Otto C, van Blitterswijk CA, de Boer J. Monitoring nutrient transport in tissue-engineered grafts. J Tissue Eng Regen Med [Internet]. 2015 Aug 1;9(8):952–60. Available from: https://doi.org/10.1002/term.1654

52. Klotz B J, Oosterhoff L A, Utomo L, Lim K S, Vallmajo-Martin Q, Clevers H, et al. A versatile biosynthetic hydrogel platform for engineering of tissue analogues. Adv Healthc Mater [Internet]. 2019;8(19):e1900979. Available from: https://doi.org/10.1002/term.1654

Chapter 6. Bioassembly of Gel-NOR and PVA-Tyr Modules for Combinatory Approaches in Tissue Vascularisation

6.1. Introduction

Combining growth factor delivery with cell therapy is a common strategy that has been applied in different contexts such as heart regeneration (1–3), bone regeneration (4,5) and tissue vascularisation (6), resulting in synergistic positive effects. The combination of these two strategies increases the complexity in the design of delivery vehicles, as the conditions for improved growth factor delivery (such as controlled release time, release profile and concentration) and improved cell delivery (such as presence of bioactive cues or controlled stiffness) need to be met at the same time. An important aspect to consider when generating these complex scaffolds is the fabrication technique. Biofabrication allows the combination of different materials that meet these conditions while providing freedom in the 3D architecture and in the arrangement of materials, cells and growth factors within the scaffold. Furthermore, it allows the inclusion of support materials that provide the necessary stiffness for the implantation into load-bearing tissues such as bone (7,8) and the generation of large, controllable pore structures that improve vascularisation and integration of the implant (9,10), making it a very flexible strategy for combined approaches in tissue engineering.

Very few studies that use biofabrication have been dedicated to the coordinated delivery of growth factors and cells to promote tissue vascularisation (6,19). One of the few examples of this is the study by Jang et al., which aimed to improve cardiac vascularisation by co-printing two hydrogel bioinks containing either cardiac progenitor cells (CPCs) or MSCs combined with VEGF. Using an *in vivo* mouse model, they demonstrated that co-printing both inks resulted in improved tissue vascularisation as compared to printing CPCs or MSCs + VEGF (19). While this study provides evidence of how adequately combining cell types and growth factors through biofabrication can help tissue vascularisation, the research did not cover the release profile of VEGF and did not include control bioinks that only delivered VEGF. The

work by Poldervaart et al. did study these aspects in more depth by generating gelatin microspheres with adsorbed VEGF that resulted in extended release up to 14 days. These microspheres were incorporated into a Matrigel/alginate bioink with encapsulated endothelial progenitor cells (EPCs), which was bioprinted to form a scaffold. After subcutaneous implantation into mice, the study demonstrated that slow release of VEGF results in an increased number of functional vessels as compared to controls with a burst release pattern (6). While this study provided more details about the release of growth factors, the bioink did not include support cells and did not undergo *in vitro* maturation to achieve pre-vascularisation. Furthermore, the capabilities of biofabrication were not exploited by arranging different cell types or materials within the scaffold. The existing information in this field is very scarce and there are still significant gaps in knowledge: key questions such as what endothelial cells and support cells result in optimal vascularisation, or how the arrangement of cells within the scaffold can affect both the pre-vascularisation process and the implant-host vessel anastomosis, still need to be answered. The presence of growth factor gradients also needs to be further explored as a key factor that could promote both these processes. Therefore, the development of models that allow studying these aspects would be key for the advancement of the field, especially if they allow studying these aspects within large constructs.

Within biofabrication techniques, bioassembly provides high flexibility on how to organise bioactive elements in the scaffold (20). This technique is based on the automated deposition of previously fabricated cell-containing building blocks, such as microspheres or microtissues, within 3D scaffolds. Bioassembly provides high flexibility on the type of building blocks used, which can either be cells or growth factor-releasing materials. These building blocks can be arranged in a controlled manner within the construct (Figure 6.1A) and the assembly process allows scalable fabrication of large tissue constructs (Figure 6.1B). Therefore, it could prove to be a useful tool not only to generate large, vascularized tissues, but also to study the effects of 3D architecture and organisation of cells and growth factors within tissue engineered scaffolds. Another significant advantage of bioassembly over bioprinting is that the materials do not need to have the specific rheological properties required for 3D printing. Instead, they only need to be adaptable to the fabrication of building blocks through less restrictive techniques such as microfluidics or mould casting.

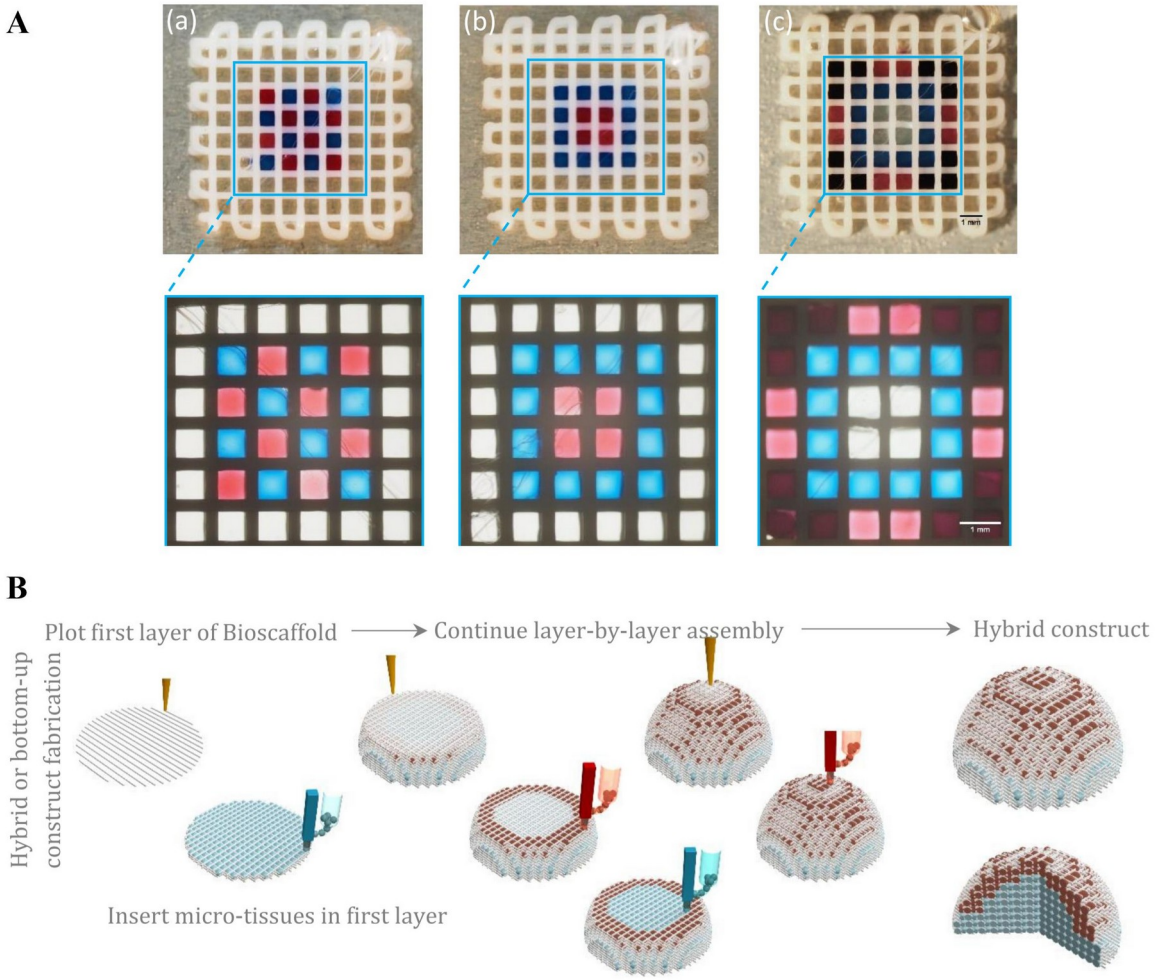

Figure 6.1. Bioassembly allows controlled arrangement of multiple bioactive modules and biofabrication of large constructs. *Blue and red microspheres represent bioactive modules such as growth factor-releasing materials or pre-vascularised constructs. (A) Demonstration of the flexibility of bioassembly on the spatial arrangement of multiple modules (B) Illustration of the hybrid bottom-up bioassembly approach that allows biofabrication of large tissue constructs. Adapted from* (21)

In this chapter, the necessary tools to fabricate engineered scaffolds that combine the PVA-Tyr GF delivery system and Gel-NOR co-cultures through bioassembly techniques were developed. The first aim of this chapter was to fabricate Gel-NOR microspheres including MSCs and/or endothelial cells and evaluate cell behaviour after the fabrication process. The second aim was to demonstrate the possible applications of this platform by performing a proof-of-concept study on how different distributions of endothelial cells and MSCs within assembled scaffolds can affect their resulting function and behaviour. The third aim was to fabricate PVA-Tyr microspheres with different degradation properties and study how this

fabrication technique affects the degradation of the material and the release of GFs. The last aim was to generate hybrid assembled constructs containing PVA-Tyr microspheres and Gel-NOR co-cultures, which could allow studying the effects of combining GF and cell delivery for vascularisation purposes.

6.2. Materials and Methods

6.2.1. Materials

Dithiothreitol (DTT), Tris(2,2′-bipyridyl)dichlororuthenium(II) hexahydrate (Ru), sodium persulfate (SPS), Phosphate buffered saline (PBS) and L-ascorbic acid-2-phosphate (ASAP) were purchased from Sigma-Aldrich. RhVEGF-165 was purchased from Gibco (PHC9394). bFGF was purchased from R&D Systems (P09038).

Human umbilical vein endothelial cells (HUVEC), vascular cell basal medium, endothelial cell growth kit-VEGF, trypsin for primary cells and trypsin neutralizing solution were purchased from ATCC. Human bone marrow-derived mesenchymal stem cells (MSCs) were purchased from RoosterBio. Alpha-MEM, Fetal bovine serum (FBS), Trypsin and Penicillin/ streptomycin were purchased from Gibco.

6.2.2. Methods

6.2.2.1. Cell Expansion

Human umbilical vein endothelial cells (HUVECs, obtained from ATCC) were cultured in Vascular Basal Media (ATCC) supplemented with Endothelial Cell Growth Kit-VEGF (ATCC) and Penicillin/Streptomycin (Referred to as endothelial growth media, EGM). Bone marrow-derived mesenchymal stem cells (MSCs, obtained from RoosterBio) were cultured in α-MEM (Gibco) supplemented with 10% foetal calf serum (Hyclone), 1% penicillin/streptomycin, 20 mM of ASAP and 5 ng/mL basic fibroblast growth factor (R&D Systems).

6.2.2.2. Hydrogel Fabrication

Dried PVA-Tyr was dissolved in PBS at 80 °C (5.9 wt%). GF and Ru/SPS stock solutions were prepared in PBS at 10x and 50x of their final concentration respectively. Upon complete dissolution, the polymer solution was cooled to room temperature (RT) and mixed with the GF, Ru and SPS stock solutions to a final PVA-Tyr concentration of 5wt%, 0.5/5 mM Ru/SPS and 500 ng/mL of GF. Dried Gel-NOR was dissolved in PBS at 37 °C and mixed with Ru, SPS and dithiothreitol (DTT) stock solutions to a final Gel-NOR concentration of 5wt% Gel-NOR, 1:4 NOR:SH ratio for DTT and 0.2/2 mM Ru/SPS. All samples were photo-crosslinked using visible light (OmniCure® S1500, Excelitas Technologies with a Rosco IR/ UV filter 400 – 450nm, 3min and 300 mW cm^{-2}).

6.2.2.3. Microsphere Generation

PVA-Tyr and Gel-NOR micro-spheres were prepared by employing a microfluidic oil-emulsion setup based on previous work (22). Briefly, PVA-7Tyr or Gel-NOR were mixed with their respective crosslinking agents and photoinitiators following the protocol for hydrogel fabrication, and the mixtures were pumped through an axisymmetric needle/tubing microfluidic device. The droplets were polymerized in situ under visible light (400–450 nm, 100 mW cm−2) irradiation to form spherical hydrogel particles. To separate the oil phase from the hydrogel microspheres, the samples were washed three times using PBS.

6.2.2.4. Cell-Laden Microspheres

Passage 2 to 3 HUVECs and passage 3 MSCs were trypsinized and mixed with Gel-NOR (5wt% Gel-NOR, DTT at 1:4 SH:NOR ratio, 0.2/2 Ru/SPS) at a concentration of either 6M HUVECs/mL (HUVECs group), 6M MSCs per mL (MSCs group) or 5M HUVECs and 1M MSCs/mL prior to pumping the mixture into the microfluidics device. The resulting microspheres were cultured up to 14 days in EGM.

6.2.2.5. Viability Assays

Live/dead staining was used to visualize cell viability of encapsulated cells on day 1 after encapsulation. Briefly, hydrogel samples were washed with PBS, cut in half, and incubated with propidium iodide (1.5 μM, from Invitrogen) and calcein-AM (1 μM, from Invitrogen) in PBS for 15 min at RT. The samples were then washed with PBS and left hydrated for imaging using a fluorescent microscope (Zeiss Axioimager Z1 microscope). Live and dead cells were counted at six different microspheres per time point using Image J (version 6.1 Fiji, National Institutes of Health). Viability was calculated using equation 6:

$$Cellviability\,(\%) = 100\,x\,\frac{Livecells}{(Livecells + Deadcells)} \qquad (6)$$

6.2.2.6. DNA Quantification

Hydrogels were digested at 56° in 1 mg mL-1 proteinase K dissolved in a 10-2 M Tris-HCl and 103 M disodium EDTA solution, following a treatment with DNase-free RNase A (Thermo Fisher). Total DNA was quantified using CyQUANT Cell Proliferation Assay Kit following the manufacturer's instructions.

6.2.2.7. Metabolic Activity Assays

AlamarBlue® was used to track the cellular health of embedded cells at days 1, 4, 7, 10 and 14 after encapsulation. Briefly, each hydrogel sample was incubated with 350 µL media containing AlamarBlue® solution, diluted according to manufacturer's instructions, for 3h. The reduction of AlamarBlue® in the solution was determined by reading absorbance at wavelengths of 570 nm and 600 nm using a spectrophotometer (Thermo Scientific Varioskan Flash, Darmstadt, Germany) followed by data processing according to manufacturer's instructions.

6.2.2.8. Immunofluorescence Examination

Cell-laden microspheres were collected after 1, 4, 7 and 14 days, washed in PBS, followed by a fixation in 4% formaldehyde for 45 min at RT. Samples were then blocked with 2% BSA for 1h at RT and permeabilized using a 0.2% Triton-X solution. Primary anti-CD 31 antibody (R&D Systems) was diluted in blocking buffer (1:100) and applied overnight at 4°C. Samples were washed three times in blocking buffer for 30 min each followed by an incubation with a goat-anti-mouse (Alexa Fluor 488, Lifetech) secondary antibody diluted in blocking buffer (1:500), in the dark overnight at 4°C. Samples were then washed 3 times in PBS during 5 min and incubated in a Rhodamine-phalloidin (1:500) solution for 30 min. Samples were then washed 3 times in PBS during 5 min, incubated in a DAPI (1:1000) solution for 2 min and washed three times in PBS for 30 min. Images were captured using a Zeiss Axioimager Z1 fluorescence microscope (Carl Zeiss Microscopy, Jena, Germany). From this staining, CD-31 and F-actin positive cells were distinguished as HUVECs, while CD-31 negative and F-actin positive cells were distinguished as MSCs. The stages of network development in Gel-NOR samples were described following previously reported criteria (18,23).

6.2.2.9. Printing of Load-Bearing Cages and Scaffolds

3D-printed Poly(ϵ-caprolactone) (PCL) cages were fabricated using a BioScaffolder (SYS+ENG, Germany). PCL was molten in the reservoir at 120°C for 45 minutes and extruded using a 23G nozzle in a repeating 0°-90°-0°-0°-90°-0° pattern. Cages were printed with a 3mm spacing in the x-axis and 1.1 mm spacing in the y-axis to include two microspheres in the same cage, while scaffolds had a 1.1mm spacing in the x-axis and 1.1 mm spacing in the y-axis to include one microsphere in each space. The auger was set at a dispensing speed of 32 RPM with x-y traverse speed of 180 mm/min. Temperature of the printing head was set at 120°C and pressure at 4 bar. Temperature of the base plate was set at 25 °C.

6.2.2.10. Release Assays

RhVEGF-165, bFGF and BDNF were labelled using Alexa Fluor 594 carboxylic acid, succinimidyl ester (ThermoFisher) following the manufacturer's instructions. Unreacted dye was separated using 3 kDa MWCO centrifuge filter units. During hydrogel and microsphere fabrication, labelled growth factors were mixed with the macromer solution before crosslinking. Hydrogels (20 μL each) with incorporated GFs were fabricated as described in 6.2.2.2 and microspheres were incubated in 1 mL of basal endothelial cell media supplemented with 1% P/S. Incubation media and microsphere samples were collected at selected time points up to total hydrogel degradation. Fluorescence in the media was measured by fluorescence spectroscopy (Thermo Scientific Varioskan Flash, Darmstadt, Germany). Release media from plain PVA-Tyr hydrogels was used as a control for background subtraction. Images from the microsphere samples were captured using a Zeiss Axioimager Z1 fluorescence microscope (Carl Zeiss Microscopy, Jena, Germany), and microspheres without loaded growth factors were used as negative controls.

6.2.2.11. Statistical Analysis

All samples were prepared in triplicates and each experiment was repeated three times (N=3) to study variability between experiments unless otherwise stated in the figures. Individual differences between groups and time points were assessed using one or two-way ANOVA and Holm-Sidak post hoc analysis (GraphPad Prism 7). Statistical significance was accepted at $p<0.05$.

6.3. Results and Discussion

6.3.1. Generation and Evaluation of Gel-NOR Microspheres Encapsulated with Endothelial Cells and Mesenchymal Stem Cells

Our first goal was to generate Gel-NOR microspheres with encapsulated HUVECs, MSCs or co-cultures for bioassembly applications. Previous research has shown that it is possible to generate methyl methacrylate polymeric microspheres by employing a microfluidic oil-water emulsion setup (22), followed by UV crosslinking using Irgacure 907 as a photoinitiator. This technique was later applied in our group to fabricate gelatin-methacryloyl (GelMA) hydrogel microspheres that were photo-crosslinked with Ru/SPS (20). Here, the same technique is applied to generate hydrogel microspheres using Gel-NOR and Ru/SPS. Gel-NOR is crosslinked through a thiol-ene step-growth reaction, which is fundamentally different to the methacryloyl-based chain-growth reaction of GelMA. These differences could affect the formation of microspheres using this oil-emulsion system. Despite this, it was possible to successfully generate Gel-NOR microspheres using the same crosslinking conditions optimised in chapter 5 for the co-culture of HUVECs and MSCs (5 wt% Gel-NOR crosslinked with DTT 1:4 NOR:SH ratio and 0.2/2 mM Ru/SPS).

As shown in Chapter 5, the selected crosslinking conditions resulted in high cell survival and metabolic activity by encapsulated HUVECs and MSCs in casted discs. However, the fabrication method could influence these results. The light attenuation through the tubing and the contact with an oil phase during the crosslinking could result in differences in the crosslinking efficiency, thereby impacting cell function and behaviour. The contact with the oil phase could also have a direct impact on cell health. To investigate if the fabrication process had a significant effect on cell survival, LIVE/DEAD assay was performed after 24h hours of culture (Figure 6.2A-C), which revealed high cell survival rates in all groups. Quantification of the images showed that the survival was above 90% in all groups with no significant differences between groups ($p>0.05$) (Figure 6.2D). These survival rates are similar to the ones obtained in chapter 5, where cell survival in photo-crosslinked Gel-NOR discs was not significantly different to Matrigel discs.

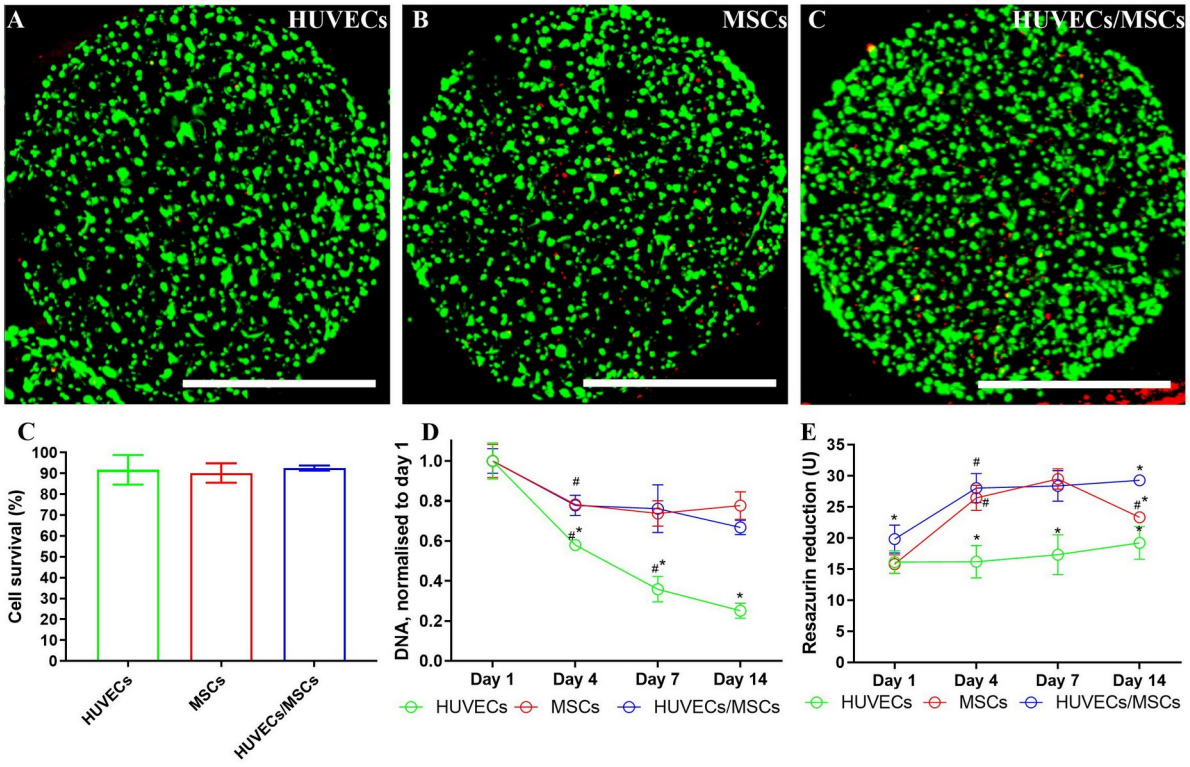

Figure 6.2. Cell survival, proliferation and metabolic activity in Gel-NOR microspheres. *Cell survival at day 1 (A-D), proliferation (E) and metabolic activity (F) of HUVECs and/or MSCs encapsulated in Gel-NOR microspheres (5 wt% Gel-NOR, 0.2/2 mM Ru/SPS and DTT at 1:4 NOR:SH ratio). Live cells are presented in green (stained with calcein) and dead cells are presented in red (stained with propidium iodide). Scale bars: 500 µm. *: Significant differences ($p<0.05$) as compared to all other groups at the same time point. #: Significant differences ($p<0.05$) as compared to the previous time point of the same group. All experiments were repeated three times with three technical replicates each (N=3). Error bars are not visible in time points where they were smaller than the symbol itself.*

DNA quantification (Figure 6.2E) revealed different trends between groups. HUVEC-laden microspheres showed a significant decrease in total DNA content at each time point, reaching 25% of the day 1 DNA content on day 14. However, microspheres containing MSCs or co-cultures decreased to approximately 80% of the day 1 DNA content between days 1 and 4 and maintained constant levels after that, with no significant differences between the two groups. These reductions in DNA content during culture period have previously been observed in similar models (24,25). For example, Barati et al. encapsulated MSCs and endothelial progenitor cells (EPCs) in patterned GelMA hydrogels and exposed them to BMP-2 and VEGF released from hydrogel-based nanoparticles. The total DNA content of the samples decreased over time regardless of the exposure to growth factors, which was interpreted as a sign of cell differentiation (25).

Metabolic activity measurements obtained using AlamarBlue® assay (Figure 6.2F) also showed differences between groups. While HUVEC-laden microspheres maintained constant levels of metabolic activity throughout the whole experiment, the metabolic activity of microspheres encapsulated with MSCs or co-cultures increased between days 1 and 4, then maintained constant levels until day 7. However, MSC-laden microspheres showed a decrease in metabolic activity between days 7 and 14 while co-culture-laden microspheres remained stable.

Overall, these results suggest that the co-encapsulation of HUVECs with MSCs within Gel-NOR microspheres improves the survival and metabolic activity of encapsulated cells during the culture process, potentially through cell-cell interactions. These interactions have been previously demonstrated multiple times in 2D (26,27) and 3D models, including microtissues (28) and photo-crosslinked gelatin methacryloyl hydrogels (24), where co-cultured endothelial cells and MSCs showed increased proliferation (24,27), metabolic activity (27) and expression of angiogenic markers (24,26,28). For example, Bidarra et al. cultured HUVECs and MSCs in a 2D model, where co-encapsulated cells showed increased overall cell number and metabolic activity as compared to HUVECs or MSCs encapsulated alone (27). Zhang et al. co-encapsulated HUVECs and MSCs in GelMA hydrogels at different cell ratios, and found that the total DNA content was lower on day 21 of the experiment as compared to day 7 regardless of the cell ratio used. This trend was, however, less marked in samples with MSCs encapsulated alone (24), similarly to the results observed in the present experiment. Thus, it was not only possible to generate cell-laden microspheres with different types of encapsulated cells, but these microspheres also showed high cell survival and followed trends that have been previously reported in the literature in terms of their proliferation and metabolic activity.

To further study the behaviour of HUVECs and MSCs after their encapsulation in fabricated Gel-NOR microspheres, CD-31 and F-actin staining was performed 4, 7 and 14 days after encapsulation. From this staining, CD-31 and F-actin positive cells were distinguished as HUVECs, while CD-31 negative and F-actin positive cells were distinguished as MSCs. Figure 6.3 shows the maximum intensity projection across 400 μm of the microsphere thickness, revealing remarkably different cell morphologies between groups. When HUVECs were encapsulated alone, they displayed round morphologies and low levels of migration throughout the construct. After 14 days of culture, most cells still showed a round morphology but some of them started to form aggregates. When MSCs were encapsulated alone, their morphologies were more elongated as compared to HUVECs and they showed the ability to migrate throughout the microsphere, progressively covering its surface. A similar phenomenon was observed in co-culture-laden microspheres, where the MSCs also migrated to the surface of the microsphere and covered it. On the other hand, HUVECs in co-culture-laden microspheres showed a more elongated morphology from day 4 onwards when compared to HUVEC that were encapsulated alone. At days 7 and 14, HUVECs were self-assembling into a partially interconnected network (Figure 6.3, bottom right image). It has been previously established that endothelial cells need the support of stromal cells to form stable 3D networks (23,29), and these results support that body of evidence. Furthermore, similar network patterns have been observed at the surface of spherical microtissues of co-cultured MSCs and HUVECs, where HUVECs formed a partially interconnected network at the surface of the structure (28,30,31).

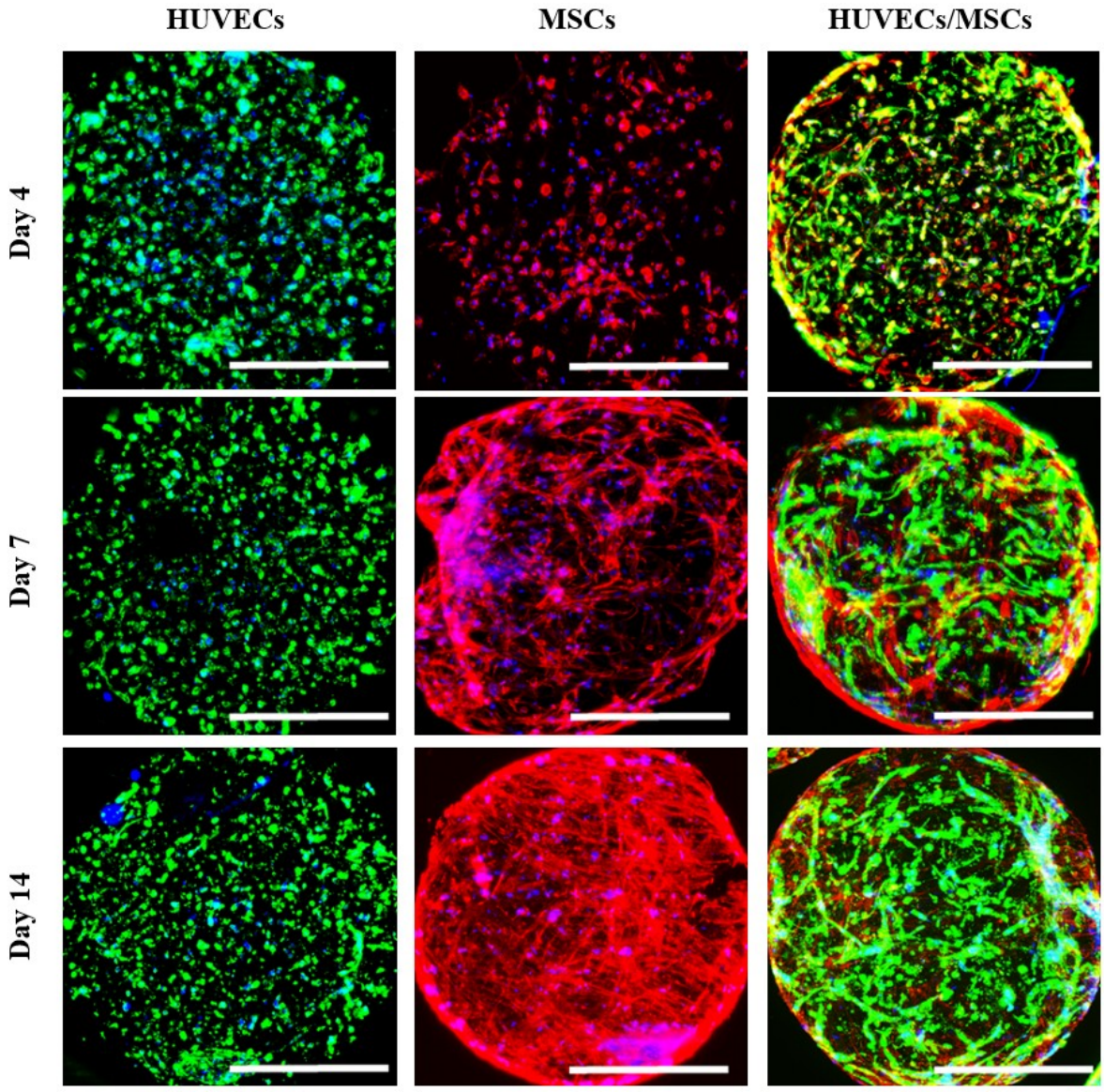

Figure 6.3. Cell morphology and self-organisation over time in Gel-NOR microspheres. *Representative images of a CD-31 and F-actin immunostaining of HUVECs, MSCs or HUVECs/MSCs co-cultures encapsulated in Gel-NOR microspheres (5 wt% Gel-NOR, 0.2/2 mM Ru/SPS and DTT at 1:4 NOR:SH ratio). CD-31 is presented in green (anti-CD31 immunostaining), F-actin is represented in red (Phalloidin) and DNA is represented in blue (DAPI). Scale bars: 500 µm. Experiments were repeated three times with three technical replicates each (N=3).*

Thorough examination of the microspheres with encapsulated co-cultures (Figure 6.4) revealed morphological differences between HUVECs and MSCs at the surface, intermediate and deep zones of the construct. The amount of MSCs was significantly lower at the intermediate and deep areas of the microspheres, suggesting that the MSCs had mostly migrated to the surface. This was potentially triggered by gradients of oxygen and/or growth factors within the microspheres coming from the culture media, which are known to stimulate MSC migration (32,33). HUVECs, on the other hand, were present both at the surface, intermediate and deep areas of the material, but the morphologies shown were different depending on the area; while cells at the surface were self-assembling into vessel-like networks, cells at the intermediate and deep areas showed lower levels of elongation and clustering. These differences are in accordance with the results shown in Chapter 5 and support that cells at the deeper areas of hydrogels do not necessarily behave in the same way as cells at the surface, as has been previously reported (34,35). It is possible that the difference in HUVEC morphology at the intermediate and deep areas of the microspheres is related to the lack of MSCs, which have migrated to the surface and are therefore unable to support network formation at the deeper areas. While the ideal result would be a homogeneous distribution of the vessel network throughout the material, the generation of microspheres could potentially allow leveraging this limitation. As long as the microspheres are smaller than the diffusion limit, which is generally considered to be 200μm of distance from the surface to the deeper area of the construct (36), the cells would receive adequate amounts of nutrients and oxygen. In this context, the presence of a vessel network at the surface of the microspheres could be enough to generate an initial microvessel template that could connect with the host vessel network and support quick vascularisation of the construct. Alternatively, a possible strategy to stimulate homogeneous vessel formation throughout the construct would be the addition of ECM proteins that have demonstrated to promote vascularisation, such as fibrin or laminin (23,37,38). Most importantly, using other cell sources such as endothelial progenitor cells could also have a significant effect in the quality and quantity of vessels formed (39). Therefore, it should be possible to improve these results and achieve a better distribution of the vessel network in the future.

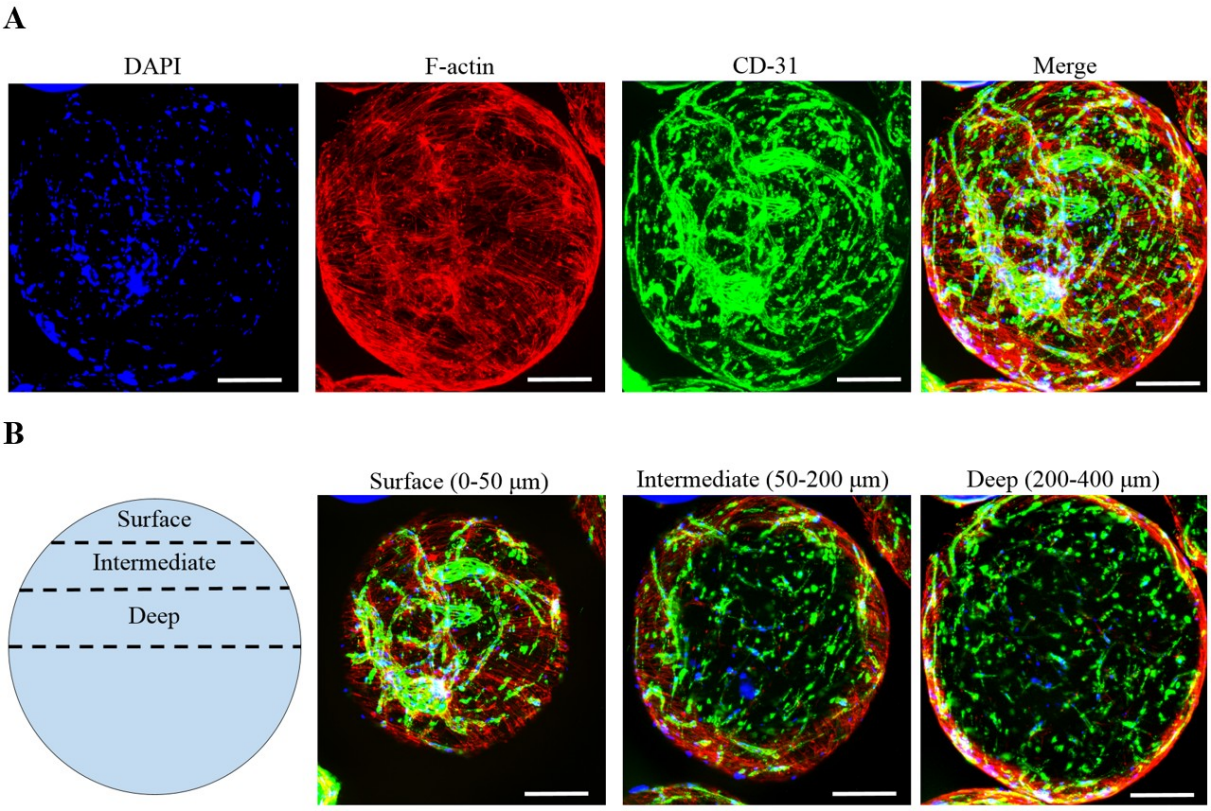

Figure 6.4. Differential cell behaviour within co-cultured Gel-NOR microspheres. *Representative maximum intensity projections of CD-31 and F-actin immunostaining of HUVECs/MSCs co-cultures encapsulated in Gel-NOR microspheres (5 wt% Gel-NOR, 0.2/2 mM Ru/SPS and DTT at 1:4 NOR:SH ratio) and cultured during 14 days. (A) Maximum intensity projection of 400 µm thickness and (B) maximum intensity projection of the surface, intermediate and deep areas of the microspheres. CD-31 is presented in green (anti-CD31 immunostaining), F-actin is represented in red (Phalloidin) and nuclei are represented in blue (DAPI). Scale bars: 200 µm. Experiments were repeated three times with three technical replicates each (N=3).*

6.3.2. Studying the Effects of Spatial Organisation of Cells in Assembled Gel-NOR Constructs

The second goal of this chapter was to perform an initial study to evaluate the interaction of different kinds of cell-laden microspheres when assembled together. When cell-laden microspheres are assembled into a larger scaffold, cells encapsulated in different microspheres interact with each other both directly through cell-cell interactions (if the microspheres are in direct contact) and indirectly through soluble signals (40). These interactions could result in changes in cell function and behaviour. For example, fusion of vascular spheroids derived from mouse allantoic tissue has been previously reported in the literature (41), and this phenomenon was not observable in a single sphere model under the same conditions (42). Thus, observing individual microspheres is not the most adequate representation of what would happen in an assembled scaffold.

To study how different cell distributions would affect cell behaviour and microsphere fusion, a proof-of concept experiment was performed by assembling microsphere pairs into 3D-printed PCL cages (Figure 6.5A-B). After 14 days of culture, a CD-31 and F-actin immunostaining was performed on the samples to evaluate cell distribution and general morphology (Figure 6.5C). When HUVEC or MSC-laden microspheres were in direct contact with cell-free microspheres, little to no migration was detected towards the cell-free microspheres (Figure 6.5C, top row). However, when co-culture-laden microspheres were assembled with cell-free microspheres, some of the HUVECs and MSCs seemed to be able to migrate onto the empty microsphere (Figure 6.5C). These observations correlate with previous reports where endothelial cells and MSCs showed increased migration when cultured together (33,43).

When two HUVEC-laden microspheres were cultured together, no fusion or interconnected structures between microspheres were observed (Figure 6.5C, middle row). This agrees with the small amount of cell migration and clustering observed in individual HUVEC-laden microspheres. When two MSC-laden microspheres were assembled together, microsphere fusion was observed (Figure 6.5C, middle row). These results correlate with the high capacity of MSCs to migrate throughout the material (33), which is also observable in individually cultured microspheres (Figures 6.3 and 6.4). In fact, MSCs had also migrated onto the PCL scaffolds at day 14 in many of the samples (Figure 6.5C). When co-culture laden microspheres were assembled together, microsphere fusion was also observed. Interestingly, the assembled structures that HUVECs formed in co-culture microspheres were also interconnected between both microspheres (Figure 6.5C, middle row). These results suggest that the presence of MSCs, either encapsulated individually or in co-cultures, is necessary for microsphere fusion. Furthermore, the presence of MSCs could be promoting the formation of interconnected HUVEC structures between microspheres. Therefore, it is possible that the assembly of co-culture-laden microspheres into a larger construct could potentially result in a large, interconnected structure of endothelial cells that could provide nutrient and oxygen supply to the whole construct.

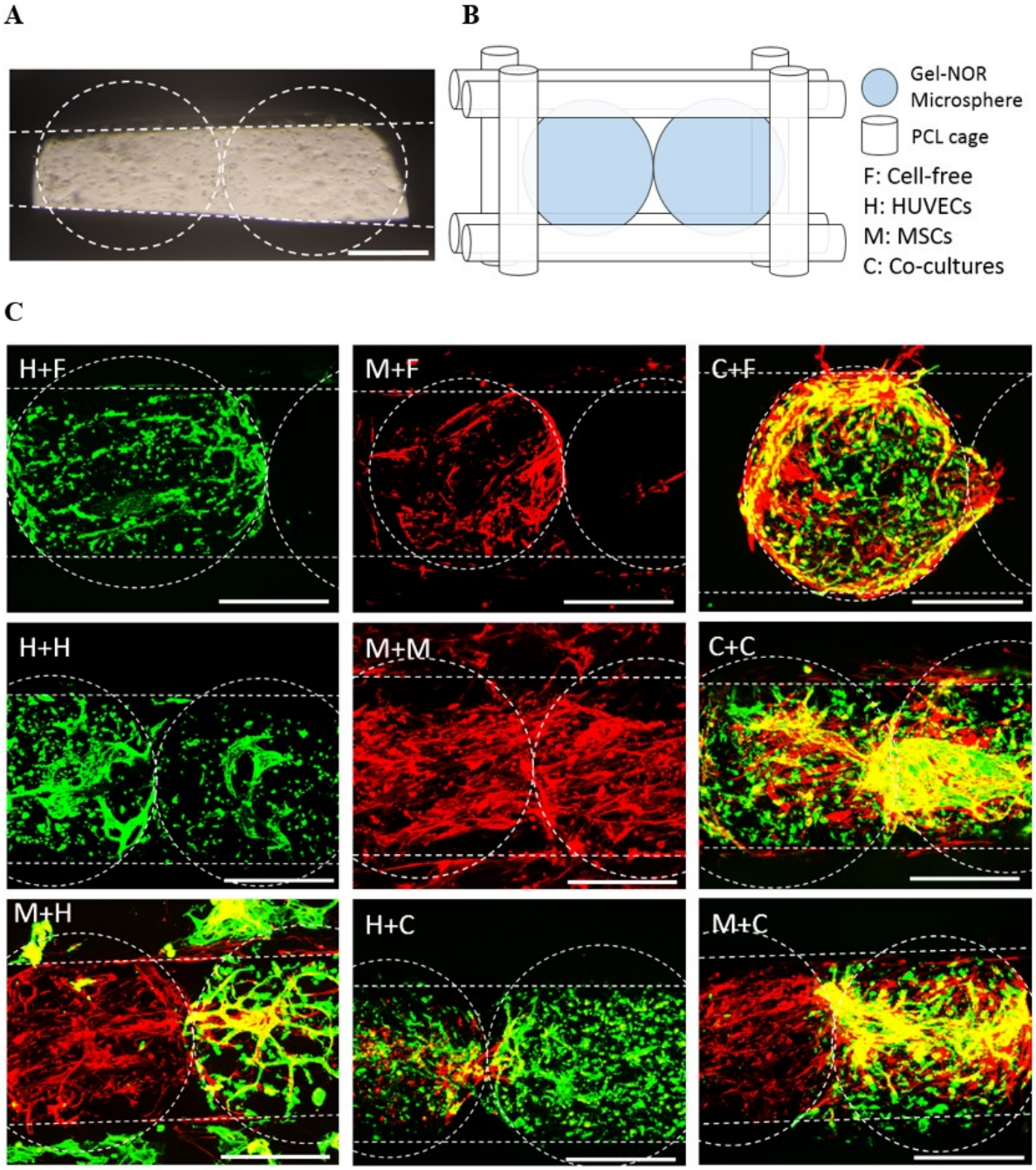

Figure 6.5. Interactions between assembled cell-laden vascular microspheres. *(A) Brightfield microscopy image of the experimental setup with assembled Gel-NOR microspheres in a 3D-printed PCL cage. (B) Schematic view of the experimental setup with assembled Gel-NOR microspheres in a 3D-printed PCL cage. (C) Representative images of a CD-31 and F-actin immunostaining of HUVECs, MSCs or HUVECs/MSCs co-cultures encapsulated in Gel-NOR microspheres (5 wt% Gel-NOR, 0.2/2 mM Ru/SPS and DTT at 1:4 NOR:SH ratio) and assembled in different combinations. CD-31 is presented in green (anti-CD31 immunostaining) and F-actin is represented in red (Phalloidin). Scale bars: 500 μm. Dashed lines represent the contour of the microspheres and the PCL cages. This experiment was repeated once (N=1).*

When MSC-laden microspheres were assembled with HUVEC-laden microspheres, some MSC migration onto the HUVEC-laden microspheres was observed (Figure 6.5C, bottom left image). Furthermore, the direct contact of these migrated MSCs with HUVECs seemed to promote the formation of interconnected structures by HUVECs, fulfilling a similar role to MSCs directly co-encapsulated with HUVECs. When co-culture-laden microspheres were assembled with HUVEC-laden microspheres, the observed MSC migration towards the HUVEC-laden microsphere was lower (Figure 6.5C, bottom middle image). A possible explanation of this phenomenon is that, when HUVECs are present in one of the microspheres, the formation of a signal gradient could be strongly attracting MSCs from adjacent microspheres. It has been shown that MSCs migration is stimulated by growth factors such as VEGF, BDNF or PDGF-ββ (33), which are secreted by HUVECs (44). However, when HUVECs are present in the same microsphere as MSCs, such signal gradient is not formed, resulting in a lower level stimulation of MSC migration. Despite the reduced migration, HUVECs that were closer to the co-culture microsphere and in contact with migrated MSCs did seem to show an increased ability to assemble into interconnected structures (Figure 6.5C, bottom middle image). When co-culture-laden microspheres were assembled with MSC-laden microspheres, a high degree of microsphere fusion was observed. However, little to no migratory activity of HUVECs was observed (Figure 6.5C, bottom right image).

Overall, the results of this experiment are preliminary (N=1) and the observations described would require further confirmation studies. However, these results provide interesting initial information on how different cell distributions would affect cell function and microsphere fusion. For optimal microsphere fusion, it seems recommendable to encapsulate MSCs in each microsphere due to their increased proliferation and migration capabilities as compared to HUVECs. For endothelial cell assembly, better results were observed when HUVECs were directly co-encapsulated with MSCs or when they were individually encapsulated and assembled together with MSC-laden microspheres. However, for vascularisation purposes it is desirable to have these interconnected endothelial cell structures distributed homogeneously throughout the scaffold, especially when fabricating large tissue engineered constructs. Therefore, it seems recommendable to co-encapsulate HUVECs and MSCs in each individual sphere for the fabrication of larger engineered constructs.

Importantly, most of the changes in cell function observed in this assembled model fit already existing data on the interactions between HUVECs and MSCs (33,43,45). Therefore, this

experiment illustrates the potential of this setup as a model of the interactions of different cell types within fabricated constructs. As stated in the introduction, the effects of the distribution of cells and materials within the scaffold is one of the largest knowledge gaps in biofabrication. This model could help answer some of these questions and provide relevant information to the field.

6.3.3. Generating and Evaluating PVA-Tyr Microspheres

The third goal of this chapter was to generate GF-loaded PVA-Tyr microspheres and to study the effects that a different fabrication technique would have on the degradation and GF release profiles of PVA-Tyr hydrogels. PVA-Tyr hydrogel microspheres were successfully generated using the same microfluidics setup used to fabricate Gel-NOR microspheres. Figure 6.6 shows representative images of the microspheres at day 1 after their fabrication.

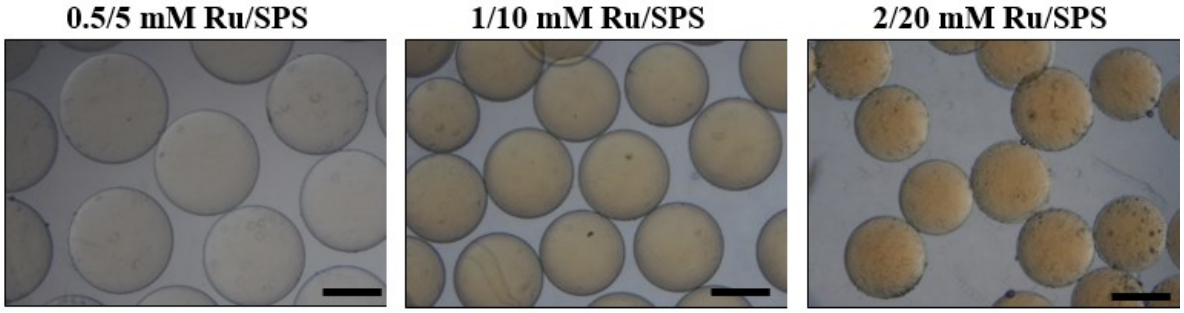

Figure 6.6. PVA-Tyr microspheres fabricated with different Ru/SPS concentrations. *Representative images of 5wt% PVA-Tyr microspheres fabricated at 0.5/5, 1/10 or 2/20 Ru/SPS mM concentrations at day one after fabrication. Scale bars: 500 µm. Experiments were repeated three times with three technical replicates each (N=3).*

It has been previously shown that differences in the size and shape of biomaterial constructs can affect their degradation time both *in vitro* and *in vivo*. In a comprehensive study, Artzi et al. studied the degradation profile of PEG:Dextran fabricated in the shape of disks, blocks or hollow cylinders both *in vitro* and in a mouse subcutaneous model. The study found that the degradation profiles differed between groups in both setups (46), where hollow cylinders were the fastest group to degrade, followed by blocks and discs. These differences in degradation were directly related to their surface to volume ratio, where hollow mesh cylinders had the highest, followed by blocks and discs. Therefore, the translation of PVA-Tyr discs to microspheres could results in large differences in their degradation profile, not only due to the difference in volume but also their difference in shape, both resulting in differences in surface-to-volume ratio. While the sphere is the geometrical shape with the lowest surface-to-volume ratio, the large differences in volume (20 mm^3 for discs against

approximately 0.5 mm^3 for microspheres) are more impactful for the surface-to-volume ratio than the geometrical shape. Therefore, we hypothesized that PVA-Tyr microspheres would degrade faster than PVA-Tyr discs. However, when comparing the degradation time of PVA-Tyr discs and microspheres (Table 6.1), it was found that both geometries were comparable in the studied crosslinking conditions. A potential explanation of the differences between these results and previous research is that PVA-Tyr hydrogels follow a bulk degradation process, as opposed to the surface erosion degradation shown by PEG:Dextran (46).

Table 6.1. Degradation time of PVA-Tyr hydrogels in the form of discs and microspheres. *Degradation time of the discs is reported as the average time point in which each sample collapsed during shaking of the PBS solution. Degradation time of the microspheres is reported as the time point in which all the microspheres had collapsed during shaking. Experiments were repeated three times with three technical replicates each (N=3).*

Form	Ru/SPS (mM)	Degradation time (Days)
Disc	**0.5/5**	8 ± 1
Microsphere	**0.5/5**	9
Disc	**1/10**	42 ± 2
Microsphere	**1/10**	40
Disc	**2/20**	63 ± 1
Microsphere	**2/20**	65

The size of the microspheres was tracked during the degradation period using bright-field microscopy (Figure 6.7). The initial diameter of PVA-Tyr microspheres crosslinked under all conditions was below 1 mm, but changed depending on the concentration of Ru/SPS utilised. This was expected from the different swelling ratios observed in chapter 3, which were caused by different degrees of crosslinking. The evolution of the microsphere size followed similar trends as the swelling ratio of discs crosslinked under the same conditions (Chapter 3, Supplementary Figure S3.1B): microspheres crosslinked at 0.5/5 mM Ru/SPS consistently showed increases in size between time points, whereas microspheres crosslinked at higher Ru/SPS concentrations showed an initial phase with no increases in size, followed by a second phase where the size started to increase between time points in a consistent manner (Figure 6.7). These results are relevant for the adaptation of these microspheres to bioassembly, as the size of the microspheres needs to initially fit the size of the printed scaffold so that the microspheres do not fall during the culture period or post-implantation. The size of the microspheres can be adapted by changing different parameters of the fabrication process (22), and the size of the scaffold can also be easily adapted by changing the printing design. The fact that the size of the microspheres increases with time, which is another sign of the bulk degradation process, is a positive result as it means that they would not fall from the printed scaffold during the degradation process.

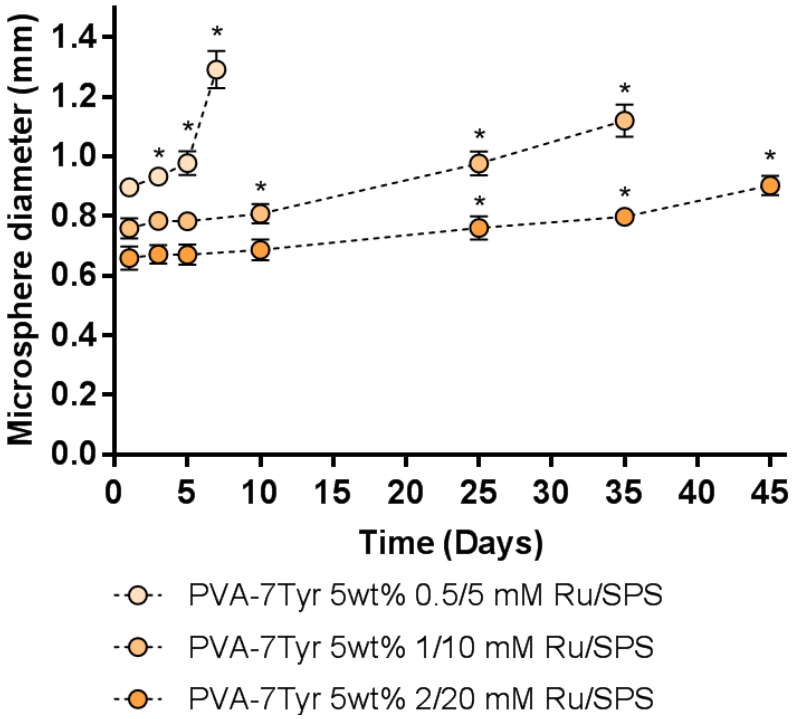

Figure 6.7. Diameter of PVA-Tyr microspheres throughout the degradation process. **: Significant difference ($p<0.05$) as compared to previous time points of the same condition. Error bars are not visible in time points where they were smaller than the symbol itself. Experiments were repeated three times with three technical replicates each (N=3).*

Taken together, the results on degradation time and sphere size show that the degradation profile of the microspheres follows similar trends as in discs. Therefore, not only it is possible to achieve controlled degradation of these microspheres, but the library of degradation profiles developed in chapter 3 can be directly translated to microspheres.

To study the changes in GF release profile from microspheres as compared to discs, fluorescently labelled VEGF, bFGF and BDNF were incorporated in both PVA-Tyr discs and microspheres. The release of GFs was tracked through fluorescence imaging of the microspheres (Figure 6.8) and through fluorescence spectroscopy of exposed culture media (Figure 6.9).

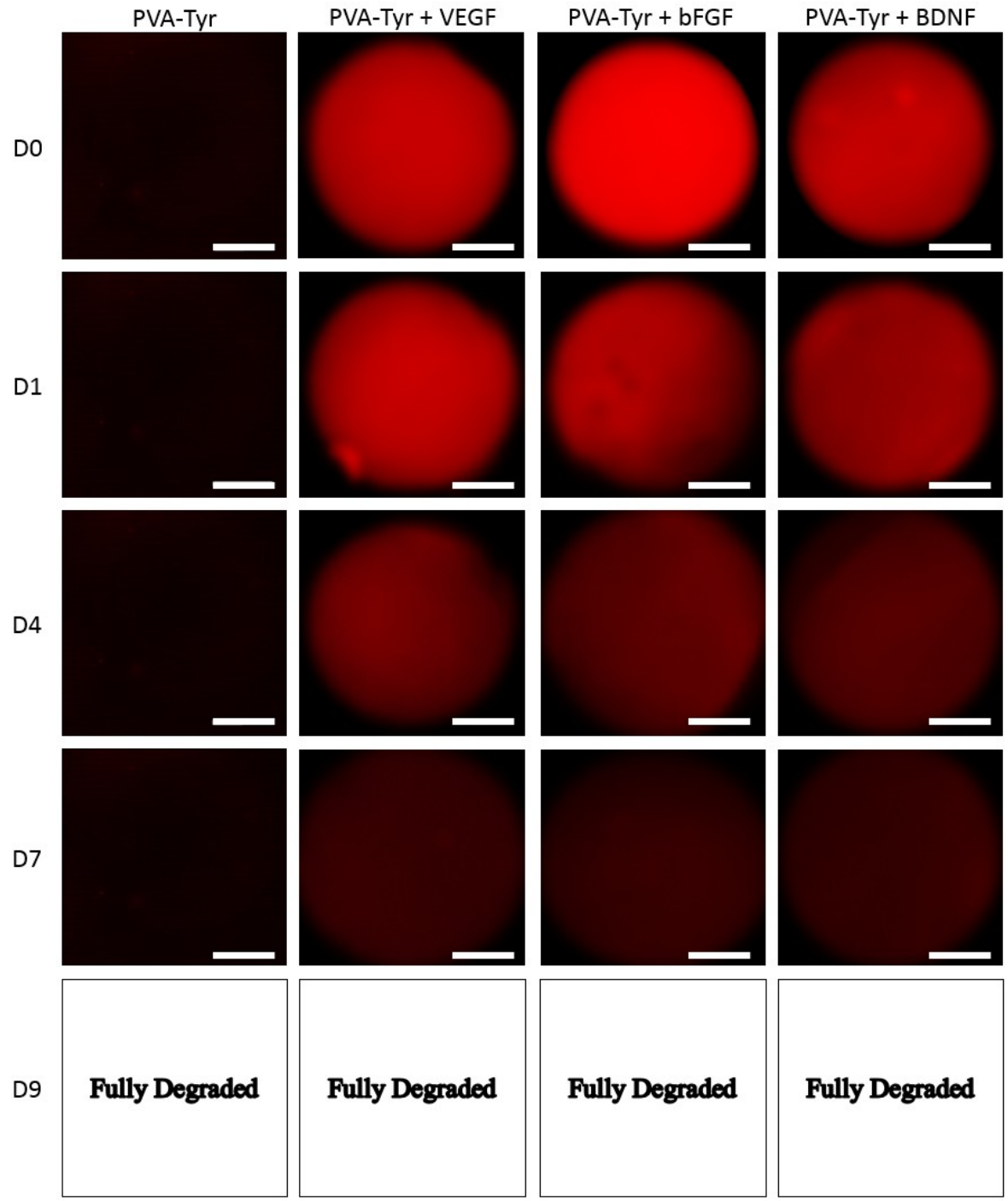

Figure 6.8. Fluorescently-labelled growth factor release from PVA-Tyr microspheres (Images). *Fluorescence images of PVA-Tyr microspheres crosslinked at 5wt% of PVA-7Tyr, 0.5/5 mM Ru/SPS loaded with fluorescently labelled VEGF, bFGF or BDNF. Scale bars: 500 µm. Experiments were repeated three times with three technical replicates each (N=3).*

Fluorescence imaging (Figure 6.8) shows that GFs were present in the microspheres during the whole degradation period, where the average fluorescence intensity of the GF-loaded microspheres was always significantly higher than the PVA-Tyr control (data not shown). Release measurements (Figure 6.9) show that the percentage release in the first 24 hours of exposure to media is significantly higher in discs than in microspheres (70-75% and 30-35%

respectively). These results were in contrast to the observed degradation times, where there were no differences between discs and microspheres. A possible explanation of the differences in the initial release is a loss of incorporated GF during the PBS washes needed to separate the microspheres from the oil phase after fabrication. As these washes happen before the beginning of the release studies, any GF lost during the process would not be detected. Interestingly, the resulting release profile is more linear, which makes it more suitable for regenerative medicine applications where burst release is not desirable (47). On the other hand, these results also mean that there is a significant loss of GF during the fabrication process (calculated to be around 55% of the initially loaded GF for this crosslinking condition), making this fabrication method less efficient. However, only GFs that have not been covalently incorporated in the network (not retained) can be lost during these initial washings. As shown in Chapter 3 (Figures 3.3A and 3.4A), the retention can be improved by increasing the Ru/SPS concentration, and therefore it was hypothesized that increasing the Ru/SPS concentrations would result in a more efficient GF incorporation during microsphere fabrication.

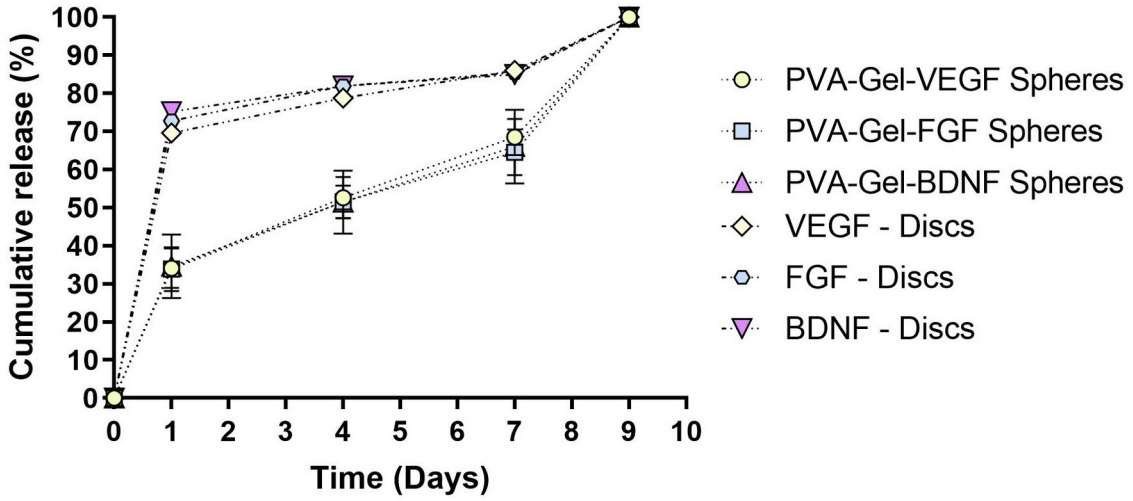

Figure 6.9. Fluorescently-labelled growth factor release from PVA-Tyr discs and microspheres. *Growth factor release from PVA-Tyr discs and microspheres crosslinked at 5wt% PVA-7Tyr, 1wt% Gelatin and 0.5/5 Ru/SPS loaded with fluorescently labelled VEGF, bFGF or BDNF. Experiments were repeated three times with three technical replicates each (N=3). Error bars are not visible in time points where they were smaller than the symbol itself.*

Overall, the results from this section show that it was possible to generate PVA-Tyr microspheres with controllable degradation times. Their degradation follows trends that are comparable to fabricated discs, making our library of degradation profiles translatable to

PVA-Tyr microspheres. Their bulk degradation process makes them increase in size during the degradation process, which will facilitate their application to bioassembly. It was possible to load VEGF, bFGF and BDNF in the microspheres and study their release profile, which was more linear than the release from discs. However, this was at the expense of losing around half the amount of GF that was initially incorporated into the microspheres, reducing the efficiency of the system.

6.3.4. Proof-of-Concept of the Combined Assembly of Gel-NOR and PVA-Tyr

In addition to controlling the distribution of cells within the construct, bioassembly allows the combination of microspheres made of different materials, which can be used for the combined delivery of growth factors and cells in a controlled manner. By controlling the arrangement of these microspheres, it would theoretically be possible to generate controlled growth factor gradients within the scaffold that attract cells to specific areas of interest or that stimulate differentiation in certain patterns (Figure 6.10A-B), mimicking the complex architecture of targeted tissues. For example, cortical bone is comprised by osteons, which are structures formed of a central channel with blood vessels surrounded by ECM and osteoblasts (48). A potential way to mimic that would be to arrange the GF-releasing microspheres in the center and surrounding them by cell-laden microspheres. Other tissues such as articular cartilage present polarized structures that are formed by gradients of growth factors. By arranging the GF-releasing microspheres on one side of the construct, it would theoretically be possible to generate a GF gradient and observe their effects on cell behaviour.

To demonstrate that it is possible to generate 3D conformations that mimic different types of tissues, Gel-NOR and PVA-Tyr microspheres were assembled into larger 3D-printed PCL scaffolds in different conformations (Figures 6.10A-B). As expected from our previous results, the PVA-Tyr microspheres were totally degraded at day 14 of culture (Figures 6.10C-D), endothelial cells were assembling into interconnected structures (Figure 6.10D) and α-SMA was detectable in MSCs (Figures6.10C-D).

These results show that it is possible to combine bioassembly techniques with the material platforms developed in this thesis, and represent a proof-of concept *(N=1)* of the future research that these tools could enable. As stated in the introduction, there is currently no research that combines growth factor delivery with the generation of pre-vascularised tissue analogues for vascularisation purposes. This platform could allow evaluation of the effects of

growth factor delivery both during the pre-vascularisation process and after implantation. Furthermore, the optimal 3D organisation of cells and GFs for vascularisation should also be studied, and this setup provides the tools to do so.

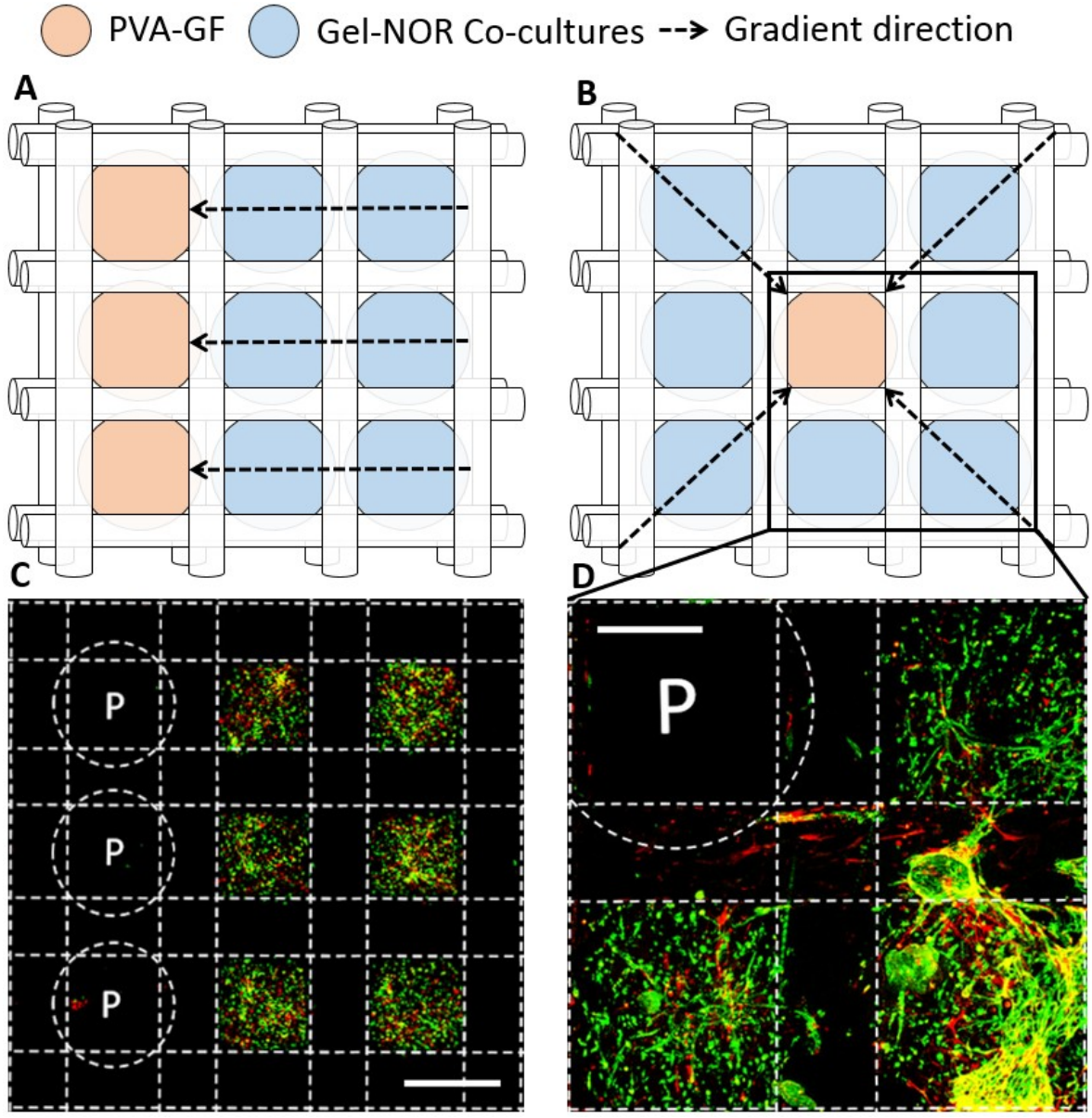

Figure 6.10: Proof-of-concept of different potential arrangements of Gel-NOR and PVA-Tyr microspheres for controlled generation of growth factor gradients within bioassembled large scaffolds. *(A-B) Schematic view of PCL scaffolds with assembled Gel-NOR and PVA-Tyr microspheres generating growth factor gradients within the scaffold. (C-D) Representative images of a CD-31 and α-SMA immunostaining of HUVECs, MSCs or HUVECs/MSCs co-cultures encapsulated in Gel-NOR microspheres (5 wt% Gel-NOR, 0.2/2 mM Ru/SPS and DTT at 1:4 NOR:SH ratio) and assembled together with PVA-Tyr microspheres (5 wt%, 0.5/5 mM Ru/SPS), at day 14 of culture in EGM. Dashed lines indicate the PCL scaffold and the initial positioning of the PVA-Tyr microspheres. P: PVA-Tyr microspheres fully degraded after two weeks of culture. Scale bars: 1mm (C) and 0.5 mm (D). This experiment was repeated once (N=1).*

6.4. Conclusions

The field of regenerative medicine is evolving towards the combination of different cells, materials and bioactive molecules to provide optimal levels of tissue regeneration (13). While several studies confirm that combining these elements can result in synergistic positive effects (1–6), there is little knowledge on the ideal ways to combine them. Bioassembly allows the combination of these elements and provides control over their spatial arrangement (12). Additionally, it allows generating large tissue analogues in a layer-by-layer fashion, facilitating translation to a clinical setting. Very few studies provide evidence of what is the ideal spatial and temporal arrangement of materials, cells and growth factors within biofabricated scaffolds. Furthermore, there are no studies yet that combine the stimulation of angiogenesis with pre-vascularisation techniques. Adapting the platforms developed in this thesis to their use as building blocks for bioassembly could allow large tissue models to be fabricated to study the effects of different cell and growth factor arrangements on tissue vascularisation.

In this chapter, PVA-Tyr and Gel-NOR microsphere modules were generated for bioassembly applications. It was demonstrated that both materials can be fabricated into microspheres with encapsulated cells and growth factors using a microfluidics system. The fabrication process did not alter the desirable properties of Gel-NOR, as both the HUVECs and MSCSs were still able to migrate and proliferate throughout the material. Furthermore, encapsulated HUVECs were able to undergo vasculogenesis and form interconnected vessel-like structures within the Gel-NOR microspheres when co-cultured with MSCs. Furthermore, it was possible to obtain proof-of-concept results on how these microspheres can be arranged to study the optimal distribution of endothelial cells and MSCs within 3D constructs for vascularisation purposes. The results suggest that both HUVECs and MSCs should be co-encapsulated in each microsphere for improved microsphere fusion and homogeneous endothelial cell network distribution. When generating GF-loaded PVA-Tyr microspheres, the fabrication process impacted the initial GF retention within the PVA-Tyr microspheres. However, PVA-Tyr microspheres still showed a linear GFs release profile throughout the degradation process. Finally, the possibility of arranging PVA-Tyr and Gel-NOR microspheres in a controlled and designed manner was demonstrated. The tools developed in this chapter should prove useful for future research in the combination of multiple strategies for tissue vascularisation.

6.5. References

1. Davis ME, Hsieh PCH, Takahashi T, Song Q, Zhang S, Kamm RD, et al. Local myocardial insulin-like growth factor 1 (IGF-1) delivery with biotinylated peptide nanofibers improves cell therapy for myocardial infarction. Proc Natl Acad Sci [Internet]. 2006 May 23;103(21):8155 LP – 8160. Available from: http://www.pnas.org/content/103/21/8155.abstract

2. Hamshere S, Arnous S, Choudhury T, Choudry F, Mozid A, Yeo C, et al. Randomized trial of combination cytokine and adult autologous bone marrow progenitor cell administration in patients with non-ischaemic dilated cardiomyopathy: the REGENERATE-DCM clinical trial. Eur Heart J [Internet]. 2015 Sep 2;36(44):3061–9. Available from: https://doi.org/10.1093/eurheartj/ehv390

3. Choudhury T, Mozid A, Hamshere S, Yeo C, Pellaton C, Arnous S, et al. An exploratory randomized control study of combination cytokine and adult autologous bone marrow progenitor cell administration in patients with ischaemic cardiomyopathy: the REGENERATE-IHD clinical trial. Eur J Heart Fail [Internet]. 2017 Jan 1;19(1):138–47. Available from: https://doi.org/10.1002/ejhf.676

4. Kim HK, Lee JS, Kim JH, Seon JK, Park KS, Jeong MH, et al. Bone-forming peptide-2 derived from BMP-7 enhances osteoblast differentiation from multipotent bone marrow stromal cells and bone formation. Exp Mol Med [Internet]. 2017;49(5):e328–e328. Available from: https://doi.org/10.1038/emm.2017.40

5. Warnke PH, Springer ING, Wiltfang J, Acil Y, Eufinger H, Wehmöller M, et al. Growth and transplantation of a custom vascularised bone graft in a man. Lancet [Internet]. 2004;364(9436):766–70. Available from: http://www.sciencedirect.com/science/article/pii/S0140673604169353

6. Poldervaart MT, Gremmels H, van Deventer K, Fledderus JO, Öner FC, Verhaar MC, et al. Prolonged presence of VEGF promotes vascularization in 3D bioprinted scaffolds with defined architecture. J Control Release [Internet]. 2014;184:58–66. Available from: http://www.sciencedirect.com/science/article/pii/S0168365914002119

7. Shim J-H, Jang K-M, Hahn SK, Park JY, Jung H, Oh K, et al. Three-dimensional bioprinting of multilayered constructs containing human mesenchymal stromal cells

for osteochondral tissue regeneration in the rabbit knee joint. Biofabrication [Internet]. 2016;8(1):14102. Available from: http://dx.doi.org/10.1088/1758-5090/8/1/014102

8. Kundu J, Shim J-H, Jang J, Kim S-W, Cho D-W. An additive manufacturing-based PCL–alginate–chondrocyte bioprinted scaffold for cartilage tissue engineering. J Tissue Eng Regen Med [Internet]. 2015 Nov 1;9(11):1286–97. Available from: https://doi.org/10.1002/term.1682

9. Zhang W, Feng C, Yang G, Li G, Ding X, Wang S, et al. 3D-printed scaffolds with synergistic effect of hollow-pipe structure and bioactive ions for vascularized bone regeneration. Biomaterials [Internet]. 2017;135:85–95. Available from: https://www.ncbi.nlm.nih.gov/pubmed/28499127

10. Daly AC, Pitacco P, Nulty J, Cunniffe GM, Kelly DJ. 3D printed microchannel networks to direct vascularisation during endochondral bone repair. Biomaterials. 2018;162:34–46.

11. Mironov V, Trusk T, Kasyanov V, Little S, Swaja R, Markwald R. Biofabrication: A 21st century manufacturing paradigm. Biofabrication. 2009 Jun 1;1:22001.

12. Groll J, Boland T, Blunk T, Burdick JA, Cho D-W, Dalton PD, et al. Biofabrication: reappraising the definition of an evolving field. Biofabrication [Internet]. 2016;8(1):13001. Available from: http://dx.doi.org/10.1088/1758-5090/8/1/013001

13. Song H-HG, Rumma RT, Ozaki CK, Edelman ER, Chen CS. Vascular Tissue Engineering: Progress, Challenges, and Clinical Promise. Cell Stem Cell [Internet]. 2018 Mar 1;22(3):340–54. Available from: https://www.ncbi.nlm.nih.gov/pubmed/29499152

14. Bertassoni LE, Cecconi M, Manoharan V, Nikkhah M, Hjortnaes J, Cristino AL, et al. Hydrogel bioprinted microchannel networks for vascularization of tissue engineering constructs. Lab Chip [Internet]. 2014;14(13):2202–11. Available from: http://dx.doi.org/10.1039/C4LC00030G

15. Kolesky DB, Homan KA, Skylar-Scott MA, Lewis JA. Three-dimensional bioprinting of thick vascularized tissues. Proc Natl Acad Sci [Internet]. 2016 Mar 22;113(12):3179 LP – 3184. Available from: http://www.pnas.org/content/113/12/3179.abstract

16. Miller JS, Stevens KR, Yang MT, Baker BM, Nguyen D-HT, Cohen DM, et al. Rapid

casting of patterned vascular networks for perfusable engineered three-dimensional tissues. Nat Mater [Internet]. 2012;11(9):768–74. Available from: https://doi.org/10.1038/nmat3357

17. Ben-Shaul S, Landau S, Merdler U, Levenberg S. Mature vessel networks in engineered tissue promote graft–host anastomosis and prevent graft thrombosis. Proc Natl Acad Sci [Internet]. 2019 Feb 19;116(8):2955 LP – 2960. Available from: http://www.pnas.org/content/116/8/2955.abstract

18. Blinder YJ, Freiman A, Raindel N, Mooney DJ, Levenberg S. Vasculogenic dynamics in 3D engineered tissue constructs. Sci Rep [Internet]. 2015;5:17840. Available from: https://www.ncbi.nlm.nih.gov/pubmed/26648270

19. Jang J, Park H-J, Kim S-W, Kim H, Park JY, Na SJ, et al. 3D printed complex tissue construct using stem cell-laden decellularized extracellular matrix bioinks for cardiac repair. Biomaterials [Internet]. 2017;112:264–74. Available from: http://www.sciencedirect.com/science/article/pii/S0142961216305695

20. Mekhileri N V, Lim K, Brown GCJ, Mutreja I, Schon BS, Hooper GJ, et al. Automated 3D bioassembly of micro-tissues for biofabrication of hybrid tissue engineered constructs. Biofabrication [Internet]. 2017; Available from: https://www.ncbi.nlm.nih.gov/pubmed/29199637

21. Mekhileri N V. Integration and automation of a micro-tissue and microsphere based tissue engineering system and its application in cartilage regeneration and cancer models. University of Otago; 2016.

22. Serra C, Berton N, Bouquey M, Prat L, Hadziioannou G. A Predictive Approach of the Influence of the Operating Parameters on the Size of Polymer Particles Synthesized in a Simplified Microfluidic System. Langmuir [Internet]. 2007 Jul 1;23(14):7745–50. Available from: https://doi.org/10.1021/la063289s

23. Lesman A, Koffler J, Atlas R, Blinder YJ, Kam Z, Levenberg S. Engineering vessel-like networks within multicellular fibrin-based constructs. Biomaterials [Internet]. 2011;32(31):7856–69. Available from: http://www.sciencedirect.com/science/article/pii/S0142961211007745

24. Zhang X, Li J, Ye P, Gao G, Hubbell K, Cui X. Coculture of mesenchymal stem cells

and endothelial cells enhances host tissue integration and epidermis maturation through AKT activation in gelatin methacryloyl hydrogel-based skin model. Acta Biomater [Internet]. 2017;59:317–26. Available from: http://www.sciencedirect.com/science/article/pii/S1742706117304294

25. Barati D, Shariati SRP, Moeinzadeh S, Melero-Martin JM, Khademhosseini A, Jabbari E. Spatiotemporal release of BMP-2 and VEGF enhances osteogenic and vasculogenic differentiation of human mesenchymal stem cells and endothelial colony-forming cells co-encapsulated in a patterned hydrogel. J Control Release [Internet]. 2016;223:126–36. Available from: http://www.sciencedirect.com/science/article/pii/S0168365915302807

26. Böhrnsen F, Schliephake H. Supportive angiogenic and osteogenic differentiation of mesenchymal stromal cells and endothelial cells in monolayer and co-cultures. Int J Oral Sci [Internet]. 2016;8(4):223–30. Available from: https://doi.org/10.1038/ijos.2016.39

27. Bidarra SJ, Barrias CC, Barbosa MA, Soares R, Amédée J, Granja PL. Phenotypic and proliferative modulation of human mesenchymal stem cells via crosstalk with endothelial cells. Stem Cell Res [Internet]. 2011;7(3):186–97. Available from: http://www.sciencedirect.com/science/article/pii/S1873506111000675

28. Saleh FA, Whyte M, Genever PG. Effects of endothelial cells on human mesenchymal stem cell activity in a three-dimensional in vitro model. Eur Cells Mater. 2011;22(Area 9):242–57.

29. Freiman A, Shandalov Y, Rozenfeld D, Shor E, Segal S, Ben-David D, et al. Adipose-derived endothelial and mesenchymal stem cells enhance vascular network formation on three-dimensional constructs in vitro. Stem Cell Res Ther [Internet]. 2016;7(1):5. Available from: https://doi.org/10.1186/s13287-015-0251-6

30. Kim EM, Lee Y Bin, Kim S, Park J, Lee J, Kim SW, et al. Fabrication of core-shell spheroids as building blocks for engineering 3D complex vascularized tissue. Acta Biomater [Internet]. 2019; Available from: http://www.sciencedirect.com/science/article/pii/S1742706119306403

31. Pitaktong I, Lui C, Lowenthal J, Mattson G, Jung W-H, Yang B, et al. Early Vascular Cells Improve Microvascularization within 3D Cardiac Spheroids. Tissue Eng Part C

Methods [Internet]. 2019 Dec 13; Available from: https://doi.org/10.1089/ten.TEC.2019.0228

32. Xu W, Xu R, Li Z, Wang Y, Hu R. Hypoxia changes chemotaxis behaviour of mesenchymal stem cells via HIF-1α signalling. J Cell Mol Med [Internet]. 2019/01/09. 2019 Mar;23(3):1899–907. Available from: https://www.ncbi.nlm.nih.gov/pubmed/30628201

33. Fu X, Liu G, Halim A, Ju Y, Luo Q, Song AG. Mesenchymal Stem Cell Migration and Tissue Repair. Cells [Internet]. 2019 Jul 28;8(8):784. Available from: https://www.ncbi.nlm.nih.gov/pubmed/31357692

34. Landau S, Guo S, Levenberg S. Localization of Engineered Vasculature within 3D Tissue Constructs. Front Bioeng Biotechnol [Internet]. 2018;6:2. Available from: https://www.ncbi.nlm.nih.gov/pubmed/29404324

35. Quade M, Knaack S, Weber D, Konig U, Paul B, Simon P, et al. Heparin modification of a biomimetic bone matrix modulates osteogenic and angiogenic cell response in vitro. Eur Cell Mater [Internet]. 2017;33:105–20. Available from: https://www.ncbi.nlm.nih.gov/pubmed/28181209

36. Lovett M, Lee K, Edwards A, Kaplan DL. Vascularization strategies for tissue engineering. Tissue Eng Part B Rev [Internet]. 2009 Sep;15(3):353–70. Available from: https://www.ncbi.nlm.nih.gov/pubmed/19496677

37. Verseijden F, Posthumus-van Sluijs SJ, van Neck JW, Hofer SOP, Hovius SER, van Osch GJVM. Vascularization of prevascularized and non-prevascularized fibrin-based human adipose tissue constructs after implantation in nude mice. J Tissue Eng Regen Med [Internet]. 2012 Mar 1;6(3):169–78. Available from: https://doi.org/10.1002/term.410

38. Simon-Assmann P, Orend G, Mammadova-Bach E, Spenlé C, Lefebvre O. Role of laminins in physiological and pathological angiogenesis. Int J Dev Biol. 2011 Jan 1;55:455–65.

39. Chen X, Aledia AS, Popson SA, Him L, Hughes CCW, George SC. Rapid anastomosis of endothelial progenitor cell-derived vessels with host vasculature is promoted by a high density of cotransplanted fibroblasts. Tissue Eng Part A [Internet]. 2010

Feb;16(2):585–94. Available from: https://www.ncbi.nlm.nih.gov/pubmed/19737050

40. Wan ACA. Recapitulating Cell–Cell Interactions for Organoid Construction – Are Biomaterials Dispensable? Trends Biotechnol [Internet]. 2016;34(9):711–21. Available from: http://www.sciencedirect.com/science/article/pii/S0167779916000494

41. Fleming PA, Argraves WS, Gentile C, Neagu A, Forgacs G, Drake CJ. Fusion of uniluminal vascular spheroids: a model for assembly of blood vessels. Dev Dyn [Internet]. 2010 Feb;239(2):398–406. Available from: https://www.ncbi.nlm.nih.gov/pubmed/19918756

42. Gentile C, Fleming PA, Mironov V, Argraves KM, Argraves WS, Drake CJ. VEGF-mediated fusion in the generation of uniluminal vascular spheroids. Dev Dyn [Internet]. 2008 Oct;237(10):2918–25. Available from: https://www.ncbi.nlm.nih.gov/pubmed/18816835

43. Potapova IA, Gaudette GR, Brink PR, Robinson RB, Rosen MR, Cohen IS, et al. Mesenchymal Stem Cells Support Migration, Extracellular Matrix Invasion, Proliferation, and Survival of Endothelial Cells In Vitro. Stem Cells. 2007;25(7):1761–8.

44. Grasman JM, Kaplan DL. Human endothelial cells secrete neurotropic factors to direct axonal growth of peripheral nerves. Sci Rep [Internet]. 2017;7(1):4092. Available from: https://doi.org/10.1038/s41598-017-04460-8

45. Wang J, Wang Y, Wang S, Cai J, Shi J, Sui X, et al. Bone marrow-derived mesenchymal stem cell-secreted IL-8 promotes the angiogenesis and growth of colorectal cancer. Oncotarget. 2015;6(40):42825–37.

46. Artzi N, Oliva N, Puron C, Shitreet S, Artzi S, bon Ramos A, et al. In vivo and in vitro tracking of erosion in biodegradable materials using non-invasive fluorescence imaging. Nat Mater [Internet]. 2011;10(9):890. Available from: https://doi.org/10.1038/nmat3095

47. Wang Z, Wang Z, Lu WW, Zhen W, Yang D, Peng S. Novel biomaterial strategies for controlled growth factor delivery for biomedical applications. Npg Asia Mater [Internet]. 2017;9:e435. Available from: http://dx.doi.org/10.1038/am.2017.171

48. Pritchard JJ. General Histology of Bone [Internet]. Second Edi. The Biology and

Physiology of Bone. ACADEMIC PRESS, INC.; 1972. 1–20 p. Available from: http://dx.doi.org/10.1016/B978-0-12-119201-3.50008-1

Chapter 7. Conclusions and Future Perspectives

7.1. Conclusions

In **Chapter 1,** a brief introduction to vascularisation in the human body was provided, together with an introduction to the main tissue engineering strategies to promote vascularisation and their current challenges. The aims of the thesis were also outlined.

In **Chapter 2**, the main strategies for growth factor delivery and for the generation of vascularised tissues were reviewed and discussed in depth. Their limitations and current gaps in the literature were identified.

This thesis systematically investigated new hydrogel-based strategies to promote vascularisation, focusing on three main aims: Developing a growth factor delivery system to promote vascularisation, combining top-down and bottom-up strategies for the generation of large vascularised tissue analogues, and combining approaches for tissue vascularisation through bioassembly. In this chapter, the achievements in each of these aims are reviewed and their implications for vascular tissue engineering are discussed, together with potential future research perspectives.

Aim I: Developing a Growth Factor Delivery System to Promote Vascularisation

In **Chapter 3**, the potential of PVA-Tyr hydrogels as a GF delivery system was investigated. The aim was to generate a novel GF delivery system that could covalently incorporate native growth factors and finely tailor their release profile, making it a flexible tool that could be adapted to different tissue engineering applications. It was demonstrated that, by changing the degree of tyramination, macromer concentration and Ru/SPS concentration, hydrogels with highly tailorable degradation profiles from seven days to up to three months could be fabricated. The release profile of covalently incorporated BSA, VEGF, bFGF and BDNF from different PVA-Tyr formulations consistently showed a linear tendency that lasted up to total degradation of the hydrogel, demonstrating potential for long term release applications and highly tailorable release profiles. It was shown that the encapsulation of VEGF, bFGF or BDNF in PVA-Tyr did not result in differences in the incorporation rate or release profile of the system, which facilitates the adaptation of the system to deliver of different GFs for a range of applications. Furthermore, proteinase K was used as a model to show that the degradation of PVA-Tyr hydrogels is driven by hydrolysis even after the covalent incorporation of high concentrations of protein. Finally, 2D and 3D in vitro models were used to demonstrate that VEGF, bFGF and BDNF still retain functionality after exposure to the oxidative stress of photo-crosslinking and to the chemical modifications associated with covalent incorporation. To our knowledge, no other GF delivery system has shown to provide such controllable release profiles in combination with the ability to covalently incorporate a wide range of proteins in the native state.

In **Chapter 4**, the PVA-Tyr system was adapted to promote vascularisation in a very specific clinical setting: revascularisation of the femoral head. Considering the design criteria reviewed in Chapter 2, VEGF was chosen to promote migration of blood vessels into the avascular femoral head. The degradation time of the hydrogels was chosen to be between 1 and 2 weeks to promote an early vascularisation process. Furthermore, it was identified that the interaction of the system with cells in the surrounding microenvironment should be improved to promote the penetration of new vessels, and the release profile and delivery method had to be considered for the specific surgical setting.

The ability of the system to directly interact with cells in the surrounding environment was improved by covalently incorporating gelatin into PVA-Tyr hydrogels. The addition of 1 wt % gelatin promoted the attachment of endothelial cells and didn't have a negative impact any of the key attributes of PVA-Tyr hydrogels (degradation time, resistance protease degradation and controlled release time frame of GFs). These results show the potential of the system to incorporate multiple proteins while still providing controlled GF release. The system was further adapted to the specific surgical procedure by performing the photo-crosslinking prior to the injection into the site of injury, which allowed avoiding unnecessary risks of uneven crosslinking or burst release into the body. Finally, PVA-Tyr hydrogels with incorporated gelatin and VEGF were applied in a piglet in vivo model of avascular necrosis. While the data from the in vivo experiment is still not conclusive and needs to be further analysed, there seems to be a tendency to improve the maintenance of the femoral head after injection of the PVA-Tyr hydrogels.

There are some aspects of the system that still need to be further investigated. Studies on the effects of increased Ru/SPS concentration in GF bioactivity should be performed. Potential strategies to reduce oxidative stress such as the addition of protective proteins in the hydrogel should be studied to avoid any loss of bioactivity that the crosslinking process could cause. We have, however, provided evidence showing that the process of covalent incorporation does not inactivate the studied GFs and, therefore, that this type of cross-linking is a viable strategy for long term GF delivery. Another key aspect for future study is the degradation profile of PVA-Tyr hydrogels in an *in vivo* environment. While we have studied the susceptibility of the system to protease degradation in vitro, other factors that could affect the process are present in the in vivo environment. Finally, the concentration of GF that needs to be delivered can only be determined through in vivo experimentation and will need to be studied for each application that the PVA-Tyr system is adapted to.

There is a range of other potential applications that the system could be translated to aside from delivery of single or multiple GFs. The capability of the system to incorporate any tyrosine-containing protein could be used to incorporate protein and cell suspensions that would otherwise be hard to deliver in a controlled manner due to their heterogeneity. One example of this type of suspensions is platelet-rich plasma (PRP). Despite the presence of a wide range of GFs in PRP, the benefits of its clinical application though direct injection have been dubious so far (1–3). In a similar way to GF delivery, these negative results could be

related to the lack of control over its release. Some studies have aimed to control the release of the GFs in PRP by incorporating it into hydrogels (4–6), but none of these platforms show the level of control over the release profile that PVA-Tyr would provide. The flexibility of the PVA-Tyr system provides can still open the door to many more novel applications in the future.

Aim II: Combining Top-down and Bottom-up Approaches for the Generation of Large Vascularised Tissue Analogues

The in vitro generation of large vascularised tissues analogues that recapitulate the different levels of vascularisation in native tissues and organs remains one of the major challenges in tissue engineering, and efforts in this direction have taken two major routes: 3D fabrication-based top-down approaches and bottom-up approaches based on endothelial cell self-assembly. One of the major barriers for these two approaches to be combined is in the incompatibility of present material platforms to be adaptable to both 3D biofabrication and to promote endothelial cell self-assembly into microvessel networks.

In **Chapter 5**, the combination of a top-down and a bottom-up approach for the biofabrication of vascularised constructs with different levels of vascularisation using a single material platform is reported. Combining thiol-ene chemistry with the visible light initiated photoinitiator system Ru/SPS allowed fine tailoring of the hydrogel mechanical properties and obtain constructs with microvasculature and homogeneous contraction. It was found that contraction of the material is tightly related to the formation of vessel-like structures by encapsulated endothelial cells. Despite the contraction, it was possible to biofabricate large constructs with an interconnected pore network of predictable diameter and spacing while allowing the elongation and migration of endothelial cells at the deeper areas of the material. To our knowledge, this was the first report of the combination of both approaches without the need of support materials and perfusion of culture media and endothelial cells. This platform was then used to study the effects of 3D architecture on the behaviour of endothelial cells both on the surface and at the deeper areas of the constructs. Our data suggests that the fabrication of interconnected pores stimulates endothelial cells to migrate to the surface of the pores and endothelialise them rather than forming a microvessel network. This resulted in full endothelialisation of the pore network regardless of the pore diameter. It was also observed that increasing the pore spacing of the constructs can affect the behaviour of endothelial cells at the deeper areas of the material, potentially by generating hypoxic conditions that stimulate microvessel formation. These results show that the fabrication parameters have an impact on cell behaviour and should be thoroughly studied to find the architecture that results in optimal outcomes. The role of hypoxia during the generation of large, pre-vascularised tissues is also an aspect that should be further studied as part of the efforts to translate these technologies to studies in larger mammals.

The findings from this chapter is a valuable proof of concept for the field as one of the first attempts to combine top-down and bottom-up approaches, in order to fabricate clinically relevant large vascularised tissues. Furthermore, we have used this novel platform to provide relevant information on how 3D design can affect endothelial cell behaviour in 3D biofabricated vascularised constructs, which will be relevant for future optimisation and translation of large vascularised constructs.

However, the quality of the microvessels at the deeper areas of biofabricated constructs was lacking in comparison to previous studies using fibrin and collagen. The addition of ECM proteins with bioactive properties such as fibrin or laminin into Gel-NOR hydrogels could help improve the formation of micro-capillaries, but could also result in changes in the degree and homogeneity of the contraction after fabrication. This would be an interesting line of research to continue using the Gel-NOR platform and biofabrication technologies.

Aim III: Combining Approaches for Tissue Vascularisation Through Bioassembly

The field of regenerative medicine is evolving towards the combination of different cells, materials and bioactive molecules to provide optimal levels of tissue regeneration. While several studies confirm that combining these elements can result in synergistic positive effects, there is little knowledge on the ideal ways to combine them. Bioassembly allows the combination of these elements and provides control over their spatial arrangement. Additionally, it allows generating large tissue analogues in a layer-by-layer fashion, facilitating translation to a clinical setting. Very few studies provide evidence of what is the ideal spatial and temporal arrangement of materials, cells and growth factors within biofabricated scaffolds. Furthermore, there are no studies yet that combine the stimulation of angiogenesis with pre-vascularisation techniques. Adapting the platforms developed in this thesis to their use as building blocks for bioassembly could allow the fabrication of large tissue models that allow studying the effects of different cell and growth factor arrangements on tissue vascularisation.

In **Chapter 6**, PVA-Tyr and Gel-NOR microsphere modules were generated for bioassembly applications. It was demonstrated that both materials can be fabricated into microspheres with encapsulated cells and GFs using a microfluidics system. The fabrication process did not alter the desirable properties of Gel-NOR, as both the HUVECs and MSCSs were still able to migrate and proliferate throughout the material. Furthermore, encapsulated HUVECs were able to undergo vasculogenesis and form interconnected vessel-like structures within the Gel-NOR microspheres when co-cultured with MSCs. Using these pre-vascularised modules, it was possible to obtain proof-of-concept results on how these microspheres can be arranged to study the optimal distribution of endothelial cells and MSCs within 3D constructs for vascularisation purposes. The results suggest that both HUVECs and MSCs should be co-encapsulated in each microsphere for improved microsphere fusion and homogeneous endothelial cell network distribution. When generating GF-loaded PVA-Tyr microspheres, the fabrication process impacted the initial GF retention within the PVA-Tyr microspheres. However, PVA-Tyr microspheres still showed a linear GFs release profile throughout the degradation process. Finally, the possibility of arranging PVA-Tyr and Gel-NOR microspheres in a controlled and designed manner was demonstrated.

The tools developed in this chapter should prove useful for future vascularisation research in in different ways. Firstly, and in contrast to the Gel-NOR biofabrication method described in

Chapter 5, it could allow the generation of large vascularised tissues by combining pre-vascularised modules with other cell-containing modules after a separate in vitro culture and differentiation process, allowing to provide each module with the conditions needed for the desired cell behaviour. Secondly, it allows combining pre-vascularised modules with GF-containing modules, enabling research on the impact of spatial and temporal arrangement of these factors in vascularised tissues. The GF-releasing microspheres could contain different GFs and could release them during different periods of time, providing a high degree of control over the microenvironment.

7.2. Future Perspectives

The stimulation of vascularisation through GF delivery has shown to be dependent on a series of parameters such as the GF used, its concentration and its release profile. The translation of any GF therapy to a clinical setting will therefore require testing a large amount of parameters. While PVA-Tyr system has shown the flexibility to adapt any of these parameters to the requirements of each therapy, technologies for high throughput screening of release conditions and better in vitro models that closely resemble in vivo conditions should be developed for quicker identification and translation of potential candidates.

The generation of large vascularised tissues in vitro is still far from clinical application. While some techniques such as pre-vascularisation and biofabrication have shown promise on generating microvessels of different diameters, no techniques so far have been able to reproduce the complex vascular beds in native tissues and organs. Novel techniques to scale up the fabrication of vascularised tissue analogues are needed, together with techniques to evaluate the adequate functionality of the fabricated vessels in terms of oxygen and nutrient diffusion to the encapsulated cells.

While the generation of constructs that only contain blood vessels could be of use for ischemic disease or for implantation in tissues that have inherent regenerative capabilities such as bone, other tissues would not be able to rely on vessels alone to recover functionality. The next challenge will be finding ways to fabricate tissues that not only contain vessels, but also contain the different types of functional cells of the targeted tissue in a way that restores or improves tissue function. For that purpose, techniques such as bioassembly could be of great help. The ability to generate smaller modules under isolated conditions that can be assembled together makes this technology appealing to achieve complex tissue biofabrication. Research aiming to optimise these conditions and techniques for automated module production would be of great help to the field.

The large evolution process that resulted in the appearance and success of the human species on Earth also resulted in our organisms being extremely complex and diverse. The field of regenerative medicine will continue studying and trying to reproduce small pieces of this puzzle to circumvent the limitations of our body. While there is still a lot of research to be done, hopefully this piece of work will be useful to someday, somehow, improve someone's life.

7.3. References

1. Bell KJ, Fulcher ML, Rowlands DS, Kerse N. Impact of autologous blood injections in treatment of mid-portion Achilles tendinopathy: double blind randomised controlled trial. BMJ [Internet]. 2013 Apr 18;346:f2310–f2310. Available from: https://www.ncbi.nlm.nih.gov/pubmed/23599320

2. de Vos R-J, Windt J, Weir A. Strong evidence against platelet-rich plasma injections for chronic lateral epicondylar tendinopathy: a systematic review. Br J Sports Med [Internet]. 2014 Jun 1;48(12):952 LP – 956. Available from: http://bjsm.bmj.com/content/48/12/952.abstract

3. Grassi A, Napoli F, Romandini I, Samuelsson K, Zaffagnini S, Candrian C, et al. Is Platelet-Rich Plasma (PRP) Effective in the Treatment of Acute Muscle Injuries? A Systematic Review and Meta-Analysis. Sport Med [Internet]. 2018;48(4):971–89. Available from: https://doi.org/10.1007/s40279-018-0860-1

4. Kurita J, Miyamoto M, Ishii Y, Aoyama J, Takagi G, Naito Z, et al. Enhanced Vascularization by Controlled Release of Platelet-Rich Plasma Impregnated in Biodegradable Gelatin Hydrogel. Ann Thorac Surg [Internet]. 2011;92(3):837–44. Available from: http://www.sciencedirect.com/science/article/pii/S0003497511010514

5. Bir SC, Esaki J, Marui A, Yamahara K, Tsubota H, Ikeda T, et al. Angiogenic properties of sustained release platelet-rich plasma: Characterization in-vitro and in the ischemic hind limb of the mouse. J Vasc Surg [Internet]. 2009;50(4):870-879.e2. Available from: http://www.sciencedirect.com/science/article/pii/S0741521409013263

6. Irmak G, Demirtaş TT, Gümüşderelioğlu M. Sustained Release of Growth Factors from Photoactivated Platelet Rich Plasma (PRP). Eur J Pharm Biopharm [Internet]. 2019; Available from: http://www.sciencedirect.com/science/article/pii/S0939641119313104